Pacific Northwest
NATIONAL LABORATORY

PNNL-38969 Rev 0
EWG-RPT-056, Rev 0

High Sodium and Potassium Glass Testing Matrix

March 2026

V Gervasio
RL Russell
J Marcial
X Lu
NA Lumetta
LM Seymour
JT Reiser
JJ Neeway
S Chong
JD Vienna
DA Cutforth
J Bai
JL George
S Choi
LQ Le
P Metheny
M Torres
A Zwoster
M Kim

U.S. DEPARTMENT of ENERGY

Prepared for the U.S. Department of Energy
under Contract DE-AC05-76RL01830

DISCLAIMER

This report was prepared as an account of work sponsored by an agency of the United States Government. Neither the United States Government nor any agency thereof, nor Battelle Memorial Institute, nor any of their employees, makes **any warranty, express or implied, or assumes any legal liability or responsibility for the accuracy, completeness, or usefulness of any information, apparatus, product, or process disclosed, or represents that its use would not infringe privately owned rights**. Reference herein to any specific commercial product, process, or service by trade name, trademark, manufacturer, or otherwise does not necessarily constitute or imply its endorsement, recommendation, or favoring by the United States Government or any agency thereof, or Battelle Memorial Institute. The views and opinions of authors expressed herein do not necessarily state or reflect those of the United States Government or any agency thereof.

PACIFIC NORTHWEST NATIONAL LABORATORY
operated by
BATTELLE
for the
UNITED STATES DEPARTMENT OF ENERGY
under Contract DE-AC05-76RL01830

Printed in the United States of America

Available to DOE and DOE contractors from
the Office of Scientific and Technical Information,
P.O. Box 62, Oak Ridge, TN 37831-0062
www.osti.gov
ph: (865) 576-8401
fax: (865) 576-5728
email: reports@osti.gov

Available to the public from the National Technical Information Service
5301 Shawnee Rd., Alexandria, VA 22312
ph: (800) 553-NTIS (6847)
or (703) 605-6000
email: info@ntis.gov
Online ordering: http://www.ntis.gov

PNNL-38969 Rev 0
EWG-RPT-056, Rev 0

High Sodium and Potassium Glass Testing Matrix

March 2026

V Gervasio
RL Russell
J Marcial
X Lu
NA Lumetta
LM Seymour
JT Reiser
JJ Neeway
S Chong
JD Vienna
DA Cutforth
J Bai
JL George
S Choi
LQ Le
P Metheny
M Torres
A Zwoster
M Kim

Prepared for
the U.S. Department of Energy
under Contract DE-AC05-76RL01830

Pacific Northwest National Laboratory
Richland, Washington 99354

Abstract

The U.S. Department of Energy Hanford Site in Washington state stores about 56 million gallons of highly radioactive waste in 155 of the original 177 tanks, with 22 already retrieved. The Tank Waste Treatment and Immobilization Plant (WTP) separately vitrify the low-activity waste (LAW) and high-level waste (HLW) fractions of this tank waste, converting them into immobilized low-activity waste (ILAW) and immobilized high-level waste (IHLW) borosilicate glass products. ILAW will be disposed of in the onsite Integrated Disposal Facility, while IHLW will be stored on site until it is sent to a national deep geological repository.

Pacific Northwest National Laboratory (PNNL) evaluated gaps in enhanced waste glass (EWG) composition-property data for both LAW and Direct-Feed HLW (DFHLW) and found that the region of high sodium and high potassium have insufficient data to optimize glass compositions. For example, the high Na and K region for Hanford LAW glasses is prone to high uncertainty or requires bias correction when predicting either product consistency test (PCT) or vapor hydration test (VHT) responses (Vienna et al. 2022). Likewise, DFHLW glasses with high Na and K concentrations are prone to high melter materials corrosion rates which limit a majority of glass compositions and are subject to high uncertainty due to limited data (Lu et al. 2026).

To expand the useable composition envelope for both DFHLW and LAW glasses, 20 glass compositions were designed in the high $Na_2O + K_2O$ composition space. The glass compositions selected were specifically targeting product consistency test (PCT) and vapor hydration test (VHT) responses near and above the contractual limits as this composition region and associated property response range has significantly less data than the range of glasses with lower $Na_2O + K_2O$ that easily pass contractual constraints. To more accurately predict the location of the constraint in composition space, data on both sides of the constraint are required. This data will expand the glass composition envelopes for both DFHLW and LAW and likely allow increased waste loading.

Of the 20 quenched glasses, seven were fully amorphous, and one had a sodium-aluminumosilicate crystalline phase > 10 wt%. The remainder of the glasses had a total crystalline fraction of < 1 wt%, with spinel being the most frequent crystalline phase identified by X-ray diffraction. Only eight of the 20 glasses met the container centerline cooling (CCC) crystallization constraint developed to prevent formation of Na-Al-silicate and Na-Ca-silicate crystals. Of these, only four did not form Na-Al-silicate and Na-Ca-silicate crystals after CCC heat-treatment. Among all 20 glass compositions tested by isothermal heat-treatment, seven compositions showed no crystal phases at or above 950 °C, eight formed $\geq$ 1 vol% crystal with Sn-containing and Al-Zr-containing crystals being most common. At the nominal melter operating temperature of 1150 °C, all the glasses met the WTP upper limit for viscosity of < 8 Pa-s. However, 55% of the glasses were below the lower limit of 2 Pa-s, which is expected since alkali decreases viscosity. Electrical conductivity (EC) at 1150 °C ranged between 40.8 and 101.8 S/m, 3 glasses had values higher than the WTP limits of $10 \leq EC_{1150} \leq 70$ S/m. This result is expected since alkali are the primary charge carriers for these glasses and thus increasing alkali leads to a higher EC. Additionally, EC wasn't constrained during glass design.

All glasses satisfied the WTP SO_3 solubility limit. Most of the quenched glasses performed poorly in the PCT durability test, exceeding the contract limit in one or two of the components: B, Na, Li, and Si. Of the 20 CCC glasses, only two had normalized elemental loss below the contract limit for B and Na. It should be emphasized that failures in specific properties were anticipated and are necessary to establish acceptable processing envelopes for DFHLW or LAW operations. The resulting dataset provides valuable information to improve model accuracy and reduce prediction uncertainty. These insights will ultimately

support the development of more robust glass formulation strategies, enabling higher waste loading, reducing operational risks, and expanding the processing envelope.

Acknowledgments

The authors gratefully acknowledge the financial support provided by the U.S. Department of Energy Hanford Field Office, Waste Treatment and Immobilization Plant project, with technical oversight by Albert Kruger. The following Pacific Northwest National Laboratory staff members are acknowledged for their contributions: Pavel Ferkl for technical review of the report; David MacPherson, Alyssa Petersen, and Aaron Sachs for quality assurance; Chrissy Charron and Cassie Martin for programmatic support during the conduct of this work; Will Eaton for project management; Matt Wilburn and Jennifer Blake for their editorial support; David Peeler for management review.

All of the other PNNL staff helping in the laboratory to complete this work are greatly appreciated and acknowledged.

Acronyms and Abbreviations

3TS	three-time saturation (method)
ARM-1	Approved Reference Material-1
BSE	backscatter electron
CCC	container centerline cooling
CF	crystal fraction
DFHLW	Direct Feed High-Level Waste
DFLAW	Direct Feed Low-Activity Waste
DIW	Type I deionized water
DOE	U.S. Department of Energy
EC	electrical conductivity
EDS	energy dispersive X-ray spectroscopy
EWG	enhanced waste glass
HLW	high-level waste
IC	ion chromatography
ICP-OES	inductively coupled plasma optical emission spectroscopy
IHLW	immobilized high-level waste
ILAW	immobilized low-activity waste
LAW	low-activity waste
NL	normalized elemental loss by 7-day PCT
NL_B	normalized B loss by 7-day PCT
NL_{Li}	normalized Li loss by 7-day PCT
NL_{Na}	normalized Na loss by 7-day PCT
NL_{Si}	normalized Si loss by 7-day PCT
NP	nepheline
NQAP	Nuclear Quality Assurance Program
PCT	product consistency test
PNNL	Pacific Northwest National Laboratory
PQM	partial quadratic model
PTFE	polytetrafluoroethylene
Q	quenched
R_s	solution resistance
RPD	relative precent difference
SCC	single-component constraint
SEM-EDS	scanning electron microscopy with energy dispersive X-ray spectroscopy
SSM	sulfur-saturated melt
SwRI	Southwest Research Institute

T_L	liquidus temperature
T_M	melting temperature
VHT	vapor hydration test
XRD	X-ray diffraction
WC	tungsten carbide
WTP	Waste Treatment and Immobilization Plant

Contents

Abstract ii
Acknowledgments iv
Acronyms and Abbreviations v
1.0 Introduction 1.1
1.1 Quality Assurance 1.1
2.0 Test Methods 2.1
2.1 Matrix Design 2.1
2.1.1 Design Method 2.1
2.1.2 Compositional Boundaries 2.3
2.1.3 Property Targets 2.4
2.1.4 Designed Glass Matrix 2.4
2.1.5 Predicted Properties 2.8
2.2 Glass Fabrication and Characterization 2.8
2.2.1 Glass Fabrication 2.8
2.2.2 Secondary Phase Investigation 2.9
2.3 Container Centerline Cooling 2.9
2.4 Isothermal Crystal Fraction 2.10
2.5 Density 2.11
2.6 SO_3 Solubility 2.11
2.7 Viscosity 2.12
2.8 Electrical Conductivity 2.12
2.9 Product Consistency Test 2.13
2.10 Vapor Hydration Test 2.13
3.0 Results and Discussion 3.1
3.1 Glass Composition 3.1
3.1.1 Secondary Phase Investigation in Quenched Glasses 3.1
3.2 Crystal Identification in Container Centerline Cooling Glasses 3.2
3.3 Crystal Fraction in Isothermally Heat-Treated Glasses 3.7
3.4 Density 3.11
3.5 SO_3 Solubility 3.13
3.5.1 Comparisons of Predicted SO_3 Saturation Concentrations 3.15
3.6 Viscosity 3.15
3.7 Electrical Conductivity 3.18
3.8 Product Consistency Test 3.21
3.9 Vapor Hydration Test 3.25
4.0 Summary 4.1
5.0 References 5.1

Appendix A – Optical Images of Fabricated Glasses A.1
Appendix B – Target and Measured Composition of Fabricated Glasses B.1
Appendix C – XRD Data on Quenched Glasses C.1
Appendix D – Container Centerline Cooling D.1
Appendix E – Crystal Fraction E.1
Appendix F – Glass Densities F.1
Appendix G – Viscosity Measurements G.1
Appendix H – Electrical Conductivity Measurements H.1
Appendix I – PCT Full Results I.1
Appendix J – VHT Images on Quenched Glasses J.1
Appendix K – VHT Images on CCC Glasses K.1

Figures

Figure 2.1. Scatterplot of pairwise elemental distributions for the designed 20 LAWHNK glasses in mass fraction. One red diamond represents the replicate glass taken from previous studies. 2.5
Figure 2.2. Plot of target temperature schedule during LAW CCC treatment. 2.10
Figure 3.1. Predicted nepheline formation (P) using the model by Lu et al. (2021) vs. nepheline formed (wt%) including Na-Al-Si phases. 3.4
Figure 3.2. BSE image of glass LAWHNK-01 after CCC at 1000×. 3.6
Figure 3.3. BSE image of glass LAWHNK-09 after CCC at 1000×. 3.7
Figure 3.4. Predicted density vs. measured density of LAWHNK glasses. 3.12
Figure 3.5. Comparison of ICP-OES vs. IC measured SO_3 wt% of each glass sample after 3TS method. 3.14
Figure 3.6. Predicted vs. measured melter SO_3 solubility of LAWHNK glasses applying the 11-term 3TS-SO_3-PQM model (Vienna et al. 2022). 3.15
Figure 3.7. Predicted vs. measured $\ln(\eta_{1150})$ where model predicted for Pa·s shown. Uncertainties for measured values are represented by SD_{pooled} reported in Vienna et al. (2022). 3.18
Figure 3.8. Predicted vs. measured $\ln(\varepsilon_{1150})$. Uncertainties for measured values are represented by SD_{pooled} reported in Vienna et al. (2022). 3.21
Figure 3.9. Normalized NL_B and NL_{Na} release in natural logarithm scale of quenched vs. CCC for LAWHNK glasses. The red line is the 1:1 line and is used to guide the eye. 3.24
Figure 3.10. $\ln(NL_B)$ and $\ln(NL_{Na})$ measured vs. predicted values from Vienna et al. (2022). The orange lines are the release limit. 3.25
Figure 3.11. Example of quenched glass (LAWHNK-18) that performed well after 24 days VHT. Red lines are the 10 equidistant measurement lines. 3.25
Figure 3.12. Example of quenched glass (LAWHNK-08) that performed extremely poorly on 24-day VHT. 3.26

Figure 3.13. Quenched glasses VHT alteration rate (r_{VHT}) compared to the total normalized alkali [Nalk = Na_2O + 0.66(K_2O) + 2(Li_2O)] content of the glass. 3.28
Figure 3.14. CCC and Q glass alteration depth comparison with the total amount of crystallinity in the CCC glass 3.29
Figure 3.15. Predicted vs. measured VHT responses using the Vienna et al. (2022) model. The red line separates glasses that passed the VHT constraint (right side) from the glass that failed (left side). 3.30

Tables

Table 2.1. Minimum and maximum values (wt%) of the matrix design ranges and rationales. 2.3
Table 2.2. Minor components in “Others”. These components were grouped together with a fixed concentration. 2.3
Table 2.3. Property targets used in the matrix design. 2.4
Table 2.4. Glass compositions (mass fraction) for LAWHNK-01 to LAWHNK-10. 2.6
Table 2.5. Glass compositions (mass fraction) for LAWHNK-11 to LAWHNK-20. 2.7
Table 2.6. List of models used to calculate predicted properties. 2.8
Table 2.7. Container centerline cooling profile for the LAW samples. 2.10
Table 3.1. Crystalline phases and wt% in as fabricated LAWHNK glasses. 3.2
Table 3.2. LAWHNK glasses that met the CCC crystal constraints. 3.3
Table 3.3. Crystal phase and mass fraction observed by XRD in CCC glasses 3.5
Table 3.4. EDS atomic % of detected elements for LAWHNK-01 after CCC. 3.7
Table 3.5. EDS atomic % of detected elements for LAWHNK-09 after CCC. 3.7
Table 3.6. Identification and crystal fraction in wt% of crystalline phases for isothermally heat-treated glasses. 3.8
Table 3.7. LAWHNK glasses that met the 950 °C crystal constraints. 3.10
Table 3.8. Measured densities of LAWHNK glasses in g/cm^3. 3.13
Table 3.9. Comparison of target, as-fabricated (quenched), and sulfate saturated samples measured SO_3 wt%. 3.14
Table 3.10. Measured η (Pa-s) values versus target temperature (in the sequence of measurement). 3.16
Table 3.11. Fitted Arrhenius coefficients and calculated η for specific temperatures. 3.17
Table 3.12. Measured electrical conductivity (S/m) values vs. temperatures. 3.19
Table 3.13. Fitted coefficients of Arrhenius model for ε_{1150}. 3.20
Table 3.14. Average normalized elemental mass losses (NL_i) in $g \cdot m^{-2}$ for the LAWHNK Q glasses. Values in bold font exceed the LAW glass limit of 2.0 $g \cdot m^{-2}$. 3.22
Table 3.15. Average normalized elemental mass losses (NL_i) in $g \cdot m^{-2}$ for the LAWHNK CCC glasses. Values in bold text exceed the DOE limit of 2 g m^{-2} d^{-1} 3.23
Table 3.16. Q and CCC sample VHT corrosion rate (r_{VHT} [$g \cdot m^{-2} \cdot d^{-1}$]), pass/fail contract rate descriptor (0/1), ln(alteration depth) (μm), and test duration (days) 3.27
Table 4.1. Summary of the 20 LAWHNK glasses passing or failing property constraints. Property constraints were taken from Vienna et al. (2025). 4.1

1.0 Introduction

The U.S. Department of Energy (DOE) Hanford Site in Washington state has roughly 56 million gallons of radioactive wastes managed as high-level waste (HLW) stored in the 155 of the original 177 underground tanks, with waste retrieved from 22 of the tanks. The Hanford Waste Treatment and Immobilization Plant (WTP) will provide DOE with the capability to treat the waste by vitrification for subsequent disposal. The tank waste will be partitioned into low-activity waste (LAW) and HLW fractions, which will then be vitrified, respectively, into immobilized low-activity waste (ILAW) and immobilized high-level waste (IHLW) products. The ILAW product will be disposed of in the Integrated Disposal Facility on the Hanford Site, while the IHLW product will be temporarily stored on site prior to disposal at a national deep geological disposal facility for high-level nuclear waste. The hot commissioning milestone was met on October 15, 2025. The HLW Facility is scheduled to follow in roughly a decade.

The immobilized waste products must satisfy a variety of requirements with respect to regulatory compliance and protection of the environment before they can be accepted for disposal. Additionally, to be efficiently processed in the WTP, melts must satisfy process-related properties. Due to the large batch-to-batch variability of these wastes, models are being developed to optimize waste loading, processability, durability, and melter component lifetime. Because property models are only reliable within the ranges where experimental data exist, certain composition boundaries (called model validity constraints) are imposed. To increase the process flexibility, model validity constraints need to be relaxed by filling data gaps.

One gap recently identified in the database of glass properties is the high alkali (specifically Na and K) region. Glasses with high alkali content tend to have lower chemical durability and can be highly corrosive to melter components. Data high Na_2O+K_2O composition region will be useful to expand the composition regions for both LAW and DFHLW vitrification as long as all appropriate properties are measured. To expand the useable composition envelope, 20 glass compositions were designed in the high $Na_2O + K_2O$ composition space. The glass compositions selected were specifically targeting product consistency test (PCT) and vapor hydration test (VHT) responses near and above the contractual limits as this property response range has significantly less data than the range of glasses that easily pass contractual constraints. To more accurately predict the location of the constraint in composition space, data on both sides of the constraints are required.

Each glass was batched and melted and then subjected to density, viscosity, and electrical conductivity (EC) measurements; container centerline cooling (CCC); crystal fraction (CF) testing; PCT measurement; VHT measurement; and 3-time sulfur solubility measurements. K-3 melter refractory corrosion tests were also performed but will be reported in a separate PNNL report.

This report details the characterization performed and the results obtained. Section 1.1 outlines quality assurance programs followed for this work. Section 2.0 describes the methods used to design, prepare, and characterize the glasses. Section 3.0 reports the results of glass preparation and characterization. Section 4.0 provides a summary of this report.

1.1 Quality Assurance

This work was performed in accordance with the Pacific Northwest National Laboratory (PNNL) Nuclear Quality Assurance Program (NQAP). The NQAP complies with the DOE Order 414.1D, *Quality Assurance*, and 10 CFR 830, Subpart A, *Quality Assurance Requirements*. The NQAP uses NQA-1-2012,

Quality Assurance Requirements for Nuclear Facility Applications, as its consensus standard and NQA-1-2012, Subpart 4.2.1, as the basis for its graded approach to quality.

The NQAP works in conjunction with PNNL's laboratory-level Quality Management Program, which is based on the requirements as defined in DOE Order 414.1D and 10 CFR 830 Subpart A.

The work on this report was performed at a technology readiness level of 4, making the data useful for technology development activities.

2.0 Test Methods

This section describes how the test matrix of 20 high-Na_2O/K_2O LAW glasses (LAWHNK) was designed and data were obtained. The descriptions include the methods for (1) glass matrix design, (2) glass fabrication and chemical composition analysis, (3) secondary phase identification from CCC treatment, (4) isothermal CF measurement, (5) density (ρ) determination, (6) sulfur solubility measurement (w_{SO3}^{cruc}), (7) viscosity (η) measurement, (8) EC (ε) measurement, (9) PCT measurement, and (10) VHT measurement.

2.1 Matrix Design

This section describes how the glasses were formulated for high Na_2O and K_2O content with high target PCT and VHT responses using the current state-of-the-art glass property-composition models and constraint sets applicable to both LAW and DFHLW.

2.1.1 Design Method

These glasses were formulated using a space-filling design approach specifically focused on relatively high Na_2O and K_2O composition space. Standard software default assumptions using JMP software (Joseph et al. 2015) were used to generate candidate glass matrices and a final matrix was selected with a fixed set of single-component constraints (SCCs) for individual oxide concentration ranges. Property constraints were applied to limit the predicted properties such as melt viscosity, VHT, and PCT response. Since the PCT constraint is more restrictive for LAW than DFHLW and because DFHLW glasses are not required to satisfy the VHT constraing, the design was specifically focused on LAW glass. LAW glasses from an existing database were used to bound the composition region and predicted properties (VHT pass/fail, elemental release from PCT, and viscosity) for this design. The matrix design was required to satisfy predefined acceptance ranges defined by the SCCs and also a broad dispersion of points across the range compared to those of external vertices.

A successful matrix must meet two success criteria: (1) the dispersion value of each component must be below 0.90 and (2) the relative range of individual components across the glasses in the matrix should be greater than or equal to 0.79 for components that can achieve their full design range (e.g., aren't limited by property constraints). The methods for calculating these two values are given below.

1. The dispersion ratio of a matrix is defined as follows.

Given a vector x of n values for a particular component (so x is a vector of length n) that are sorted in increasing order, we define d to be the differences of the entries in x. So, d is a vector of length $n - 1$, such that:

$$d_i = x_{i+1} - x_i \text{ for } i = 1, 2, 3, \ldots, n - 1 \quad (2.1)$$

Thus, these d_i values are the lengths of the segments of the partition formed by the component values contained in the vector x.

The formula for the single-component dispersion metric is:

$$D = \frac{\sum_{i=1}^{n-1} \left| d_i - \frac{R}{n-1} \right|}{R} \quad (2.2)$$

where D = the dispersion metric
R = the intended range of the particular component or predicted property
n = number of glasses in the matrix

Note that if the points formed an "ideal" uniform or regular partition of the range of the particular component, each d_i would have a length of $\frac{R}{n-1}$, and D would be 0. So, the dispersion metric describes the sum of absolute differences from a uniform or regular partition of the range of the particular component, relative to the range of the component. Thus, a value of $D = 1.45$ would mean that the absolute differences in the actual segment lengths of the partition formed by the vector x and the length of an "ideal" segment would sum to 1.45 times the intended range of the component.

The single-component dispersion metric, $D \leq 0.9$, identifies sets of component values that are close to a uniform or regular partition. Smaller values of D are better in the sense that the corresponding x vector would be closer to a regular spaced points.

Additionally, the multi-component dispersion is monitored qualitatively by plotting the pairwise elemental distributions (see Figure 2.1 for an example) and inspecting the two-dimensional range coverage for the various pairwise plots.

2. The relative range of each individual component across the glasses in the matrix is calculated according to: [min(g_{matrix})-max(g_{matrix})]/[min(g_{target})-max(g_{target})].

The matrix was designed following these general steps:

1. Identify compositional gaps in the database.
2. Filter the database to exclude glasses without PCT or VHT response measurements.
3. Set component concentration boundaries and property boundaries (both within and beyond the typical processing and product quality constraints so that constraints can be successfully predicted). The normalized elemental release of boron by PCT (NL_B), VHT, and viscosity bounds were selected to provide more data where available data is sparse.
4. Further filter glass database to remove glasses with mass fraction of components outside the selected SCC's, resulting in a database containing 245 glasses.
5. Generate a significant amount of simulated glass compositions (40,000) using JMP within the selected SCC's, allowing for Na and Li to independently vary.
6. Calculate the predicted properties for the similated points using various models.
7. Select the glasses that fall within the target property ranges among the 40,000 simulated points.
8. Combine the selected glasses with existing data that are within the component concentration boundaries, and add duplicates from previous tested glass matrices.
9. Design 6 candidate glass matrices (20 glasses per matrix with one from a previously tested matrix as a duplicate) using JMP to back fill with a few different random seeds.
10. Calculate matrix dispersion ratio and range coverage to select one matrix for testing.

11. Plot scatter plot of elemental pairwise distributions figures to check compositional coverage and predicted property distribution.

2.1.2 Compositional Boundaries

The concentration boundaries were determined by filtering out the entries that did not include NL_B or VHT results from available LAW database. Afterward, NL_B response, VHT response, and $\eta_{1150°C}$ were calculated using the partial quadratic models (PQMs) in Vienna et al. (2022). Database entries were then further filtered following property targets outlined in the next section. Lastly, to ensure that a high Na_2O composition space was targeted, entries were removed in which (1) $Na_2O < 20$ wt%, and (2) $Cl > 1.9$ wt%, $Cr_2O_3 > 0.63$ wt%, $F > 0.49$ wt%, $P_2O_5 > 0.68$ wt%, $SO_3 > 1.3$ wt%, and $Cl + Cr_2O_3 + F + P_2O_5 + SO_3 > 2.9$ wt%. A database of 245 glasses remained, for which the min/max mass fractions of Al_2O_3, B_2O_3, CaO, Fe_2O_3, K_2O, Li_2O, MgO, Na_2O, SiO_2, SnO_2, TiO_2, V_2O_5, ZnO, ZrO_2, and others were input into the space-filling design algorithm.

Table 2.1 presents these boundaries. Table 2.2 presents the minor components that were grouped together with a fixed concentration under "Others."

Table 2.1. Minimum and maximum values (wt%) of the matrix design ranges and rationales.

Component	Min	Max
Al_2O_3	8.65	13.66
B_2O_3	6.00	14.01
CaO	0.00	12.24
Fe_2O_3	0.00	9.98
K_2O	0.00	5.88
Li_2O	0.00	1.93
MgO	0.00	10.02
Na_2O	20.00	26.57
SiO_2	30.26	45.05
SnO_2	0.00	5.00
TiO_2	0.00	4.00
V_2O_5	0.00	4.09
ZnO	0.00	4.50
ZrO_2	0.00	5.50
Others[(a)]	0.23	2.96

(a) See list in Table 2.2.

Table 2.2. Minor components in "Others". These components were grouped together with a fixed concentration.

Component	Mean Mass Fraction	Median Mass Fraction	Mass Fraction of "Others"
Cl	0.002	0.004	0.269
Cr_2O_3	0.004	0.003	0.206
F	0.001	0.001	0.058
P_2O_5	0.001	0.002	0.104
SO_3	0.005	0.005	0.362
Total	0.014	0.015	1.000

2.1.3 Property Targets

Table 2.3 shows the property targets used to select glasses generated from the space filling step that pass the constraints. These targets were modified compared to the LAW and DFHLW enhanced waste glass (EWG) limits (Vienna et al. 2022, Lu et al. 2026) so that the glasses have predicted values on/near the database extremes, where the available data is sparse.

Table 2.3. Property targets used in the matrix design.

Property	LAW EWG Limit	DFHLW EWG Limit	Design Targets
PCT	$NL_B \leq 2$ g/m^2	$NL_B \leq 8.35$ g/m^2	$NL_B \leq 10$ g/m^2
VHT[(a)]	*P/F threshold ≤ 0.19*	n/a	0.65 ≤ P/F threshold ≤ 0.83
Viscosity	$2 \leq \eta_{1150} \leq 8$ Pa·s	$2 \leq \eta_{1150} \leq 8$ Pa·s	$1 \leq (\eta_{1150°C}$, Pa·s) ≤ 10

(a) The probability values of 0.19, 0.65, and 0.83 translate to logit values of -1.45, 0.6, and 1.6, which roughly translate to VHT rate values of 0.1, 46, and 902 g m^{-2} d^{-1}.

2.1.4 Designed Glass Matrix

Figure 2.1 shows a scatterplot matrix for the designed 20 LAWHNK glasses. The glass compositions listed in mass fraction of the 20 glasses are reported in Table 2.4 and Table 2.5. LAWHNK-20 is a duplicate of glass ORPLA26 (Muller et al. 2012).

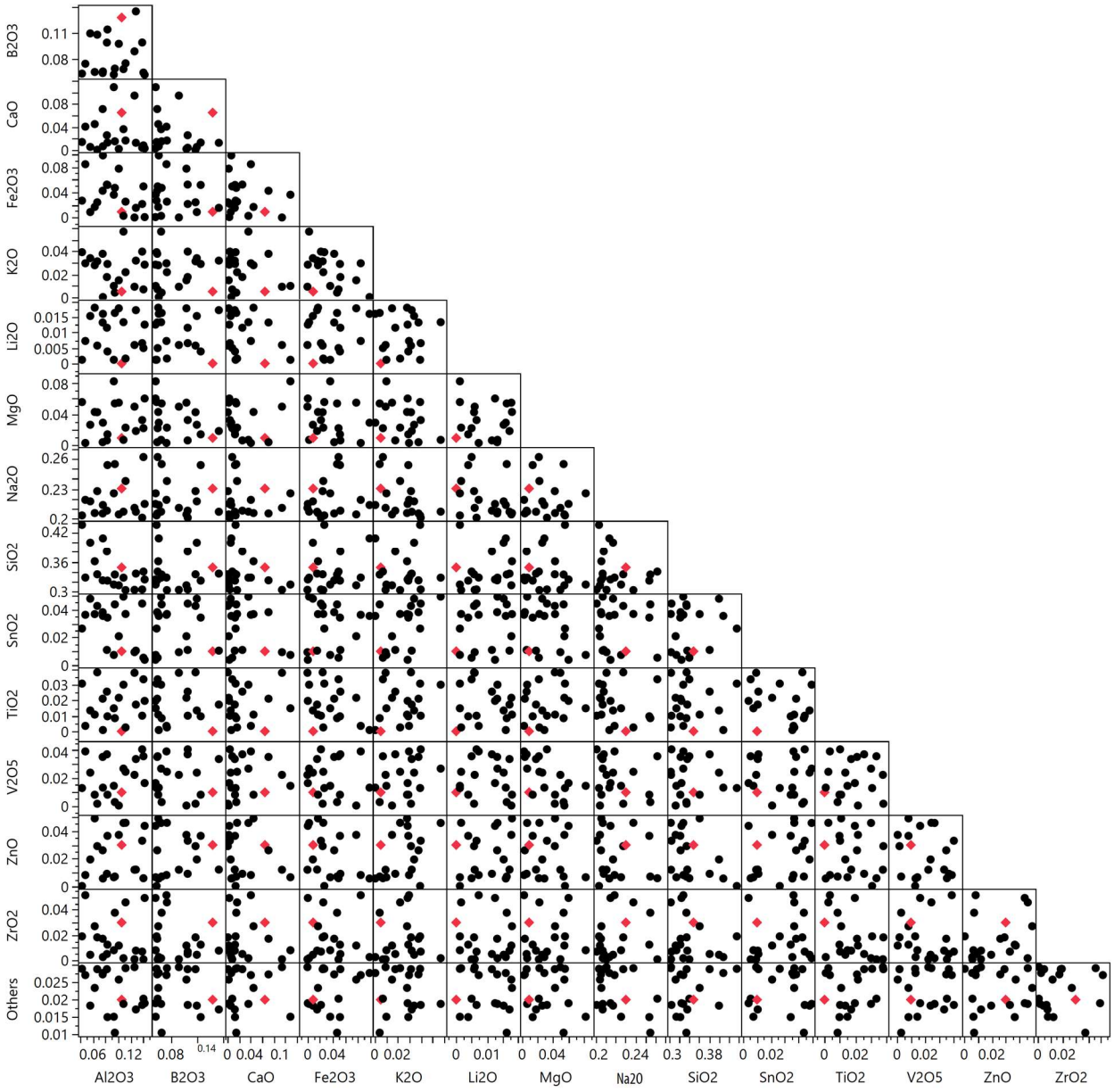


Figure 2.1. Scatterplot of pairwise elemental distributions for the designed 20 LAWHNK glasses in mass fraction. One red diamond represents the replicate glass taken from previous studies.

Table 2.4. Glass compositions (mass fraction) for LAWHNK-01 to LAWHNK-10.

Component	LAWHNK-01	LAWHNK-02	LAWHNK-03	LAWHNK-04	LAWHNK-05	LAWHNK-06	LAWHNK-07	LAWHNK-08	LAWHNK-09	LAWHNK-10
Al_2O_3	0.12619	0.13841	0.14225	0.11200	0.06711	0.10870	0.14045	0.09502	0.09343	0.12837
B_2O_3	0.08887	0.09914	0.06195	0.07509	0.10806	0.06838	0.06437	0.06904	0.06215	0.13505
CaO	0.09427	0.00407	0.00305	0.01658	0.00060	0.03616	0.00824	0.01523	0.10893	0.01263
Fe_2O_3	0.00003	0.02141	0.00064	0.02512	0.02409	0.00263	0.04925	0.04696	0.03611	0.01527
K_2O	0.00933	0.03971	0.02836	0.02192	0.03127	0.05699	0.00696	0.00416	0.01003	0.03193
Li_2O	0.00601	0.00664	0.01258	0.00162	0.00580	0.01336	0.00500	0.01635	0.00118	0.01728
MgO	0.04957	0.03222	0.06020	0.02240	0.04236	0.00655	0.02169	0.05378	0.08249	0.01804
Na_2O	0.21076	0.20093	0.21482	0.23794	0.22770	0.20696	0.26211	0.25498	0.22553	0.20687
SiO_2	0.30315	0.30397	0.32419	0.30267	0.33455	0.32781	0.34008	0.33412	0.31388	0.33605
SnO_2	0.00943	0.04437	0.00390	0.03692	0.04273	0.04936	0.00544	0.04379	0.00736	0.01053
TiO_2	0.03790	0.01013	0.01971	0.00250	0.03824	0.03017	0.03368	0.00847	0.01487	0.01727
V_2O_5	0.02227	0.04074	0.01640	0.02452	0.00146	0.02676	0.03565	0.00274	0.01438	0.03366
ZnO	0.01211	0.03296	0.04365	0.04586	0.02914	0.04576	0.00603	0.00724	0.00667	0.01219
ZrO_2	0.00086	0.00695	0.04937	0.04591	0.01816	0.00167	0.00082	0.03770	0.00800	0.00771
Cl	0.00788	0.00494	0.00510	0.00780	0.00774	0.00505	0.00545	0.00281	0.00404	0.00462
Cr_2O_3	0.00603	0.00378	0.00390	0.00597	0.00592	0.00386	0.00417	0.00215	0.00309	0.00354
F	0.00170	0.00107	0.00110	0.00168	0.00167	0.00109	0.00118	0.00061	0.00087	0.00100
P_2O_5	0.00304	0.00191	0.00197	0.00301	0.00299	0.00195	0.00210	0.00108	0.00156	0.00178
SO_3	0.01060	0.00665	0.00686	0.01049	0.01041	0.00679	0.00733	0.00377	0.00543	0.00621
Sum	1.00000	1.00000	1.00000	1.00000	1.00000	1.00000	1.00000	1.00000	1.00000	1.00000

Table 2.5. Glass compositions (mass fraction) for LAWHNK-11 to LAWHNK-20.

Component	LAWHNK-11	LAWHNK-12	LAWHNK-13	LAWHNK-14	LAWHNK-15	LAWHNK-16	LAWHNK-17	LAWHNK-18	LAWHNK-19	LAWHNK-20
Al_2O_3	0.04285	0.08237	0.06313	0.07612	0.05601	0.10131	0.07573	0.04824	0.08331	0.10585
B_2O_3	0.06316	0.09895	0.06512	0.06570	0.10964	0.09762	0.06386	0.07458	0.11407	0.12788
CaO	0.01398	0.02565	0.04500	0.00657	0.00553	0.00209	0.07105	0.04053	0.01299	0.06479
Fe_2O_3	0.02670	0.05224	0.01673	0.09853	0.00863	0.07739	0.04241	0.08453	0.05157	0.00901
K_2O	0.03915	0.01771	0.02787	0.00038	0.03404	0.01488	0.03778	0.02963	0.02899	0.00511
Li_2O	0.00117	0.01155	0.01806	0.01610	0.01536	0.01786	0.01325	0.00725	0.00385	0.00000
MgO	0.05556	0.00582	0.04266	0.02880	0.02609	0.05478	0.00345	0.00247	0.01371	0.00901
Na_2O	0.20318	0.20797	0.20557	0.21370	0.21740	0.20422	0.20517	0.21895	0.25397	0.23033
SiO_2	0.43603	0.38110	0.36094	0.40874	0.39998	0.31240	0.32242	0.32801	0.32186	0.34850
SnO_2	0.02636	0.01096	0.03679	0.03550	0.04794	0.02091	0.03816	0.03630	0.03428	0.01001
TiO_2	0.03085	0.02565	0.01084	0.00076	0.01345	0.02171	0.02111	0.00347	0.00969	0.00000
V_2O_5	0.01278	0.03714	0.00798	0.01315	0.02389	0.00021	0.03516	0.03919	0.00797	0.00971
ZnO	0.00039	0.00924	0.04906	0.00580	0.01946	0.03722	0.02609	0.00826	0.03654	0.02994
ZrO_2	0.01902	0.00497	0.02698	0.00255	0.00435	0.01169	0.01715	0.05157	0.01235	0.02994
Cl	0.00776	0.00773	0.00627	0.00744	0.00491	0.00693	0.00733	0.00728	0.00400	0.00641
Cr_2O_3	0.00594	0.00591	0.00480	0.00569	0.00376	0.00530	0.00561	0.00557	0.00306	0.00521
F	0.00168	0.00167	0.00135	0.00160	0.00106	0.00149	0.00158	0.00157	0.00086	0.00000
P_2O_5	0.00300	0.00298	0.00242	0.00287	0.00190	0.00268	0.00283	0.00281	0.00155	0.00000
SO_3	0.01044	0.01039	0.00843	0.01000	0.00660	0.00931	0.00986	0.00979	0.00538	0.00830
Sum	1.00000	1.00000	1.00000	1.00000	1.00000	1.00000	1.00000	1.00000	1.00000	1.00000

2.1.5 Predicted Properties

Predicted properties were calculated using the target composition and a set of models listed in Table 2.6.

Table 2.6. List of models used to calculate predicted properties.

Property	Model	Ref
Viscosity	(a) 21-Term reduced partial quadratic mixture model on the natural logarithm of viscosity at 1150 °C for LAW glasses	(a)
	(b) AM PQM viscosity-temperature-composition models	(a)
EC	13-Term reduced partial quadratic mixture model on the natural logarithm of electrical conductivity at 1150 °C for LAW glasses	(a)
Sulfur Solubility	11-Term reduced partial quadratic mixture model on melter SO_3 tolerance at 1150 ºC for LAW glasses with offset	(a)
K3-Corrosion	13-Term reduced partial quadratic mixture model on the natural logarithm of K-3 corrosion at 1208 °C for LAW glasses	(a)
VHT	19-Component logistic partial quadratic mixture model on the Pass/Fail VHT response on LAW glasses using a threshold for classification of 0.19	(a)
NL_B	22-Term bias corrected partial quadratic mixture model on the natural logarithm of normalized PCT boron loss from LAW glasses	(a)
NL_{Na}	22-Term bias corrected partial quadratic mixture model on the natural logarithm of normalized PCT sodium loss from LAW glasses	(a)
Density	Partial-specific volume model for density	(b)
	Combined partial molar volume model for density	(c)
Nepheline	Location above the line separating the nepheline forming glasses in sub-mixture space	(d)

(a) Vienna et al. 2022, (b) Vienna et al. 2009, (c) Vienna et al. 2002, (d) Lu et al. 2021

2.2 Glass Fabrication and Characterization

This section describes the fabrication method of the LAWHNK glasses and their characterization methods.

2.2.1 Glass Fabrication

The LAWHNK glasses were batched using chemicals composed of single-metal oxides, single-metal carbonates, sodium salts, and boric acid in the appropriate masses to form the target composition for each glass. For each glass, a ~2 kg batch was prepared. Laboratory crucible-scale fabrication of glasses is not intended to mimic the actual melter process or feed processability; rather, it is intended to fabricate a glass sample with a controlled composition for property testing.

The batched powders were thoroughly hand mixed in a plastic bag until a uniform color developed and then milled for 4 min in a vibratory mill (Angstrom TE110). The batched powders were melted using Deltech furnaces. Based on the quality of glass after melting, each glass was melted 2 or more times.

For the Deltech furnace, the powders were placed in a clean platinum (Pt)-10% rhodium (Rh) (Pt-alloy) crucible for melting. Initial melting was performed at 1150 ± 10 °C for 1 h ± 10 min. After the first melt was air quenched on a stainless-steel pouring plate, the glass was observed under an optical microscope, and the presence of undissolved particles and/or salts was reported. The quenched glass was then

separated into aliquots that would fit into a 500-g tungsten carbide (WC) vibratory mill (AngstromTE110) and ground to a fine powder for 5 min. If any glass pieces were still present after 5 min, the sample was ground for an additional 1 min and then hand mixed. A second melt was performed at 1150 °C for 1 h ± 10 min, except for glass LAWHNK-01, which was melted at 1200 °C ± 10 °C for 1 h ± 10 min to determine if an increase in melting temperature would help reduce the amount of undissolved particles observed after the first melt. The results were insufficient to justify risking loss of volatile components; thus, the remainder of the glasses were remelted at 1150 ± 10 °C, except for two glasses: LAWHNK-08 and LAWHNK-09. These glasses were melted a third time at 1200 ± 10 °C and 1150 ± 10 °C, respectively, to aid the absorption of sulfate salt into the melt.

Some glasses showed the presence of yellow salt phases on the surfaces (see images in Appendix A). The seven glasses with large amounts of salt phases (LAWHNK-03, LAWHNK-04, LAWHNK-05, LAWHNK-09, LAWHNK-11, LAWHNK-14, and LAWHNK-16) were washed with Type 1 deionized water (DIW). For washing the glasses, ~2 kg of glass was placed into a 2-L polytetrafluoroethylene (PTFE) vessel, and DIW (~ 55% of glass mass) was added to the vessel. The sealed vessel was shaken for 1-2 min by hand and then placed on a tumbler for 10 min. The glass was removed from the vessel and placed in a 1-L glass beaker, put into an oven, and dried at 90 °C overnight. A sample of all the LAWHNK glasses were ground to a fine powder, and the powders were analyzed by inductively coupled plasma-optical emission spectroscopy (ICP-OES) analysis to validate the chemical composition.

These results are discussed in Section 3.1.

2.2.2 Secondary Phase Investigation

X-ray diffraction (XRD) analysis was performed on all the quenched glasses to identify and quantify the crystalline phases within the glasses. Powdered glass samples were prepared for XRD using ~5 mass% CeO_2 as an internal standard phase with between 1 and 2 g of powdered glass. A glass piece representative of the whole sample was milled alone for 1 min and then homogenized with the CeO_2 for 30 s in a 10-cm^3 WC disc mill. The homogenized samples were loaded into plastic holders and analyzed using a Bruker D8 Advance XRD (Bruker AXS Inc., Madison, Wisconsin) with Cu Kα emission. Samples were scanned at a 0.015° 2θ step size with 1.5-s dwell time from 5° to 75° 2θ scan range. XRD spectra were analyzed with DIFFRAC.EVA (Bruker Corporation, Billerica, Massachusetts) for phase identification. Full-pattern Rietveld refinement using TOPAS 5 Software (Bruker AXS Inc., Madison) was performed to quantify the fraction of each crystal phase present. Comparing the quantified fraction by Rietveld refinement to the quantity of the crystalline internal standard used allowed quantification of the crystalline phases and amorphous phase in the sample. The percentage of crystals measured by XRD was finally corrected by the standard crystallinity of the CeO_2 of 51.28%.

These results are discussed in Section 3.1.1.

2.3 Container Centerline Cooling

A portion (~150 g) of each test glass was subjected to the simulated CCC temperature profile shown in Table 2.7 and Figure 2.2. This profile is the CCC schedule for Hanford LAW glasses produced at the WTP [(1)] and modified by PNNL to include a 30-min soak at the glass melt temperature before the cooling begins. The LAW container cooling schedule was chosen over the HLW canister cooling schedule because it is slower and therefore more conservative. Pieces of quenched glass, < 3 cm in diameter, were placed in a Pt-alloy crucible and covered with a Pt-alloy lid. The glass samples were placed in a furnace

[1] Memorandum, Low Activity Container Centerline Cooling Data, CCN: 074181, RPP-WTP, October 16, 2003.

preheated to the glass melting temperature. After 30 min at 1150°C, the temperature was quickly decreased to 1114 °C and the cooling profile started. Temperature progressed down to about 600 °C based on the cooling segments shown in Table 2.7 and Figure 2.2.

Table 2.7. Container centerline cooling profile for the LAW samples.

Segment	Start Temp (°C)	Stop Temp (°C)	Rate (°C/min)
1[(a)]	T_M[(a)]	T_M[(a)]	0.000[(a)]
2	T_M	1114	-7.125
3	1114	1000	-1.754
4	1000	900	-0.615
5	900	825	-0.312
6	825	775	-0.175
7	775	725	-0.130
8	725	600	-0.095
9	600	Room temp	NA

(a) 30 min at the melting temperature

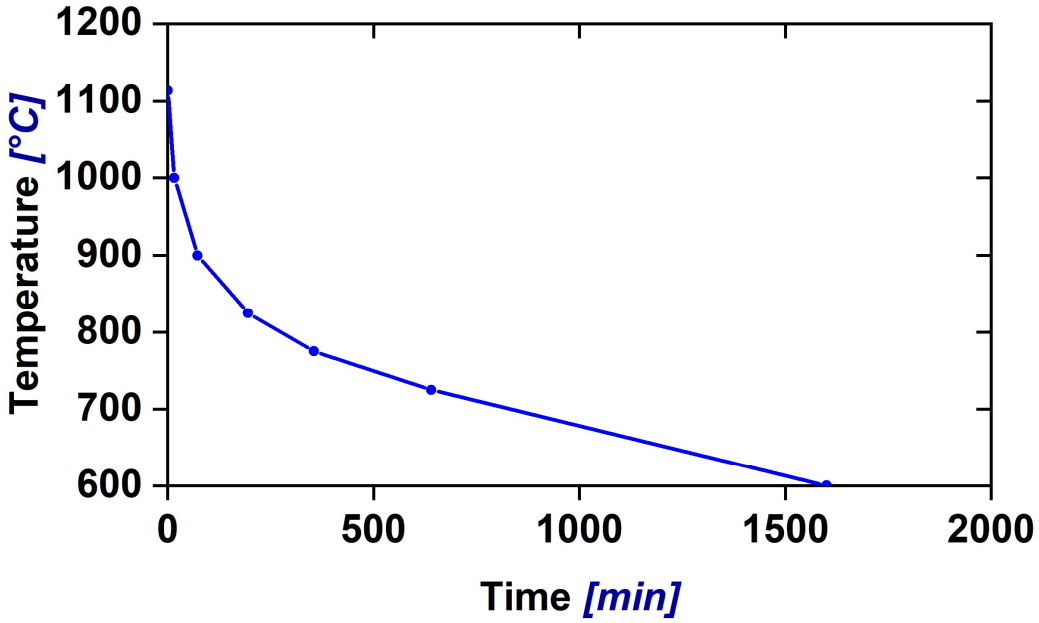


Figure 2.2. Plot of target temperature schedule during LAW CCC treatment.

The amounts and types of crystalline phases that formed during CCC were determined by XRD according to Section 2.2.2. Results are discussed in Section 3.2.

2.4 Isothermal Crystal Fraction

Prior to measuring the CF, the furnace temperature accuracy was verified using standard glass ARG-1 (Smith 1993). Data measured and captured for the standard glass check is stored in project records as a data package.

The CF heat-treatments were completed on each glass composition by selecting pieces of glass between 4 mm and 425 µm, washing with DIW (three times) in a sonic bath, then performing a final wash with clean ethanol and drying in air for at least 12 h or by using an appropriate explosion-proof drying oven at 90 °C

for at least 2 h. These pieces were then loaded into a Pt-alloy crucible of roughly 1 cm^3 prepared following procedure ASTM C1720. The crucible was first held for 30 min at the melt temperature (T_M) prior to moving into a second furnace preheated to the desired measurement temperature of either 1050 °C for 24 h, 950 °C for 24 h, or 850 °C for 48 h. The Pt-alloy crucibles were removed from the furnace and placed on a ceramic brick to cool after the designated time. Due to the small sample size, water quenching was unnecessary to prevent crystal formation from cooling. The crystals that formed during heat-treatment were determined using XRD according to Section 2.2.2 and the CF results are discussed in Section 3.3.

2.5 Density

Density of each glass was measured at room temperature using a MicroMeritics AccuPyc II 1340 gas pycnometer (MicroMeritics, Norcross, Georgia). Approximately 1 g of glass pieces were loaded into a sample holder and placed within the instrument. The pycnometer was purged 10 times with He gas prior to volume measurement, and the volume of each glass was measured 10 times. The average of 10 volume measurements and the measured mass of the sample were used to calculate the glass density. The pycnometer calibration was verified before and after measurements for that day using a National Institute of Standards and Technology traceable standard tungsten carbide ball.

These results are discussed in Section 3.4.

2.6 SO_3 Solubility

The SO_3 solubility (w_{SO3}^{cruc}) was determined using the three-time saturation melt method (3TS) developed by Jin et al. (2019), with minor modifications introduced in this study. Approximately 60 g of the quenched LAWHNK glasses were ground into fine particles using a WC chamber in the Angstrom mill, with a milling time of ~3 min. For each sample, 3.84 g of Na_2SO_4 (Fisher Chemical) was added to 50.00 g of the crushed quenched glass fraction and mixed in the WC mill for 30 s to ensure homogeneity. The resulting glass-Na_2SO_4 blend was melted in a Pt-alloy crucible at 1150 ± 10 °C for 1 h ± 10 min. After 1 h, the melt was quenched on a stainless-steel plate, producing a glass phase alongside a separated sulfate salt. After cooling, the glass and the salt phase, were re-ground together to fine particles and remelted at 1150 ± 10 °C for another hour.

This melting and quenching cycle was repeated three times to produce sulfur-saturated melt (SSM) glasses. The final SSM glass was crushed incrementally in the WC mill for ~1.2 s and sieved to obtain a 106- to 180-µm fraction using a Ro-Tap shaker (RX-29 model, W.C. Tyler) for 6 min for each session. Approximately 5 to 10 sessions were required to crush and sieve the SSM glass fraction, resulting in > 15 g of the 106- to 180-µm fraction available for the washing steps. Two grams of SSM 106-180-µm fraction glass was combined with 20 g of DIW in a centrifuge tube fitted with a 0.45-µm nylon filter. The tube was sealed and manually shaken for approximately 2 min to ensure full contact between the glass particles and the water. The tube was then centrifuged at 3175 rpm for 5 min in a centrifuge (Sorvall Legend Mach 1.6 model, Thermo Electron Corporation). After centrifuging, the filter containing the rinsed glass powder was removed, and the supernatant (rinse solution) was poured off and saved for possible future analysis. The washing step was repeated twice before the filter containing the glass powder was dried overnight in an oven at 80 °C. Once dry, the glass powder was carefully separated from the filter and prepared for ICP-OES and ion chromatography (IC) analysis.

These results are discussed in Section 3.5.

2.7 Viscosity

The viscosity of each glass was measured as a function of temperature using the viscosity dependance to the shear stress and shear rate [Eq. (2.3)]:

$$\eta = \frac{\tau}{\gamma} \tag{2.3}$$

where η is the viscosity, γ is the shear rate, and τ is the shear stress.

A rotating spindle digital viscometer capable of measuring viscosities from 1 to 400 Pa·s (Brookfield Digital Model LVTD) was staged above a high-temperature Deltech furnace (Model DT-31-RS, Denver, Colorado) equipped with a Pt-alloy spindle fit through a hole in the top of the furnace. A 50-mL glass sample was added to a 100-mL Pt-alloy crucible with approximate dimensions of 5 cm diameter × 6 cm height. The crucible was placed into the furnace, which was set at 1150 °C, and the glass was left to melt for about 20 min. The spindle was then lowered into the molten glass in the center of the crucible with the lower end of the rod suspended 5 mm above the bottom of the crucible. The furnace was programmed to follow a set ramp schedule at the following temperatures: 1150 °C, 1050 °C, 950 °C, 1150 °C, 1200 °C, and back to 1150 °C. The soak time was 45 min at each temperature. This temperature profile allowed for the potential impacts of crystallization (at lower temperatures) and volatility (at higher temperatures) to be assessed (via reproducibility) at the repeated 1150 °C temperature. The viscometer was calibrated using the Defense Waste Processing Facility startup frit (Crum et al. 2012). At each target temperature, the maximum and minimum spindle torque values were recorded three times each in 3-min intervals. The average of the three measurements was used for data analysis. A secondary thermocouple was placed below the crucible and temperature was recorded continuously during measurement to ensure thermal equilibrium was reached before measurement. Results are discussed in Section 3.6.

2.8 Electrical Conductivity

The EC (ε in S/m) as a function of temperature was calculated from the resistance (R' in Ω) and cell constant (K in m^{-1}) by:

$$\varepsilon = K/R_s \tag{2.4}$$

where R_s is the solution resistance obtained for the KCl calibration solutions and K is the cell constant and is linked to the geometry of the system.

Approximately 18 g of quenched glass was added to an alumina crucible with the two-blade Pt-alloy probes attached perpendicular to one another ~20 mm apart, and the assembly was loaded into the furnace at room temperature. The furnace was then slowly (~10 °C/min) ramped to 900 °C to prevent thermal shock to the crucibles and was successively fast ramped to 1200 °C to complete glass melting. The furnace was then held (~30 min) at 1200 °C to homogenize the glass before taking the first measurement. Each change in temperature was performed at a slow rate (~10 °C/min) and the glass was allowed to equilibrate at each temperature for ~30 min before the corresponding measurement was taken.

A Biologic VSP-3E potentiostat connected to a two-blade Pt-alloy probe staged above a high-temperature Sentrotech furnace (Model ST-1200-7812, Strongsville, Ohio) was used to measure the molten glass impedance. Data was recorded at 1200, 1150, 1050, and 950 °C after roughly 30-min soaks at each temperature, allowing the program to collect impedance data at an applied voltage of 100 mV, frequencies of 0.5 to $5x10^5$ Hz, measuring 25 data points per decade, and repeating the scan three times for a total of four measurements per glass per temperature.

Solution resistance (R_s) was calculated by fitting the impedance spectra (i.e., Nyquist plots). A cell constant was determined using 0.1 M and 1.0 M KCl solutions measured at the same volume in the same alumina crucible and Pt-alloy probe apparatus. The conductivity was then calculated from Eq. (2.6).

These results are discussed in Section 3.7.

2.9 Product Consistency Test

The PCT responses were measured for quenched (Q) and CCC samples of each glass using Method A of ASTM C1285, *Standard Test Methods for Determining Chemical Durability of Nuclear, Hazardous, and Mixed Waste Glasses and Multiphase Glass Ceramics: The Product Consistency Test (PCT)*. Tests were performed in triplicate for each Q and CCC glass. Alongside each triplicate of the measured composition, the Approved Reference Material-1 (ARM-1, Mellinger and Daniel 1984) glass was also tested in triplicate. Two blanks, which consisted of DIW in a cleaned vessel without glass, were added with each set of tests. Glasses were ground, sieved to -100 +200 mesh, washed, and prepared according to Section 19.6 of ASTM C1285. Then 1.5 g of the prepared glass was added to 15 mL of DIW in a Type 304L Parr stainless steel vessel with a PTFE gasket. The vessels were closed, sealed, and placed into an oven at 90 ± 2 °C for 7 days ± 3 h.

After 7 days, the vessels were removed from the oven and allowed to cool to the touch. The final mass of the vessel and the solution pH were recorded. The leachate from each test vessel was then filtered through a 0.45-µm-size filter and acidified with concentrated, high-purity HNO_3 to 1 vol% before analysis. The leachates were analyzed using ICP-OES for Si, Na, Li, and B.

The normalized elemental mass loss (NL, g m^{-2}) was calculated with the following formula:

$$\mathrm{NL}_i = \frac{C_i}{f_i(SA/V)} \tag{2.5}$$

where:

C_i = the concentration of element i in solution ($g_i \cdot L^{-1}$)
f_i = mass fraction of element i in the glass ($g_i \cdot glass^{-1}$)
SA/V = surface area divided by the leachate volume ($m^2\ L^{-1}$)

An assumed SA/V of 2.0 $m^2\ L^{-1}$ was used based on a geometric estimate of SA with a glass density of ~2.68 g cm^3 (Lonergan et al. 2020). See Section X1.2 in ASTM C1285 for a description of the calculation of a specific surface of a -100 +200 mesh glass particle with a given density.

These results are discussed in Section 3.8.

2.10 Vapor Hydration Test

Monolithic glass samples were exposed to water vapor at 200 °C in sealed stainless-steel vessels according to the ASTM International standard procedure *Standard Test Method for Measuring Waste Glass or Glass Ceramic Durability by Vapor Hydration Test* (ASTM C1663). Roughly 1.5 mm × 10.3 mm × 10.3 mm samples were cut from annealed Q or CCC-treated LAW glass bars using a diamond-impregnated saw. All sides of the cut sample were polished to 600-grit surface finishes with silicon carbide paper.

Polished samples were hung from stainless-steel supports with Pt wire within a stainless-steel container. DIW was added to the bottom of the vessel so that enough water was present to react with the specimen,

but without enough water to reflux during testing (~0.20 g). The samples were heated and held at 200 °C ± 2 °C in a convection oven for 24 days. Samples found to have fully reacted in 24 days were then tested for 7 days to enable estimation of a numerical alteration rate.

After removal from the oven, vessels were weighed and then quenched in cold water. The post-VHT monoliths were removed from the vessels, air-dried, mounted in epoxy, cross-sectioned, and polished to 600-grit for optical microscopy-image analysis to determine the amount of remaining unaltered glass after the VHT. The solution pH in the vessel was measured and noted. No action was taken based on the resulting pH as the cause of high pH values (> 10) could not be resolved. Possible reasons for high pH values include solution reflux during the VHT, solution dripping off the monolith while moving vessels during termination, and portions of altered products falling into solution.

The remaining glass thicknesses of the monoliths were determined on the cross section of the sample mounted in epoxy and polished down to 600-grit surface finish on both sides. Ten measurements were performed fairly equally distributed across the cross section of the sample. The amount of glass altered per unit surface area of specimen (m_a, g·mm^{-2}) was determined from the average thickness of remaining glass according to Eq. (2.6) (from ASTM C1663-21, Equation 6):

$$m_a = \frac{m_i}{2 \cdot w_i \cdot l_i} \cdot \left(1 - \frac{d_r}{d_i}\right) \tag{2.6}$$

where:

m_i = initial glass monolith mass (g); treated as a constant for error propagation as only one mass measurement was made
w_i = average initial glass monolith width (mm)
l_i = average initial glass monolith length (mm)
d_i = average initial thickness of the glass monolith (mm)
d_r = average thickness of remaining glass (mm)

When the VHT corrosion rate (r_{VHT}), defined as m_a divided by test duration in days, is < 50 g m^{-2} d^{-1} for a given glass, it satisfies the current DOE requirement for LAW glass response. Although the contract limit for VHT response is provided as a rate (50 g m^{-2} d^{-1}), the test directly measures alteration depth (D) in µm at different times. In previous studies (Piepel et al. 2007; Muller et al. 2014), the directly measured parameter of D in µm after 24 days was modeled. This value can be converted to a rate by D (µm) ×10^{-6} (m/µm) × density (g/cm^3) ×10^6 (cm^3/m^3) /t(d). Assuming a density of 2.65 g·cm^{-3}, the limit of 50 g·m^{-2}·d^{-1} is equivalent to a D of 453 µm for a 24-day test duration. In the present study, the density was assumed to be 2.65 g·cm^{-3}.

These results are discussed in Section 3.9.

3.0 Results and Discussion

This section describes the results for the chemical composition, CCC, CF,liquidus temperature (T_L), sulfur solubility, density, viscosity, EC, PCT, and VHT.

3.1 Glass Composition

Optical images of the quenched LAWHNK glasses after the final melt are shown in Appendix A. Appendix B provides the target and ICP-OES measured compositions, except for F and Cl, in wt%. The ICP-OES results showed that the sums of measured oxides and adding target masses of F and Cl were between 93.1 and 98.8 wt%, indicating acceptable recovery of the glass components since the noted difference falls within the experimental error and analytical uncertainties ranges. For all further calculations, the target values for all components but SO_3 were used. For SO_3 measured values were substituted to target and compositions were renormalized.

The ICP-OES results showed that the relative precent difference (RPD) was below 10% except for the following:

1. Al_2O_3 in three glasses, LAWHNK-02, LAWHNK-07, and LAWHNK-10 (RPDs of -12.77%, -13.09 %, and -16.98 %)
2. B_2O_3 in one glass, LAWHNK-01 (RPD of -17.38 %)
3. SnO_2 in two glasses, LAWHNK-02 and LAWHNK-04 (RPDs of -31.03% and -16.44%)
4. SO_3 in three glasses, LAWHNK-01, LAWHNK-05, and LAWHNK-11 (RPDs of -10.94% -10.28%, and -13.70%)
5. SiO_2 in one glass, LAWHNK-07 (RPD of 10.05%)

The differences between target and measured Al_2O_3, and SiO_2, were close enough to an RPD value of 10% to be considered within experimental error. Due to higher analytical uncertainties for B, B_2O_3 content < 20% is considered within experimental error. Low measured SO_3 in double crucible melts is expected due to S evaporation. The two SnO_2 quantities below target were most likely due to sequestration of Sn into crystals (see Section 3.1.1).

3.1.1 Secondary Phase Investigation in Quenched Glasses

The crystalline phases identified in the Q samples and their wt% values are provided in Table 3.1. The refined XRD plots with quantified crystalline fractions are shown in Appendix C. The normalized wt% was calculated using Eq. (3.1), where *P* is the phase wt%, *C* is the standard crystallinity of 51.28 wt% for the internal standard, and *S* is the added standard wt%:

$$\text{Normalized wt\% of a Phase} = \frac{PC}{100 - S} \tag{3.1}$$

Seven glasses out of 20 were fully amorphous. Overall, 12 glasses had a total crystalline fraction of < 1 wt%. The most frequent crystalline phase identified by XRD was spinel. Three different spinel phases

with < 1 wt% were observed and used for refinement: $ZnFe_{1.9}Cr_{0.1}O_4$, $ZnFe_2O_4$, and $ZnCr_{1.8}Al_{0.2}O_4$. With small amounts of spinel phases in the glasses, only two small peaks of diffraction from (h k l) planes of (2 2 0) and (3 1 1) were present in the XRD patterns. Glass LAWHNK-03 contained a high amount of sodium aluminosilicate ($Na_{1.55}Al_{1.55}Si_{0.45}O_4$), which had a different space group compared to a nepheline phase. The wt% of $Na_{1.55}Al_{1.55}Si_{0.45}O_4$ from XRD analysis was 41.48, but this wt% was not possible with the glass given target composition. This indicated that the chemistry of the phase must be different, although the structure of the phase satisfies the XRD fitting of peaks. However, no alternative phase was available in Powder Diffraction Database, and this phase in LAWHNK-03 might be a new phase that is isostructural to $Na_{1.55}Al_{1.55}Si_{0.45}O_4$ but with a different chemistry. LAWHNK-03 had the highest target wt% of ZrO_2 (4.94 wt%) and was the only glass with ZrO_2 phase in the XRD pattern. SnO_2 was observed in glasses with high target masses of SnO_2 (3.7 to 4.94 wt%): LAWHNK-02, LAWHNK-04, LAWHNK-05, and LAWHNK-06.

Table 3.1. Crystalline phases and wt% in as fabricated LAWHNK glasses.

Glass ID	$Na_{1.55}(Al_{1.55}Si_{0.45}O_4)$	$ZnFe_{1.9}Cr_{0.1}O_4$	$ZnCr_{1.8}Al_{0.2}O_4$	ZrO_2	$ZnFe_2O_4$	SnO_2
LAWHNK-01	x	x	0.39	x	x	x
LAWHNK-02	x	0.29	x	x	x	0.66
LAWHNK-03	41.48	x	x	1.02	x	x
LAWHNK-04	x	0.35	x	x	x	0.26
LAWHNK-05	x	x	x	x	x	0.05
LAWHNK-06	x	x	x	x	x	0.12
LAWHNK-07	x	0.20	x	x	x	x
LAWHNK-08	x	x	x	x	x	x
LAWHNK-09	x	x	x	x	x	x
LAWHNK-10	x	0.10	x	x	x	x
LAWHNK-11	x	x	x	x	x	x
LAWHNK-12	x	0.19	x	x	x	x
LAWHNK-13	x	0.16	x	x	x	x
LAWHNK-14	x	0.14	x	x	x	x
LAWHNK-15	x	x	x	x	x	x
LAWHNK-16	x	x	x	x	0.51	x
LAWHNK-17	x	0.09	x	x	x	x
LAWHNK-18	x	x	x	x	x	x
LAWHNK-19	x	x	x	x	x	x
LAWHNK-20	x	x	x	x	x	x

3.2 Crystal Identification in Container Centerline Cooling Glasses

This section presents and discusses the CF results from CCC-treated glasses. Details on the methods are discussed in Section 2.3 and the effects of CCC on PCT and VHT are reported in Sections 3.8 and 3.9, respectively. Pictures of the CCC glasses are presented in Appendix D.

The CCC treatment simulates the slow cooling profile of the molten glass inside the LAW glass container core. Crystal formation during the slow cooling might impact glass durability by altering the residual glass composition, depending on the type of crystals formed (Kim et al. 1995; Kroll et al. 2019). Two primary crystalline phases have been recognized as exerting a significant adverse impact on glass durability (PCT and VHT): Na-Al silicate and Na-Ca (including Na-Ca-Al) silicate groups. CCC

crystallization constraints have been developed to prevent formation of Na-Al and Na-Ca silicates, respectively (Lonergan et al. 2021):

$$g_{Al_2O_3} \leq 0.158 - 0.28\,(g_{Na_2O} + 0.66 g_{K_2O}) \quad (3.2)$$

$$g_{CaO} \leq 0.2084 - 0.528\,(g_{Na_2O} + 0.66 g_{K_2O}) \quad (3.3)$$

Of the 20 glasses, only eight met both CCC crystallization constraints as shown in Table 3.2. Of these, only five did not form Na-Al and Na-Ca silicates after CCC heat-treatment, as shown in Table 3.2.

Table 3.2. LAWHNK glasses that met the CCC crystal constraints.

Glass ID	Al_2O_3 CCC Crystal Constraints Met?	Formed Na-Al Crystals?	CaO CCC Crystal Constraints Met?	Formed Na-Ca Crystals?	P, NP Model by Lu et al. 2021	NP Formed (wt%)
LAWHNK-01	No	Yes	No	No	-0.038	28.2
LAWHNK-02	No	Yes	Condition met	No	-0.027	23.7
LAWHNK-03	No	Yes	Condition met	No	-0.054	64.6[(a)]
LAWHNK-04	No	Yes	Condition met	No	-0.034	58.7[(a)]
LAWHNK-05	Condition met	No	Condition met	No	0.033	0.0
LAWHNK-06	No	Yes	Condition met	No	-0.023	14.8
LAWHNK-07	No	Yes	Condition met	No	-0.056	27.2
LAWHNK-08	No	Yes	Condition met	No	-0.017	79.2[(a)]
LAWHNK-09	No	Yes	No	No	-0.023	81.6[(a)]
LAWHNK-10	No	No	Condition met	No	0.003	0.0
LAWHNK-11	Condition met	No	Condition met	No	0.066	0.0
LAWHNK-12	Condition met	No	Condition met	No	0.029	0.0
LAWHNK-13	**Condition met**	**Yes**	Condition met	No	**0.025**	**8.4**
LAWHNK-14	**Condition met**	**Yes**	Condition met	No	0.026	0.0
LAWHNK-15	Condition met	No	Condition met	No	0.056	0.0
LAWHNK-16	No	Yes	Condition met	No	-0.003	10.3
LAWHNK-17	**Condition met**	**Yes**	Condition met	No	0.001	0.0
LAWHNK-18	Condition met	No	Condition met	No	0.037	0.0
LAWHNK-19	No	No	Condition met	No	0.012	0.0
LAWHNK-20	No	Yes	Condition met	No	**0.008**	**4.9**

(a) Crystal fraction may be overestimated due to the small fraction (5 wt%) of internal standard added for XRD quantification compared to the crystalline phase present in the sample.

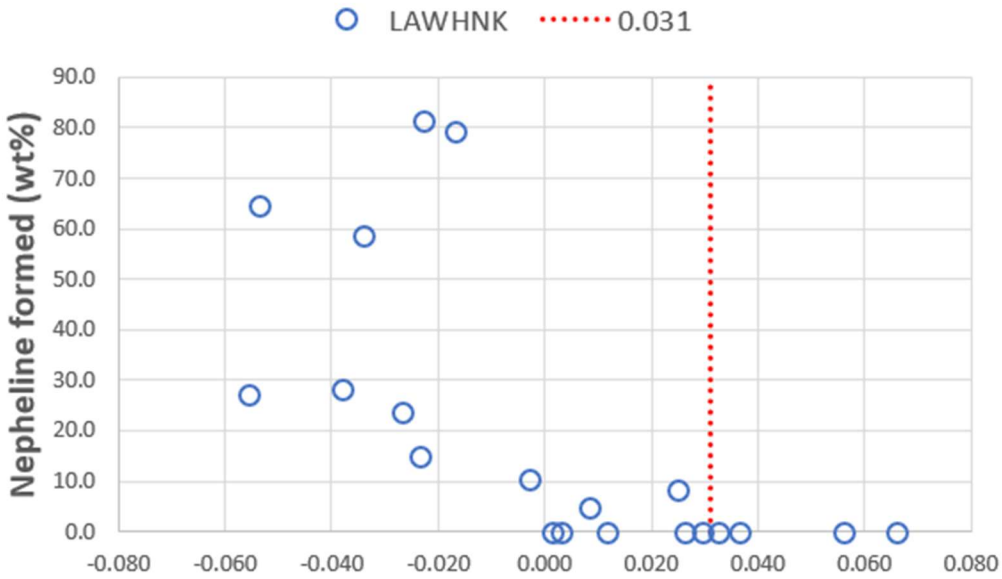


Figure 3.1. Predicted nepheline formation (P) using the model by Lu et al. (2021) vs. nepheline formed (wt%) including Na-Al-Si phases.

The three remaining glasses that met both CCC crystallization constraints developed a variety of Na–Al silicate crystals even though both constraints were met (see Table 3.2 for details). The rest of the glasses formed one or more types of crystals. A detailed list of identified crystals is presented in Table 3.3. Most of the glasses that formed SnO_2 (LAWHNK-02, LAWHNK-04, LAWHNK-05, LAWHNK-06, LAWHNK-08, LAWHNK-13, and LAWHNK-17) had high SnO_2 target quantities (≥ 3.69 wt%) compared to the other glasses. However, there was no observed correlation between ZnO concentration and formation of Zn-containing crystals. Overall, the diverse distribution of crystalline phases formed underscores the distinct crystallization behavior across the compositional range of the glass matrix, but there were certain dominating phases formed like sodium aluminum silicate ($Na_{1.55}Al_{1.55}Si_{0.45}O_4$) during the CCC treatment.

Table 3.3. Crystal phase and mass fraction observed by XRD in CCC glasses.

Glass ID	Crystalline Phase	Chemical Formula	wt%
LAWHNK-01	Nepheline	$NaAlSiO_4$	5.96
	Sodium Aluminum Silicate	$Na_{1.55}Al_{1.55}Si_{0.45}O_4$	22.22
	Franklinite	$ZnFe_{1.9}Cr_{0.1}O_4$	0.53
	Nosean	$Na_8(Al_6Si_6O_{24})(SO_4)$	11.5
	Sodalite	$Na_8Al_6(SiO_4)_6S_{0.1}Cl_{1.9}$	2.45
LAWHNK-02	Nepheline	$NaAlSiO_4$	23.66
	Tin Oxide	SnO_2	1.86
LAWHNK-03	Nepheline	$NaAlSiO_4$	16.85
	Sodium Aluminum Silicate	$Na_{1.55}Al_{1.55}Si_{0.45}O_4$	47.77
	Nosean	$Na_8(Al_6Si_6O_{24})(SO_4)$	2.46
	Potassium Iron Silicon Oxide	$K_{0.97}Fe_{0.97}Si_{1.03}O_4$	0.59
LAWHNK-04	Sodium Aluminum Silicate	$Na_{1.55}Al_{1.55}Si_{0.45}O_4$	58.7
	Nosean	$Na_8(Al_6Si_6O_{24})(SO_4)$	8.78
	Sodalite	$Na_8Al_6(SiO_4)_6S_{0.1}Cl_{1.9}$	3.63
	Tin Oxide	SnO_2	1.7
	Potassium Aluminum Silicon Oxide	$K_{9.6}Al_{9.6}Si_{38.4}O_{96}$	2.55
	Calcium Iron Oxide	$CaFeO_3$	3.08
LAWHNK-05	Franklinite	$ZnFe_{1.9}Cr_{0.1}O_4$	1.86
	Tin Oxide	SnO_2	0.5
LAWHNK-06	Nepheline	$NaAlSiO_4$	14.83
	Nosean	$Na_8(Al_6Si_6O_{24})(SO_4)$	3.17
	Sodalite	$Na_8Al_6(SiO_4)_6S_{0.1}Cl_{1.9}$	1.32
	Tin Oxide	SnO_2	1.14
LAWHNK-07	Nepheline	$NaAlSiO_4$	27.15
	Franklinite	$ZnFe_{1.9}Cr_{0.1}O_4$	0.82
LAWHNK-08	Sodium Aluminum Silicate	$Na_{1.55}Al_{1.55}Si_{0.45}O_4$	79.18
	Tin Oxide	SnO_2	0.78
	Potassium Aluminum Silicon Oxide	$K_{9.6}Al_{9.6}Si_{38.4}O_{96}$	2.75
	Calcium Iron Oxide	$CaFeO_3$	3.34
LAWHNK-09	Sodium Aluminum Silicate	$Na_{1.55}Al_{1.55}Si_{0.45}O_4$	81.59
	Calcium Olivine	Ca_2SiO_4	3.29
LAWHNK-10	Franklinite	$ZnFe_{1.9}Cr_{0.1}O_4$	0.27
LAWHNK-11	None		
LAWHNK-12	Franklinite	$ZnFe_{1.9}Cr_{0.1}O_4$	0.52
LAWHNK-13	Franklinite	$ZnFe_{1.9}Cr_{0.1}O_4$	0.23
	Tin Oxide	SnO_2	0.2
	Sodium Aluminum Silicate	$Na_4Al_2Si_2O_9$	8.38
LAWHNK-14	Franklinite	$ZnFe_{1.9}Cr_{0.1}O_4$	0.35
	Nosean	$Na_8(Al_6Si_6O_{24})(SO_4)$	1.01
	Sodalite	$Na_8Al_6(SiO_4)_6S_{0.1}Cl_{1.9}$	1.25
LAWHNK-15	None		
LAWHNK-16	Sodium Aluminum Silicate	$Na_{1.55}Al_{1.55}Si_{0.45}O_4$	10.35
	Nosean	$Na_8(Al_6Si_6O_{24})(SO_4)$	4.13
	Sodalite	$Na_8Al_6(SiO_4)_6S_{0.1}Cl_{1.9}$	2.57
	Magnetite	Fe_3O_4	5.62
LAWHNK-17	Franklinite	$ZnFe_{1.9}Cr_{0.1}O_4$	0.26
	Nosean	$Na_8(Al_6Si_6O_{24})(SO_4)$	12.53
	Sodalite	$Na_8Al_6(SiO_4)_6S_{0.1}Cl_{1.9}$	3.56
	Magnetite	Fe_3O_4	0.15
	Tin Oxide	SnO_2	0.16
LAWHNK-18	None		
LAWHNK-19	None		
LAWHNK-20	Nepheline	$NaAlSiO_4$	4.9
	Nosean	$Na_8(Al_6Si_6O_{24})(SO_4)$	3.86
	Sodalite	$Na_8Al_6(SiO_4)_6S_{0.1}Cl_{1.9}$	1.31

Two LAWHNK glasses with high crystal content (LAWHNK-01 and LAWHNK-09) after CCC treatment were selected for scanning electron microscopy with energy dispersive X-ray spectroscopy (SEM-EDS) analysis to confirm chemical compositions of the crystalline phases. Backscatter electron (BSE) images were taken to show the morphology of different phases in CCC samples as shown in Figure 3.2 and Figure 3.3. Generally, phases composed of lighter elements (low atomic number) appear darker while phases composed of heavier elements (high atomic number) appear brighter. EDS analysis was performed on multiple (2 to 4) spots on each phase, and the averaged values of atomic percentage of elements are reported in Table 3.4 and Table 3.5.

For the LAWHNK-01 CCC sample, there are two dark phases (phases 1 and 3) with different morphology as shown in Figure 3.2. EDS results show that phase 1 contains the major elements of Na, K, Al, Si, and O with an approximately 1:1:1 ratio of (Na+K):Al:Si. This is consistent with the nepheline ($NaAlSiO_4$) identified by XRD but with partial substitution of Na by K. Phase 3 is also rich in Na, Al, and Si, but the approximate ratio of Na:Al:Si is 1:1.6:2. This phase could be correlated to the sodalite or nosean phase observed by XRD. Phase 2 is rich in Na (17.6%) and Si (28.7%) with a negligible amount of Al (0.6%), while no crystalline phase match can be found from the XRD results. Phase 4 is rich in Mg (9.0%) and Zn (6.8%) with a relatively low concentration of Na (2.1%), Al (2.8%), and Si (7.2%), suggesting it is likely correlated to a spinel phase primarily composed of Mg and Zn.

For the LAWHNK-09 CCC sample, the dark phase 1 was found to be rich in Na, Al, Mg, and Si with an approximate ratio of Na:Mg:Al:Si=1:0.5:1:2. The branch shape indicates this phase could be nepheline. It also contains a noticeable amount of Fe (2.6%). Phase 2 has high concentrations of Na (14.5%), Mg (12.8%), and Si (22.6%) with negligible amount of Al (0.6%). Phase 3 is rich in Na (10.9%) and Si (16.4%), with the minor incorporation of Mg, Al, P, Ca, Ti, and Fe. The chemistry of the three phases in the LAWHNK-09 CCC sample doesn't match the XRD result, which showed $Na_{1.55}Al_{1.55}Si_{0.45}O_4$ and Ca_2SiO_4 as the crystalline phases. It is possible that the crystallization in the CCC samples involves element substitution, while maintaining a similar crystal structure (i.e., K substituting Na in nepheline). The XRD phase identification could be limited by the available candidates in the database, and non-stoichiometric crystals with new chemistry may have formed within the CCC samples.

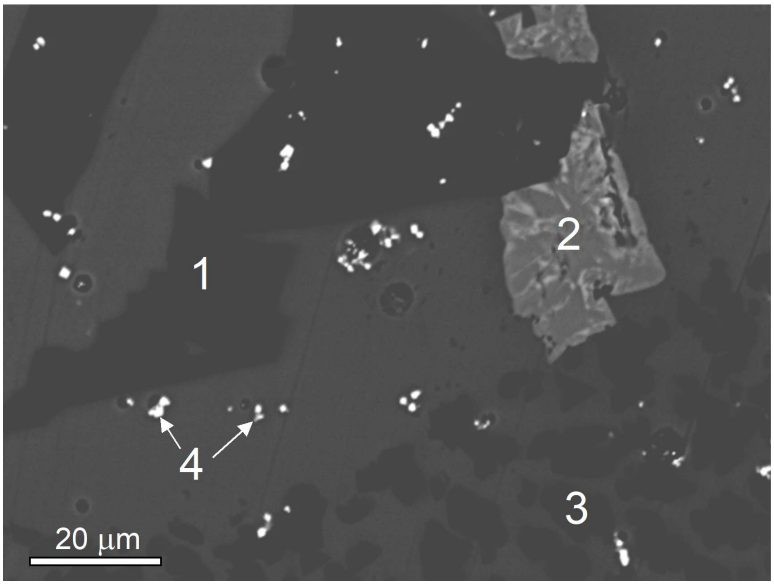


Figure 3.2. BSE image of glass LAWHNK-01 after CCC at 1000×.

Table 3.4. EDS atomic % of detected elements for LAWHNK-01 after CCC.

	O	Na	Mg	Al	Si	P	Cl	K	Ca	Ti	V	Fe	Zn
Phase 1	47.1	13.2	0.5	18.6	18.6	0.3	0.0	1.6	0.0	0.0	0.0	0.0	0.0
Phase 2	47.7	17.6	1.3	0.6	28.7	0.8	0.0	0.0	1.6	0.5	0.0	1.0	0.1
Phase 3	50.1	10.2	2.6	16.3	19.7	0.0	0.0	0.0	0.1	0.1	0.0	0.0	0.7
Phase 4	68.5	2.1	9.0	2.8	7.2	0.5	0.2	0.5	1.9	0.5	0.0	0.0	6.8
Residual Glass	55.7	6.9	6.5	1.8	22.1	0.3	0.7	0.0	2.0	1.9	1.0	0.0	1.1

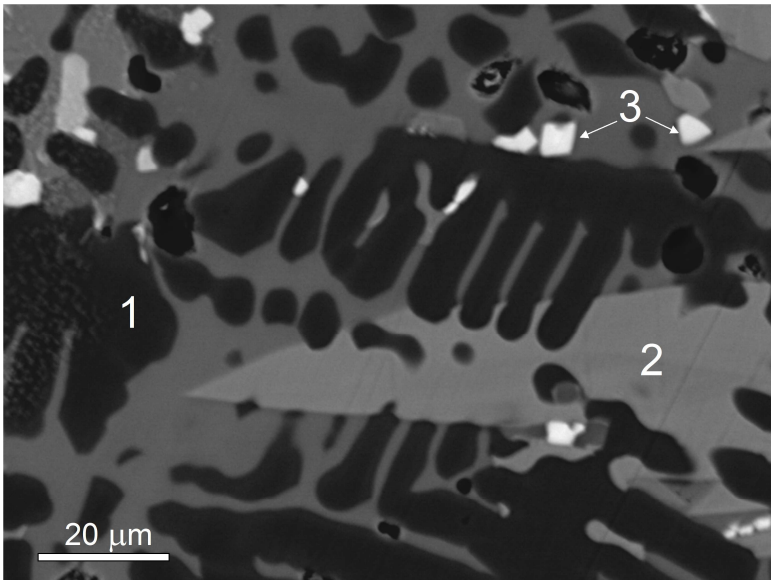


Figure 3.3. BSE image of glass LAWHNK-09 after CCC at 1000×.

Table 3.5. EDS atomic % of detected elements for LAWHNK-09 after CCC.

	O	Na	Mg	Al	Si	P	Cl	K	Ca	Ti	V	Fe	Zn	Zr
Phase 1	51.2	9.2	5.7	10.3	19.3	0.2	0.1	0.3	0.2	0.1	0.1	2.6	0.8	0.0
Phase 2	45.8	14.5	12.8	0.6	22.6	1.4	0.0	0.0	2.1	0.0	0.0	0.0	0.1	0.0
Phase 3	53.9	10.9	3.8	1.9	16.4	2.0	0.0	0.0	2.0	3.7	0.0	4.2	0.2	1.0
Residual Glass	53.1	11.3	6.7	1.5	13.7	0.7	0.4	2.8	1.7	1.2	1.8	4.3	0.4	0.0

3.3 Crystal Fraction in Isothermally Heat-Treated Glasses

Crystal formation may affect the melter operation by clogging the pour spout after settling in the melter (Bunnell 1988) or altering the composition of the residual glass phase and deteriorating the chemical durability of the final waste form (Kim et al. 1995). Generally, crystal formation is favored at lower heat-treatment temperatures; thus, the extended idling periods at temperatures lower than the melter operational temperature might encourage crystal formation. The crucial criteria are to avoid the formation of undesirable crystalline phases below the melting temperature without compromising other glass properties such as chemical durability and EC. To investigate the crystal formation in waste glass, isothermal heat-treatment was conducted to study the crystalline phases that formed and their quantities at various testing temperatures under equilibrium or pseudo-equilibrium conditions. Table 3.6 summarizes

the isothermal test temperatures, identification of crystalline phases, and CF (in wt%) of each phase. Photos and XRD patterns of the 950 °C samples are reported in Appendix E.

A diverse group of crystalline phases was identified across the glass compositions in the matrix (Table 3.6). The commonly observed phases were tin oxide (SnO_2) in nine compositions, franklinite ($ZnFe_{1.9}Cr_{0.1}O_4$) in seven compositions, nosean ($Na_8(Al_6Si_6O_{24})(SO_4)$) in seven compositions, and nepheline ($Na_3KAl_4Si_4O_{16}$) in six compositions. Less common phases were sodium aluminum silicate ($Na_{1.55}Al_{1.55}Si_{0.45}O_4$) in three compositions, sodium zirconium silicate ($Na_4Zr_2(SiO_4)_3$) in two compositions, magnetite (Fe_3O_4) in one composition, calcium aluminum oxide ($Ca_3Al_2O_6$) in one composition, and potassium iron silicon oxide ($K_{0.97}Fe_{0.97}Si_{1.03}O_4$) in one composition.

The high frequency of sodium aluminum silicate phases is not surprising since the glass matrix was designed to push the Na content boundaries. For other common phases, the highest CFs of SnO_2 (2.47 wt%) were observed in glasses with high Sn content, indicating that the Sn solubility limit may have been exceeded. In general, these results highlight the disparity in crystal formation within compositional variation of the glass matrix.

Table 3.6. Identification and crystal fraction in wt% of crystalline phases for isothermally heat-treated glasses.

Glass ID	Temperature (°C)	Crystalline Phase	Chemical Formula	Crystal Fraction (wt%)	Crystal Fraction (vol%)[a]
LAWHNK-01	850	Nepheline	$NaAlSiO_4$	5.54	ND
		Franklinite	$ZnFe_{1.9}Cr_{0.1}O_4$	0.84	ND
		Nosean	$Na_8(Al_6Si_6O_{24})(SO_4)$	11.6	ND
		Calcium Aluminum Oxide	$Ca_3Al_2O_6$	3.13	ND
	950	Franklinite	$ZnFe_{1.9}Cr_{0.1}O_4$	0.54	0.26
		Nosean	$Na_8(Al_6Si_6O_{24})(SO_4)$	7.78	9.21
		Calcium Aluminum Oxide	$Ca_3Al_2O_6$	2.46	2.13
	1050	Nosean	$Na_8(Al_6Si_6O_{24})(SO_4)$	1.51	ND
LAWHNK-02	850	Nepheline	$NaAlSiO_4$	17.23	ND
		Franklinite	$ZnFe_{1.9}Cr_{0.1}O_4$	0.9	ND
		Tin Oxide	SnO_2	2.47	ND
	950	Nepheline	$NaAlSiO_4$	1.91	1.95
		Franklinite	$ZnFe_{1.9}Cr_{0.1}O_4$	0.39	0.19
		Tin Oxide	SnO_2	2.08	0.80
	1050	Tin Oxide	SnO_2	1.69	ND
LAWHNK-03	850	Nepheline	$NaAlSiO_4$	12.86	ND
		Sodium Aluminum Silicate	$Na_{1.55}Al_{1.55}Si_{0.45}O_4$	25.34[b]	ND
		Nosean	$Na_8(Al_6Si_6O_{24})(SO_4)$	4.17	ND
		Potassium Iron Silicon Oxide	$K_{0.97}Fe_{0.97}Si_{1.03}O_4$	0.55	ND
	950	Sodium Aluminum Silicate	$Na_{1.55}Al_{1.55}Si_{0.45}O_4$	36.11[b]	35.83
		Nosean	$Na_8(Al_6Si_6O_{24})(SO_4)$	1.81	2.16
		Potassium Iron Silicon Oxide	$K_{0.97}Fe_{0.97}Si_{1.03}O_4$	0.45	0.41
	1050	Sodium Aluminum Silicate	$Na_{1.55}Al_{1.55}Si_{0.45}O_4$	57.42[b]	ND
		Potassium Iron Silicon Oxide	$K_{0.97}Fe_{0.97}Si_{1.03}O_4$	0.5	ND
LAWHNK-04	850	Nepheline	$NaAlSiO_4$	6.19	ND
		Franklinite	$ZnFe_{1.9}Cr_{0.1}O_4$	0.82	ND
		Nosean	$Na_8(Al_6Si_6O_{24})(SO_4)$	7.7	ND
		Tin Oxide	SnO_2	1.52	ND

Glass ID	Temperature (°C)	Crystalline Phase	Chemical Formula	Crystal Fraction (wt%)	Crystal Fraction (vol%)[a]
		Sodium Zirconium Silicate	$Na_4Zr_2(SiO_4)_3$	3.67	ND
	950	Franklinite	$ZnFe_{1.9}Cr_{0.1}O_4$	0.6	0.29
		Nosean	$Na_8(Al_6Si_6O_{24})(SO_4)$	1.16	1.40
		Tin Oxide	SnO_2	1.65	0.63
		Sodium Zirconium Silicate	$Na_4Zr_2(SiO_4)_3$	0.89	0.69
	1050	Tin Oxide	SnO_2	1.41	ND
LAWHNK-05	850	Tin Oxide	SnO_2	1.14	ND
	950	Tin Oxide	SnO_2	1.08	0.41
	1050	Tin Oxide	SnO_2	0.95	ND
LAWHNK-06	850	Nepheline	$NaAlSiO_4$	9.23	ND
		Franklinite	$ZnFe_{1.9}Cr_{0.1}O_4$	0.21	ND
		Nosean	$Na_8(Al_6Si_6O_{24})(SO_4)$	1.11	ND
		Tin Oxide	SnO_2	2.08	ND
	950	Tin Oxide	SnO_2	1.98	0.76
	1050	Tin Oxide	SnO_2	1.59	ND
LAWHNK-07	850	Nepheline	$NaAlSiO_4$	20.84	ND
		Nosean	$Na_8(Al_6Si_6O_{24})(SO_4)$	2.76	ND
	950	Nepheline	$NaAlSiO_4$	8.42	8.45
		Nosean	$Na_8(Al_6Si_6O_{24})(SO_4)$	1.79	2.13
	1050	None			-
LAWHNK-08	850	Sodium Aluminum Silicate	$Na_{1.55}Al_{1.55}Si_{0.45}O_4$	35.71	ND
		Tin Oxide	SnO_2	1.42[c]	ND
		Sodium Zirconium Silicate	$Na_4Zr_2(SiO_4)_3$	6.87	ND
	950	Sodium Aluminum Silicate	$Na_{1.55}Al_{1.55}Si_{0.45}O_4$	10.41	10.48
		Tin Oxide	SnO_2	1.72[c]	0.66
		Sodium Zirconium Silicate	$Na_4Zr_2(SiO_4)_3$	1.02	0.79
	1050	Tin Oxide	SnO_2	0.9	ND
LAWHNK-09	850	Sodium Aluminum Silicate	$Na_{1.55}Al_{1.55}Si_{0.45}O_4$	60.67[b]	ND
	950	Sodium Aluminum Silicate	$Na_{1.55}Al_{1.55}Si_{0.45}O_4$	63.25[b]	63.07
	1050	None			-
LAWHNK-10	850	Franklinite	$ZnFe_{1.9}Cr_{0.1}O_4$	0.25	ND
	950	None			-
	1050	None			-
LAWHNK-11	850	None			-
	950	None			-
LAWHNK-12	850	Franklinite	$ZnFe_{1.9}Cr_{0.1}O_4$	0.36	ND
	950	None			-
LAWHNK-13	850	Franklinite	$ZnFe_{1.9}Cr_{0.1}O_4$	0.12	ND
		Tin Oxide	SnO_2	1.38	ND
	950	Tin Oxide	SnO_2	1.02	0.39
	1050	Tin Oxide	SnO_2	0.61	ND
LAWHNK-14	850	Tin Oxide	SnO_2	0.25[c]	ND
	950	Tin Oxide	SnO_2	0.65[c]	0.25
	1050	Tin Oxide	SnO_2	0.48[c]	ND
LAWHNK-15	850	None			-
	950	None			-
LAWHNK-16	850	Nosean	$Na_8(Al_6Si_6O_{24})(SO_4)$	7.61	ND
		Magnetite	Fe_3O_4	3.86	ND
	950	Magnetite	Fe_3O_4	2.02	1.03
		Tin Oxide	SnO_2	0.16	0.06
	1050	None			-

Glass ID	Temperature (°C)	Crystalline Phase	Chemical Formula	Crystal Fraction (wt%)	Crystal Fraction (vol%)[a]
LAWHNK-17	850	Tin Oxide	SnO_2	0.95	ND
	950	Tin Oxide	SnO_2	0.86	0.33
	1050	Tin Oxide	SnO_2	0.79	ND
LAWHNK-18	850	None			-
	950	None			-
LAWHNK-19	850	None			-
	950	None			-
LAWHNK-20	850	Nosean	$Na_8(Al_6Si_6O_{24})(SO_4)$	2.47	ND
	950	None			-

(a) Crystal Fraction (vol%) is calculated only at 950 °C. ND = not determined.
(b) The unusual increase of sodium aluminum silicate wt% at higher temperatures might be due to the fact that the quenched sample is already highly crystallized (see Table 3.1). If the glass is already separated or crystallized during melt-quench, it might not follow the normal trends of decreasing crystal fraction with increasing temperature.(c) The increase of tin oxide crystals wt% at some of the higher temperatures might be due to the use of the suggested minimal treatment hours required by ASTM for each temperature, to keep the efficiency of testing. However, the actual sufficient treatment time needed for the CF sample to reach equilibrium varies from compositions.

Among all 20 glass compositions tested by isothermal heat-treatment, seven compositions showed no crystal phases at or above 950 °C: LAWHNK-10, LAWHNK-11, LAWHNK-12, LAWHNK-15, LAWHNK-18, LAWHNK-19, and LAWHNK-20.

Two primary crystalline constraints had been identified to significantly reduce the risk of ≥ 1 vol% of either cassiterite (SnO_2) or zirconia containing phases (e.g., baddeleyite, zircon, parakeldyshite) (Lonergan et al. 2022):

$$g_{SnO_2} \leq 0.045 \tag{3.4}$$

$$g_{Al_2O_3} + 0.677\, g_{SnO_2} + 0.827\, g_{ZrO_2} \leq 0.1655 \tag{3.5}$$

Of the 20 glasses, 90% met the Sn CF crystallization constraint and 85% met the Al-Zr constraint (Table 3.7). As expected, the glasses that didn't meet one or both constraints formed crystals except for one glass, LAWHNK-15. LAWHNK-15 didn't form any Sn containing crystals even though it didn't meet the Sn constraint, indicating the constraint should be revised with more data. Some crystalline phases formed at > 1 vol% at 950°C (Nosean, Calcium Aluminum Oxide, Nepheline, that were not constrained by the Lonergan et al. 2022 limit, suggesting that further crystal constraints are needed.

Table 3.7. LAWHNK glasses that met the 950 °C crystal constraints.

Glass ID	SnO_2 Crystal Constraints Met?	Formed >1 vol% Sn Crystals?	Al_2O_3 and ZrO_2 Crystal Constraints Met?	Formed >1 vol% Zr Crystals?
LAWHNK-01	Yes	No	Yes	No
LAWHNK-02	Yes	No	No	Yes
LAWHNK-03	Yes	No	No	No
LAWHNK-04	Yes	No	No	Yes
LAWHNK-05	Yes	No	Yes	No
LAWHNK-06	No	No	Yes	No
LAWHNK-07	Yes	No	Yes	No

Glass ID	SnO_2 Crystal Constraints Met?	Formed >1 vol% Sn Crystals?	Al_2O_3 and ZrO_2 Crystal Constraints Met?	Formed >1 vol% Zr Crystals?
LAWHNK-08	Yes	No	Yes	Yes
LAWHNK-09	Yes	No	Yes	No
LAWHNK-10	Yes	No	Yes	No
LAWHNK-11	Yes	No	Yes	No
LAWHNK-12	Yes	No	Yes	No
LAWHNK-13	Yes	No	Yes	No
LAWHNK-14	Yes	No	Yes	No
LAWHNK-15	No	No	Yes	No
LAWHNK-16	Yes	No	Yes	No
LAWHNK-17	Yes	No	Yes	No
LAWHNK-18	Yes	No	Yes	No
LAWHNK-19	Yes	No	Yes	No
LAWHNK-20	Yes	No	Yes	No

3.4 Density

Densities of the LAWHNK glasses were obtained using the methods discussed in Section 2.5 and are provided in Table 3.8. The average density of the LAWHNK glasses was 2.69 g/cm³, with a minimum and a maximum of 2.59 and 2.79 g/cm³, respectively. The predicted densities using two models are compared to the measured densities in Figure 3.4. Both models provide reasonably accurate density predictions, with increased scatter observed for the Vienna et al. (2009) model.

Appendix F presents the pycnometer calibration checks performed before and after the sample densities were measured.

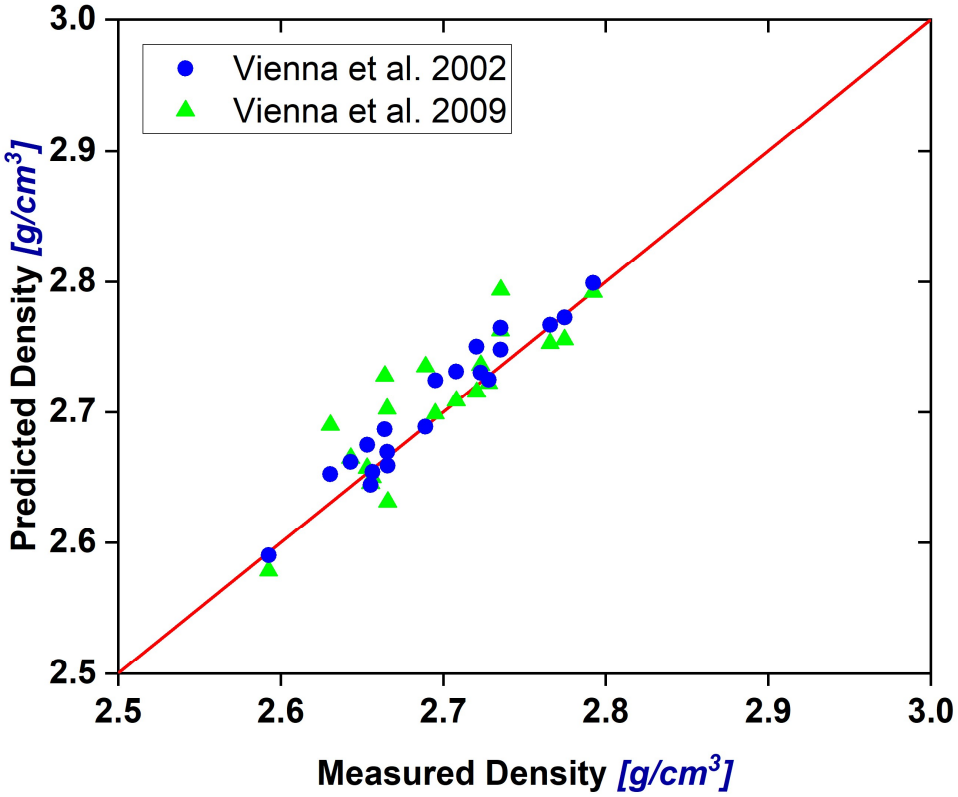


Figure 3.4. Predicted density vs. measured density of LAWHNK glasses.

Table 3.8. Measured densities of LAWHNK glasses in g/cm^3.

Glass ID	Density (g/cm³)	Standard Deviation (g/cm³)
LAWHNK-01	2.6532	0.0054
LAWHNK-02	2.6655	0.0080
LAWHNK-03	2.6640	0.0058
LAWHNK-04	2.7354	0.0070
LAWHNK-05	2.6952	0.0024
LAWHNK-06	2.7279	0.0038
LAWHNK-07	2.6306	0.0037
LAWHNK-08	2.7352	0.0029
LAWHNK-09	2.7205	0.0040
LAWHNK-10	2.5926	0.0014
LAWHNK-11	2.6431	0.0027
LAWHNK-12	2.6554	0.0047
LAWHNK-13	2.7658	0.0040
LAWHNK-14	2.6891	0.0044
LAWHNK-15	2.6659	0.0034
LAWHNK-16	2.7231	0.0031
LAWHNK-17	2.7747	0.0024
LAWHNK-18	2.7923	0.0035
LAWHNK-19	2.7080	0.0046
LAWHNK-20	2.6564	0.0035

3.5 SO_3 Solubility

Melter SO_3 tolerance (w_{SO3}^{melter}), defined as the feed SO_3 concentration above which a salt phase accumulates in the melter, is a critical parameter. At the processing temperature of 1150 °C, w_{SO3}^{melter} must surpass feed SO_3 concentration to avoid excessive corrosion of the melter and increased radionuclide volatility (Vienna et al. 2014; Muller et al. 2015).

Studies have shown a strong correlation between melter SO_3 tolerance and crucible-scale SO_3 solubility (i.e., saturated SO_3 concentrations) at 1150 °C, with a constant offset between w_{SO3}^{melter} and w_{SO3}^{cruc} of −0.33 wt% ± 0.02 wt% SO_3 (Skidmore et al. 2019). Consequently, SO_3 solubility data derived from crucible-scale tests can be used to estimate melter SO_3 tolerance, which would otherwise require resource-intensive scaled melter testing or laborious methods such as bubbling SO_3 through the glass during a furnace run for an extended period.

Sulfur solubility for each glass sample was experimentally determined by measuring SO_3 retention after three cycles of saturation as described in Section 2.6. The saturation results are shown in Table 3.9 together with target and as-fabricated (quenched) SO_3 wt% content. The SO_3 wt% of sulfate saturated samples is an average of both the ICP-OES and IC results. Comparison of IC and ICP-OES shows excellent agreement between the two measurement methods, validating the reliability of both methods (see Figure 3.5).

Table 3.9. Comparison of target, as-fabricated (quenched), and sulfate saturated samples measured SO_3 wt%.

Glass ID	SO_3 wt%		
	Targeted SO_3 (wt%)	As-Fabricated SO_3 (wt%)	Sulfate Saturated (wt%)
LAWHNK-01-SSM	1.060	0.944	1.239
LAWHNK-02-SSM	0.665	0.659	1.058
LAWHNK-03-SSM[(a)]	0.686	0.647	0.728
LAWHNK-04-SSM[(a)]	1.049	1.014	1.452
LAWHNK-05-SSM[(a)]	1.041	0.934	0.958
LAWHNK-06-SSM	0.679	0.692	1.219
LAWHNK-07-SSM	0.733	0.757	1.271
LAWHNK-08-SSM	0.377	0.420	1.245
LAWHNK-09-SSM[(a)]	0.543	0.552	0.928
LAWHNK-10-SSM	0.621	0.584	1.615
LAWHNK-11-SSM[(a)]	1.044	0.901	1.124
LAWHNK-12-SSM	1.039	1.011	1.536
LAWHNK-13-SSM	0.843	0.877	1.212
LAWHNK-14-SSM[(a)]	1.000	0.986	1.147
LAWHNK-15-SSM	0.660	0.662	1.866
LAWHNK-16-SSM[(a)]	0.931	0.764	0.901
LAWHNK-17-SSM	0.986	1.031	1.525
LAWHNK-18-SSM	0.979	1.071	1.476
LAWHNK-19-SSM	0.538	0.584	1.670
LAWHNK-20-SSM	0.830	0.829	1.494

(a) Denotes that quenched glasses were washed to remove the salts on the surfaces.

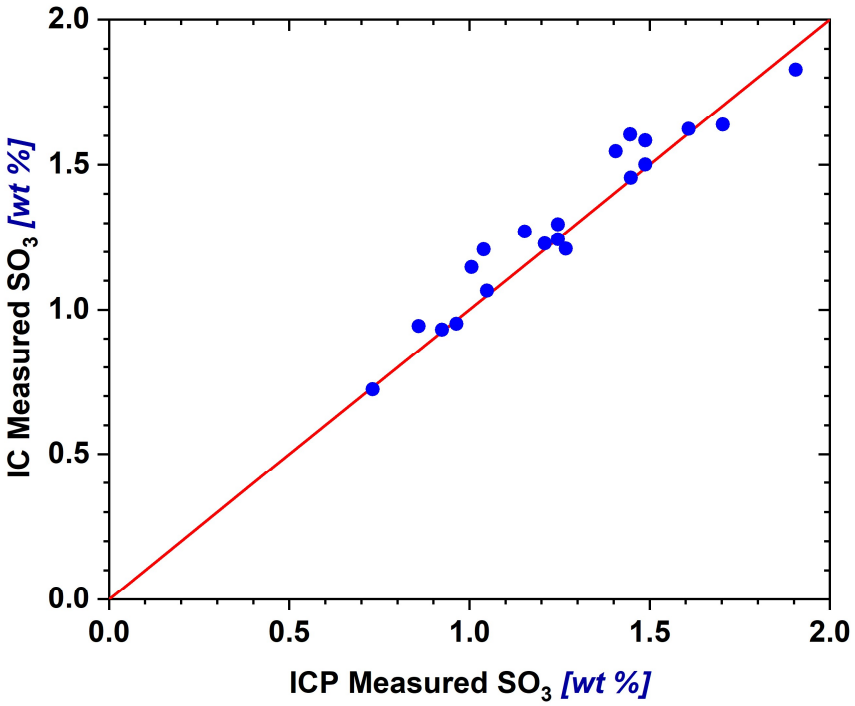


Figure 3.5. Comparison of ICP-OES vs. IC measured SO_3 wt% of each glass sample after 3TS method.

Overall, all glasses satisfied the SO_3 solubility limit and fall within the range of melter SO_3 tolerance and solubility specified in Table A.3 of Appendix A (Vienna et al. 2022) for the 576 glasses in the modeling dataset, which vary from 0.150 to 2.603 wt%.

3.5.1 Comparisons of Predicted SO_3 Saturation Concentrations

The SO_3 saturation concentrations determined experimentally were compared to predicted values calculated using the 11-Term reduced partial quadratic mixture model from Vienna et al. (2022). Figure 3.6 shows a one-to-one comparison of the measured and predicted SO_3 solubilities. Most glasses were on or close to the 45° line, meaning the model predicted correctly. A systematic underestimation of SO_3 tolerance by the model was observed at higher concentrations of SO_3, which is expected since the same behavior was observed when the model was created. One glass was predicted to have significantly higher concentration than measured (LAWHNK-09).

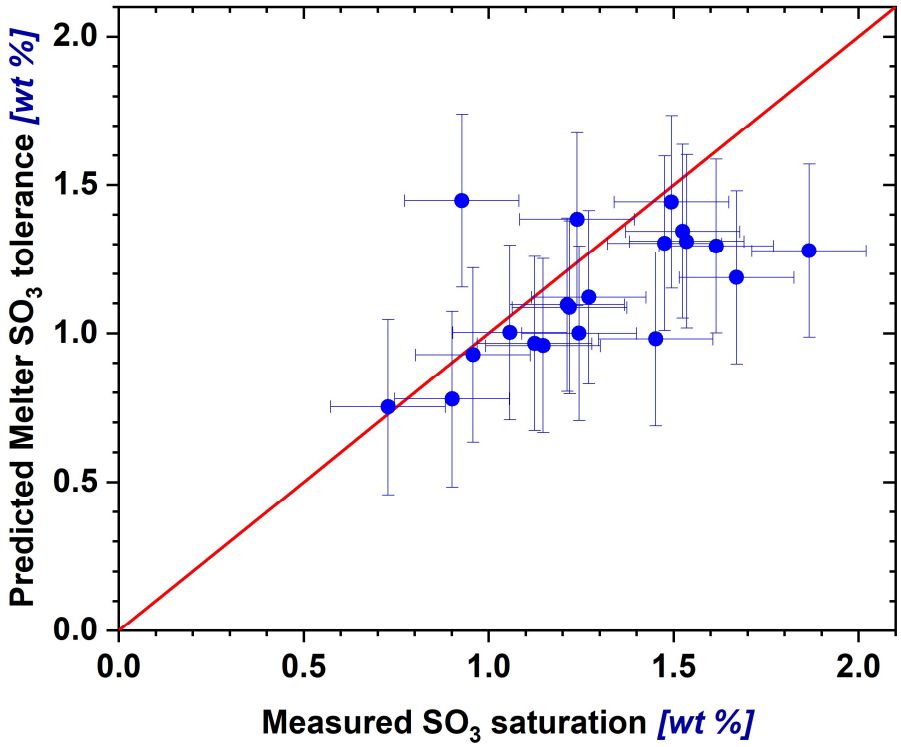


Figure 3.6. Predicted vs. measured melter SO_3 solubility of LAWHNK glasses applying the 11-term 3TS-SO_3-PQM model (Vienna et al. 2022).

3.6 Viscosity

Viscosity is a of the critical processing constraint that must remain between 2 and 8 Pa·s at 1150 °C to ensuring proper pouring without underfilling the container (Perez 2006), prevent melter corrosion (if too low), and maintain adequate melting rates (if too high).

Viscosity was measured as discussed in Section 2.7. The results are summarized in Table 3.10 and individually reported in Appendix G. Note that the reported temperatures may be different than target temperatures listed in Section 2.7 because of a difference between the furnace control thermocouple and the viscosity measurement thermocouple.

Table 3.10. Measured η (Pa-s) values versus target temperature (in the sequence of measurement).

Target *T*, °C	1150	1050	950	1150	1250	1150
Glass ID	η (Pa-s)[a]	η (Pa-s)[a]	η (Pa-s)[a]	η (Pa-s)[a]	η (Pa-s)[a]	η (Pa-s)[a]
LAWHNK-01	1.57	3.30	9.65	1.43	0.74	1.39
LAWHNK-02	3.15	8.54	27.53	3.07	1.78	n.m.[c]
LAWHNK-03	4.93	13.61	--[b]	4.49	2.05	4.53
LAWHNK-04	4.59	10.89	38.48	3.61	1.43	3.25
LAWHNK-05	1.45	22.78	--[b]	1.36	0.73	1.34
LAWHNK-06	1.88	8.21	37.64	1.84	0.82	3.96
LAWHNK-07	2.99	6.70	16.78	3.18	1.68	3.26
LAWHNK-08	1.61	4.12	14.17	1.54	0.76	1.53
LAWHNK-09	1.38	3.21	--[b]	1.30	0.66	1.34
LAWHNK-10	1.70	3.47	8.00	1.77	0.98	1.85
LAWHNK-11	4.70	12.38	39.05	4.59	2.09	4.70
LAWHNK-12	2.16	4.58	11.34	2.20	1.27	2.26
LAWHNK-13	1.61	3.81	43.89	1.47	0.72	1.47
LAWHNK-14	4.41	11.28	44.42	4.43	2.07	4.38
LAWHNK-15	1.75	3.71	9.53	1.70	0.92	1.75
LAWHNK-16	1.49	3.56	10.12	1.42	0.71	1.40
LAWHNK-17	1.33	9.38	147.62	1.16	0.65	1.27
LAWHNK-18	1.22	2.94	9.19	1.27	0.66	1.34
LAWHNK-19	1.10	2.17	5.37	1.05	0.60	1.08
LAWHNK-20	2.41	5.46	15.76	2.25	1.12	2.23

(a) Average of three measurements.
(b) Too viscous to get a reading.
(c) n.m. = not measured.

All of the glasses were formulated to have viscosity 1150 °C higher than 1 Pa s, and their measured η_{1150} ranged between 1.05 and 4.93 Pa-s. All met the WTP upper limit of < 8 Pa-s, though 55% of the glasses were below the lower limit of 2 Pa-s, which is expected since the matrix was designed to push the Na boundary and alkali are known to decrease viscosity by breaking bridging bonds between silica and other glass formers to create more non-bridging oxygens.

The Arrhenius model was used to fit the viscosity-temperature data for each waste glass. The model form is the Arrhenius equation:

$$\ln(\eta) = A + \frac{B}{T_K} \tag{3.6}$$

where A and B are independent of temperature (T_K), which is in Kelvin (T(°C) + 273.15). For each glass, Table 3.11 provides the values for the A and B coefficients and summarizes the viscosity results at six target temperatures calculated using the Arrhenius equation [Eq. (3.6)].

Table 3.11. Fitted Arrhenius coefficients and calculated η for specific temperatures.

	Arrhenius Coefficients		Temperature (°C)					
			950	1050	1100	1150	1200	1250
	A	B	η [Pa-s]					
Glass ID	(ln Pa-s)	(ln Pa-s*K)						
LAWHNK-01	-12.0654	17714.5	11.24	3.76	2.31	1.47	0.96	0.65
LAWHNK-02	-12.3661	19352.8	31.75	9.60	5.64	3.43	2.16	1.41
LAWHNK-03	-13.3997	21239.7	52.84	14.22	7.92	4.60	2.77	1.73
LAWHNK-04	-14.6126	22655.7	50.00	12.33	6.61	3.70	2.16	1.30
LAWHNK-05	-26.8995	39202.4	173.27	15.36	5.22	1.91	0.75	0.31
LAWHNK-06	-18.8910	27897.1	50.37	8.98	4.17	2.04	1.05	0.56
LAWHNK-07	-10.0245	15933.5	20.16	7.53	4.86	3.23	2.21	1.55
LAWHNK-08	-13.9244	20539.9	17.64	4.96	2.82	1.66	1.02	0.65
LAWHNK-09	-12.1659	17789.1	10.80	3.60	2.20	1.40	0.91	0.62
LAWHNK-10	-9.6327	14566.3	9.75	3.96	2.66	1.83	1.29	0.93
LAWHNK-11	-12.9411	20688.1	53.24	14.82	8.39	4.94	3.02	1.90
LAWHNK-12	-9.9704	15386.3	13.60	5.26	3.44	2.32	1.61	1.14
LAWHNK-13	-19.5525	28592.1	45.89	7.84	3.57	1.72	0.87	0.46
LAWHNK-14	-13.4406	21330.4	54.62	14.62	8.13	4.71	2.83	1.76
LAWHNK-15	-10.8652	16276.4	11.51	4.21	2.69	1.77	1.20	0.84
LAWHNK-16	-12.7030	18676.7	13.04	4.11	2.46	1.52	0.98	0.64
LAWHNK-17	-27.5123	40027.6	184.34	15.53	5.16	1.85	0.71	0.29
LAWHNK-18	-12.6941	18484.2	11.24	3.59	2.16	1.34	0.86	0.57
LAWHNK-19	-10.6439	15309.8	6.52	2.53	1.66	1.12	0.78	0.55
LAWHNK-20	-12.0515	18390.7	19.80	6.35	3.83	2.39	1.54	1.02

The η_{1150} values interpolated from measured data were compared to predicted viscosity values calculated using the Vienna et al. (2022) η_{1150} model and are shown in Figure 3.7. Overall, there is good agreement between predicted and measured values for viscosity among all the LAWHNK glasses. A few glasses are slightly above or below the 45° line, but no significant outliers were noted.

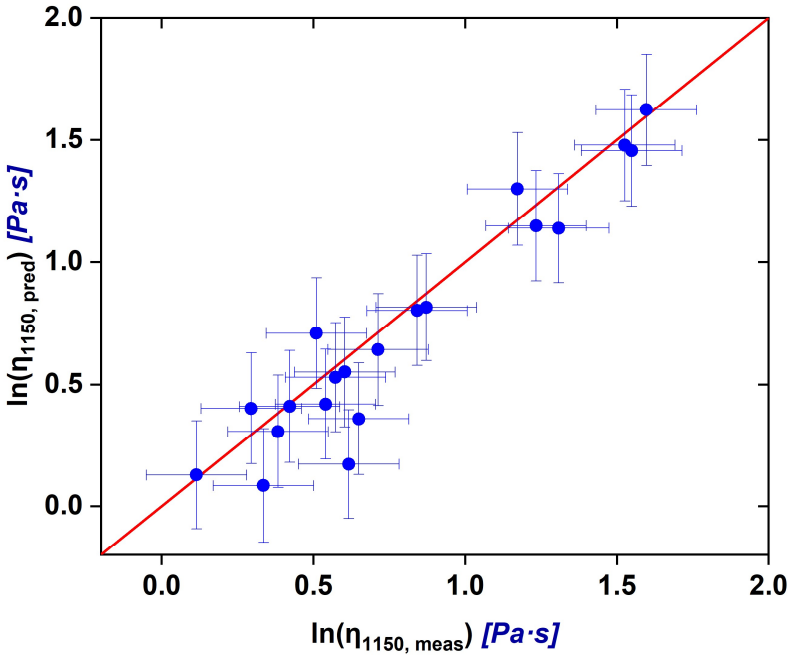


Figure 3.7. Predicted vs. measured $\ln(\eta_{1150})$ where model predicted for Pa·s shown. Uncertainties for measured values are represented by SD_{pooled} reported in Vienna et al. (2022).

3.7 Electrical Conductivity

Electrical conductivity is a constraint that needs to be met when formulating glasses to be processed at WTP. The melters are Joule-heated, so melts need to fall within the range between 10 and 70 S/m over the temperature range from 1100 to 1200 °C.

EC was measured using the methods discussed in Section 2.8. The results are summarized in Table 3.12. Measured EC (S/m) values vs. temperatures are individually reported in Appendix H.

Table 3.12. Measured electrical conductivity (S/m) values vs. temperatures.

Glass ID	Target *T*, °C			
	950	1050	1150	1200
LAWHNK-01	22.89	37.38	56.49	67.24
LAWHNK-02	29.58	39.40	47.99	50.54
LAWHNK-03	58.65	72.14	91.44	100.7
LAWHNK-04	37.21	51.54	64.31	72.35
LAWHNK-05	27.28	40.02	46.46	61.98
LAWHNK-06	30.51	44.05	60.98	70.26
LAWHNK-07	61.93	81.62	101.82	111.07
LAWHNK-08	38.51	53.18	72.56	82.01
LAWHNK-09	24.22	30.46	40.81	48.83
LAWHNK-10	33.94	50.67	66.01	75.53
LAWHNK-11	23.73	35.31	47.90	54.29
LAWHNK-12	29.65	43.22	57.31	64.98
LAWHNK-13	30.85	46.82	64.87	77.04
LAWHNK-14	24.30	35.99	53.52	62.76
LAWHNK-15	35.41	49.44	63.82	71.71
LAWHNK-16	20.56	31.27	43.50	51.65
LAWHNK-17	20.84	34.71	47.99	55.49
LAWHNK-18	32.79	48.27	63.77	70.92
LAWHNK-19	34.66	48.02	62.71	70.46
LAWHNK-20	20.60	31.84	44.50	53.94

EC at 1150 °C ranged between 40.8 and 101.8 S/m, 3 glasses had values higher than the WTP limits of $20 \leq EC_{1150} \leq 70$ S/m. This result is expected since alkali are the primary charge carriers for these glasses and thus increasing alkali leads to a higher EC and EC wasn't constrained during glass design (Ezz Eldin and El Alaily 1998; Maji et al. 2016).

The Arrhenius equation [Eq. (3.6)] was used to fit EC-temperature data for each waste glass. Arrhenius coefficients and calculated ε_{1150} are reported in Table 3.13.

Table 3.13. Fitted coefficients of Arrhenius model for ε_{1150}.

	Arrhenius Coefficients		ε_{1150}
Glass ID	A, ln[S/m]	B, ln[S/m]·K	(S/m)
LAWHNK-01	9.501	-7786	56.21
LAWHNK-02	6.606	-3915	47.22
LAWHNK-03	7.277	-3936	91.05
LAWHNK-04	7.500	-4736	64.83
LAWHNK-05	7.729	-5401	51.08
LAWHNK-06	8.340	-6021	60.86
LAWHNK-07	7.589	-4228	101.3
LAWHNK-08	8.136	-5492	72.02
LAWHNK-09	7.236	-4988	41.68
LAWHNK-10	8.207	-5706	66.47
LAWHNK-11	8.062	-5974	47.65
LAWHNK-12	8.013	-5642	57.28
LAWHNK-13	8.775	-6534	65.60
LAWHNK-14	8.815	-3893	53.08
LAWHNK-15	7.721	-5072	63.88
LAWHNK-16	8.406	-6579	43.95
LAWHNK-17	8.359	-6386	47.98
LAWHNK-18	8.067	-5578	63.24
LAWHNK-19	7.731	-5114	62.61
LAWHNK-20	8.622	-6841	45.33

Figure 3.8 compares the measured and predicted values using the Vienna et al. (2022) model. Generally, glasses sat on both sides of the 45° line, with most of the glasses falling reasonably close to the line. LAWHNK-03 and LAWHNK-07 were both measured to be significantly higher than predicted. LAWHNK-03 was found to have a sodium aluminosilicate phase present upon melting, which persisted in CF measurements at 1050 and 950 °C, suggesting that the residual glass may be richer in sodium, resulting in a higher measured conductivity. LAWHNK-07 was also found to have nepheline crystals at 950 °C, though it did not have crystals at higher temperatures. LAWHNK-07 is also sodium rich, potentially explaining the high measured conductivity.

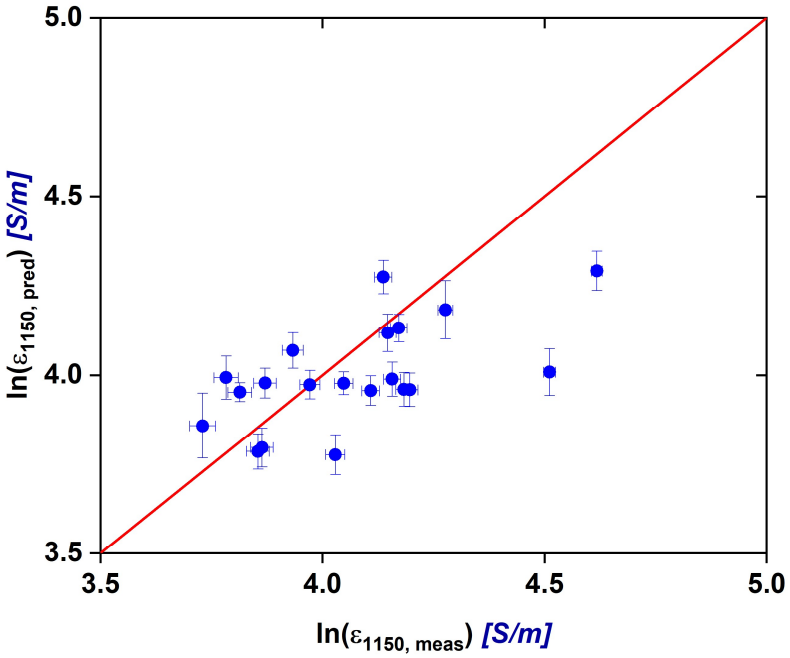


Figure 3.8. Predicted vs. measured $\ln(\varepsilon_{1150})$. Uncertainties for measured values are represented by SD_{pooled} reported in Vienna et al. (2022).

3.8 Product Consistency Test

PCT is one of two main tests used to evaluate glass durability. The PCT limits for LAW glass are normalized losses of boron and sodium (NL_B, NL_{Na}) < 2.0 g m^{-2} and VHT rate < 50 g m^{-2} d^{-1}, respectively. PCT requirements for DFHLW are NL_B, NL_{Li}, and $NL_{Na} \leq$ 8.35, 4.785, and 6.675 g m^{-2}, respectively.

The average normalized elemental mass losses [NL_i; see Eq. (3.7)] from the triplicate samples for B, Na, Si, and Li for Q and CCC glass are reported in Table 3.14 and Table 3.15, respectively. The normalized elemental mass losses for each test are reported in Appendix I. As per ASTM C1285, the NL_i values presented in Table 3.14 and Table 3.15 are determined from triplicate tests with the following expression:

$$NL_i = exp\,[avg\,\ln(NL_i)] \tag{3.7}$$

The NL_i for the individual tests are presented in Appendix I. The relative standard deviations between triplicate samples were found to be less than 5%.

Table 3.14. Average normalized elemental mass losses (NL_i) in $g \cdot m^{-2}$ for the LAWHNK Q glasses. Values in bold font exceed the LAW glass limit of 2.0 $g \cdot m^{-2}$.

Glass ID	NL_B	NL_{Si}	NL_{Na}	NL_{Li}[(a)]
LAWHNK-01	1.40	0.28	1.92	1.52
LAWHNK-02	**2.08**	0.27	1.73	1.67
LAWHNK-03	**7.87**	0.35	**4.59**	2.95
LAWHNK-04	1.26	0.25	1.29	0.51
LAWHNK-05	**2.35**	0.40	**2.12**	1.63
LAWHNK-06	0.53	0.37	1.21	0.25
LAWHNK-07	1.47	0.40	1.49	0.29
LAWHNK-08	1.84	0.41	1.95	0.83
LAWHNK-09	**2.60**	0.30	**3.33**	1.87
LAWHNK-10	**2.75**	0.28	**2.22**	2.48
LAWHNK-11	**13.50**	1.78	**9.74**	3.27
LAWHNK-12	1.24	0.26	1.13	0.96
LAWHNK-13	**4.64**	0.83	**4.21**	3.88
LAWHNK-14	0.58	0.31	0.73	0.30
LAWHNK-15	**6.46**	1.18	**5.21**	4.91
LAWHNK-16	1.77	0.36	1.60	1.36
LAWHNK-17	1.04	0.37	1.54	1.22
LAWHNK-18	1.26	0.30	1.44	0.86
LAWHNK-19	**2.64**	0.48	**2.59**	1.42
LAWHNK-20	0.81	0.19	0.97	1.00

(a) NL_i values above 2.0 $g \cdot m^{-2}$ are not in bold for Li because Li is not an element that is specified in the contract requirement.

Table 3.15. Average normalized elemental mass losses (NL_i) in $g \cdot m^{-2}$ for the LAWHNK CCC glasses. Values in bold text exceed the DOE limit of 2 g m^{-2} d^{-1}.

Glass ID	NL_B	NL_{Si}	NL_{Na}	NL_{Li}[(a)]
LAWHNK-01	**3.71**	0.24	**2.91**	2.27
LAWHNK-02	**47.83**	0.64	**28.23**	32.80
LAWHNK-03	**49.06**	0.92	**22.26**	11.88
LAWHNK-04	**45.56**	0.99	**21.23**	15.13
LAWHNK-05	**2.87**	0.47	**2.40**	2.16
LAWHNK-06	**44.01**	**3.22**	**27.96**	25.33
LAWHNK-07	**49.43**	**2.06**	**26.67**	15.41
LAWHNK-08	**45.16**	0.83	**20.42**	14.93
LAWHNK-09	**12.46**	0.31	**5.64**	1.45
LAWHNK-10	**4.38**	0.36	**3.07**	3.85
LAWHNK-11	**15.34**	**2.00**	**10.26**	3.54
LAWHNK-12	**4.61**	0.71	**3.15**	3.71
LAWHNK-13	**2.73**	0.63	**3.92**	2.01
LAWHNK-14	0.59	0.30	0.68	0.42
LAWHNK-15	**6.68**	1.11	**5.00**	4.73
LAWHNK-16	**7.47**	0.53	**4.80**	4.02
LAWHNK-17	**17.86**	1.69	**11.48**	11.70
LAWHNK-18	1.40	0.32	1.45	1.01
LAWHNK-19	**2.51**	0.46	**2.39**	1.64
LAWHNK-20	**3.19**	0.43	**2.74**	1.00

(a) NLi values above 2.0 $g \cdot m^{-2}$ are not in bold for Li because Li is not an element that is specified in the contract requirement.

Nine of the Q glasses exceed the LAW contract limit for B, eight of the Q glasses exceed the limit for Na. Only two of the 20 CCC glasses satisfied the LAW contract requirement for B and Na, and two of the 20 CCC glasses fail the Si limit with a third right on the line. These results achieved one of the objectives of this matrix design, which was to produce glasses at or near the PCT limit.

The high PCT release values can be associated with the presence of crystalline phases in the glasses that remove network-forming elements from the glass, which leads to a less chemically durable glass. However, in this matrix, though nine of the 20 Q glasses exceed the PCT limit for B, only one Q glass (LAWHNK-03) contains a $Na_{1.55}$ ($Al_{1.55}$ $Si_{0.45}$ O_4) phase at 41.48 wt% that removes either Si or Al from the glass. The other crystalline phases in the Q glasses contained Zn, Fe, Cr, Sn, and Zr at amounts near or less than 1.0 wt%. Thus, the presence of crystalline phases does not appear to be a major driving force behind the poor performance of the Q glasses. Large amounts of alkalis have been also known to increase PCT releases. Due to an ion exchange reaction with the alkalis in the glass, where a H_3O^+ ion in solution exchanges with M^+ (where M^+ is an alkali ion), more alkalis from the glass are released. This causes a higher pH in the solution, thereby promoting the dissolution of the silica network (Ojovan et al. 2006). However, this also does not appear to be the only driver of durability as the two poorest performing glasses (LAWHNK-03 and LAWHNK-11) are near the middle of the matrix in total alkali content in this high Na and K matrix. Another possible reason for poor PCT response is the low amount of SiO_2 in the glass. The low amount of SiO_2 results in a low amount of network formers, which may make the glass more susceptible to attack by water and lead to a higher PCT response.

As for the CCC glasses, many of the glasses contained nepheline and $Na_{1.55}Al_{1.55}$ $Si_{0.45}$ O_4, both of which remove the network formers Si and Al from the glass (Table 3.2). As discussed in Section 3.2, when the $Na_{1.55}Al_{1.55}$ $Si_{0.45}$ O_4 phases were examined by XRD, the chemistry was most similar to nepheline. Of the six CCC glasses with the highest PCT response (LAWHNK-02, LAWHNK-03, LAWHNK-04, LAWHNK-06, LAWHNK-07, and LAWHNK-08), all contained near or greater than 15 wt% of the two Si containing phases listed above (e.g. $Na_{1.55}Al_{1.55}$ $Si_{0.45}$ O_4,). All six of these CCC glasses had a NL_B response greater than 45 g/m^2 and, because a value of 50 g/m^2 is equivalent to complete dissolution in a PCT-A test, these glasses may be considered completely dissolved in the 7-d tests. Only two of the CCC glasses met the LAW PCT requirements (LAWHNK-14 and LAWHNK-18).

Lastly, a characteristic of this set of LAWHNK glasses is that the NL_{Na} values tend to bias lower than NL_B, especially for the glasses with higher NL_i values. This characteristic can be attributed to the need for charge compensation of $[AlO_4]^-$ units in the alteration layer. The charge compensation is initially performed by Ca^{2+}, but when that source has been exhausted, Na^+ is retained.

A method that relies on a pooled standard deviation of PCT responses can be employed to determine if the difference between Q and CCC heat-treated glasses are within experimental error (Russell et al. 2025). Briefly, the method creates a range for $\ln(NL_{Na})$ and $\ln(NL_B)$ where if the measured $\ln(NL_{Na})$ and $\ln(NL_B)$ for Q and CCC glasses fall within that range, then the Q and CCC responses can be considered to be within experimental uncertainty. Twelve of the 20 LAWHNK glasses did not have quenched PCT responses that were within experimental uncertainty for B, while 11 of the 20 LAWHNK glasses did not have CCC PCT responses that were within experimental uncertainty for Na.

The differences between $\ln(NL_i)$ values for Q and CCC glasses are presented in Figure 3.9. For most of the Q and CCC responses, the high degree of crystallinity in the CCC resulted in a disruption to the network connectivity and less durable glass. For this reason, the CCC responses are greater than or equivalent to the quenched glass responses.

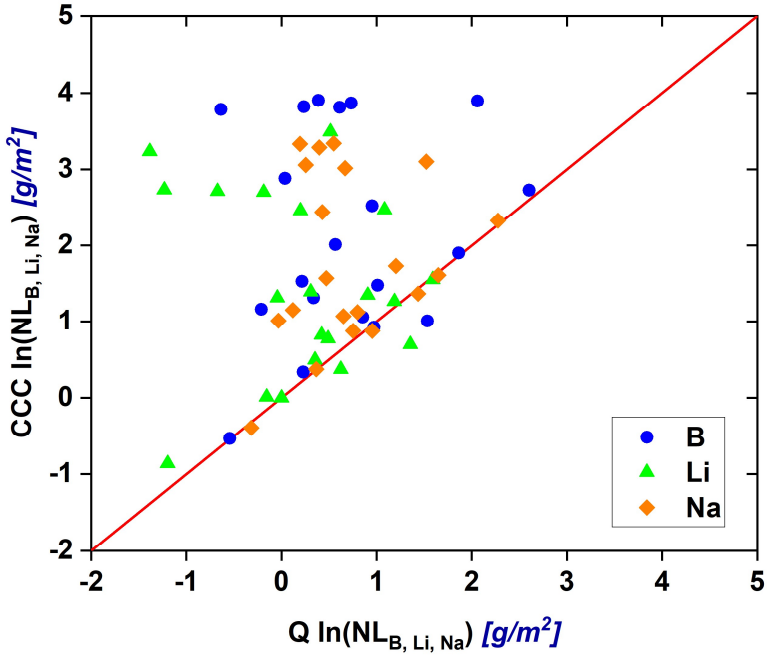


Figure 3.9. Normalized NL_B and NL_{Na} release in natural logarithm scale of quenched vs. CCC for LAWHNK glasses. The red line is the 1:1 line and is used to guide the eye.

Figure 3.10 shows measured average ln(NL_B) and ln(NL_{Na}) values plotted against model predictions from Vienna et al. (2022). All LAWHNK glasses were designed to have a release at or near the PCT limit of 2.0 g/m^2. Visually, the model adequately predicts the ln(NL_B) releases within model uncertainty except for LAWHNK-18. The model also adequately predicts the ln(NL_{Na}) releases within model uncertainty except for the cases of LAWHNK-07, LAWHNK-18, and LAWHNK-19. Of the cases where the model prediction is not within agreement with the measured value, the model overpredicts the test response, which demonstrates that the model predictions are conservative.

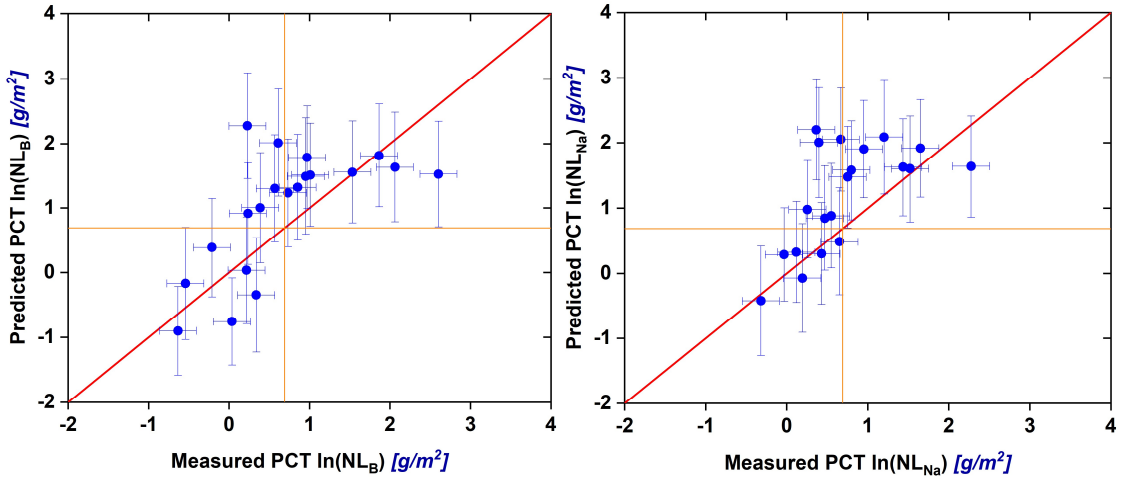


Figure 3.10. ln(NL_B) and ln(NL_{Na}) measured vs. predicted values from Vienna et al. (2022). The orange lines are the release limit.

3.9 Vapor Hydration Test

The VHT is another test used by WTP to evaluate durability in LAW glasses. Per the WTP contract, the VHT alteration rate (r_{VHT}) of LAW glasses subjected to > 7-day VHT shall be less than 50 g/m^2/d (DOE 2000).

The majority of the glasses failed VHT both as Q and as CCC with r_{VHT} above the WTP contract limit. Only three Q glasses passed the 24-day VHT test with r_{VHT} < 50 g/m^2/d. The remaining glasses failed either the 24-day or the 7-day VHT. One Q glass (LAWNHK-16) was not tested because it was too friable to successfully cut a coupon and one glass (LAWHK-20) was removed from the analysis because of experimental difficulties. Examples of post VHT samples are presented in Figure 3.11 and Figure 3.12. Results are presented in Table 3.16. Photos of the glass samples before and after the VHT are presented in Appendix J and Appendix K.

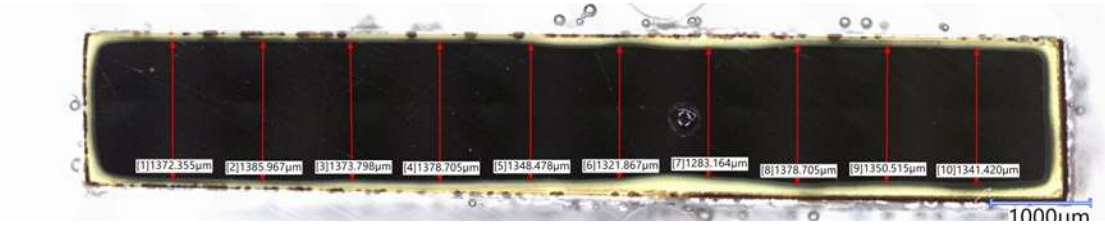


Figure 3.11. Example of quenched glass (LAWHNK-18) that performed well after 24 days VHT. Red lines are the 10 equidistant measurement lines.

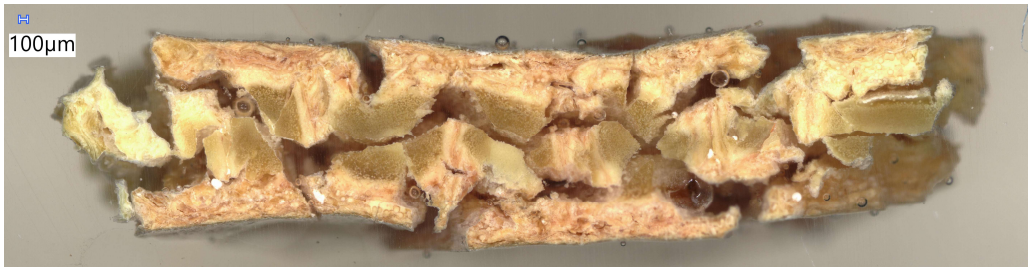


Figure 3.12. Example of quenched glass (LAWHNK-08) that performed extremely poorly on 24-day VHT.

Table 3.16. Q and CCC sample VHT corrosion rate (r_{VHT} [$g \cdot m^{-2} \cdot d^{-1}$]), pass/fail contract rate descriptor (0/1), ln(alteration depth) (μm), and test duration (days).

Glass ID	Q r_{VHT} ($g/m^2/d$)	Q ln(Alteration depth) (um)	Q Test Duration (days)	Q Solution pH	CCC r_{VHT} ($g/m^2/d$)	CCC Test Duration (days)	CCC ln(Alteration depth) (um)	CCC Solution pH
LAWHNK-01	77.6	5.31	7	10.0	441.4	7	7.09	10.5
LAWHNK-02	299.9	6.67	7	9.5	87.6	24	6.70	9.0
LAWHNK-03	276.7	6.62	7	11.0	85.5	24	6.64	N/A[a]
LAWHNK-04	9.5	4.40	24	11.5	87.8	24	6.59	12
LAWHNK-05	278.6	6.59	7	11.0	273.7	7	6.59	10.5
LAWHNK-06	313.3	6.66	7	12.0	80.9	24	6.56	12
LAWHNK-07	355.1	6.86	7	N/A[a]	NM[b]	N/A[a]	N/A[a]	N/A[a]
LAWHNK-08	317.3	6.68	7	9.0	112.2	24	6.90	N/A[a]
LAWHNK-09	120.1	5.78	7	11.0	NM[b]	N/A[a]	NA[a]	N/A[a]
LAWHNK-10	271.9	6.60	7	10.0	277.8	7	6.64	9.5
LAWHNK-11	61.0	6.33	24	9.5	59.8	24	6.28	9.0
LAWHNK-12	66.7	6.42	24	9.5	216.4	7	6.37	9.5
LAWHNK-13	283.2	6.61	7	10.0	378.6	7	6.63	11.0
LAWHNK-14	252.9	6.51	7	9.5	290.0	7	6.62	9.0
LAWHNK-15	76.9	6.54	24	9.5	179.9	7	6.15	9.0
LAWHNK-16	NM[b]	NM[b]	N/A[a]	N/A[a]	297.3	7	6.63	11.0
LAWHNK-17	74.0	6.50	24	11.5	83.0	24	6.61	10.5
LAWHNK-18	16.9	5.03	24	11.0	286.5	7	6.58	10.5
LAWHNK-19	91.7	6.69	24	N/A[a]	264.9	7	6.66	10.5
LAWHNK-20	NM[b)]	NM[b]	N/A[a]	N/A[a]	NM[b]	N/A[a]	N/A[a]	N/A[a]

(a) Not available, (b) Not measured

Most of the glasses failed VHT, likely due to the presence of crystals in both Q and CCC glasses and the high amounts of alkali (Na and K) in the glass compositions (Figure 3.13). The main crystallinity phases found in the Q glasses were Zn-Fe-Cr and/or Sn containing oxides. Spinel has previously been shown to have minimal effects on glass durability while SnO_2 is added primarily to reduce VHT responses (Fox et al. 2016). If SnO_2 precipitates out of glass, it likely will cause increased VHT rate. On the other hand, CCC glasses contained mostly Na-Al silicates, one of the main crystal groups well known to negatively impact glass durability and therefore increase VHT. High alkali glasses are prone to corrode more quickly due to ion exchange increasing solution pH. This is why high alkali glasses were selected in designing glasses with high VHT and PCT responses.

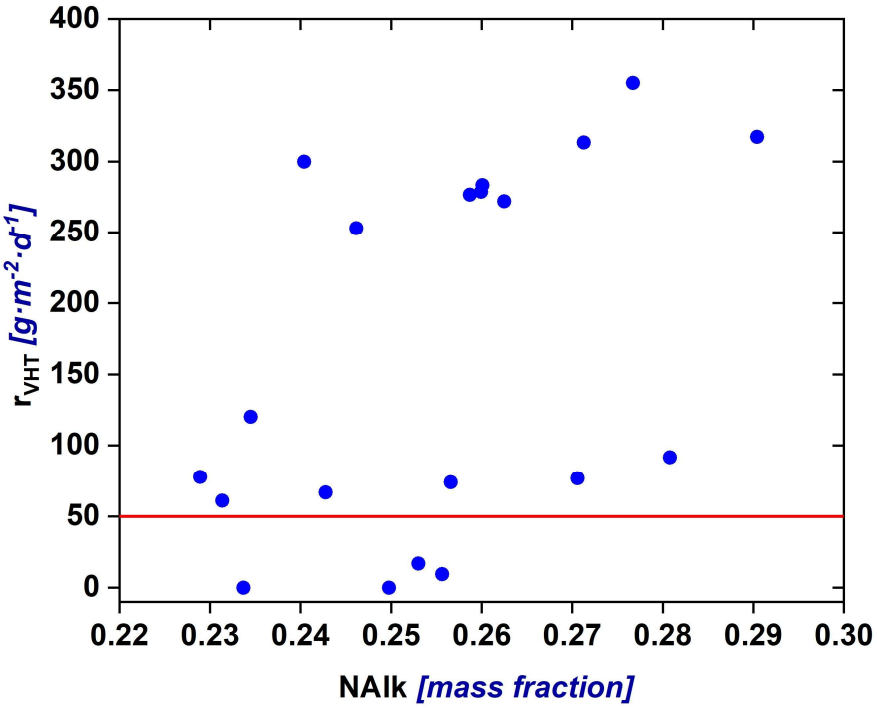


Figure 3.13. Quenched glasses VHT alteration rate (r_{VHT}) compared to the total normalized alkali [Nalk = $Na_2O + 0.66(K_2O) + 2(Li_2O)$] content of the glass.

Figure 3.14 compares the quenched glass alteration depth with the CCC glass alteration depth results and the amount of crystallinity in the quenched glass. There does not appear to be any correlation between the amount of crystallinity in the glass and the depth of glass alteration. The alteration rate was also evaluated (not shown) and did not appear to have a direct correlation either.

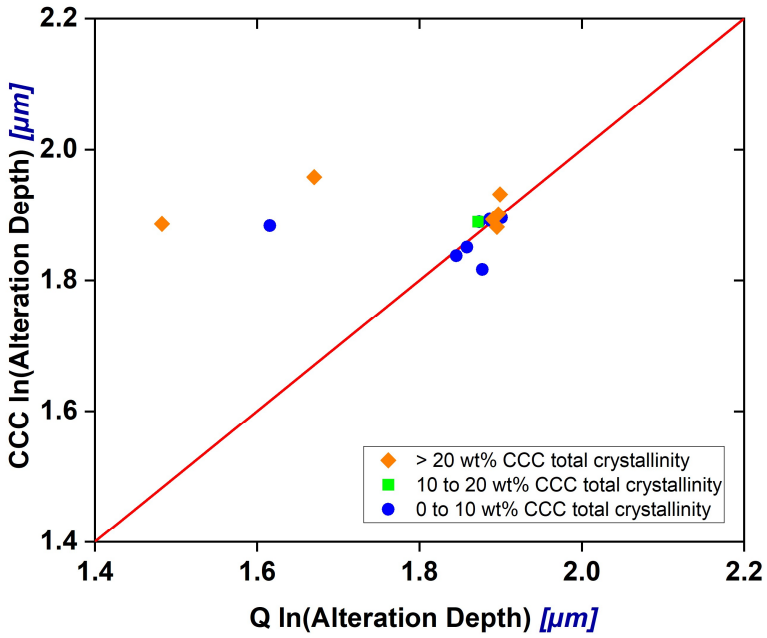


Figure 3.14. CCC and Q glass alteration depth comparison with the total amount of crystallinity in the CCC glass

The Q r_{VHT} values were compared to predictions calculated using the Vienna et al. (2022) model. The Vienna et al. (2022) VHT model is in the form of a logistic model. Logistic models are often used to predict binary responses, in this case expressed as pass/fail for the contract VHT limit. The predictor variables in the model represent glass compositions in the form of a PQM model, while the response is a logit of the binary response. The model is used to calculate the probability that a given glass will fail the VHT constraint:

$$\hat{y} = ln\left[\frac{P(g)}{1-P(g)}\right] = \sum_{i=1}^{q} b_i \cdot g_i \tag{3.8}$$

where:

$\hat{y}$ = the model predicted logit value for a given glass
g = the composition for a given glass, expanded to match the model form
b = the vector of model coefficients
$P(g)$ = the model predicted "score" or probability that the binary response for a given glass composition (g) is "successful" (in this case, suggesting that the glass will fail the VHT)
q = the number of model parameters

Note that the predicted probability or "score" for a given glass, P(g), is calculated by inverting the logit transformation:

$$P(g) = \frac{e^{\hat{y}}}{1+e^{\hat{y}}} \tag{3.9}$$

The suggested threshold for predicted model "scores" when classifying a given glass as pass or fail with respect to the VHT was set at 0.19. Thus, a glass having P(g) < 0.19 is predicted to pass the VHT constraint, whereas a glass having P(g) ≥ 0.19 is predicted to fail the VHT constraint (Vienna et al. 2022).

Because of the binary nature of the model, only prediction uncertainties were applied. The measured alteration rate was converted to an observed pass/fail status for each glass, and measurement uncertainty was not included in this process.

Figure 3.15 illustrates results comparing VHT model predictions to corresponding observed pass/fail binary responses determined from measured alteration rates for validation of quenched glasses. The x-axis in this figure indicates the actual pass/fail status of the validation glasses; the y-axis shows model-predicted logit values for the validation glasses. The red vertical line in Figure 3.15 separates those glasses that pass VHT constraint (right side) from the glass that failed (left side).

Of the 20 glasses, only two (LAWHNK-04, and LAWHNK-18) were erroneously predicted to fail the VHT, whereas they actually passed the test indicating that the model is conservative.

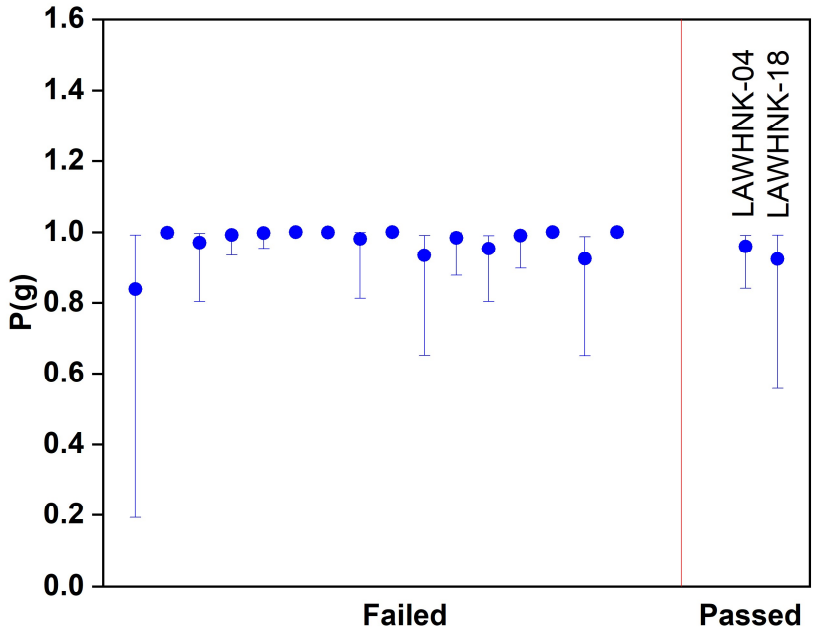


Figure 3.15. Predicted vs. measured VHT responses using the Vienna et al. (2022) model. The red line separates glasses that passed the VHT constraint (right side) from the glass that failed (left side).

4.0 Summary

A matrix of 20 glasses was designed to simultaneously expand the LAW and DFHLW composition range by increasing Na_2O and K_2O content and adding to the data for properties of interest to both facilities. The glasses were primarily designed for LAW since VHT response is only available for LAW glasses. The glasses were designed to be near and exceed property limits to improve predictions at the limits. The designed glasses were fabricated and tested for CCC and isothermal heat-treatments, density, viscosity, EC, chemical durability, and sulfate solubility. Refractory corrosion testing will be reported separately.

The glass compositions were verified by ICP-OES. After the final melt, seven glasses out of 20 were fully amorphous. Overall, 12 glasses had a total crystalline fraction of < 1 wt%. The most frequent crystalline phase identified by XRD was spinel.

Crystal formation during the LAW CCC slow cooling profile showed the formation of two primary crystalline phases, Na-Al silicate and Na-Ca (including Na-Ca-Al) silicate groups, both recognized as exerting a significant adverse impact on glass durability (PCT and VHT). CCC crystal constraints were previously developed to avoid these crystalline phases, however they were not included in matrix design. A total of 90% of the glasses met the CaO CCC crystal constraints, and 60% met the Al_2O_3 CCC crystal constraints. Only two glasses failed both constraints (Table 3.2). Three of the 20 glasses predicted to avoid the alumino silicate phase were found to form them. Applying the nepheline constraint from Lu et al. 2021 accurately predicted formation of nepheline in all glasses forming nepheline or other alumino-silicates in this matrix.

Among all 20 glass compositions tested by isothermal heat-treatment, seven compositions showed no crystal phases at or above 950 °C and the rest formed a variety of crystals, with Na containing ones being the more frequent. The high frequency of sodium aluminum silicate phases is not surprising since the glass matrix was designed to push the Na content boundaries.

Glass densities were measured, and the results fell within the range of LAW glasses found in the literature. Measurements were compared to predictions using Vienna et al. (2002 and 2009) models. Both models provide reasonably accurate density predictions, with increased scatter observed for the Vienna et al. (2009) model.

The SO_3 solubility was determined using the 3TS method developed by Jin et al. (2019). Overall, the observed values fall within the range of melter SO_3 tolerance. Measured vs. predicted values calculated using the Vienna et al. (2022) model were shown to be in good agreement, demonstrating that the model correctly predicts in this LAW and DFHLW high Na_2O and K_2O compositional space.

Measured η_{1150} ranged between 1.05 and 4.93 Pa-s. All of the glasses met the WTP upper limit of < 8 Pa-s, though 55% of the glasses were below the lower limit of 2 Pa-s, which is expected since the matrix was designed to push the Na boundary and alkali are known to decrease viscosity by breaking bridging bonds between silica and other glass formers to create more non-bridging oxygens (Wang et al. 2013). The η_{1150} values interpolated from measured data were compared to predicted viscosity values calculated using the Vienna et al. (2022) η_{1150} model. Overall, good agreement between predicted and measured η_{1150} values was observed, with a few glasses slightly above or below the 45° line, but no significant outliers.

EC at 1150 °C ranged between 40.8 and 101.8 S/m, 3 glasses had values higher than the WTP limits of $20 \leq EC_{1150} \leq 70$ S/m. This result is expected since alkali are the primary charge carriers for these glasses and

thus increasing alkali leads to a higher EC and EC wasn't constrained during glass design. When compared to predictions calculated using the Vienna et al. (2022) EC model, the majority of the glasses sat on both sides of the 45° line, falling reasonably close to the line, except for two glasses that were measured to be significantly higher than predicted, possibly due to crystal formation.

Most of the quenched glasses performed poorly in the PCT durability test, exceeding the contract limit in one or two of the components (B, Na, Li, and Si). Of the 20 CCC glasses, only two had NL values below the LAW contract limit for B and Na. Although high PCT release values are often linked to crystallization that removes network formers and reduces durability, this matrix showed little correlation: of the nine glasses exceeding the NL_B limit, only one contained a significant Na-Al silicate crystalline phase at 41.48 wt%, while others had only minor crystal quantities close to or less than 1 wt%. Likewise, alkali content alone does not appear to explain the poor durability of this glass matrix – some glasses with intermediate $Na_2O + K_2O$ content performed worst. Average $\ln(NL_B)$ and $\ln(NL_{Na})$ values were plotted against model predictions from Vienna et al. (2024). All LAWHNK glasses were designed to have a release at or near the PCT limit of 2.0 g/m^2. Visually, the model adequately predicts the $\ln(NL_B)$ releases within model uncertainty except for LAWHNK-18. The model also adequately predicts the $\ln(NL_{Na})$ releases within model uncertainty except for the cases of LAWHNK-07, LAWHNK-18, and LAWHNK-19. Of the cases where the model prediction is not within agreement with the measured value, the model overpredicts the test response, which demonstrates that the model predictions are conservative.

Most of the glasses failed VHT, likely due to the presence of crystals in both Q and CCC glasses, and the high amounts of alkali (Na_2O and K_2O) in the glass compositions. The main crystallinity phases found in the Q glasses were Zn-Fe-Cr and/or Sn containing oxides. VHT results for Q glasses were transformed into pass/fail binary responses determined from measured alteration rates and compared to the Vienna et al. (2022) binary model. All the glasses were predicted to fail, but two passed the test, demonstrating the model's conservative nature.

Overall, the Vienna et al. (2022) models appear to predict well in the high Na and K compositional space, although additional effort is likely required to control crystallinity in this composition region, as that wasn't adequately predicted (Table 4.1).

Table 4.1. Summary of the 20 LAWHNK glasses passing or failing property constraints. Property constraints were taken from Vienna et al. (2025).

z	w_{SO3}	η_{1150}	ε_{1150}	PCT Q	PCT CCC	VHT Q	VHT CCC	Isothermally	Isothermally	CCC	Pred NP F/P	Meas NP F/P
Constraints	SO_3 in glass < w_{SO3}	20 to 80 Poise	12 to 59 S/m	<2 g/m^2	<2 g/m^2	< 50 g m^{-2} d^{-1}	< 50 g m^{-2} d^{-1}	Formed Sn Crystals	Formed >1 vol% Zr Crystals	Formed Na-Al Crystals	Model Predicted Nepheline Formation	Measured Nepheline Formation
LAWHNK-01	P	F	P	P	F	F	F	P	P	F	F	F
LAWHNK-02	P	P	P	F	F	F	F	F	F	F	F	F
LAWHNK-03	P	P	F	F	F	F	F	P	P	F	F	F
LAWHNK-04	P	P	F	P	F	P	F	F	F	F	F	F
LAWHNK-05	F	F	P	F	F	F	F	F	P	P	P	P
LAWHNK-06	P	P	F	P	F	F	F	F	P	F	F	F
LAWHNK-07	P	P	F	P	F	F	P	P	P	F	F	F
LAWHNK-08	P	F	F	P	F	F	F	F	F	F	F	F
LAWHNK-09	P	F	P	F	F	F	P	P	P	F	F	F
LAWHNK-10	P	F	F	F	F	F	F	P	P	P	P	P
LAWHNK-11	P	P	P	F	F	F	F	P	P	P	P	P
LAWHNK-12	P	P	P	P	F	F	F	P	P	P	P	P
LAWHNK-13	P	F	F	F	F	F	F	F	P	F	P	F
LAWHNK-14	P	P	P	P	P	F	F	F	P	F	P	P
LAWHNK-15	P	F	F	F	F	F	F	P	P	P	P	P
LAWHNK-16	F	F	P	P	F	F	F	F	P	F	F	F
LAWHNK-17	P	F	P	P	F	F	F	F	P	F	P	P
LAWHNK-18	P	F	F	P	P	P	F	P	P	P	P	P
LAWHNK-19	P	F	F	F	F	F	F	P	P	P	P	P
LAWHNK-20	P	P	P	P	F	F	F	P	P	F	P	F
Total F	2	11	10	9	18	18	18	9	3	13	9	11

5.0 References

10 CFR 830, Subpart A, *Quality Assurance Requirements*. Code of Federal Regulations.

ASTM C1285, *Standard Test Methods for Determining Chemical Durability of Nuclear, Hazardous, and Mixed Waste Glasses and Multiphase Glass Ceramics: The Product Consistency Test (PCT)*. ASTM International, West Conshohocken, PA.

ASTM C1663, *Standard Test Method for Measuring Waste Glass or Glass Ceramic Durability by Vapor Hydration Test*. ASTM International, West Conshohocken, PA.

ASTM C1720, *Standard Test Method for Determining Liquidus Temperature of Immobilized Waste Glasses and Simulated Waste Glasses*. ASTM International, West Conshohocken, PA.

Bunnell, L. R. 1988. *Laboratory Work in Support of West Valley Glass Development.* Prepared for the U.S. Department of Energy under Contract DE-AC06-76RLO 1830, Pacific Northwest Laboratory, PNL-6539, UC-510, Richland, WA.

Crum J. V., T. B. Edwards, R. L. Russell, P. J. Workman, M. J. Schweiger, R. F. Schumacher, D. E. Smith, D. K. Peeler, and J. D. Vienna. 2012. "DWPF Startup Frit Viscosity Measurement Round Robin Results." *Journal of the American Ceramic Society*, 95 (7): 2196-2205.

DOE Order 414.1D, Quality Assurance. U.S. Department of Energy, Washington, D.C.

DOE. 2000. *Design, Construction, and Commissioning of the Hanford Tank Waste Treatment and Immobilization Plant*. Contract DE-AC27-01RV14136, as amended, U.S. Department of Energy, Office of River Protection, Richland, WA.

Ezz Eldin FM, and NA El Alaily. 1998. "Electrical conductivity of some alkali silicate glasses." *Materials Chemistry and Physics*, 52 (2): 175-179.

Fox, K. M., and M. D. Fowley. 2016. D. H. Miller Crystal Accumulation in the Hanford Waste Treatment Plant High Level Waste Melter: Summary of FY2016 Experiments. Savannah River National Laboratory, SRNL-STI-2016-00644, Aiken, S.C.

Jin, T., D. Kim, L. P. Darnell, B. L. Weese, N. L. Canfield, M. Bliss, M. J. Schweiger, J. D. Vienna, and A. A. Kruger. 2019. "A crucible salt saturation method for determining sulfur solubility in glass melt." *International Journal of Applied Glass Science* 10 (1): 92-102.

Joseph, R., E. Gui, and S. Ba. 2015. "Maximum Projection Designs for Computer Experiments." *Biometrika* 102 (2): 371-380.

Kim, D. S., D. Peeler, and P. Hrma. 1995. "Effect of Crystallization on the Chemical Durability of Simulated Nuclear Waste Glasses." *Environmental Issues and Waste Management Technologies in the Ceramic and Nuclear Industries*, 177-186.

Kroll, J. O., Z. J. Nelson, C. H. Skidmore, D. A. Dixon, and J. D. Vienna. 2019. "Formulation of High-Al_2O_3 Waste Glasses from Projected Hanford Waste Compositions and Assessment of Current Glass Property Models." *Journal of Non-Crystalline Solids* 517: 17-25.

Lonergan, C. E., J.L. George, D. A. Cutforth, T. Jin, P. Cholsaipant, S. E. Sannoh, C. H. Skidmore, B. A. Stanfill, S. K. Cooley, G. F. Piepel, R. L. Russell, J. D. Vienna. 2020. *Enhanced Hanford Low-Activity Waste Glass Property Data Development (Phase 3)*. Pacific Northwest National Laboratory, PNNL-29847. Richland, WA

Lonergan, C.E., D.S. Kim, and J.D. Vienna. 2021. *Crystallization Constraints for WTP LAW Operations: Assessment of CCC Impacts on VHT and PCT*, PNNL-31138, Pacific Northwest National Laboratory, Richland, WA.

Lu, X., Sargin I., and Vienna J. D. 2021. "Predicting nepheline precipitation in waste glasses using ternary submixture model and machine learning." *Journal of the American Ceramic Society*. 2021; 104: 5636–5647.

Lu, X., J. D. Vienna, and P. Ferkl. 2024. *Evaluation of DFHLW EWG Formulations and Processing Rates*. Pacific Northwest National Laboratory, PNNL-36196. Richland, WA

Maji, B. K., J. Hrudananda, and R. Asuvathraman. 2016. "Electrical conductivity and glass transition temperature (Tg) measurements on some selected glasses used for nuclear waste immobilization," *Journal of Non-Crystalline Solids*, 434: 102-107.

Mellinger, G. B. and J. L. Daniel. 1984. *Approved Reference and Testing Materials for Use in Nuclear Waste Management Research and Development Programs*. Pacific Northwest Laboratory, PNL-4955-2, Richland, WA.

Muller, I. S., H. Gan, K. Gilbo, I. L. Pegg, and I. Joseph. 2015. *LAW Glass Property-Composition Models for K-3 Refractory Corrosion and Sulfate Solubility*. Vitreous State Laboratory, The Catholic University of America, VSL-15R3270-1, Washington, D.C.

Muller, I. S., K. Gilbo, I. Joseph, and I. L. Pegg. 2014. *Enhanced LAW Glass Property-Composition Models—Phase 1*. Vitreous State Laboratory, The Catholic University of America, VSL-13R2940-1, Washington, DC.

Muller, I. S., W. K. Kot, H. K. Pasieka, K. Gilbo, F. C. Perez-Cardenas, I. Joseph, and I. L. Pegg. 2012. *Compilation and Management of ORP Glass Formulation Database*. Vitreous State Laboratory, The Catholic University of America, VSL-12R2470-1 (ORP-53934), Washington, D.C.

NQA-1-2012, *Quality Assurance Requirements for Nuclear Facility Applications*. American Society of Mechanical Engineers, New York, NY.

Ojovan, M. I., A. Pankov, and W. E. Lee. 2006. "The ion exchange phase in corrosion of nuclear waste glasses." *Journal of Nuclear Materials*, 358 (1): 57-68.

Perez, J. M. 2006. "Practical and Historical Bases for a Glass Viscosity Range for Joule-Heater Ceramic Melter Operation." Email to J. D. Vienna, Dec. 22, 2006. River Protection Project, Hanford Waste Treatment and Immobilization Plant, CCN: 150054, Richland, WA.

Piepel, G. F., S. K. Cooley, I. S. Muller, H. Gan, I. Joseph, and I. L. Pegg. 2007. *ILAW PCT, VHT, Viscosity, and Electrical Conductivity Model Development*. Vitreous State Laboratory, The Catholic University of America, VSL-07R1230-4, Rev. 0, ORP-56502, Washington, D.C.

Russell, R. L., V. Gervasio, X. Lu, S. Chong, J. T. Reiser, N. L. Canfield, J. L. George, N. A. Lumetta, J. Neeway, L. M. Seymour. 2025. *Direct Feed High Level Waste APPS Model Glass Testing (DFHLW APPS) Matrix, Phase 2*. Pacific Northwest National Laboratory, PNNL-37506, Richland, WA.

Skidmore, C. H., J. D. Vienna, T. Jin, D. Kim, B. A. Stanfill, K. M. Fox, and A. A. Kruger. 2019. "Sulfur solubility in low activity waste glass and its correlation to melter tolerance." *International Journal of Applied Glass Science*, 10 (4): 558-568.

Smith, G. L. 1993. *Characterization of Analytical Reference. Glass-1 (ARG-1)*. Pacific Northwest Laboratory, PNL-8992, Richland, WA.

Vienna, J. D., A. Fluegel, D. S. Kim, and P. Hrma. 2009. *Glass Property Data and Models for Estimating High-Level Waste Glass Volume*. Pacific Northwest National Laboratory, PNNL-18501, Richland, WA.

Vienna, J. D., A. Heredia-Langner, S. K. Cooley, A. E. Holmes, D. S. Kim, and N. A. Lumetta. 2022. *Glass Property-Composition Models for Support of Hanford WTP LAW Facility Operation*. Pacific Northwest National Laboratory, PNNL-30932, Rev. 2, Richland, WA.

Vienna, J. D., and D. S. Kim. 2014. *Preliminary IHLW Formulation Algorithm Description*. River Protection Project, Hanford Tank Waste Treatment and Immobilization Plant, 24590-HLW- RPT-RT-05-001, Rev. 1, Richland, WA.

Vienna, J. D., D. Kim, and P. Hrma. 2002. *Database and Interim Glass Property Models for Hanford HLW and LAW Glasses*. Pacific Northwest National Laboratory, PNNL-14060, Richland, WA.

Wang, J., J. Cheng, and Z. Deng. 2013. "Effect of alkali metal oxides on viscosity and crystallization of the $MgO–Al_2O_3–SiO_2$ glasses." *Physica B: Condensed Matter*, 415: 34-37.

Appendix A – Optical Images of Fabricated Glasses

This appendix presents optical images of the fabricated LAWHNK glasses. Details on batching and melting are in Section 2.1.



Figure A.1. Photograph of LAWHNK-01 after the second melt.



Figure A.2. Photograph of LAWHNK-02 after the second melt.



Figure A.3. Photograph of LAWHNK-03 after the second melt.



Figure A.4. Photograph of LAWHNK-04 after the second melt.



Figure A.5. Photograph of LAWHNK-05 after the second melt.



Figure A.6. Photograph of LAWHNK-06 after the second melt.



Figure A.7. Photograph of LAWHNK-07 after the second melt.



Figure A.8. The photograph of LAWHNK-08 after the second melt. A picture after the third and final melt was not taken.



Figure A.9. Photograph of LAWHNK-09 after the third melt.



Figure A.10. Photograph of LAWHNK-10 after the second melt.



Figure A.11. Photograph of LAWHNK-11 after the second melt.



Figure A.12. Photograph of LAWHNK-12 after the second melt.



Figure A.13. Photograph of LAWHNK-13 after the second melt.



Figure A.14. Photograph of LAWHNK-14 after the second melt.

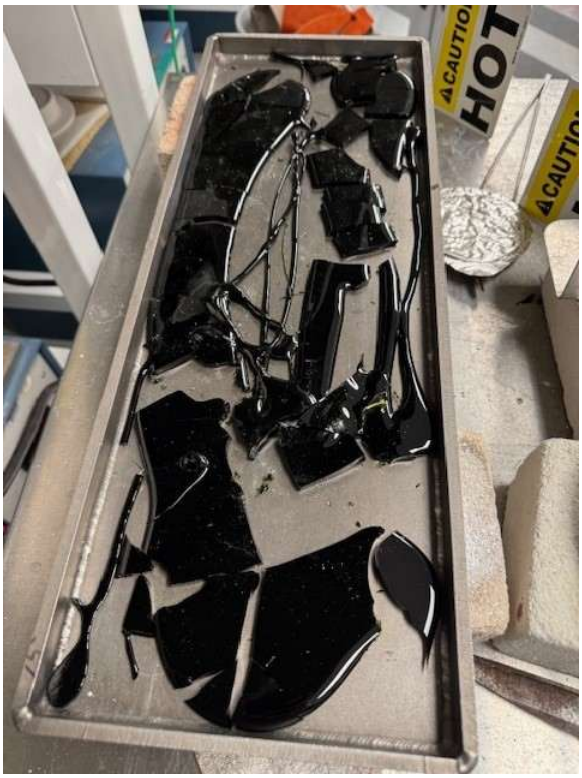


Figure A.15. Photograph of LAWHNK-15 after the second melt.



Figure A.16. Photograph of LAWHNK-16 after the second melt.



Figure A.17. Photograph of LAWHNK-17 after the second melt.



Figure A.18. Photograph of LAWHNK-18 after the second melt.



Figure A.19. Photograph of LAWHNK-19 after the second melt.

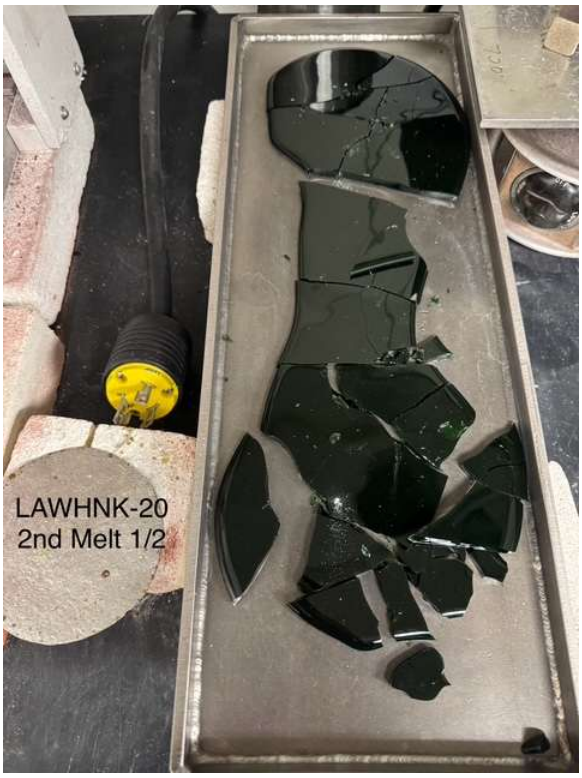


Figure A.20. Photograph of LAWHNK-20 after the second melt.

Appendix B – Target and Measured Composition of Fabricated Glasses

The tables in this appendix provide the target glass compositions, the analyzed glass compositions, and the relative percent differences.

Table B.1. Target and analyzed (ICP-OES) compositions of LAWHNK glasses. Shadowed cells highlight main components (> 1 wt%) with a %RPD greater than 10.

	LAWHNK-01			LAWHNK-02			LAWHNK-03			LAWHNK-04			LAWHNK-05		
	Target wt%	Measured wt%	%RPD	Target wt%	Measured wt%	%RPD	Target wt%	Measured wt%	%RPD	Target wt%	Measured wt%	%RPD	Target wt%	Measured wt%	%RPD
Al_2O_3	12.62	12.00	-4.92	13.84	12.07	-12.77	14.23	13.60	-4.37	11.20	10.71	-4.35	6.71	6.44	-3.99
B_2O_3	8.89	7.34	-17.38	9.91	9.69	-2.23	6.20	5.83	-5.91	7.51	7.18	-4.37	10.81	10.66	-1.36
CaO	9.43	9.65	2.41	0.41	0.42	3.19	0.31	0.34	12.46	1.66	1.71	2.96	0.06	0.09	53.33
Cl	0.79	NM[(a)]		0.49	NM[(a)]		0.51	NM[(a)]		0.78	NM[(a)]		0.77	NM[(a)]	
Cr_2O_3	0.60	0.59	-2.32	0.38	0.36	-3.70	0.39	0.32	-16.92	0.60	0.57	-4.69	0.59	0.53	-11.15
F	0.17	NM[(a)]		0.11	NM[(a)]		0.11	NM[(a)]		0.17	NM[(a)]		0.17	NM[(a)]	
Fe_2O_3	0.00	0.06		2.14	2.03	-5.18	0.06	0.12	81.25	2.51	2.42	-3.82	2.41	2.37	-1.49
K_2O	0.93	0.95	2.04	3.97	3.99	0.40	2.84	2.87	1.09	2.19	2.19	0.00	3.13	3.11	-0.61
Li_2O	0.60	0.62	2.83	0.66	0.67	1.51	1.26	1.29	2.31	0.16	0.17	2.47	0.58	0.59	2.07
MgO	4.96	4.99	0.69	3.22	3.18	-1.18	6.02	6.09	1.10	2.24	2.27	1.43	4.24	4.30	1.39
Na_2O	21.08	20.22	-4.06	20.09	19.68	-2.05	21.48	20.62	-3.99	23.79	22.92	-3.69	22.77	21.84	-4.09
P_2O_5	0.30	0.32	3.95	0.19	0.19	1.57	0.20	0.21	4.06	0.30	0.31	1.33	0.30	0.31	4.35
SiO_2	30.32	28.45	-6.15	30.40	27.38	-9.92	32.42	30.16	-6.96	30.27	28.88	-4.59	33.46	31.23	-6.64
SnO_2	0.94	0.72	-24.07	4.44	3.06	-31.03	0.39	0.38	-2.05	3.69	3.09	-16.44	4.27	4.06	-4.91
SO_3	1.06	0.94	-10.94	0.67	0.66	-0.90	0.69	0.65	-5.69	1.05	1.01	-3.34	1.04	0.93	-10.28
TiO_2	3.79	3.92	3.43	1.01	1.10	8.49	1.97	2.07	4.92	0.25	0.29	17.60	3.82	3.94	2.96
V_2O_5	2.23	2.18	-2.20	4.07	3.98	-2.28	1.64	1.62	-1.46	2.45	2.39	-2.45	0.15	0.14	-3.42
ZnO	1.21	1.23	1.32	3.30	3.34	1.21	4.37	4.42	1.24	4.59	4.63	0.98	2.91	2.98	2.09
ZrO_2	0.09	0.10	12.79	0.70	0.67	-3.17	4.94	4.57	-7.51	4.59	4.43	-3.49	1.82	1.80	-1.05
Sum[(b)]	100.00	95.23		100.00	93.09		100.00	95.77		100.00	96.11		100.00	96.26	

(a) NM - not measured
(b) Includes target Cl and F.

Table B.2. Target and analyzed (ICP-OES) compositions of LAWHNK glasses. Shadowed cells highlight main components (> 1 wt%) with a %RPD greater than 10.

	LAWHNK-06			LAWHNK-07			LAWHNK-08			LAWHNK-09			LAWHNK-10		
	Target wt%	Measured wt%	%RPD	Target wt%	Measured wt%	%RPD	Target wt%	Measured wt%	%RPD	Target wt%	Measured wt%	%RPD	Target wt%	Measured wt%	%RPD
Al_2O_3	10.87	10.18	-6.31	14.05	12.21	-13.09	9.50	9.15	-3.76	9.34	8.84	-5.35	12.84	10.66	-16.98
B_2O_3	6.84	6.63	-2.98	6.44	6.09	-5.45	6.90	6.67	-3.45	6.22	5.99	-3.62	13.51	13.46	-0.33
CaO	3.62	3.72	2.93	0.82	0.83	1.09	1.52	1.58	3.81	10.89	11.14	2.25	1.26	1.26	-0.16
Cl	0.51	NM[(a)]		0.55	NM[(a)]		0.28	NM[(a)]		0.40	NM[(a)]		0.46	NM[(a)]	
Cr_2O_3	0.39	0.38	-1.81	0.42	0.41	-2.64	0.22	0.22	0.47	0.31	0.28	-8.74	0.35	0.34	-4.52
F	0.11	NM[(a)]		0.12	NM[(a)]		0.06	NM[(a)]		0.09	NM[(a)]		0.10	NM[(a)]	
Fe_2O_3	0.26	0.32	20.53	4.93	4.72	-4.20	4.70	4.53	-3.49	3.61	3.49	-3.41	1.53	1.46	-4.52
K_2O	5.70	5.67	-0.44	0.70	0.74	6.03	0.42	0.48	14.42	1.00	1.00	-0.40	3.19	3.17	-0.78
Li_2O	1.34	1.35	1.35	0.50	0.51	2.40	1.64	1.68	2.45	0.12	0.12	3.39	1.73	1.72	-0.23
MgO	0.66	0.66	0.76	2.17	2.17	0.14	5.38	5.46	1.43	8.25	8.08	-2.11	1.80	1.74	-3.49
Na_2O	20.70	19.95	-3.60	26.21	25.61	-2.29	25.50	24.26	-4.84	22.55	21.16	-6.16	20.69	19.68	-4.86
P_2O_5	0.20	0.20	4.10	0.21	0.22	5.24	0.11	0.11	5.56	0.16	0.16	3.85	0.18	0.18	1.69
SiO_2	32.78	30.59	-6.68	34.01	30.59	-10.05	33.41	31.23	-6.52	31.39	29.95	-4.58	33.61	30.38	-9.61
SnO_2	4.94	4.60	-6.89	0.54	0.54	-1.47	4.38	4.30	-1.71	0.74	0.72	-2.04	1.05	1.01	-3.99
SO_3	0.68	0.69	1.91	0.73	0.76	3.27	0.38	0.42	11.41	0.54	0.55	1.66	0.62	0.58	-5.96
TiO_2	3.02	3.10	2.85	3.37	3.57	6.00	0.85	0.91	7.08	1.49	1.55	3.90	1.73	1.82	5.27
V_2O_5	2.68	2.62	-1.94	3.57	3.52	-1.35	0.27	0.27	-2.19	1.44	1.39	-3.55	3.37	3.25	-3.48
ZnO	4.58	4.59	0.37	0.60	0.62	2.32	0.72	0.73	0.69	0.67	0.66	-0.75	1.22	1.22	0.00
ZrO_2	0.17	0.17	1.20	0.08	0.08	1.22	3.77	3.70	-1.83	0.80	0.79	-1.75	0.77	0.75	-2.98
Sum[(b)]	100.00	96.06		100.00	93.84		100.00	96.03		100.00	96.36		100.00	93.24	

(a) NM - not measured
(b) Includes target Cl and F.

Table B.3. Target and analyzed (ICP-OES) compositions of LAWHNK glasses. Shadowed cells highlight main components (> 1 wt%) with a %RPD greater than 10.

	LAWHNK-11			LAWHNK-12			LAWHNK-13			LAWHNK-14			LAWHNK-15		
	Target wt%	Measured wt%	%RPD	Target wt%	Measured wt%	%RPD	Target wt%	Measured wt%	%RPD	Target wt%	Measured wt%	%RPD	Target wt%	Measured wt%	%RPD
Al_2O_3	4.29	4.12	-3.87	8.24	7.79	-5.49	6.31	6.01	-4.82	7.61	7.28	-4.43	5.60	5.29	-5.53
B_2O_3	6.32	6.22	-1.60	9.90	9.53	-3.67	6.51	6.22	-4.56	6.57	6.44	-1.98	10.96	10.76	-1.91
CaO	1.40	1.51	8.08	2.57	2.67	4.17	4.50	4.76	5.71	0.66	0.70	7.15	0.55	0.59	5.97
Cl	0.78	NM[(a)]		0.77	NM[(a)]		0.63	NM[(a)]		0.74	NM[(a)]		0.49	NM[(a)]	
Cr_2O_3	0.59	0.57	-4.71	0.59	0.58	-1.86	0.48	0.45	-5.62	0.57	0.53	-7.21	0.38	0.36	-3.19
F	0.17	NM[(a)]		0.17	NM[(a)]		0.14	NM[(a)]		0.16	NM[(a)]		0.11	NM[(a)]	
Fe_2O_3	2.67	2.66	-0.41	5.22	5.10	-2.30	1.67	1.62	-3.41	9.85	9.12	-7.43	0.86	0.90	3.82
K_2O	3.92	3.88	-0.92	1.77	1.83	3.39	2.79	2.81	0.72	0.04	0.00	-100.00	3.40	3.41	0.15
Li_2O	0.12	0.12	3.42	1.16	1.18	1.99	1.81	1.87	3.32	1.61	1.64	1.61	1.54	1.54	0.20
MgO	5.56	5.52	-0.61	0.58	0.59	1.72	4.27	4.28	0.28	2.88	2.89	0.17	2.61	2.60	-0.23
Na_2O	20.32	19.28	-5.13	20.80	19.95	-4.07	20.56	19.95	-2.95	21.37	20.49	-4.12	21.74	21.03	-3.27
P_2O_5	0.30	0.30	0.67	0.30	0.31	2.35	0.24	0.25	3.31	0.29	0.29	0.70	0.19	0.19	1.58
SiO_2	43.60	41.50	-4.82	38.11	36.79	-3.45	36.09	34.01	-5.77	40.87	39.79	-2.65	40.00	36.15	-9.62
SnO_2	2.64	2.60	-1.25	1.10	1.07	-2.37	3.68	3.57	-3.02	3.55	3.40	-4.14	4.79	4.69	-2.27
SO_3	1.04	0.90	-13.70	1.04	1.01	-2.69	0.84	0.88	4.03	1.00	0.99	-1.40	0.66	0.66	0.30
TiO_2	3.09	3.19	3.27	2.57	2.65	3.39	1.08	1.15	5.72	0.08	0.11	38.16	1.35	1.39	3.35
V_2O_5	1.28	1.24	-2.90	3.71	3.64	-1.94	0.80	0.79	-1.38	1.32	1.29	-1.75	2.39	2.32	-2.85
ZnO	0.04	0.04	7.69	0.92	0.93	1.08	4.91	4.95	0.98	0.58	0.58	0.69	1.95	1.95	0.41
ZrO_2	1.90	1.82	-4.10	0.50	0.50	0.20	2.70	2.63	-2.37	0.26	0.26	0.78	0.44	0.43	-0.23
Sum[(b)]	100.00	96.41		100.00	97.07		100.00	96.94		100.00	96.69		100.00	94.86	

(a) NM - not measured
(b) Includes target Cl and F.

Table B.4. Target and analyzed (ICP-OES) compositions of LAWHNK glasses. Shadowed cells highlight main components (> 1 wt%) with a %RPD greater than 10.

	LAWHNK-16			LAWHNK-17			LAWHNK-18			LAWHNK-19			LAWHNK-20		
	Target wt%	Measured wt%	%RPD	Target wt%	Measured wt%	%RPD	Target wt%	Measured wt%	%RPD	Target wt%	Measured wt%	%RPD	Target wt%	Measured wt%	%RPD
Al_2O_3	10.13	9.56	-5.63	7.57	7.20	-4.94	4.82	4.71	-2.47	8.33	7.77	-6.78	10.59	10.00	-5.57
B_2O_3	9.76	9.53	-2.36	6.39	6.02	-5.70	7.46	7.34	-1.56	11.41	11.34	-0.63	12.79	12.27	-4.06
CaO	0.21	0.26	26.32	7.11	7.35	3.39	4.05	4.18	3.23	1.30	1.36	4.93	6.48	6.67	3.01
Cl	0.69	NM[(a)]		0.73	NM[(a)]		0.73	NM[(a)]		0.40	NM[(a)]		0.64	NM[(a)]	
Cr_2O_3	0.53	0.49	-7.92	0.56	0.54	-3.39	0.56	0.57	3.05	0.31	0.30	-0.98	0.52	0.51	-2.11
F	0.15	NM[(a)]		0.16	NM[(a)]		0.16	NM[(a)]		0.09	NM[(a)]		0.00	NM[(a)]	
Fe_2O_3	7.74	7.52	-2.83	4.24	3.89	-8.30	8.45	7.76	-8.16	5.16	4.99	-3.24	0.90	0.87	-3.88
K_2O	1.49	1.47	-1.21	3.78	3.76	-0.53	2.96	2.98	0.40	2.90	2.89	-0.28	0.51	0.54	5.87
Li_2O	1.79	1.81	1.23	1.33	1.35	2.19	0.73	0.74	2.21	0.39	0.39	1.82	0.00	0.00	
MgO	5.48	5.41	-1.31	0.35	0.34	-1.45	0.25	0.25	1.21	1.37	1.35	-1.68	0.90	0.91	0.89
Na_2O	20.42	19.28	-5.61	20.52	19.82	-3.42	21.90	21.30	-2.73	25.40	24.13	-4.99	23.03	22.11	-4.02
P_2O_5	0.27	0.28	2.61	0.28	0.29	2.83	0.28	0.29	1.78	0.16	0.16	2.58	0.00	0.00	
SiO_2	31.24	29.95	-4.13	32.24	30.80	-4.46	32.80	33.16	1.09	32.19	31.45	-2.30	34.85	32.94	-5.47
SnO_2	2.09	2.04	-2.25	3.82	3.72	-2.52	3.63	3.53	-2.78	3.43	3.30	-3.70	1.00	0.97	-2.70
SO_3	0.93	0.76	-17.94	0.99	1.03	4.56	0.98	1.07	9.40	0.54	0.58	8.55	0.83	0.83	-0.12
TiO_2	2.17	2.25	3.73	2.11	2.19	3.51	0.35	0.38	10.09	0.97	1.02	5.37	0.00	0.03	
V_2O_5	0.02	0.02	0.00	3.52	3.41	-3.01	3.92	3.84	-2.07	0.80	0.78	-1.63	0.97	0.95	-1.96
ZnO	3.72	3.76	0.99	2.61	2.64	1.15	0.83	0.83	0.48	3.65	3.70	1.18	2.99	3.03	1.04
ZrO_2	1.17	1.15	-1.45	1.72	1.68	-2.33	5.16	4.98	-3.35	1.24	1.21	-1.86	2.99	2.90	-3.01
Sum[(b)]	100.00	96.38		100.00	96.91		100.00	98.80		100.00	97.21		100.00	96.17	

(a) NM - not measured
(b) Includes target Cl and F.

Appendix C – XRD Data on Quenched Glasses

The refined XRD data on quenched glasses with wt% of crystalline phases are shown in this appendix. CeO_2 was added as a standard to quantify the crystalline phases. Red is calculated, and blue is experimental data. The percentage of crystals in the plots are reported before correcting for the CeO_2 standard crystallinity of 51.28%.

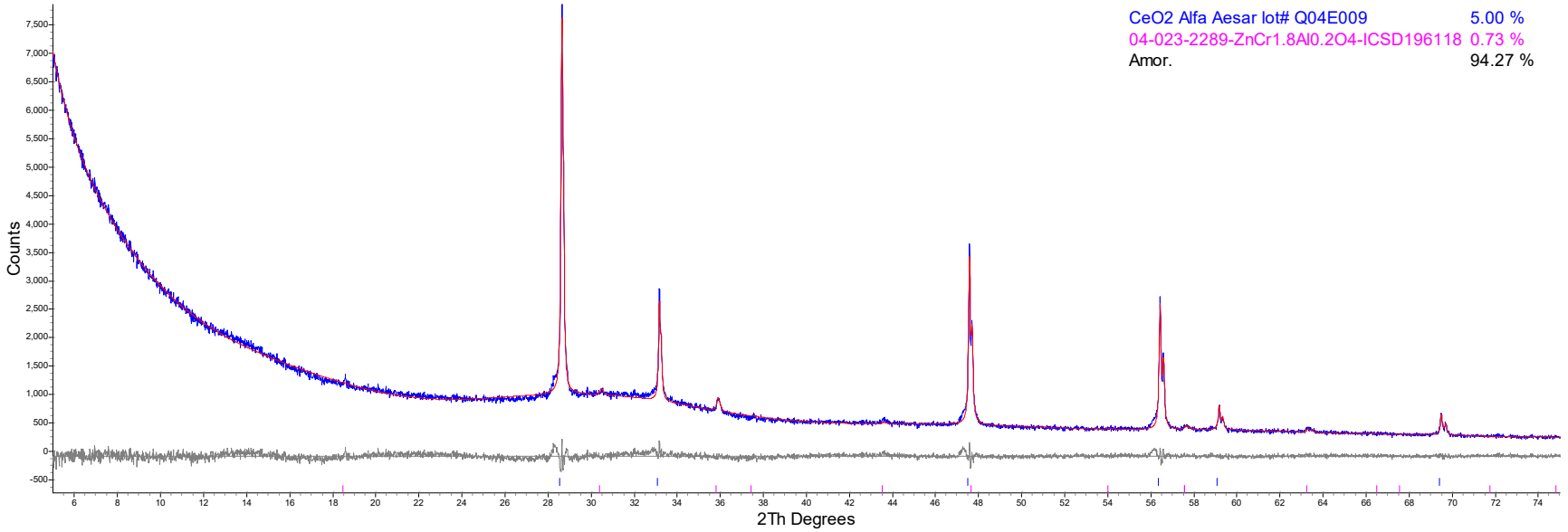


Figure C.1. Refined XRD data of LAWHNK-01.

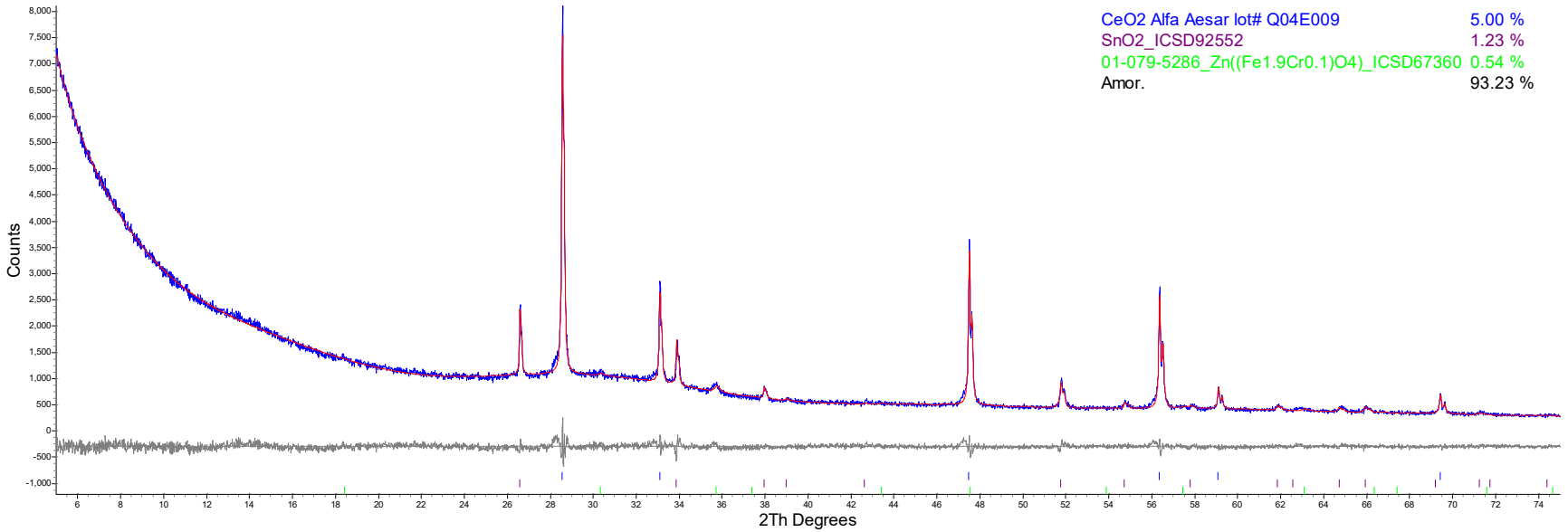


Figure C.2. Refined XRD data of LAWHNK-02.

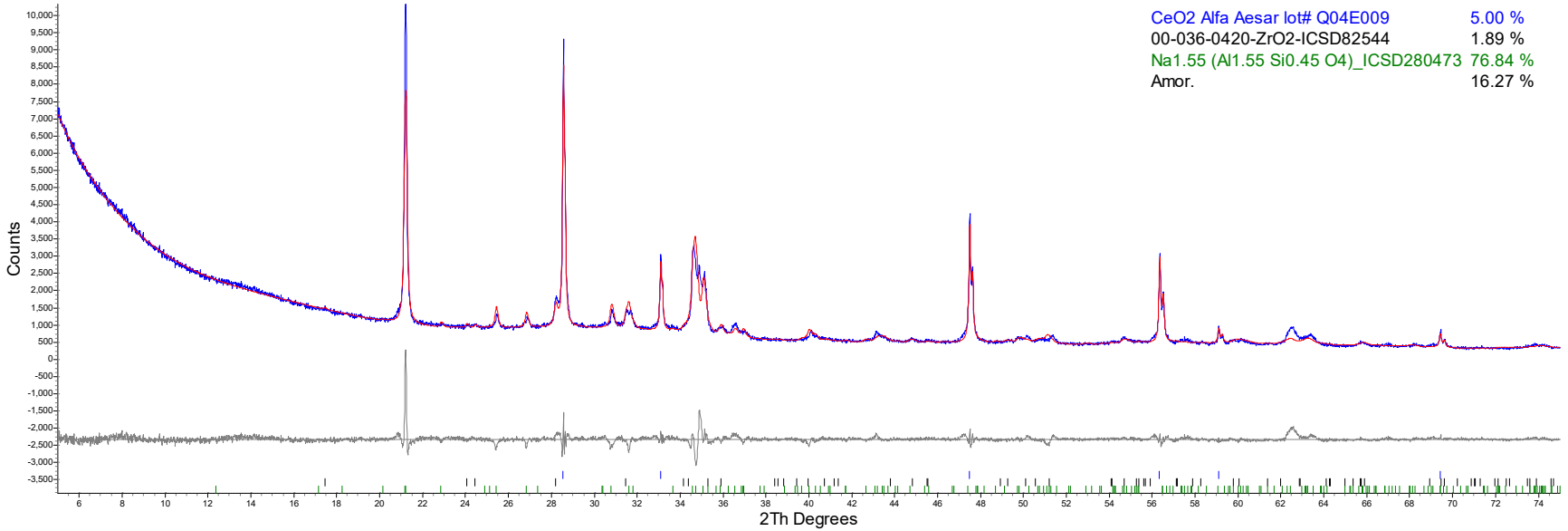


Figure C.3. Refined XRD data of LAWHNK-03.

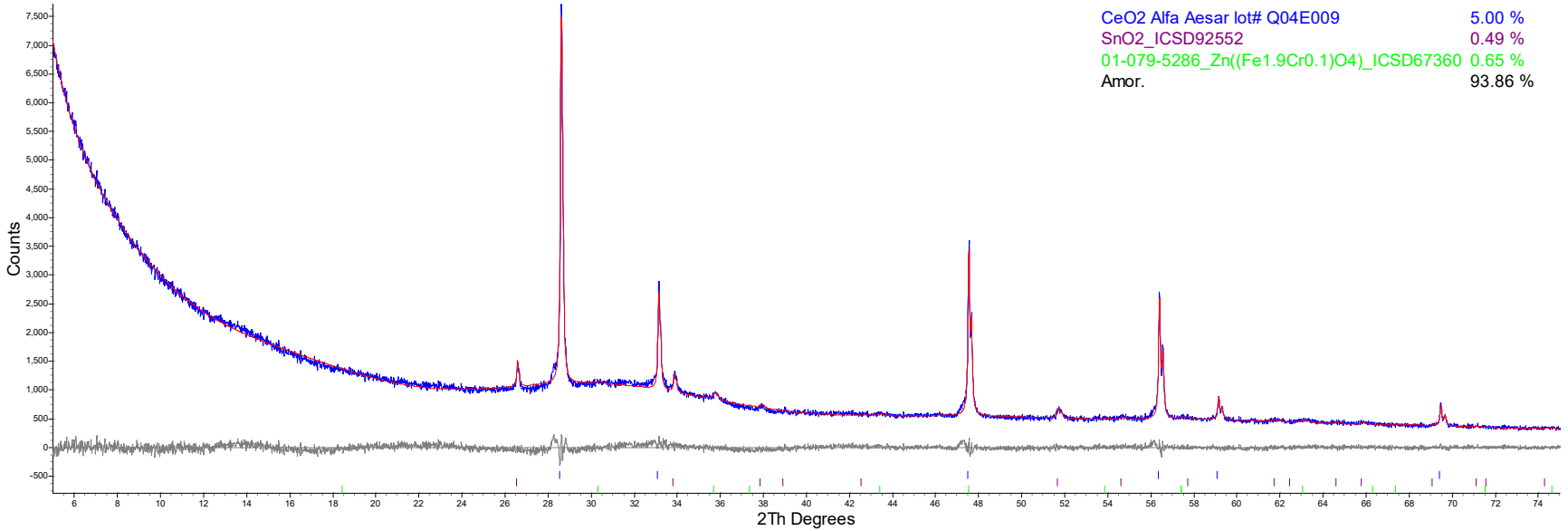


Figure C.4. Refined XRD data of LAWHNK-04.

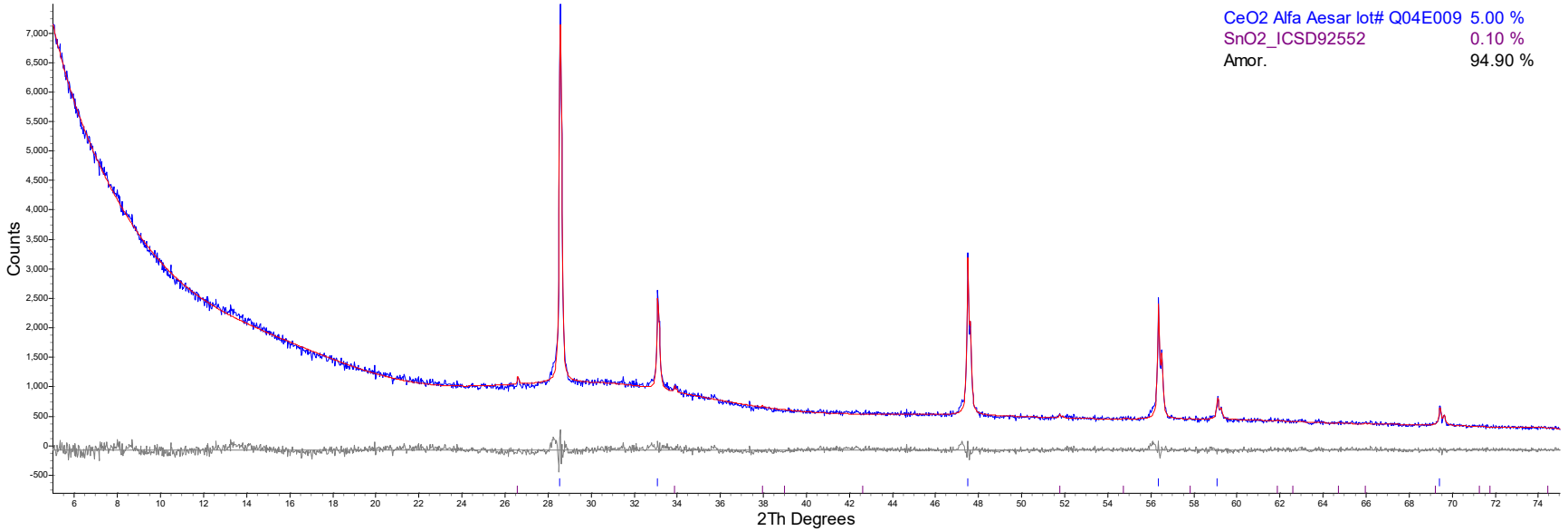


Figure C.5. Refined XRD data of LAWHNK-05.

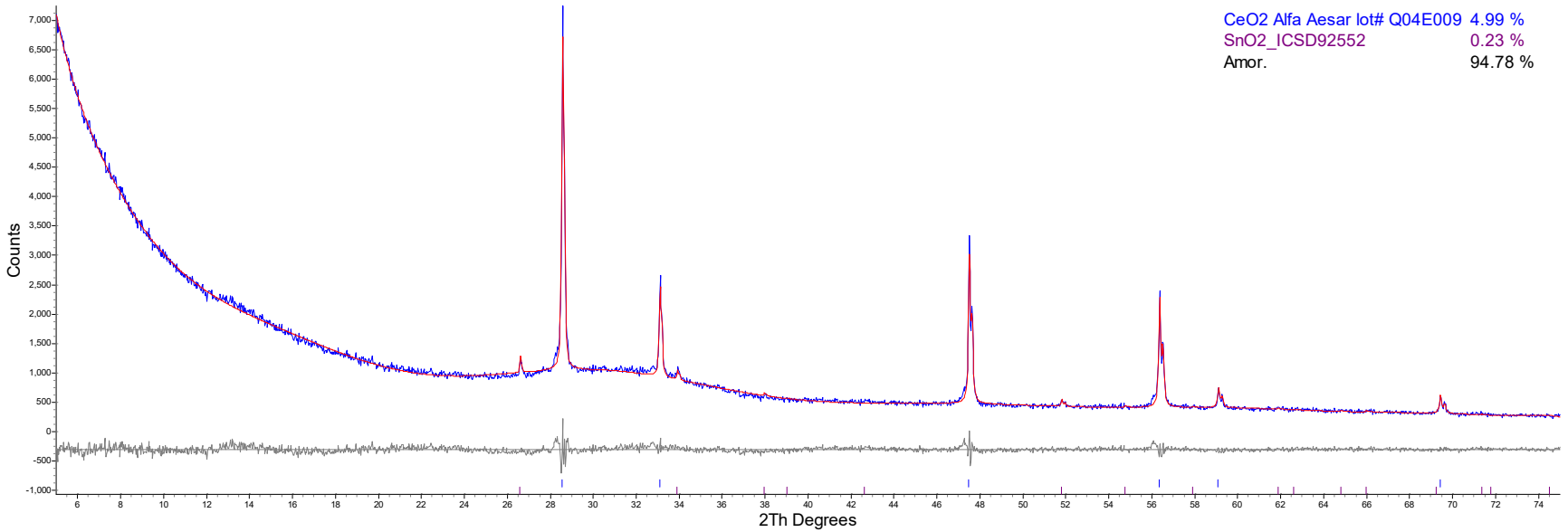


Figure C.6. Refined XRD data of LAWHNK-06.

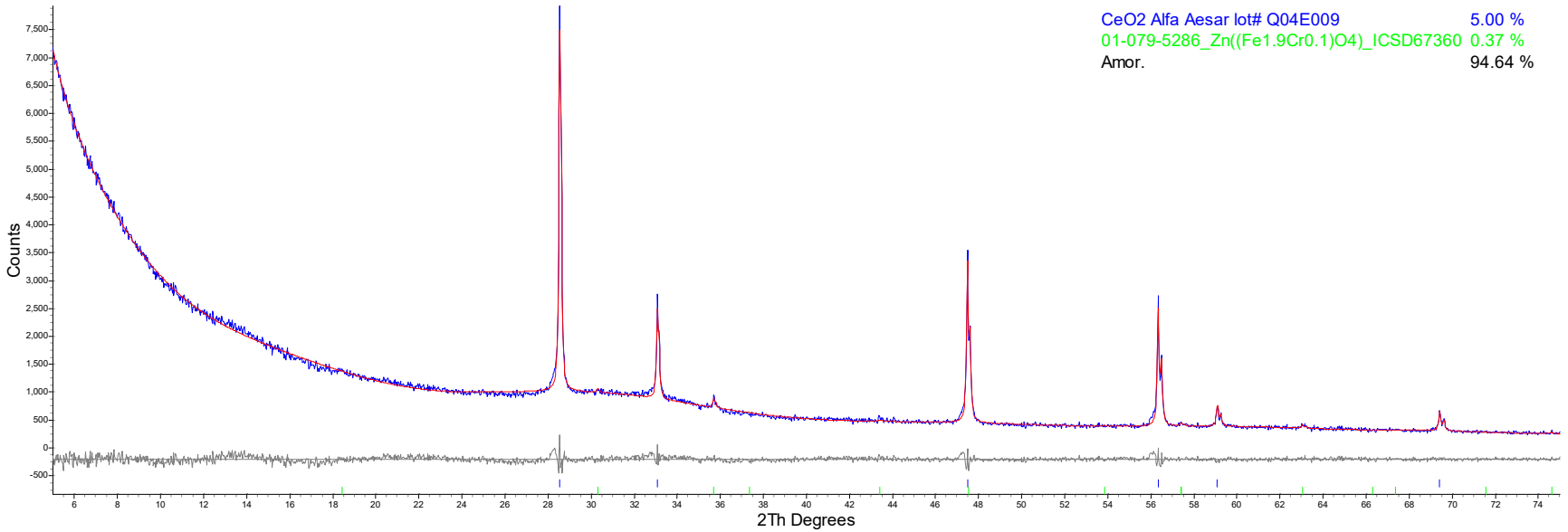


Figure C.7. Refined XRD data of LAWHNK-07.

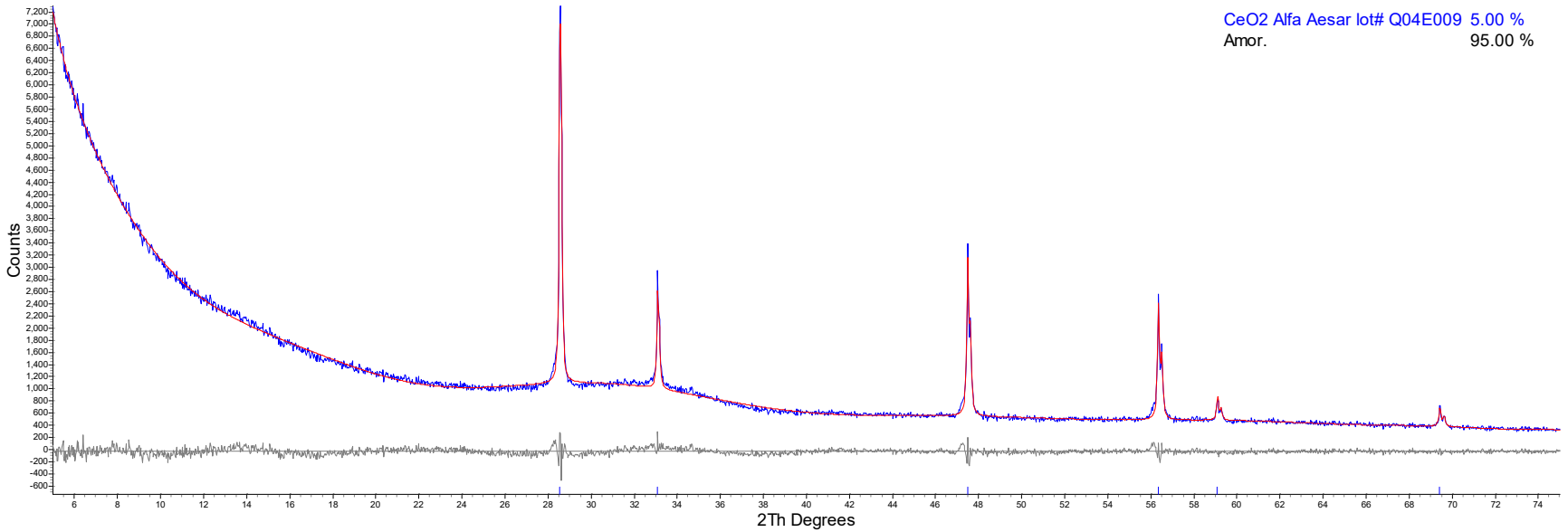


Figure C.8. Refined XRD data of LAWHNK-08.

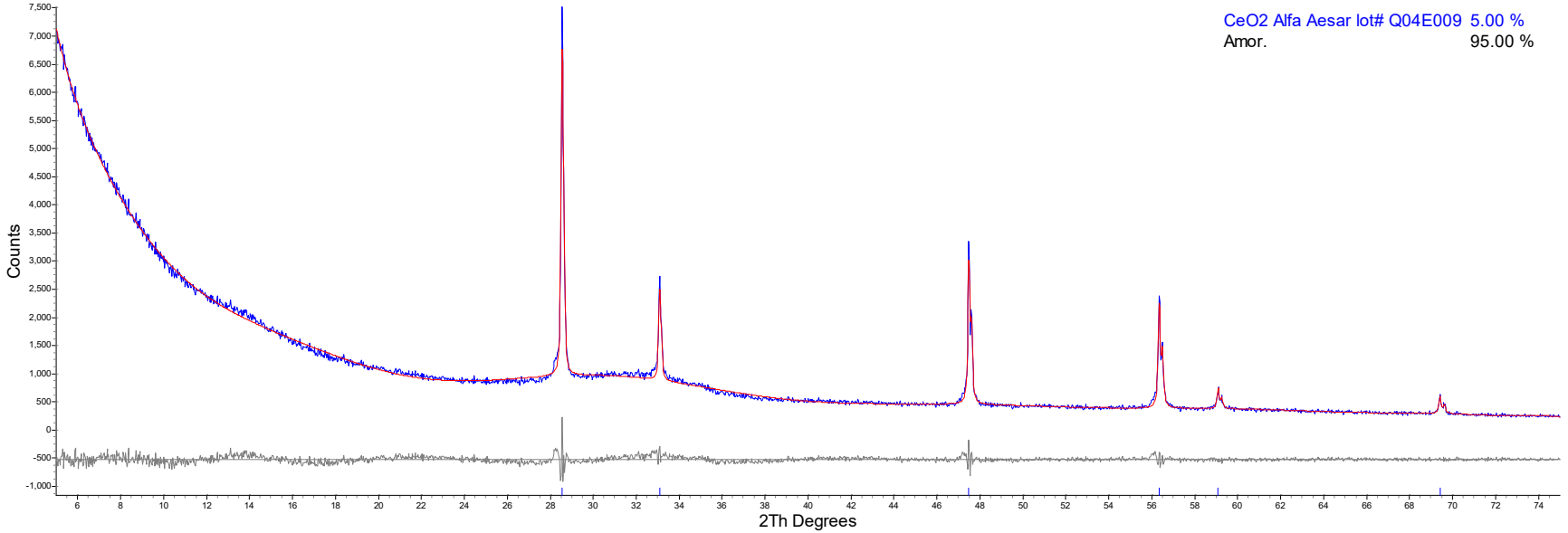


Figure C.9. Refined XRD data of LAWHNK-09.

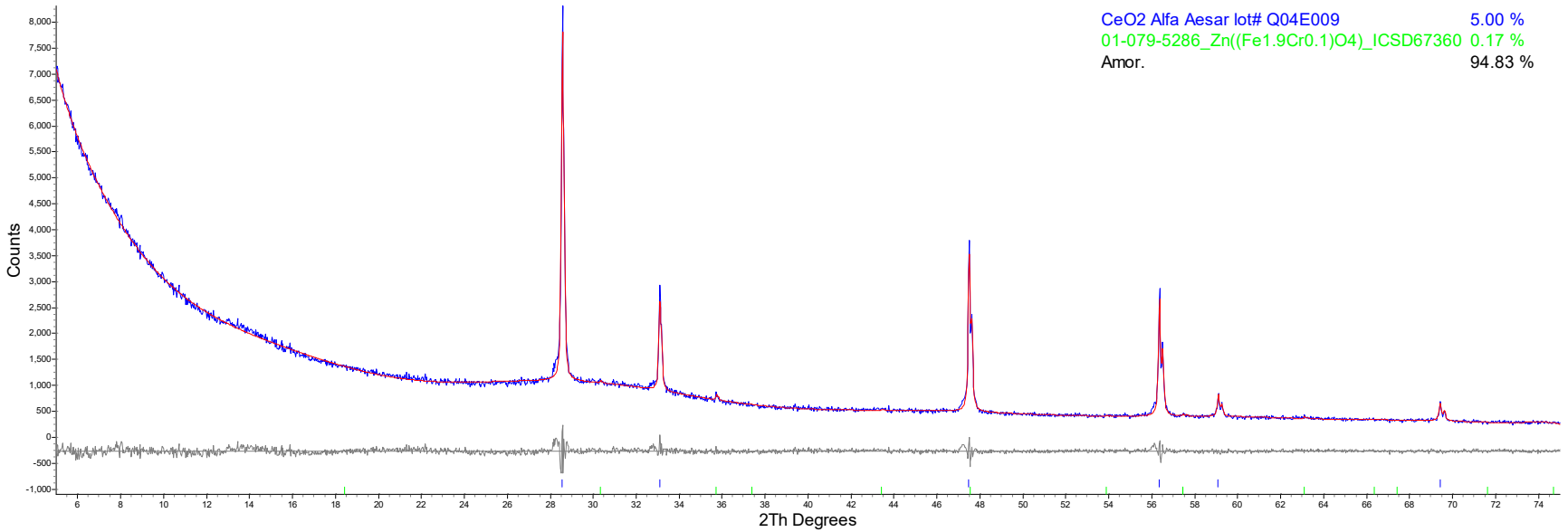


Figure C.10. Refined XRD data of LAWHNK-10.

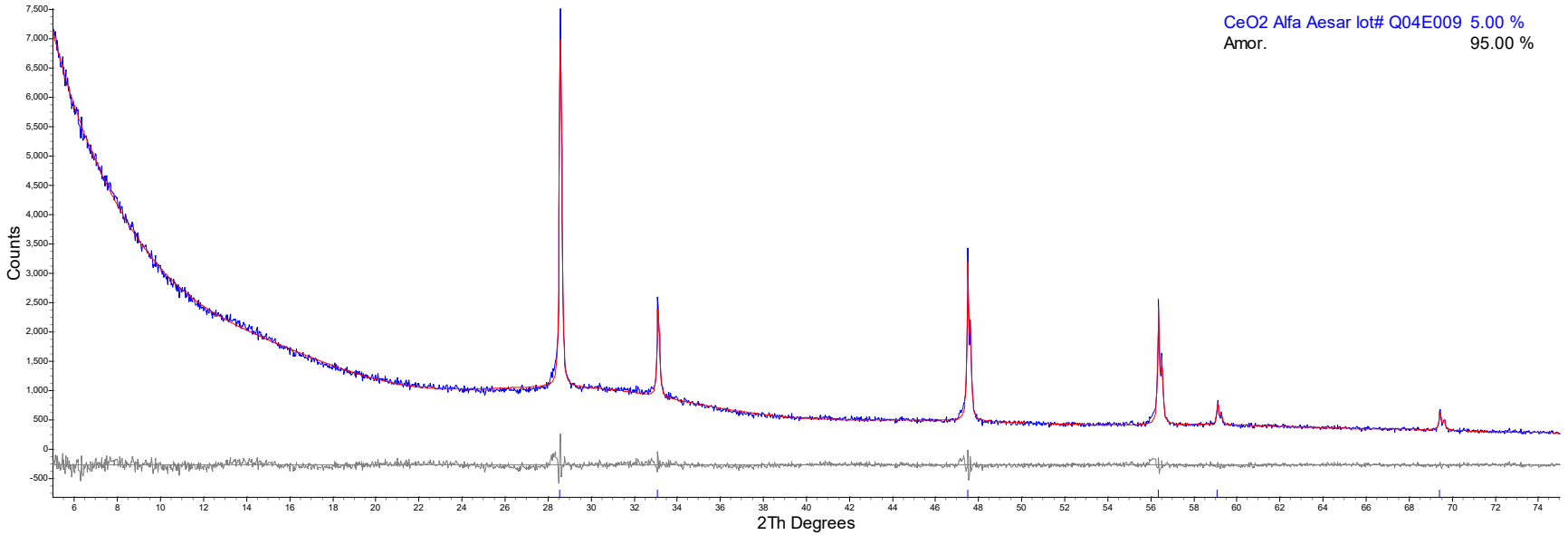


Figure C.11. Refined XRD data of LAWHNK-11.

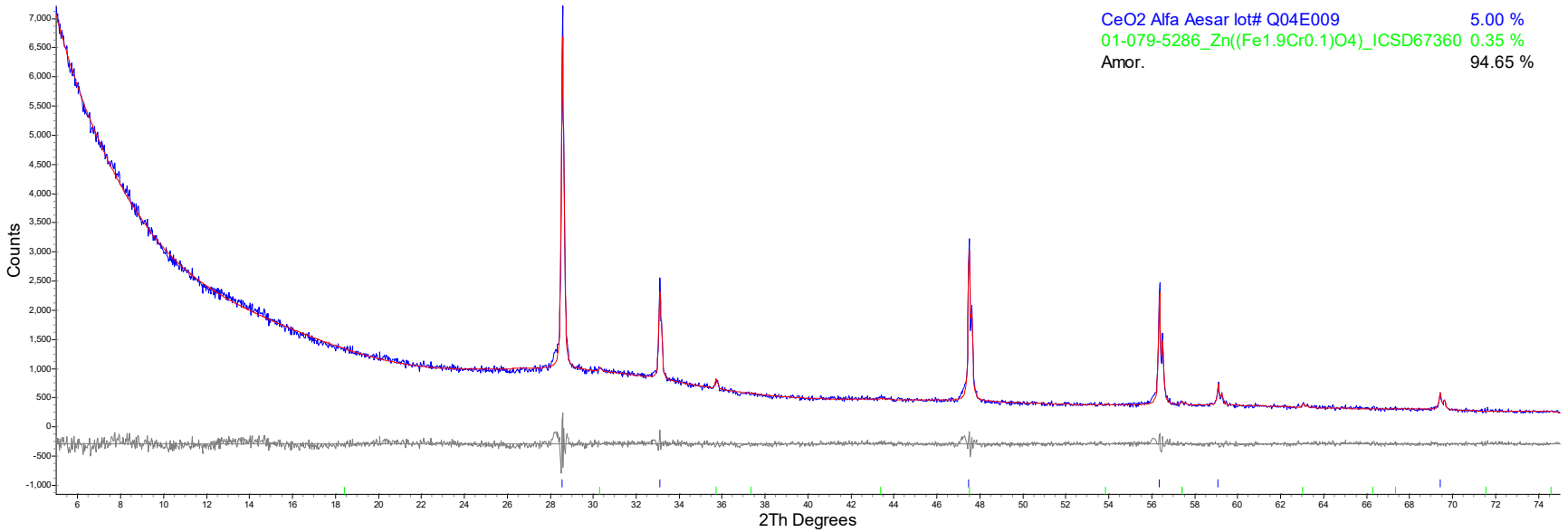


Figure C.12. Refined XRD data of LAWHNK-12.

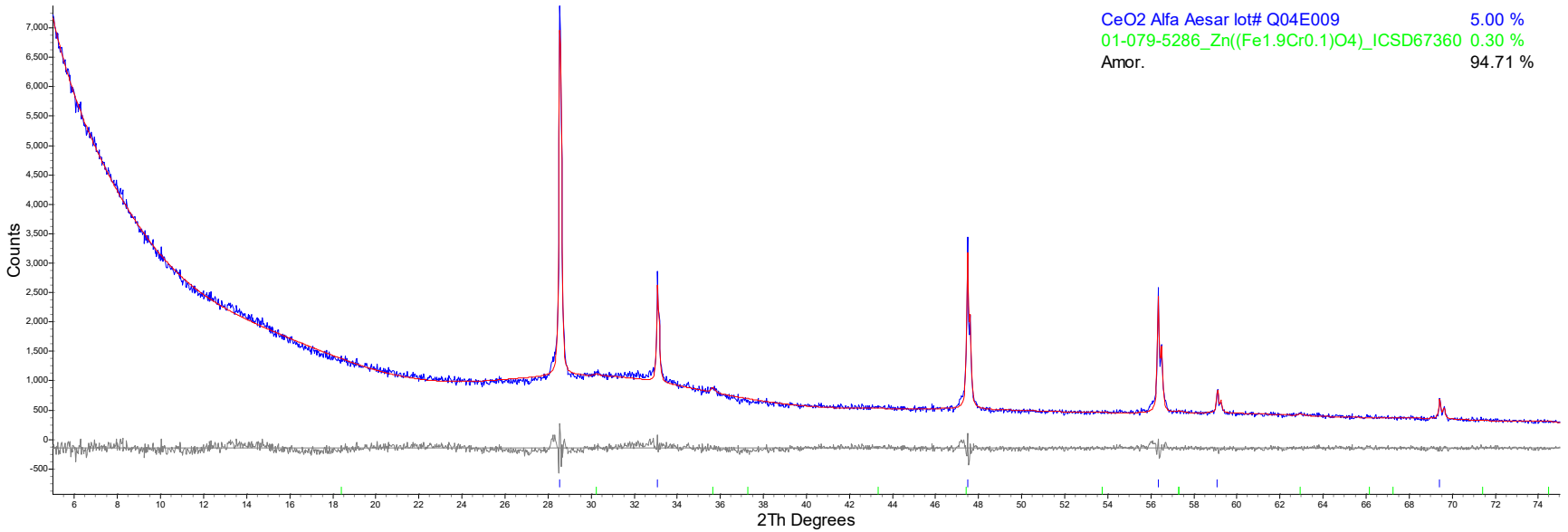


Figure C.13. Refined XRD data of LAWHNK-13.

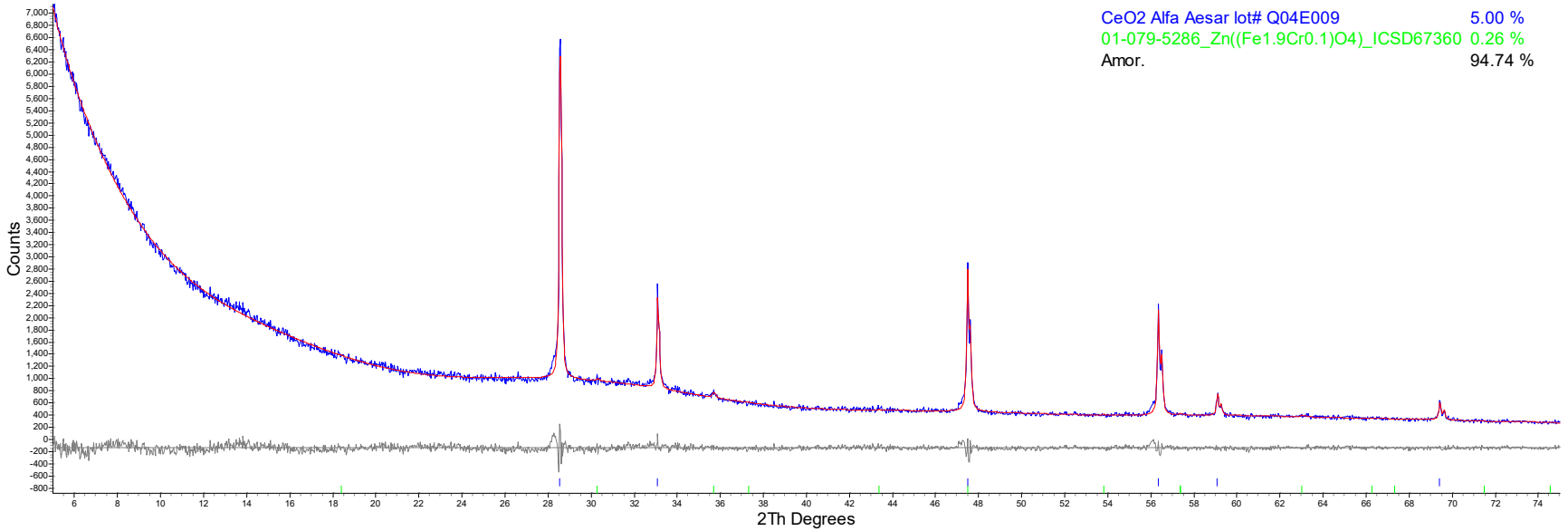


Figure C.14. Refined XRD data of LAWHNK-14-1.

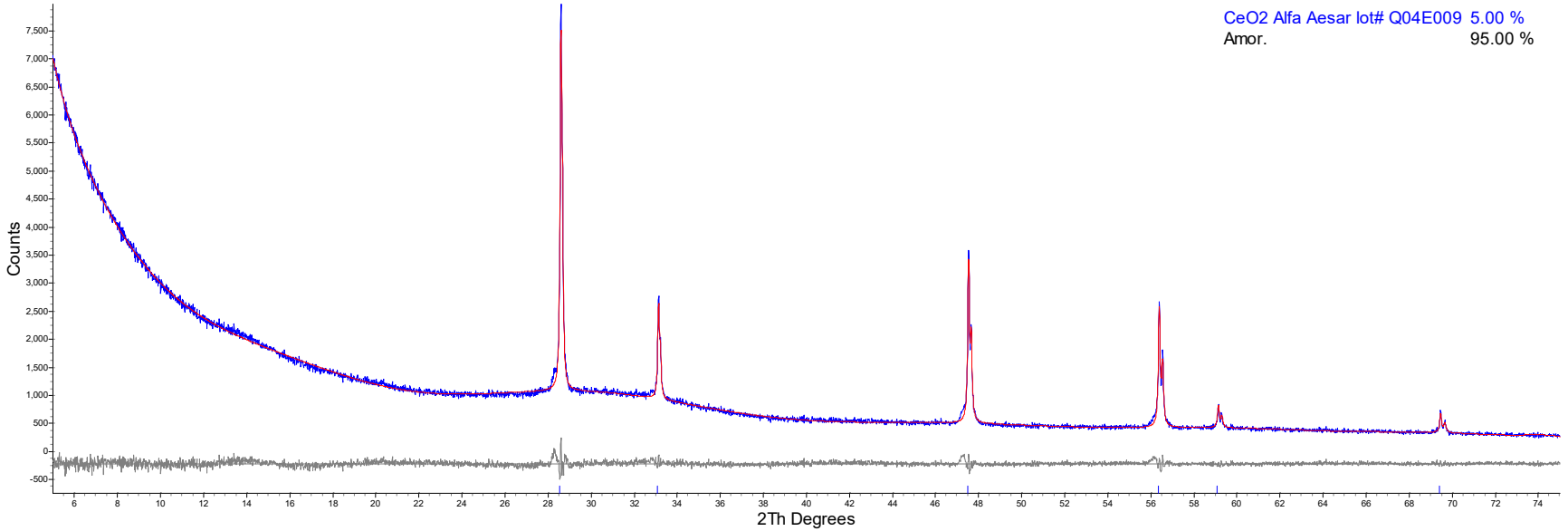


Figure C.15. Refined XRD data of LAWHNK-15.

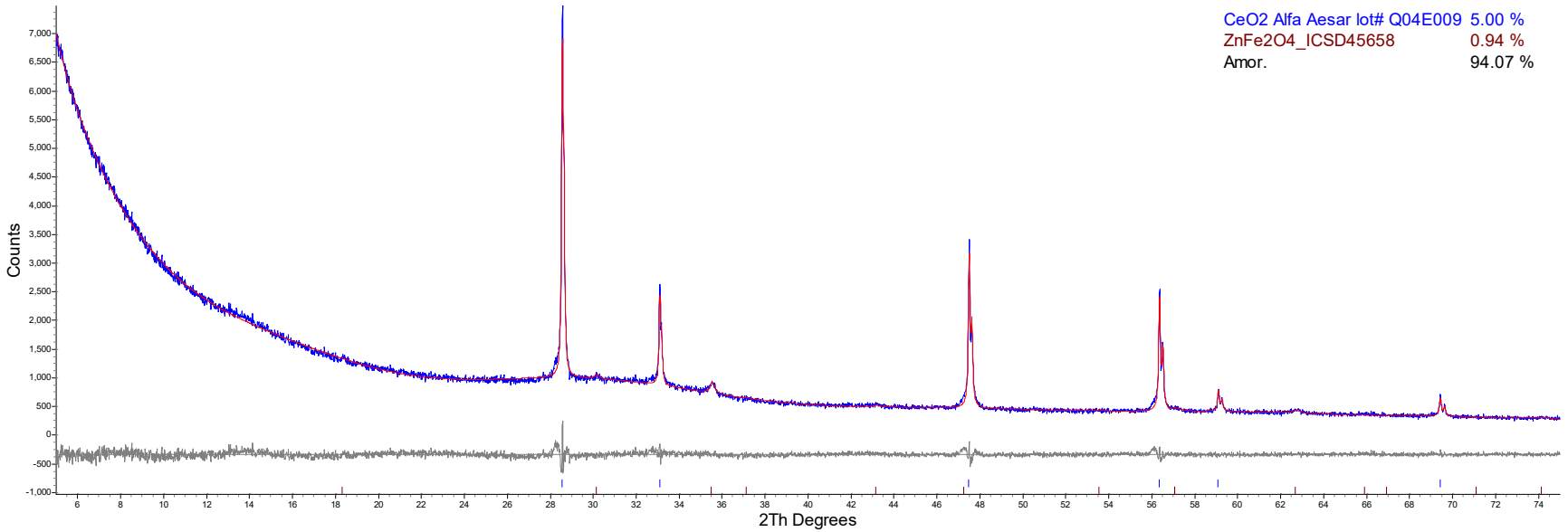


Figure C.16. Refined XRD data of LAWHNK-16.

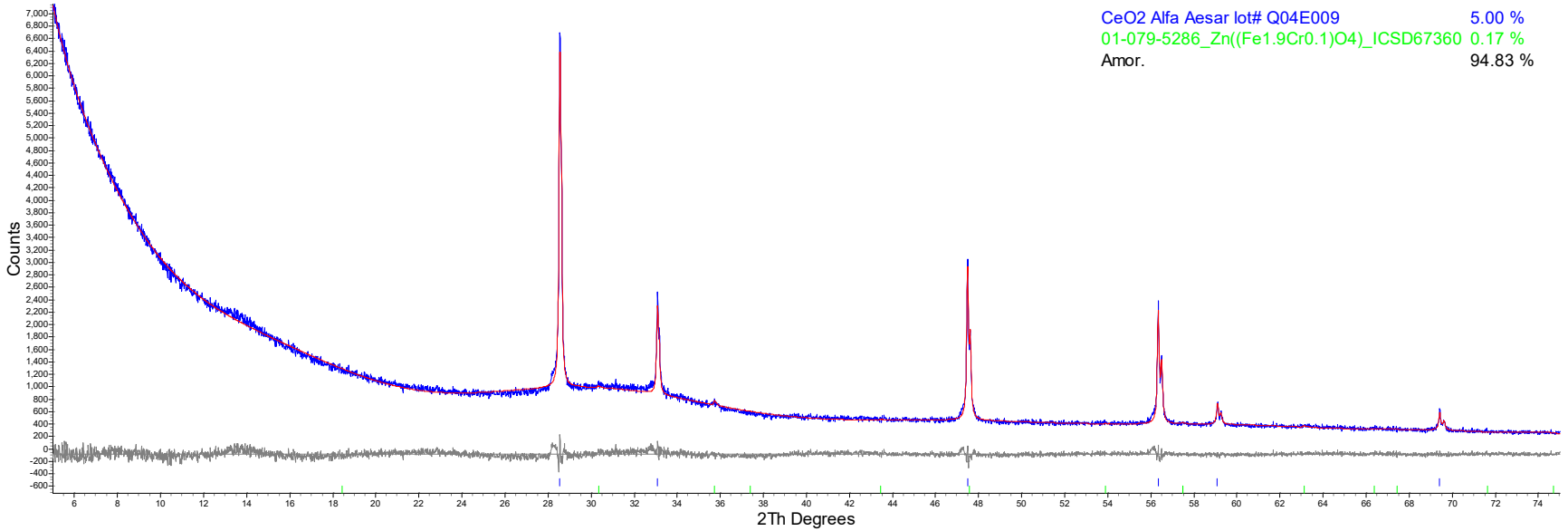


Figure C.17. Refined XRD data of LAWHNK-17.

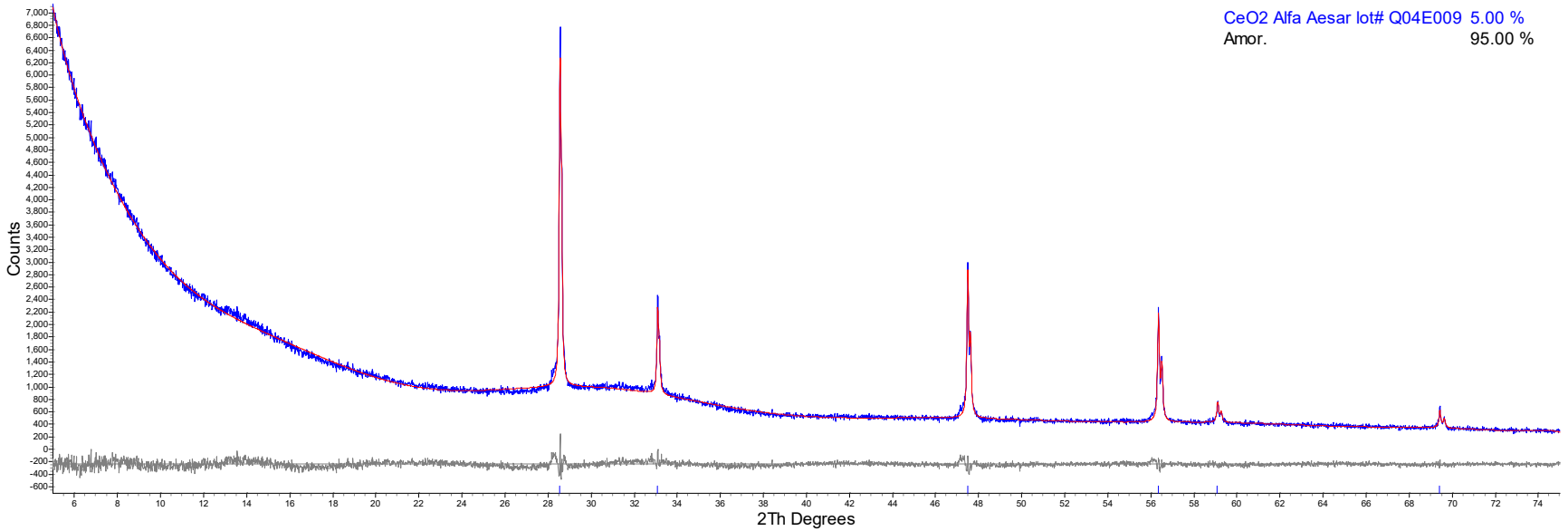


Figure C.18. Refined XRD data of LAWHNK-18.

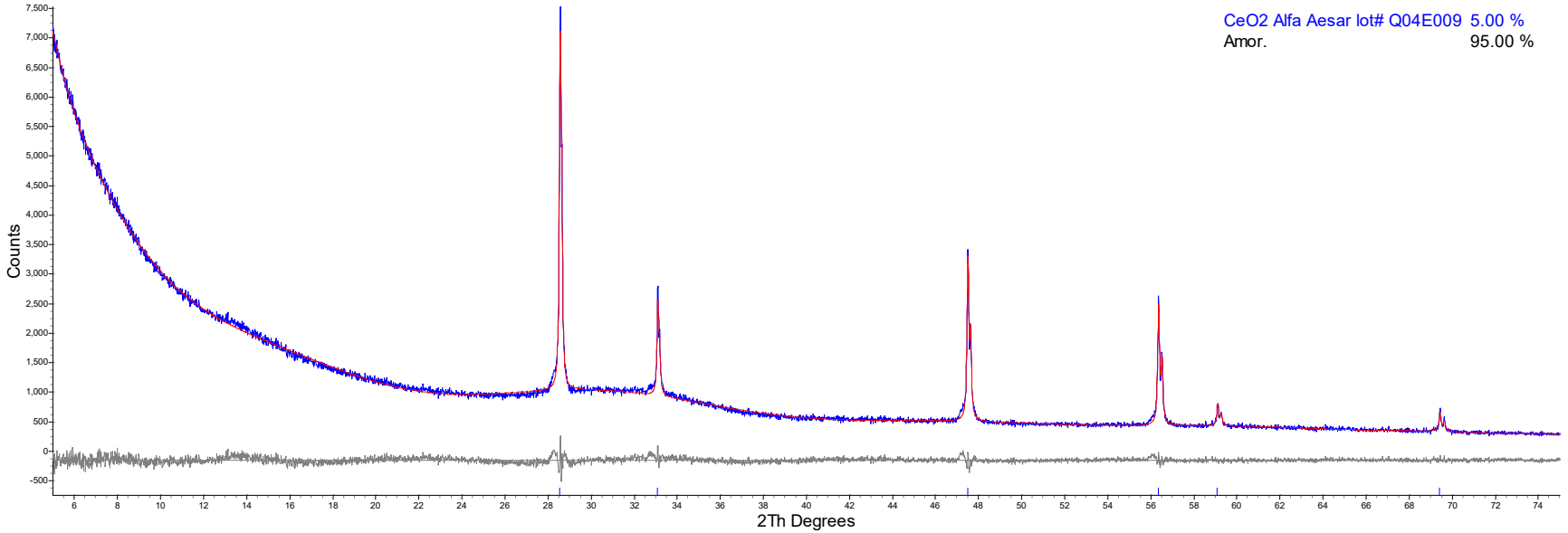


Figure C.19. Refined XRD data of LAWHNK-19.

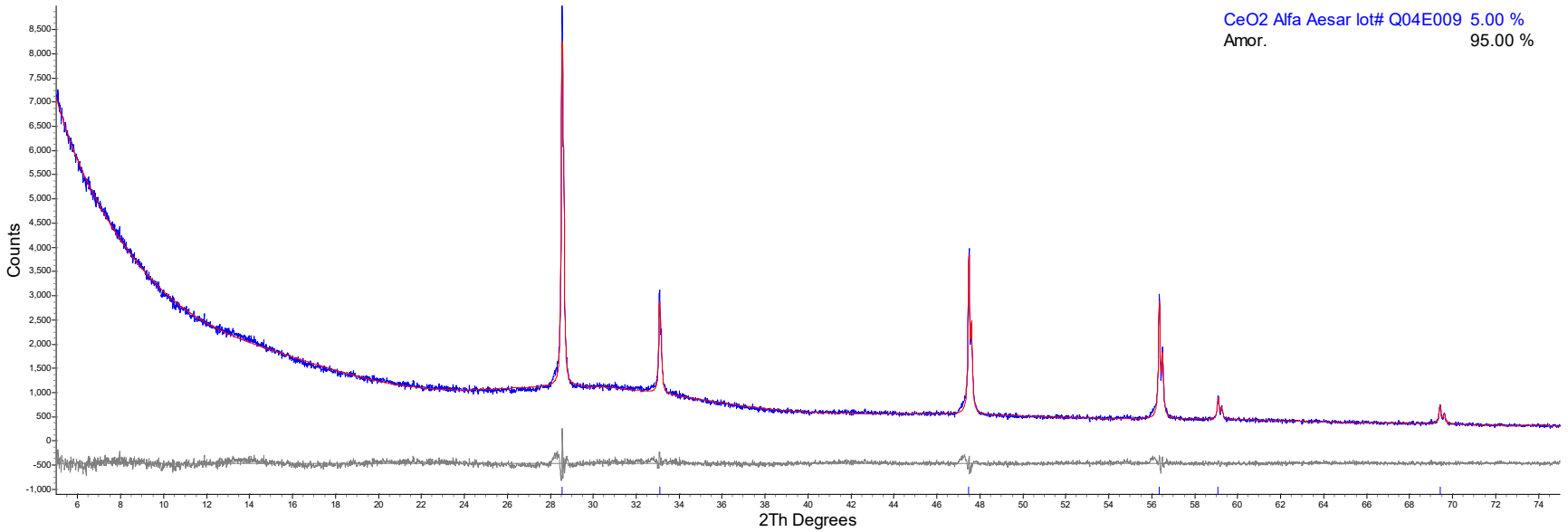


Figure C.20. Refined XRD data of LAWHNK-20.

Appendix D – Container Centerline Cooling

The photographs in this appendix show each glass after container centerline cooling (CCC) as described in Section 2.4. When applicable, X-ray diffraction (XRD) scans are reported. The percentage of crystals in the plots are reported before correcting for the TiO_2 standard crystallinity of 91.26%.



Figure D.1. Morphology of glass LAWHNK-01 after CCC.

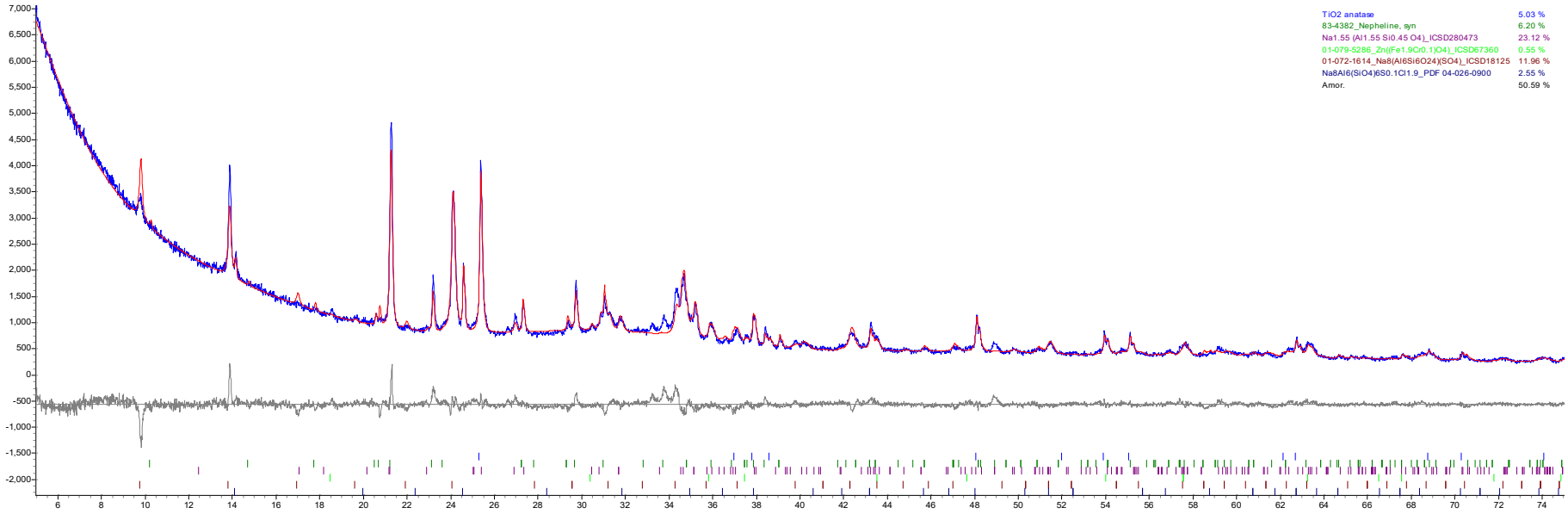


Figure D.2. XRD scan of glass LAWHNK-01 after CCC.



Figure D.3. Morphology of glass LAWHNK-02 after CCC.

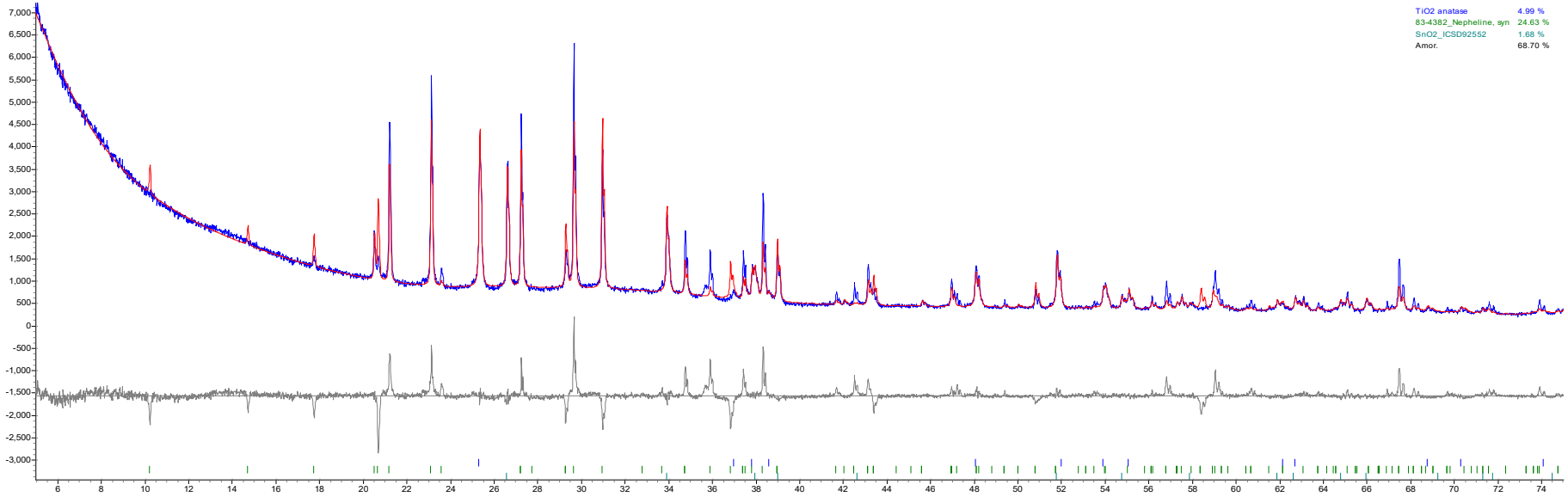


Figure D.4. XRD scan of glass LAWHNK-02 after CCC.



Figure D.5. Morphology of glass LAWHNK-03 after CCC.

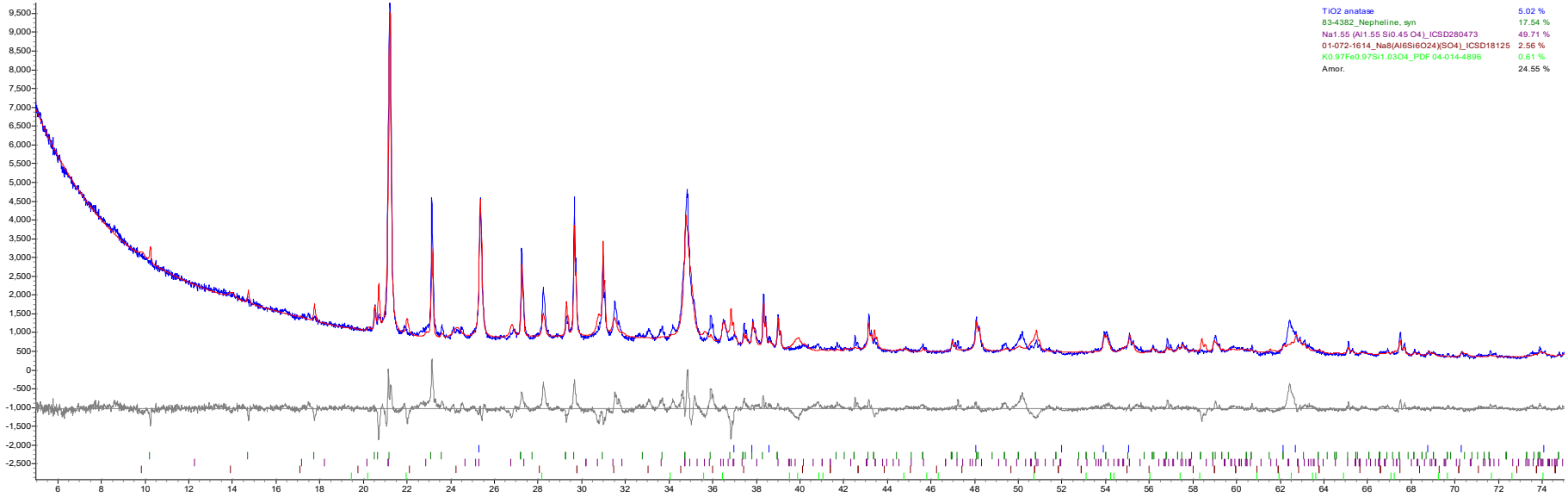


Figure D.6. XRD scan of glass LAWHNK-03 after CCC.



Figure D.7. Morphology of glass LAWHNK-04 after CCC.

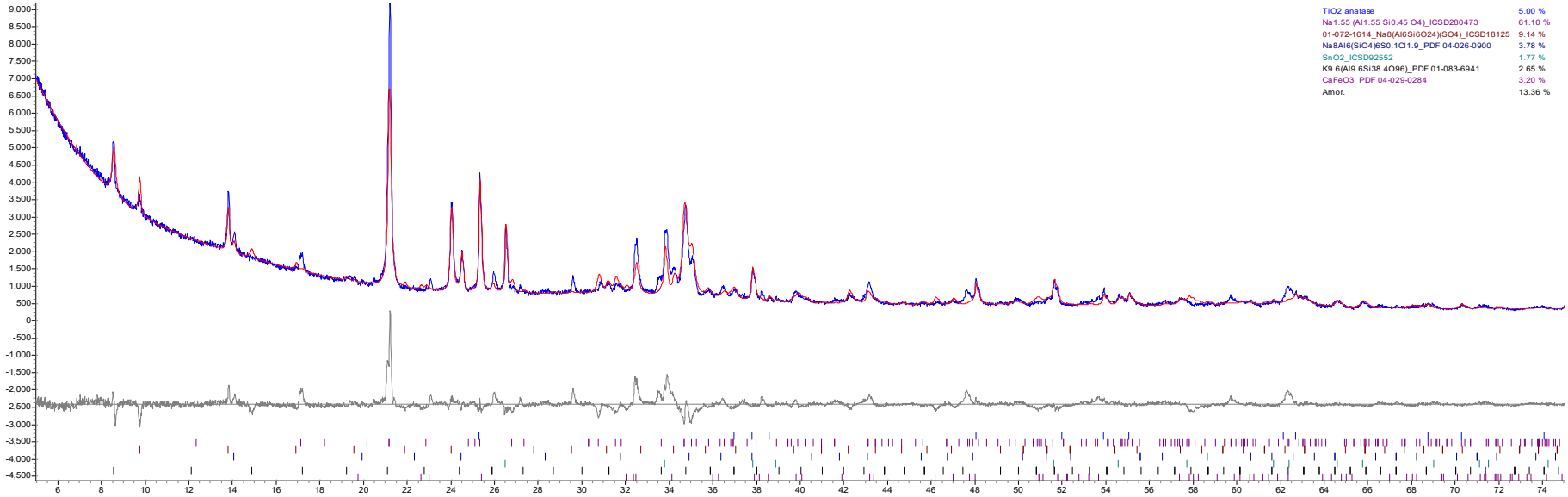


Figure D.8. XRD scan of glass LAWHNK-04 after CCC.



Figure D.9. Morphology of glass LAWHNK-05 after CCC.

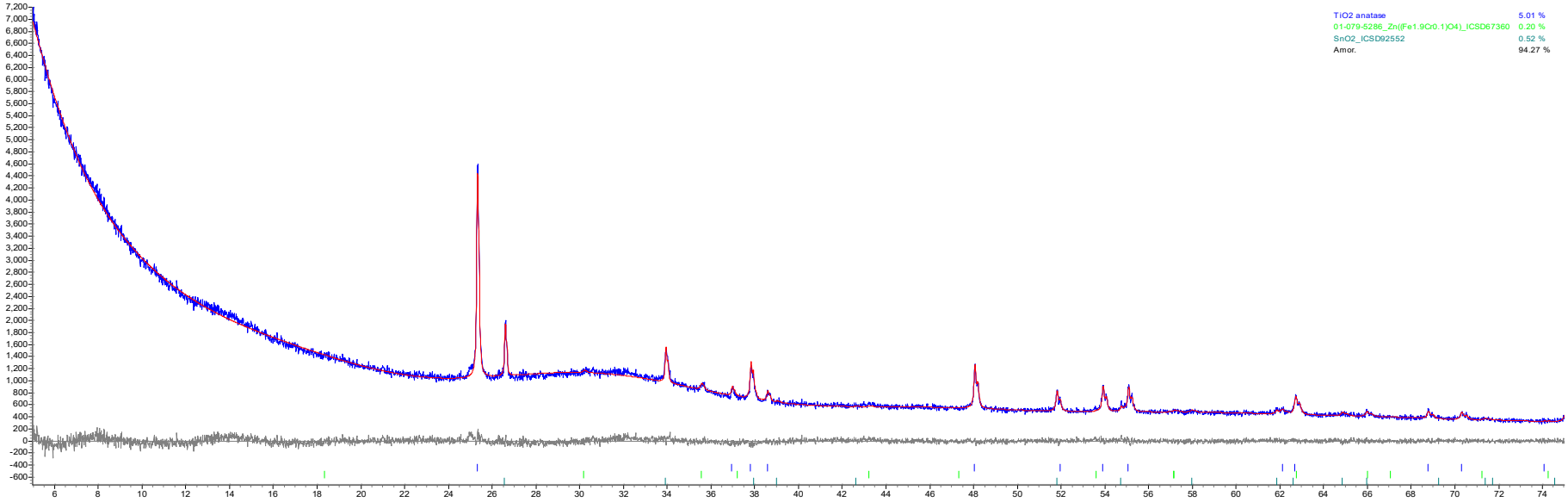


Figure D.10. XRD scan of glass LAWHNK-05 after CCC.



Figure D.11. Morphology of glass LAWHNK-06 after CCC.

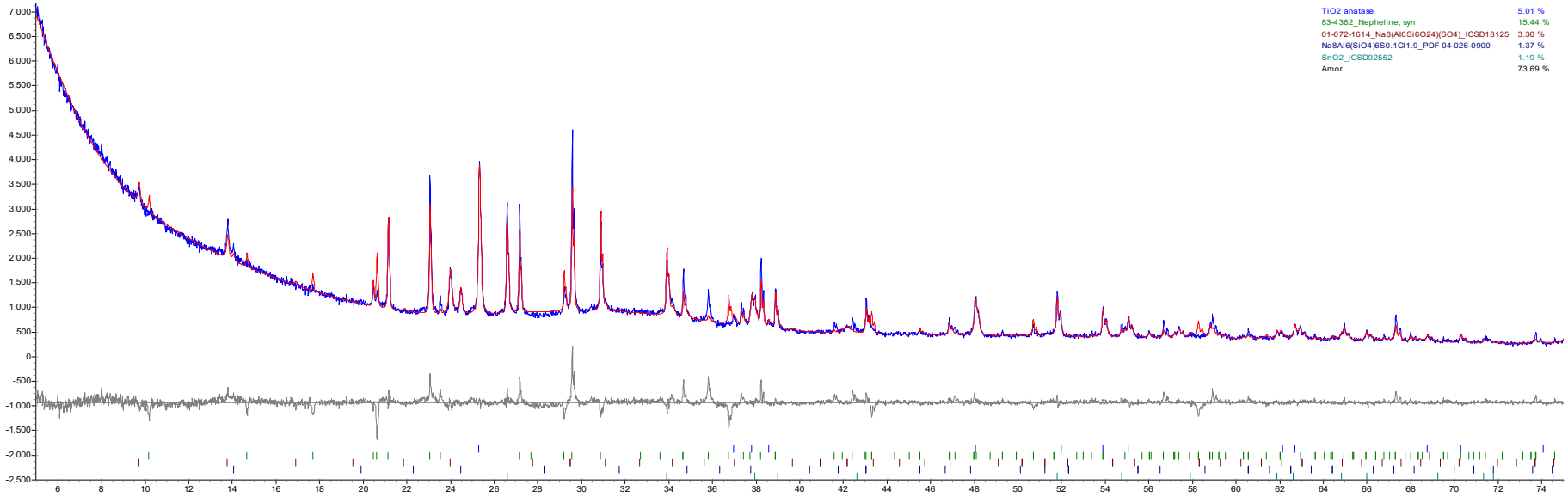


Figure D.12. XRD scan of glass LAWHNK-06 after CCC.



Figure D.13. Morphology of glass LAWHNK-07 after CCC.

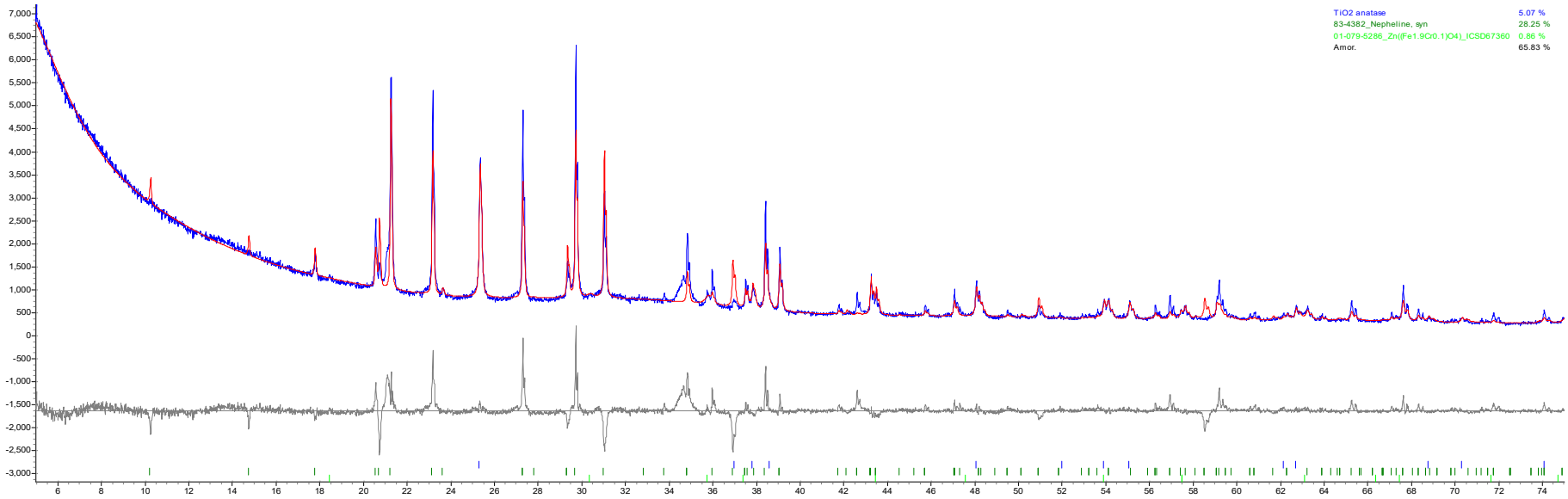


Figure D.14. XRD scan of glass LAWHNK-07 after CCC.



Figure D.15. Morphology of glass LAWHNK-08 after CCC.

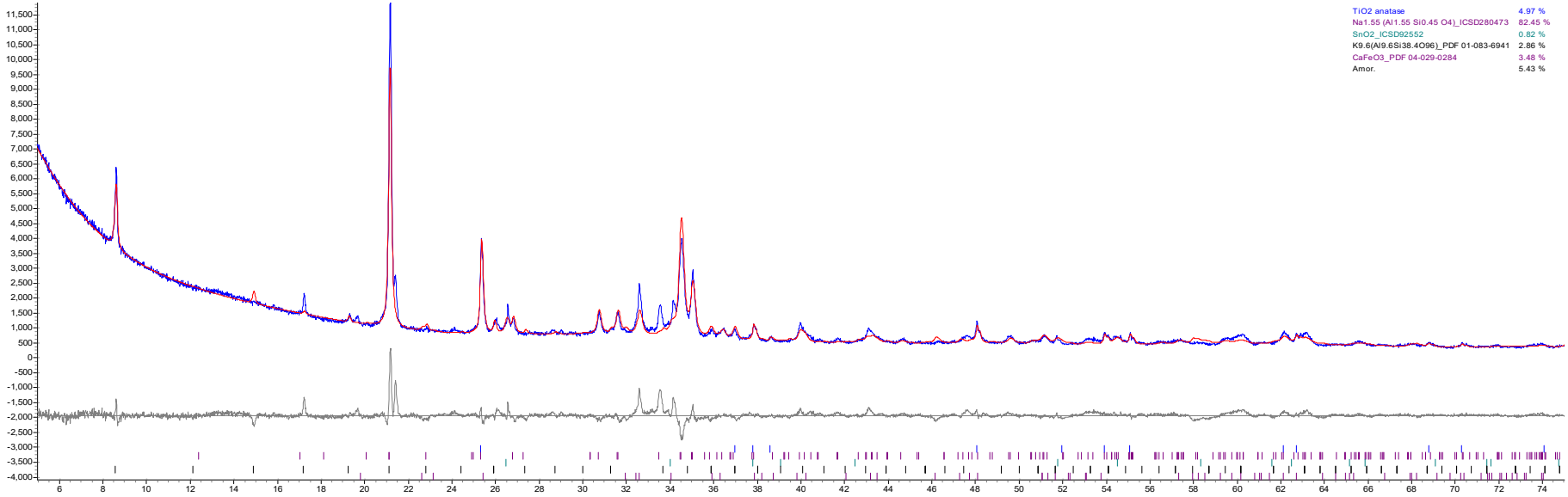


Figure D.16. XRD scan of glass LAWHNK-08 after CCC.



Figure D.17. Morphology of glass LAWHNK-09 after CCC.

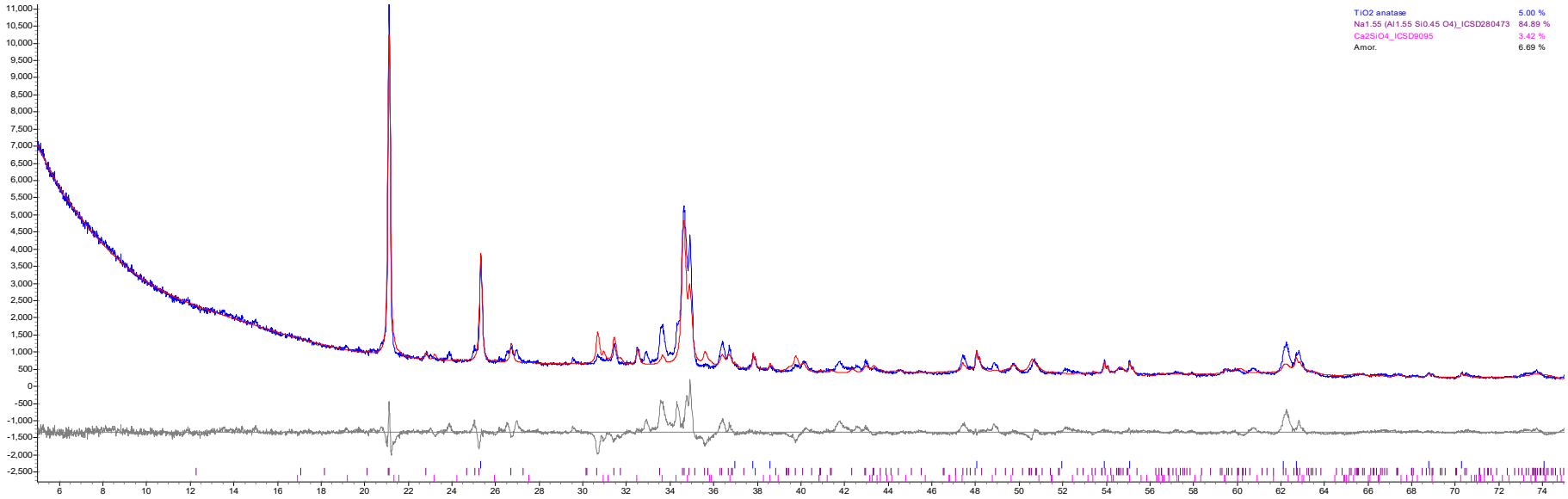


Figure D.18. XRD scan of glass LAWHNK-09 after CCC.



Figure D.19. Morphology of glass LAWHNK-10 after CCC.

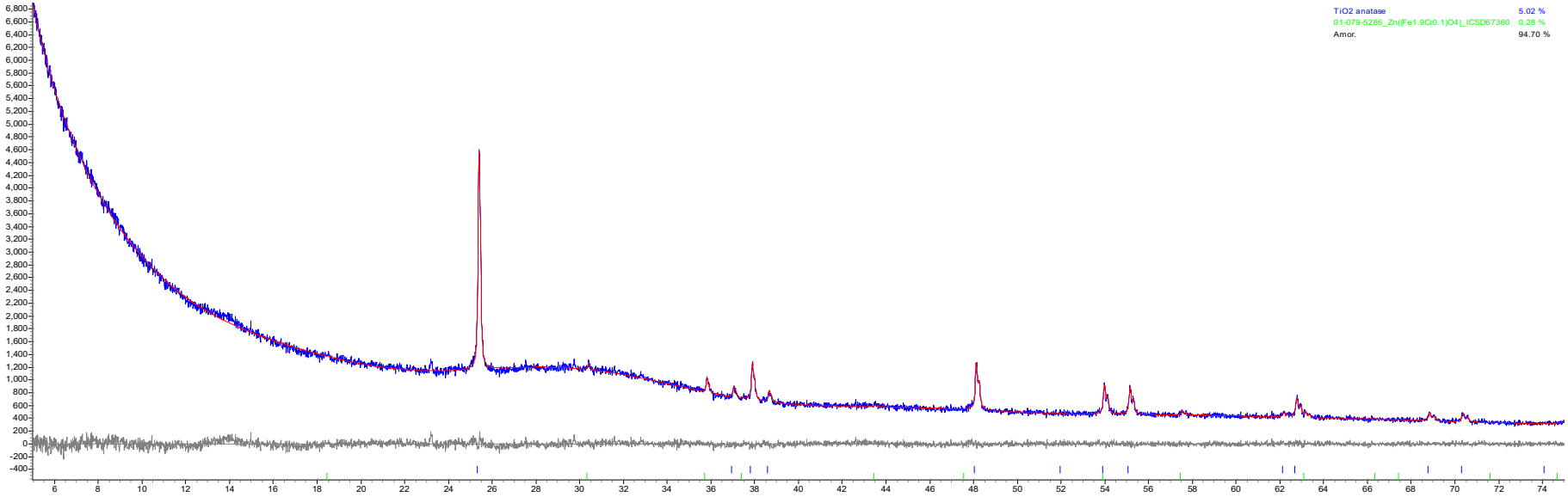


Figure D.20. XRD scan of glass LAWHNK-10 after CCC.



Figure D.21. Morphology of glass LAWHNK-11 after CCC.

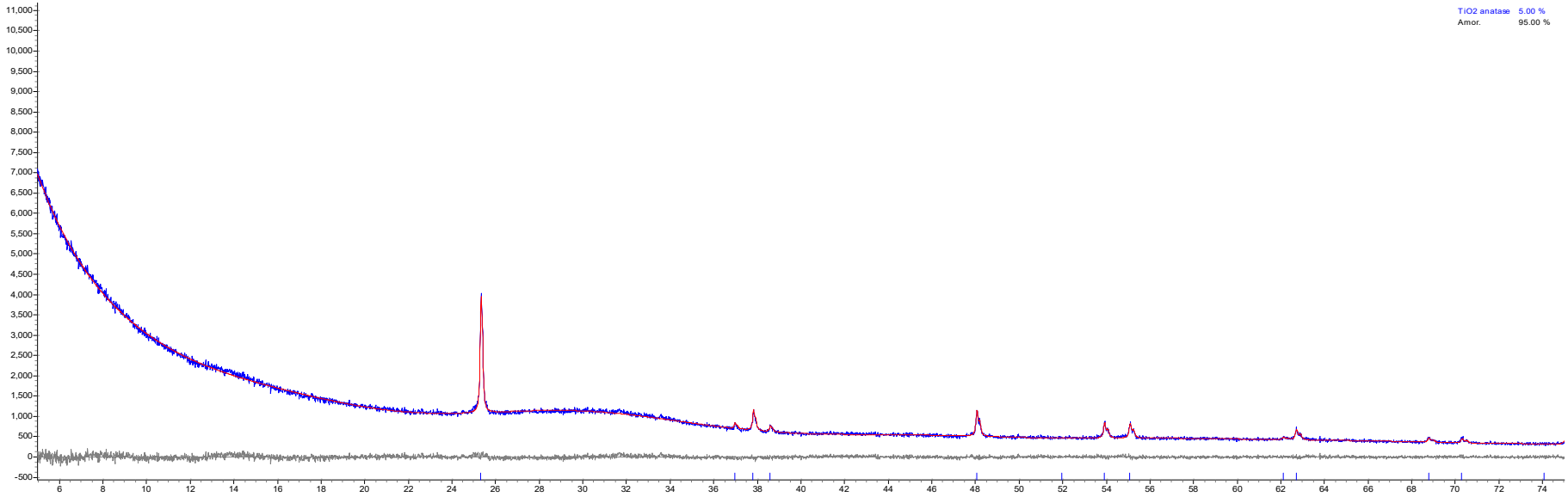


Figure D.22. XRD scan of glass LAWHNK-11 after CCC.



Figure D.23. Morphology of glass LAWHNK-12 after CCC.

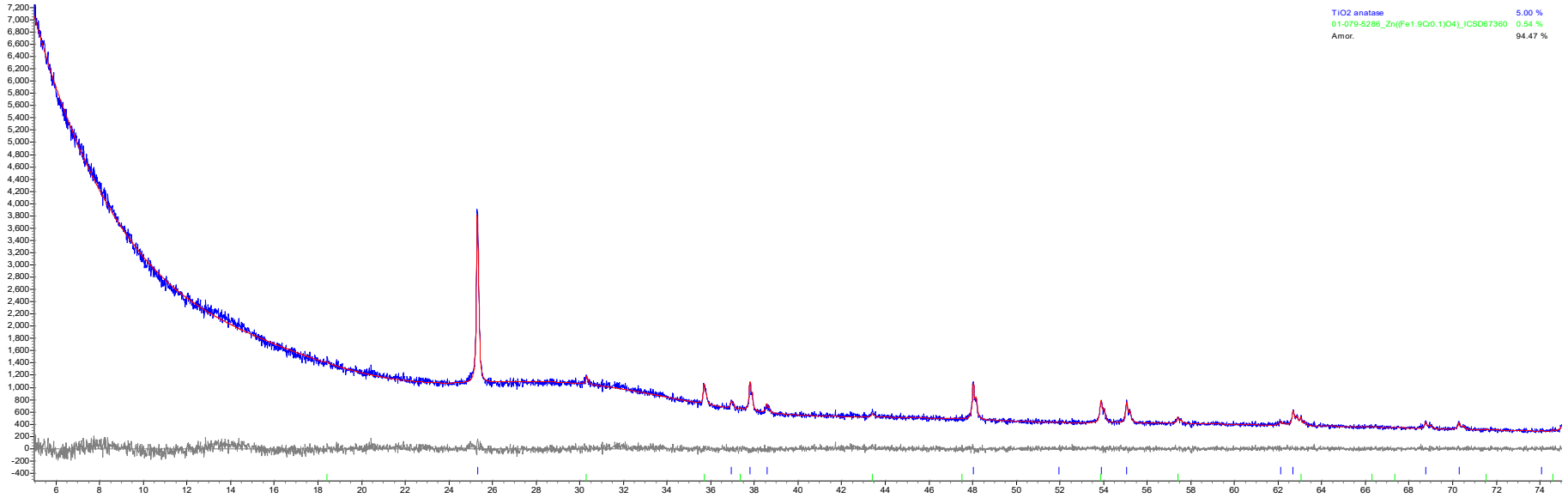


Figure D.24. XRD scan of glass LAWHNK-12 after CCC.



Figure D.25. Morphology of glass LAWHNK-13 after CCC.

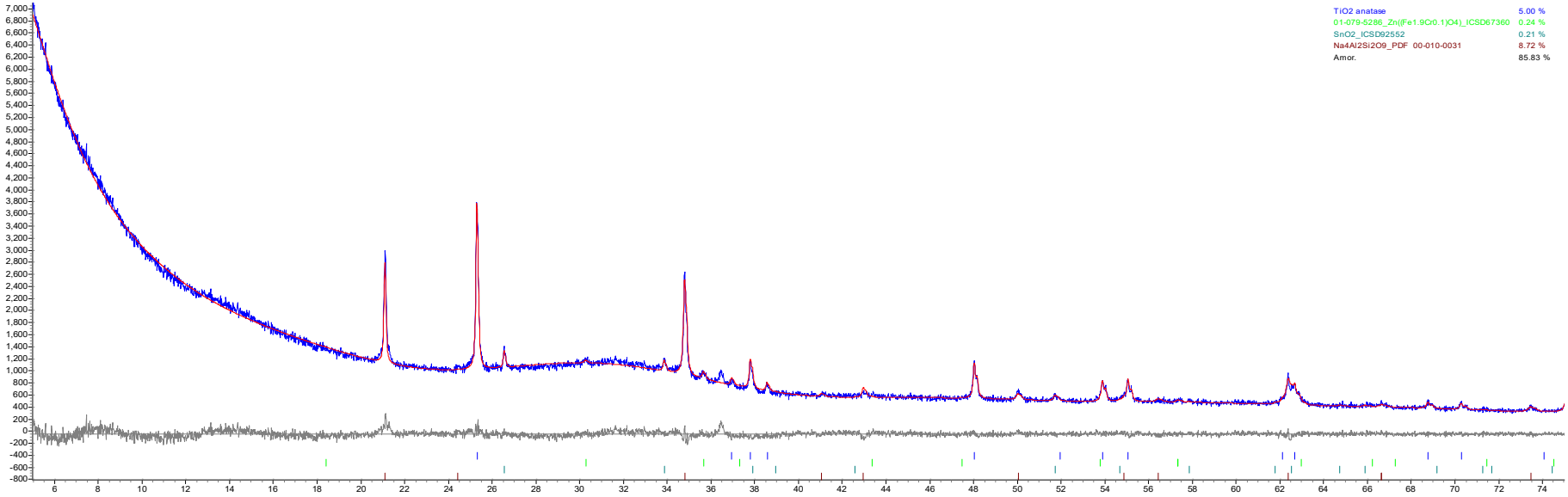


Figure D.26. XRD scan of glass LAWHNK-13 after CCC.



Figure D.27. Morphology of glass LAWHNK-14 after CCC.

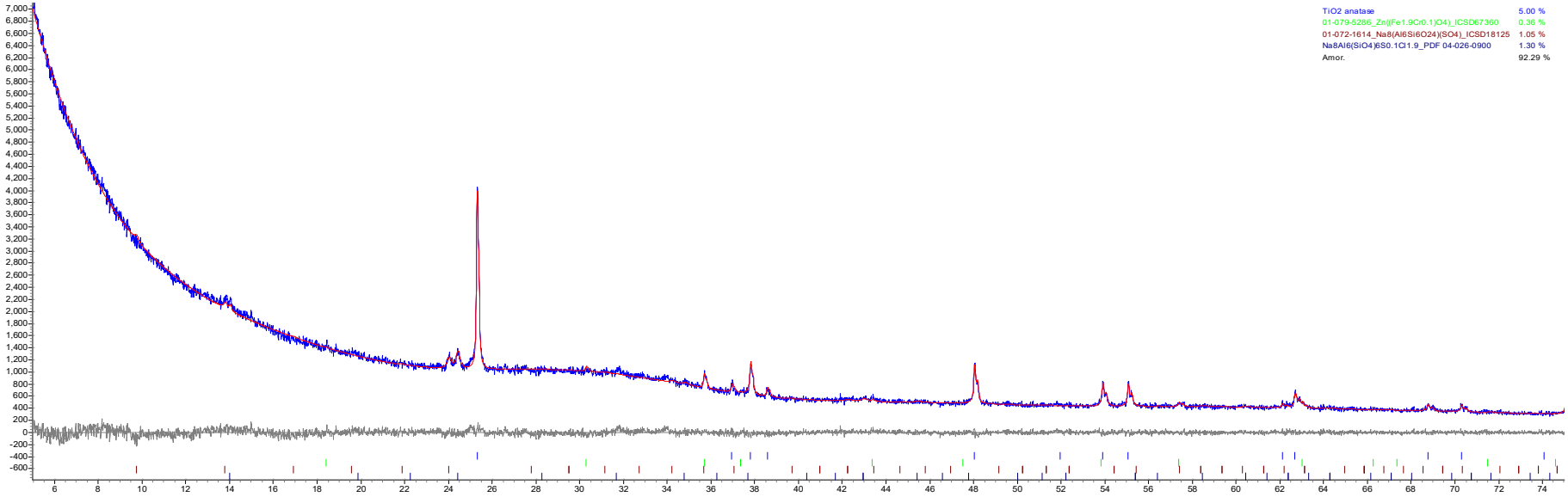


Figure D.28. XRD scan of glass LAWHNK-14 after CCC.



Figure D.29. Morphology of glass LAWHNK-15 after CCC.

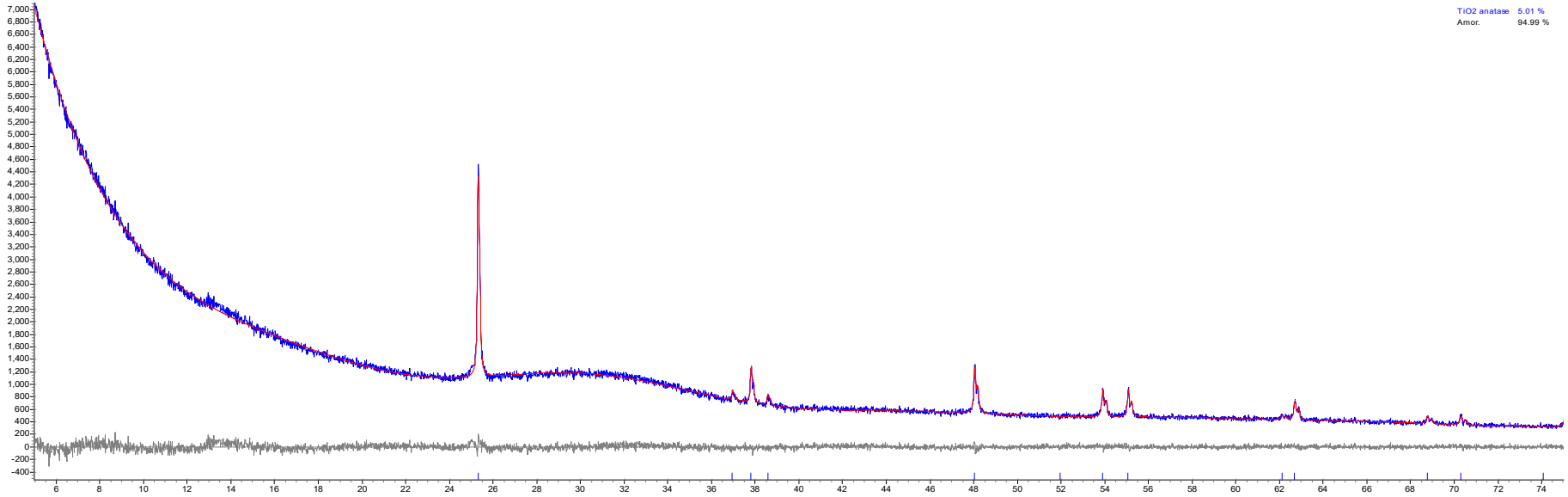


Figure D.30. XRD scan of glass LAWHNK-15 after CCC.



Figure D.31. Morphology of glass LAWHNK-16 after CCC.

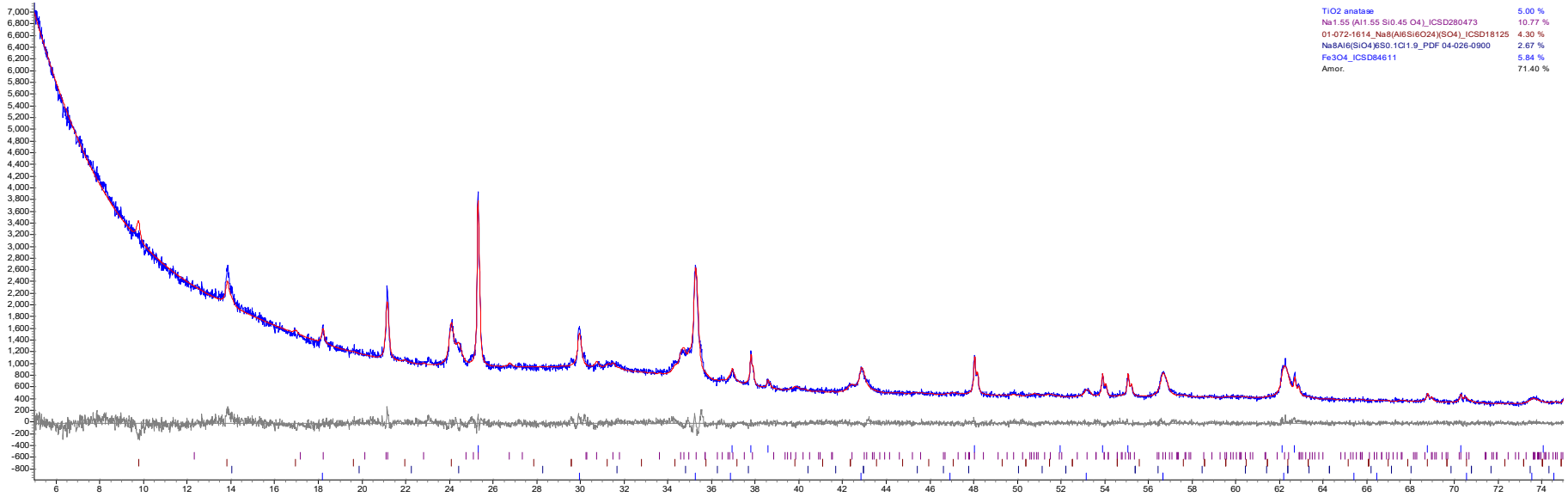


Figure D.32. XRD scan of glass LAWHNK-16 after CCC.



Figure D.33. Morphology of glass LAWHNK-17 after CCC.

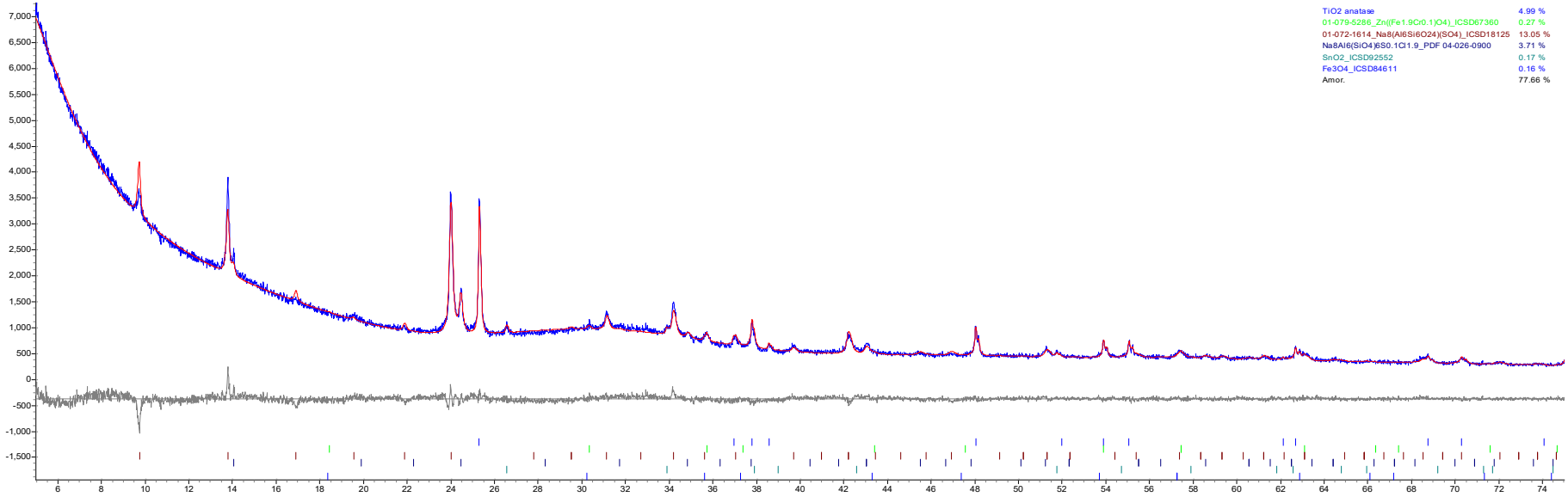


Figure D.34. XRD scan of glass LAWHNK-17 after CCC.



Figure D.35. Morphology of glass LAWHNK-18 after CCC.

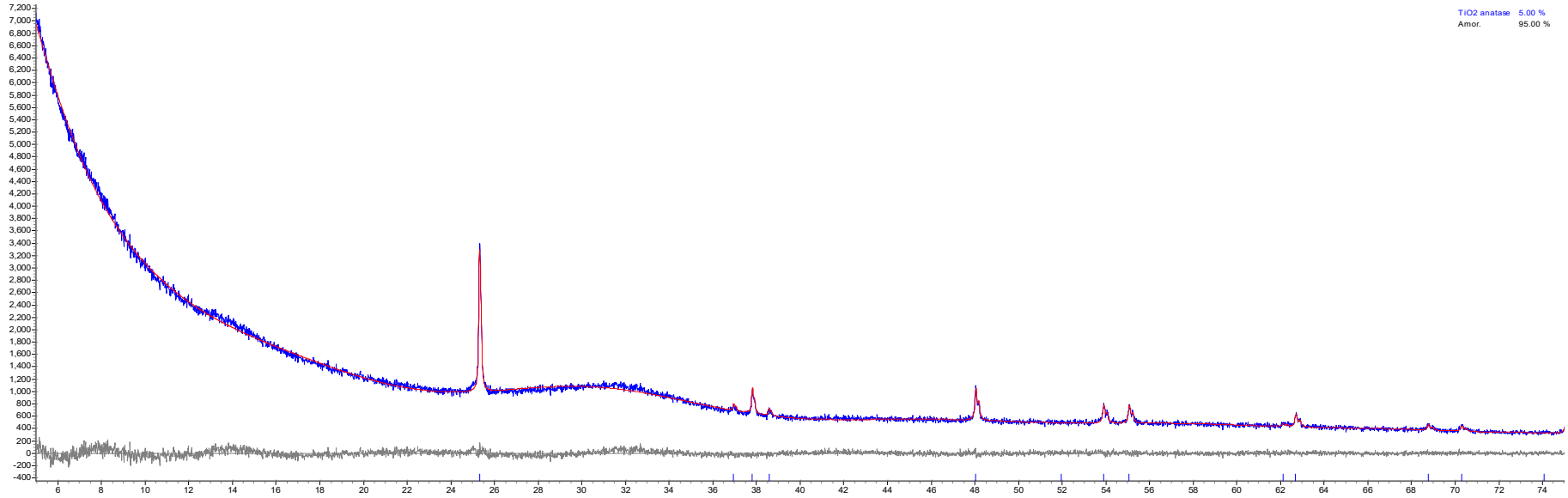


Figure D.36. XRD scan of glass LAWHNK-18 after CCC.



Figure D.37. Morphology of glass LAWHNK-19 after CCC.

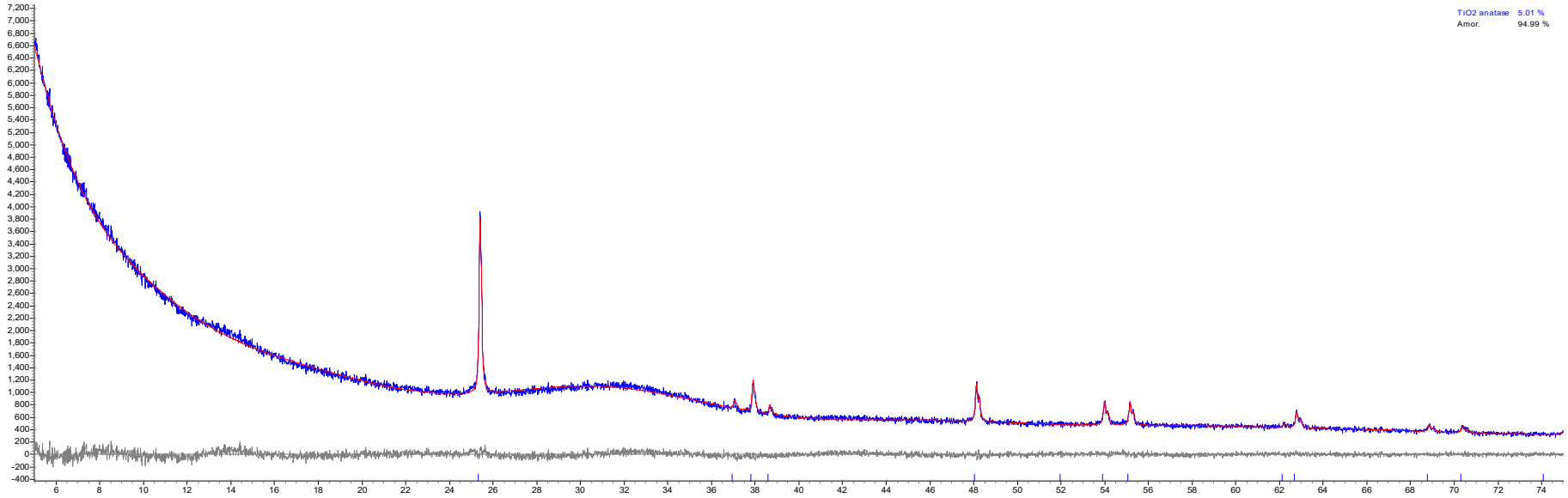


Figure D.38. XRD scan of glass LAWHNK-19 after CCC.



Figure D.39. Morphology of glass LAWHNK-20 after CCC.

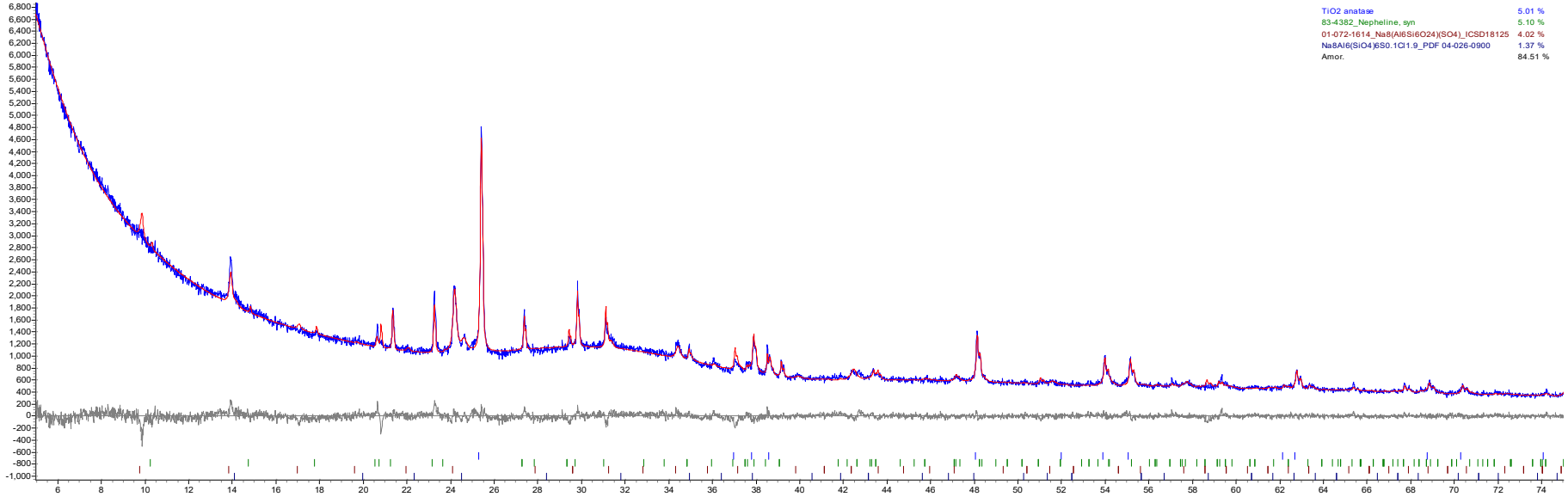


Figure D.40. XRD scan of glass LAWHNK-20 after CCC.

Appendix E – Crystal Fraction

This appendix contains photographs of the LAWHNK glasses after they were heat-treated at 950 °C for 24 h, which should conservatively represent the potential presence of crystal formation. XRD scans are included except for fully amorphous samples. The mass percentage of crystal fraction in the XRD images reported before adjustment was made from spiking with 5 wt% high purity TiO_2.



Figure E.1. Glass LAWHNK-01 after isothermal heat treatment at 950 °C for 24 h.

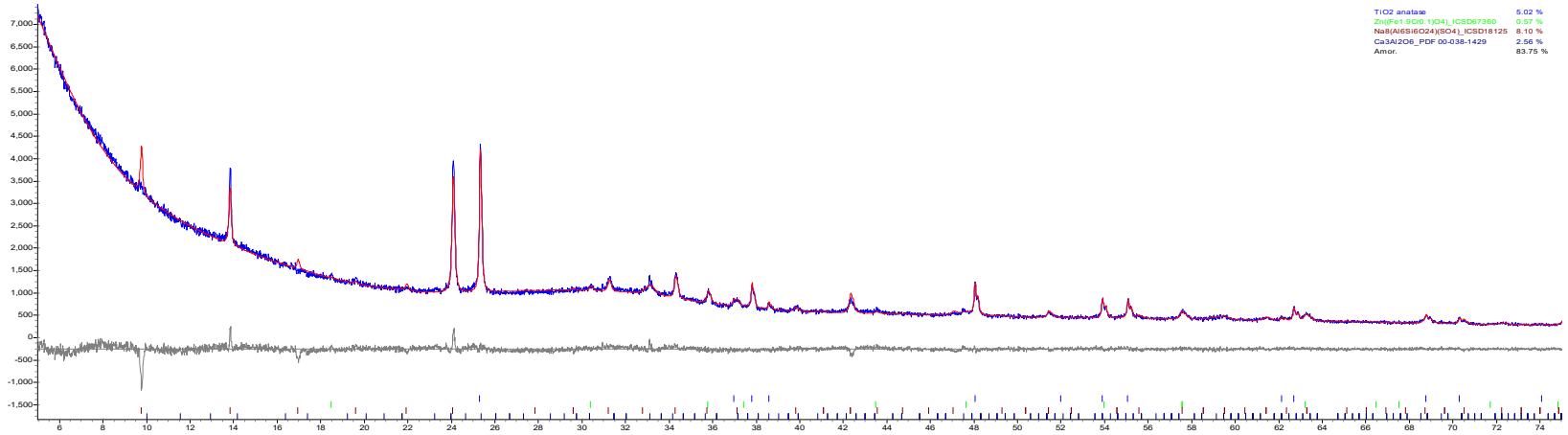


Figure E.2. XRD scan of glass LAWHNK-01 after isothermal heat treatment at 950 °C for 24 h.



Figure E.3. Glass LAWHNK-02 after isothermal heat treatment at 950 °C for 24 h.

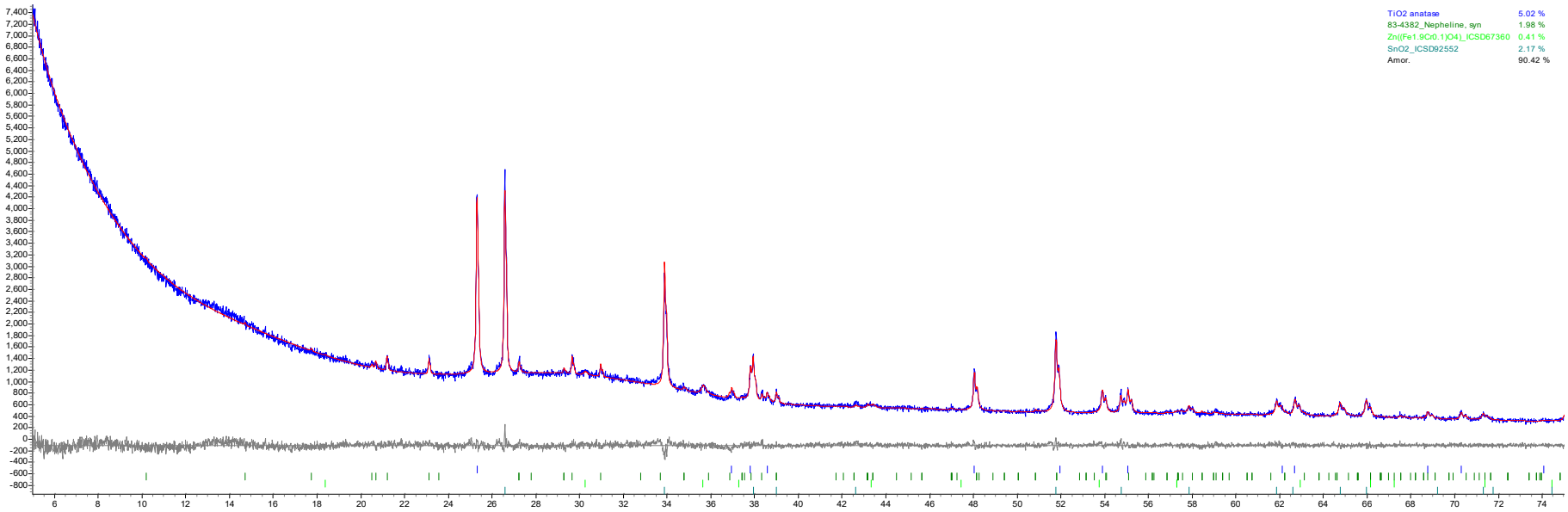


Figure E.4. XRD scan of glass LAWHNK-02 after isothermal heat treatment at 950 °C for 24 h.



Figure E.5. Glass LAWHNK-03 after isothermal heat treatment at 950 °C for 24 h.

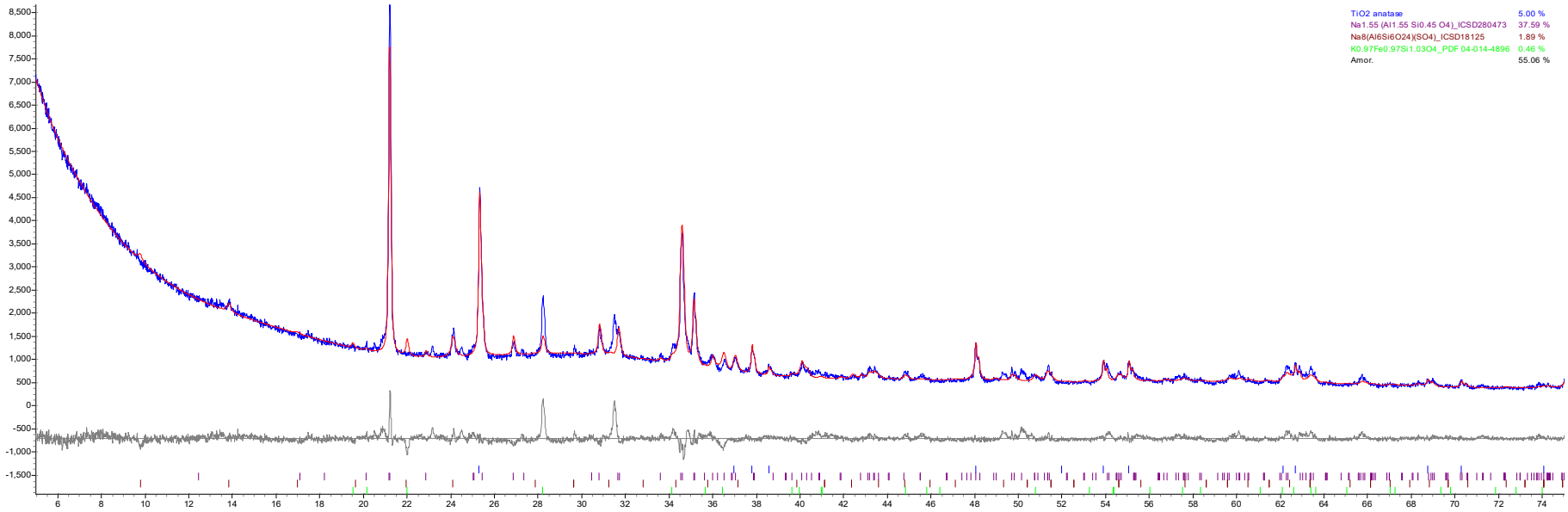


Figure E.6. XRD scan of glass LAWHNK-03 after isothermal heat treatment at 950 °C for 24 h.



Figure E.7. Glass LAWHNK-04 after isothermal heat treatment at 950 °C for 24 h.

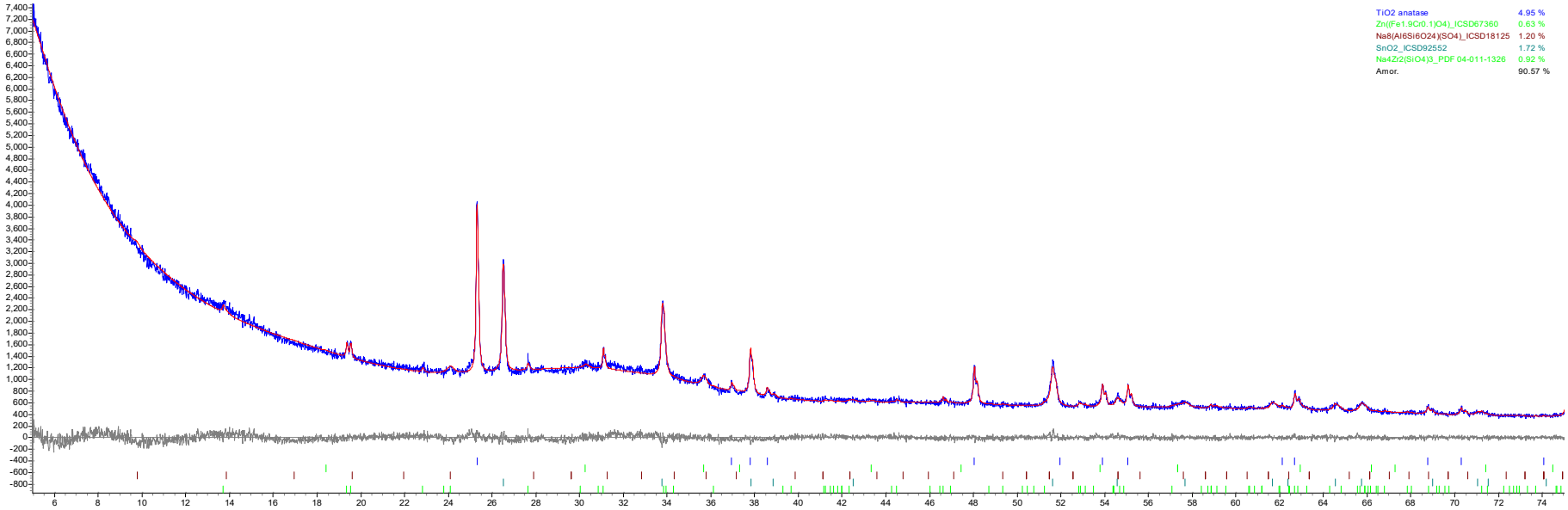


Figure E.8. XRD scan of glass LAWHNK-04 after isothermal heat treatment at 950 °C for 24 h.



Figure E.9. Glass LAWHNK-05 after isothermal heat treatment at 950 °C for 24 h.

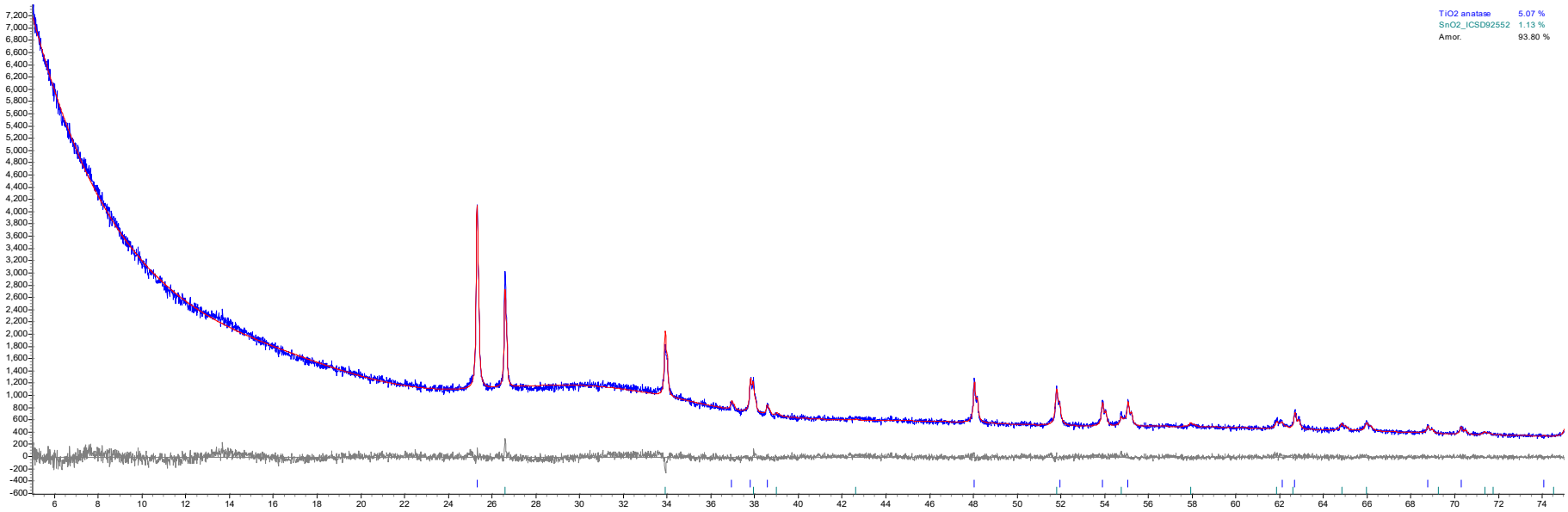


Figure E.10. XRD scan of glass LAWHNK-05 after isothermal heat treatment at 950 °C for 24 h.



Figure E.11. Glass LAWHNK-06 after isothermal heat treatment at 950 °C for 24 h.

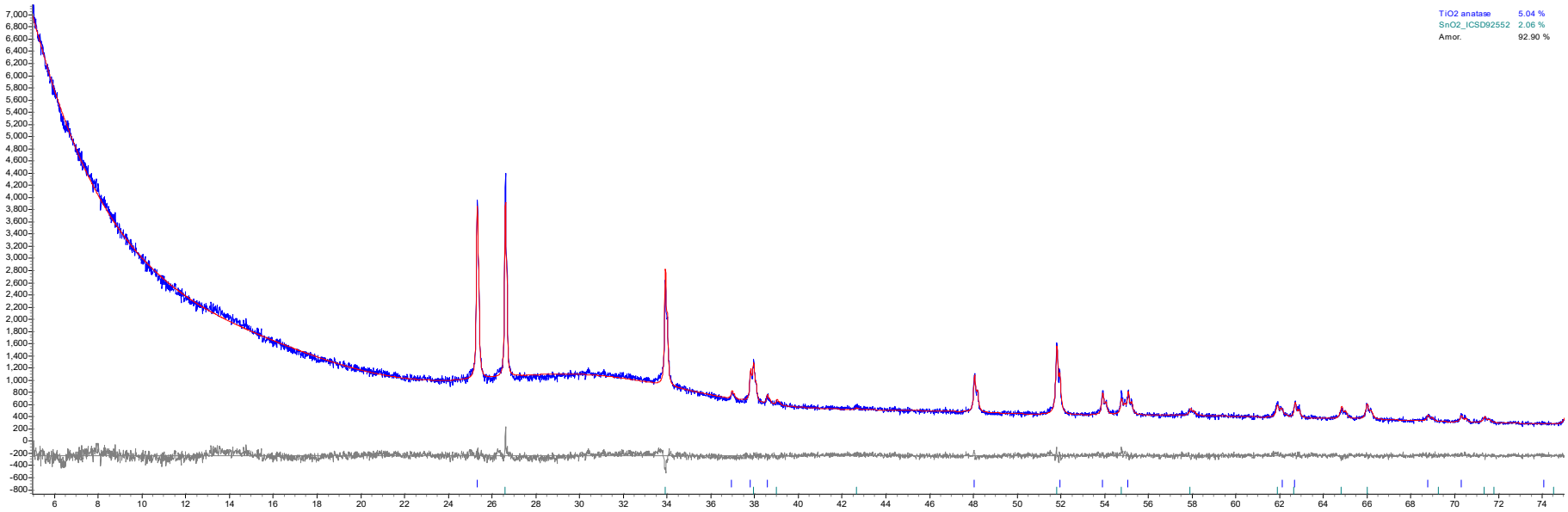


Figure E.12. XRD scan of glass LAWHNK-06 after isothermal heat treatment at 950 °C for 24 h.



Figure E.13. Glass LAWHNK-07 after isothermal heat treatment at 950 °C for 24 h.

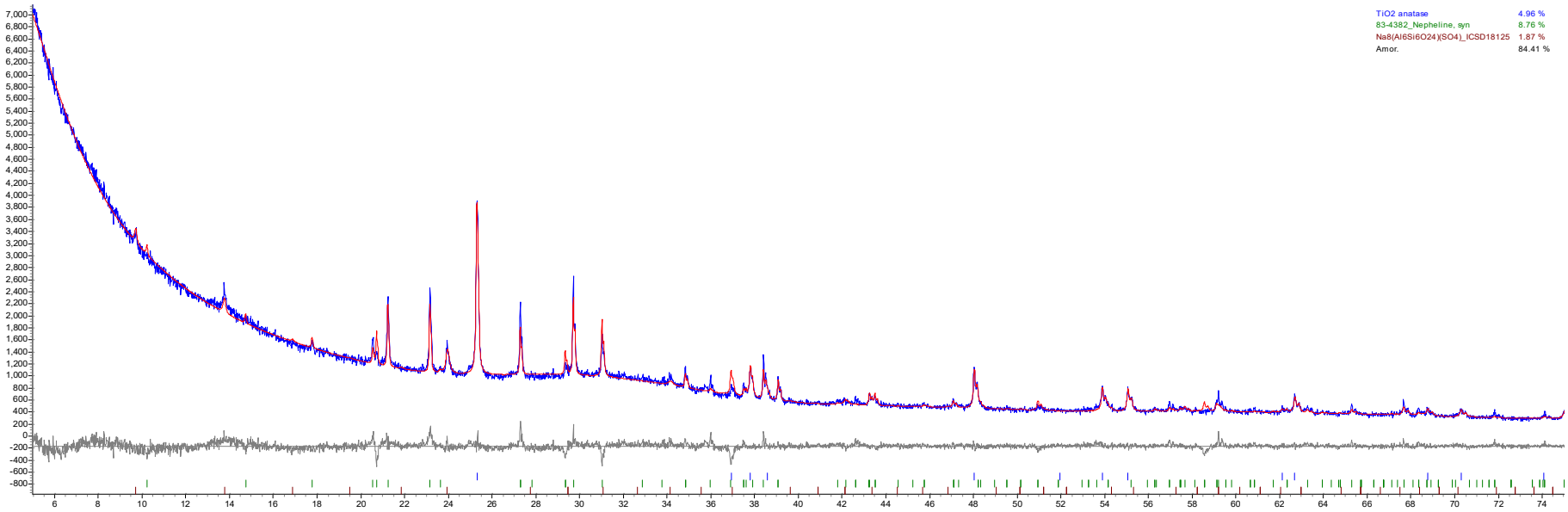


Figure E.14. XRD scan of glass LAWHNK-07 after isothermal heat treatment at 950 °C for 24 h.



Figure E.15. Glass LAWHNK-08 after isothermal heat treatment at 950 °C for 24 h.

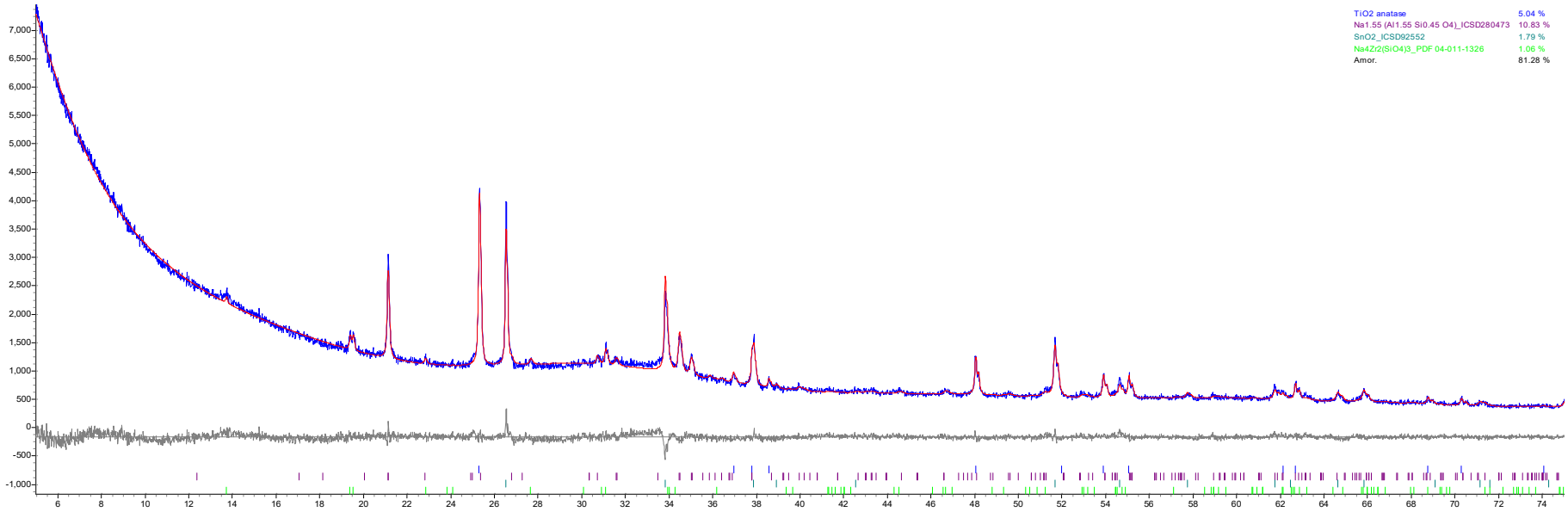


Figure E.16. XRD scan of glass LAWHNK-08 after isothermal heat treatment at 950 °C for 24 h.



Figure E.17. Glass LAWHNK-09 after isothermal heat treatment at 950 °C for 24 h.

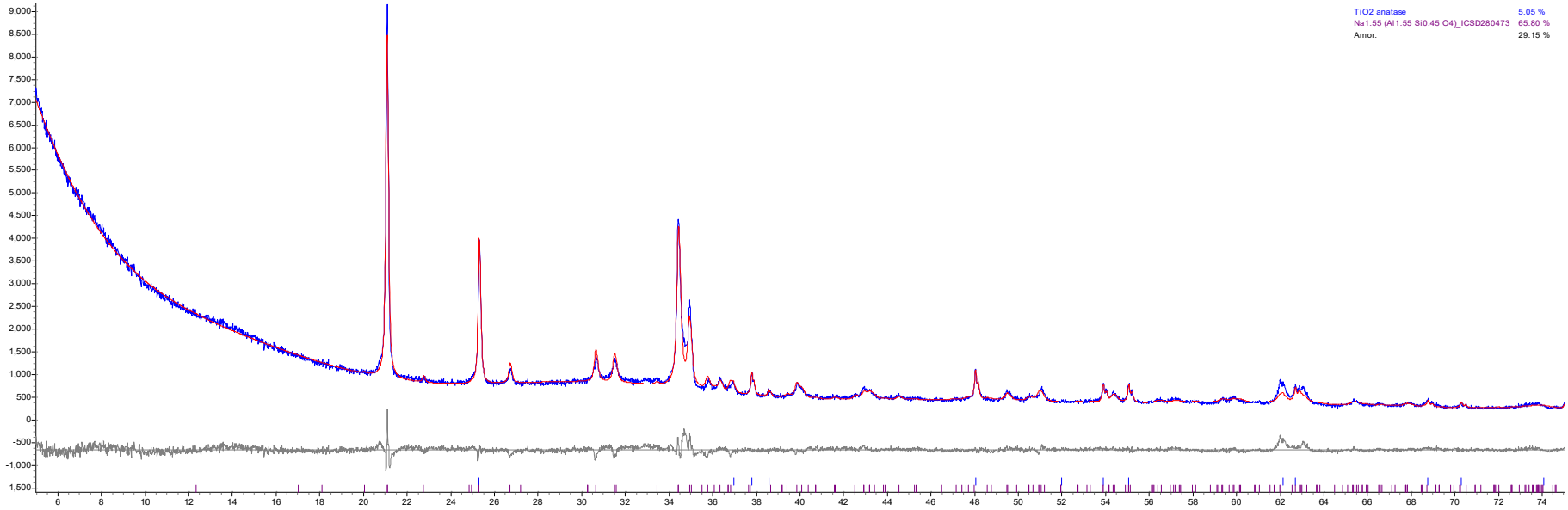


Figure E.18. XRD scan of glass LAWHNK-09 after isothermal heat treatment at 950 °C for 24 h.



Figure E.19. Glass LAWHNK-10 after isothermal heat treatment at 950 °C for 24 h. Amorphous by XRD scan (not shown).



Figure E.20. Glass LAWHNK-11 after isothermal heat treatment at 950 °C for 24 h. Amorphous by XRD scan (not shown).



Figure E.21. Glass LAWHNK-12 after isothermal heat treatment at 950 °C for 24 h. Amorphous by XRD scan (not shown).



Figure E.22. Glass LAWHNK-13 after isothermal heat treatment at 950 °C for 24 h.

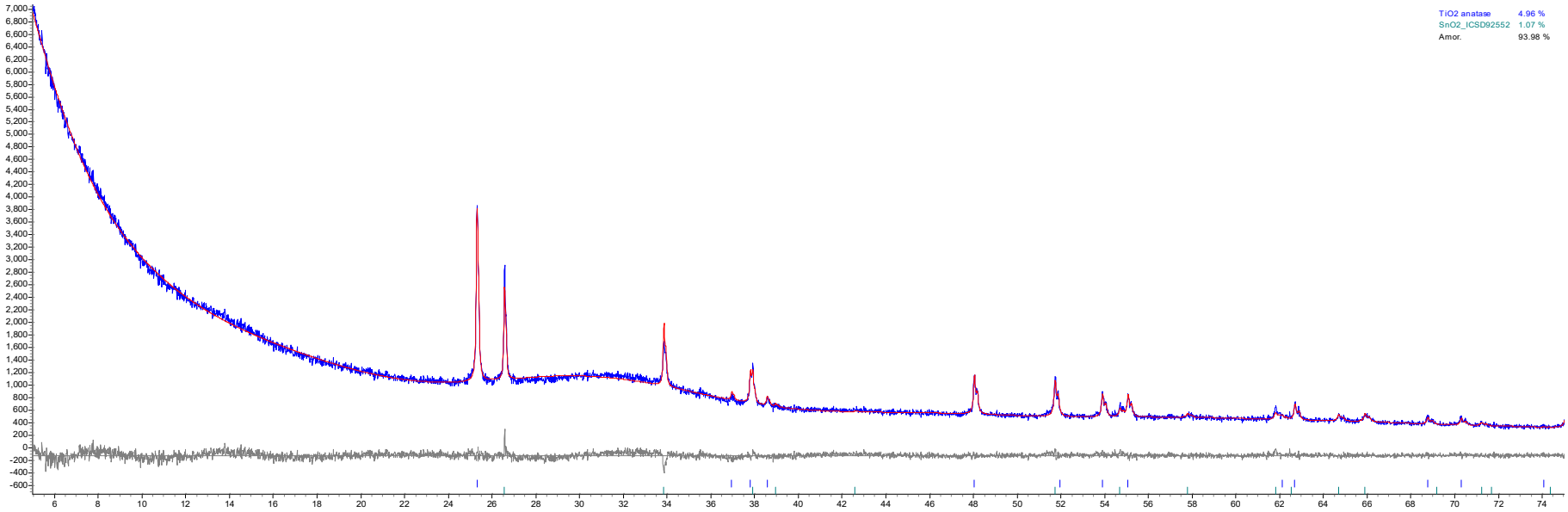


Figure E.23. XRD scan of glass LAWHNK-13 after isothermal heat treatment at 950 °C for 24 h.



Figure E.24. Glass LAWHNK-14 after isothermal heat treatment at 950 °C for 24 h.

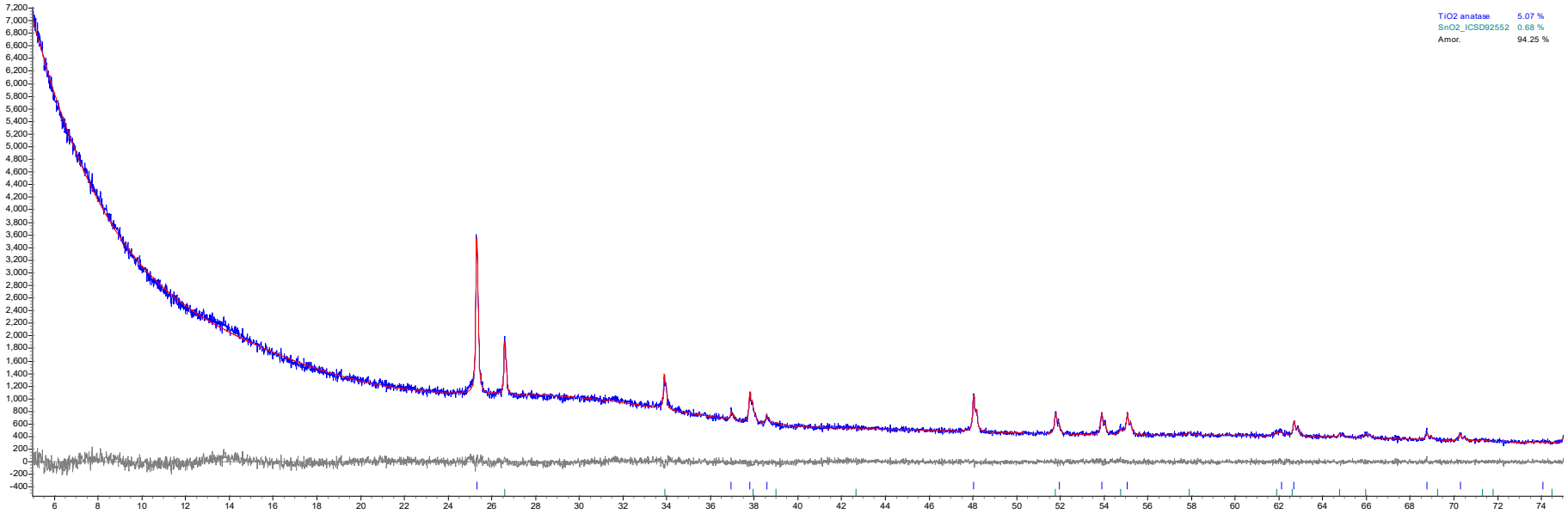


Figure E.25. XRD scan of glass LAWHNK-14 after isothermal heat treatment at 950 °C for 24 h.

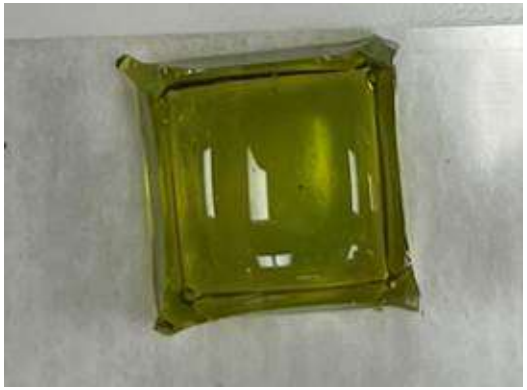


Figure E.26. Glass LAWHNK-15 after isothermal heat treatment at 950 °C for 24 h. Amorphous by XRD scan (not shown).



Figure E.27. Glass LAWHNK-16 after isothermal heat treatment at 950 °C for 24 h.

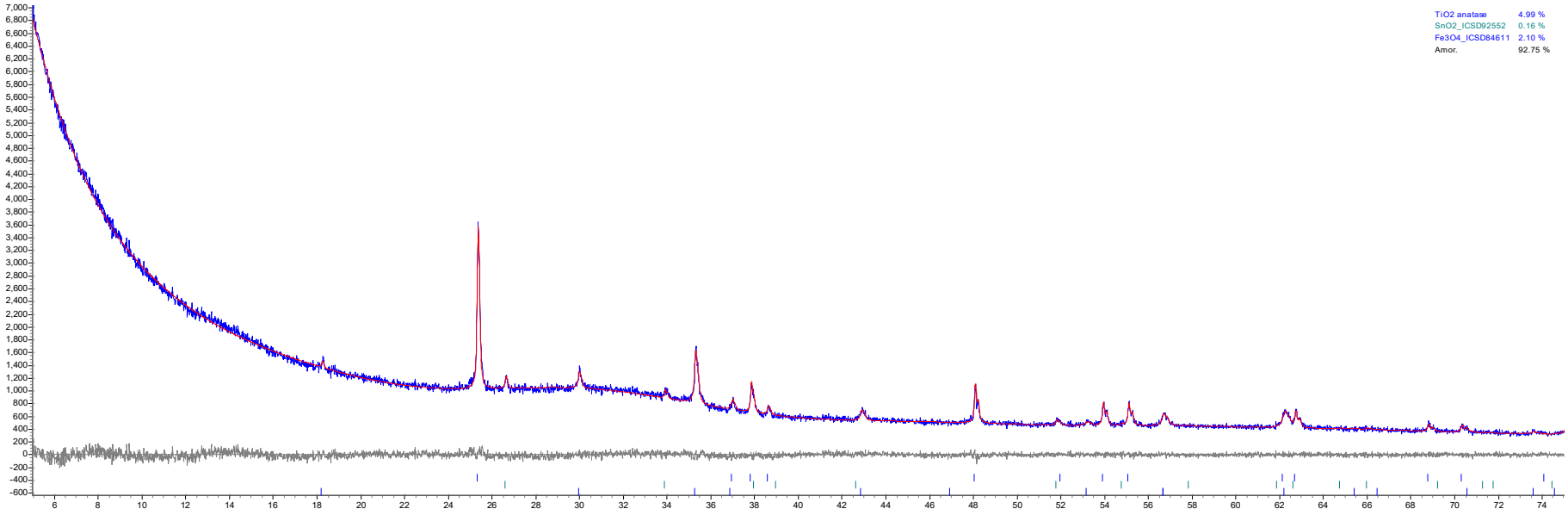


Figure E.28. XRD scan of glass LAWHNK-16 after isothermal heat treatment at 950 °C for 24 h.



Figure E.29. Glass LAWHNK-17 after isothermal heat treatment at 950 °C for 24 h.

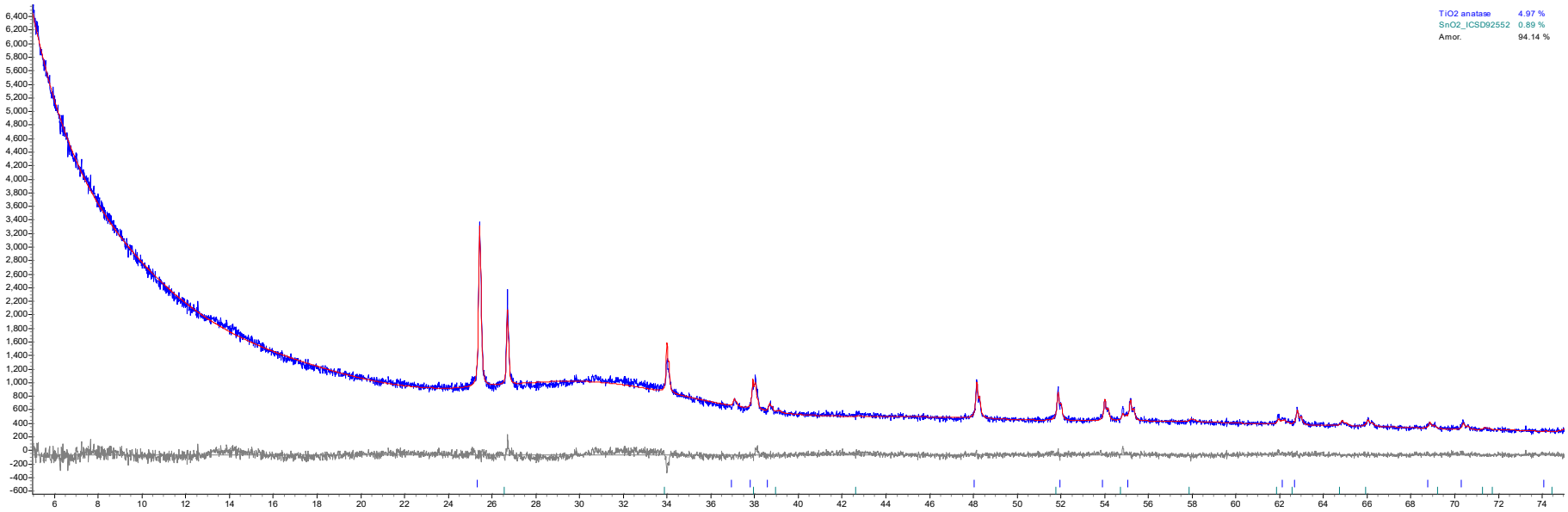


Figure E.30. XRD scan of glass LAWHNK-17 after isothermal heat treatment at 950 °C for 24 h.



Figure E.31. Glass LAWHNK-18 after isothermal heat treatment at 950 °C for 24 h. Amorphous by XRD scan (not shown).



Figure E.32. Glass LAWHNK-19 after isothermal heat treatment at 950 °C for 24 h. Amorphous by XRD scan (not shown).



Figure E.33. Glass LAWHNK-20 after isothermal heat treatment at 950 °C for 24 h. Amorphous by XRD scan (not shown).

Appendix F – Glass Densities

This appendix contains the pycnometer calibration checks performed before and after measuring sample. density of LAWHNK glasses as described in Section 2.6.

Table F.1. Calibration check performed on 03-13-2025.

	Pressure		Volume			
Cycle#	Volume (cm^3)	Deviation (psig)	Density (g/cm^3)	Deviation (cm^3)	Temperature (°C)	Porosity* (%)
1	0.7202	-0.012	1.3885	0.0011	24.78	27.98
2	0.7192	-0.013	1.3904	0.0001	24.84	28.08
3	0.72	-0.001	1.3890	0.0009	24.89	28.00
4	0.7188	0.005	1.3913	-0.0003	24.88	28.12
5	0.7184	0.001	1.3919	-0.0007	24.92	28.16
6	0.7195	0.006	1.3899	0.0004	24.91	28.05
7	0.7188	0.006	1.3913	-0.0003	24.91	28.12
8	0.7188	0.008	1.3912	-0.0003	24.91	28.12
9	0.7178	-0.004	1.3931	-0.0013	24.92	28.22
10	0.7197	0.004	1.3895	0.0006	24.91	28.03

*Calculated from envelope density

Table F.2. Calibration check performed on 03-24-2025.

	Pressure		Volume			
Cycle#	Volume (cm^3)	Deviation (psig)	Density (g/cm^3)	Deviation (cm^3)	Temperature (°C)	Porosity* (%)
1	0.7193	-0.006	1.3902	-0.0001	24.57	28.07
2	0.719	0.005	1.3909	-0.0004	24.62	28.1
3	0.7192	0.003	1.3904	-0.0002	24.62	28.08
4	0.7192	-0.016	1.3904	-0.0002	24.58	28.08
5	0.7194	0.004	1.3900	0.0000	24.57	28.06
6	0.71932	0.008	1.3904	-0.0002	24.66	28.08
7	0.7191	-0.003	1.3905	-0.0002	24.65	28.09
8	0.7196	0.002	1.3896	0.0003	24.67	28.04
9	0.7195	0.006	1.3899	0.0001	24.68	28.05
10	0.7202	-0.003	1.3885	0.0008	24.62	27.98

*Calculated from envelope density

Appendix G – Viscosity Measurements

This appendix contains the temperatures at which viscosity was measured, and the measured viscosity data for each of the glasses in this matrix. The plots shown in this appendix are fitted to the Arrhenius equation:

$$\ln(\eta) = A + \frac{B}{T_K}$$

where A and B are independent of temperature and temperature (T_K) is in K (T(°C) + 273.15).

Table G.1. Temperatures at which viscosity was measured

Glass ID	Temperature (°C)					
LAWHNK-01	1149.0	1058.8	966.4	1146.6	1238.8	1150.5
LAWHNK-02	1149.7	1060.3	966.0	1149.3	1239.7	1150.9
LAWHNK-03	1143.4	1057.7	NM	1145.6	1237.2	1148.5
LAWHNK-04	1149.2	1058.5	967.7	1146.9	1239.2	1150.6
LAWHNK-05	1146.7	1056.4	NM	1145.6	1236.7	1148.8
LAWHNK-06	1149.2	1061.2	969.7	1150.0	1241.3	1151.8
LAWHNK-07	1150.7	1061.8	969.2	1152.3	1242.5	1152.5
LAWHNK-08	1151.3	1062.8	970.7	1151.3	1243.1	1153.8
LAWHNK-09	1153.6	1063.2	NM	1152.7	1243.0	1153.3
LAWHNK-10	1154.1	1063.7	972.2	1153.8	1243.6	1153.9
LAWHNK-11	1153.3	1064.3	974.6	1154.3	1244.1	1154.1
LAWHNK-12	1152.5	1063.7	971.4	1153.5	1244.0	1154.0
LAWHNK-13	1151.8	1065.7	971.7	1152.5	1243.7	1153.3
LAWHNK-14	1152.1	1063.5	971.1	1153.7	1244.2	1153.5
LAWHNK-15	1150.4	1060.9	970.3	1151.0	1241.7	1152.1
LAWHNK-16	1153.8	1063.9	972.4	1153.0	1244.5	1154.5
LAWHNK-17	1154.8	1064.2	972.8	1154.1	1244.8	1154.8
LAWHNK-18	1152.7	1063.3	971.5	1153.2	1243.0	1153.0
LAWHNK-19	1153.8	1064.0	972.4	1153.8	1243.6	1153.3
LAWHNK-20	1153.5	1062.4	970.8	1152.8	1243.2	1153.9
NM=not measured						

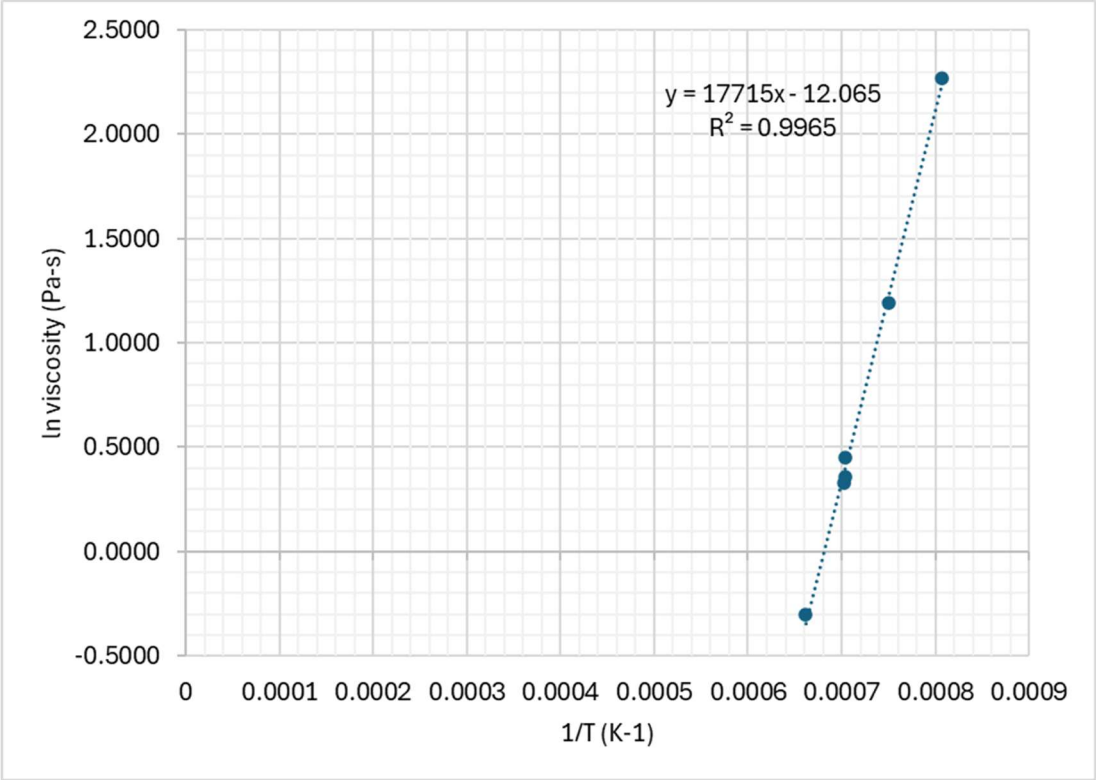


Figure G.1. Viscosity-Temperature Data and Arrhenius Equation Fit for LAWHNK-01.

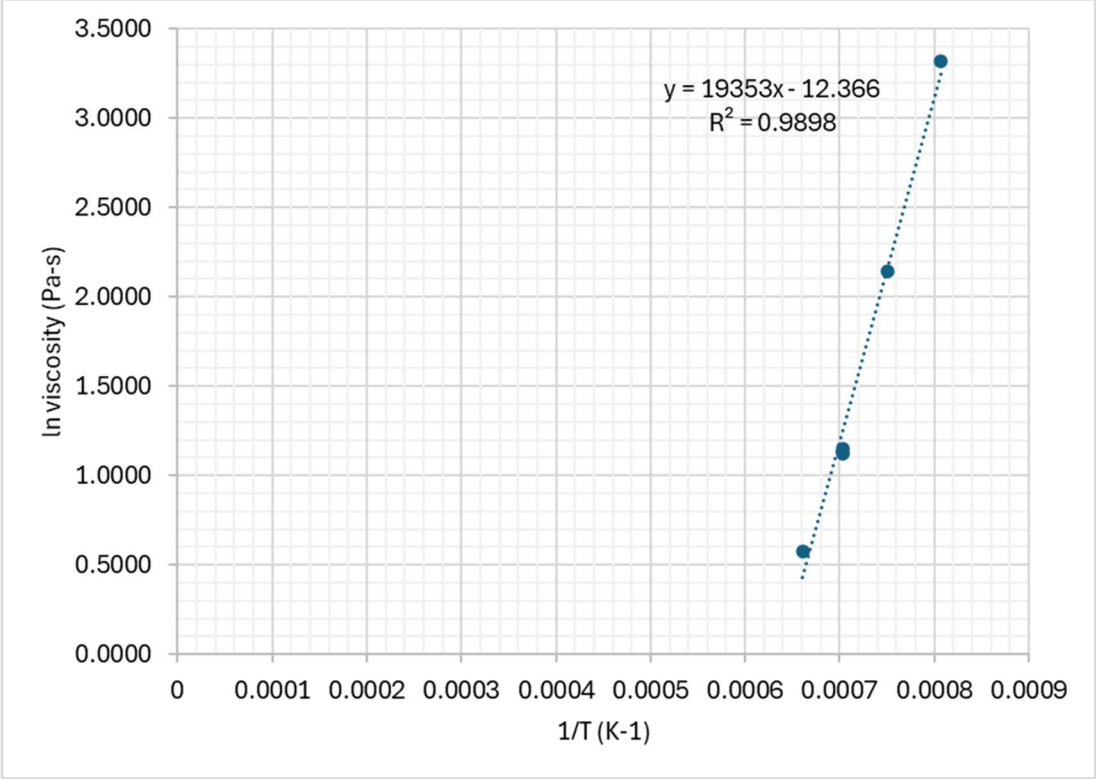


Figure G.2. Viscosity-Temperature Data and Arrhenius Equation Fit for LAWHNK-02.

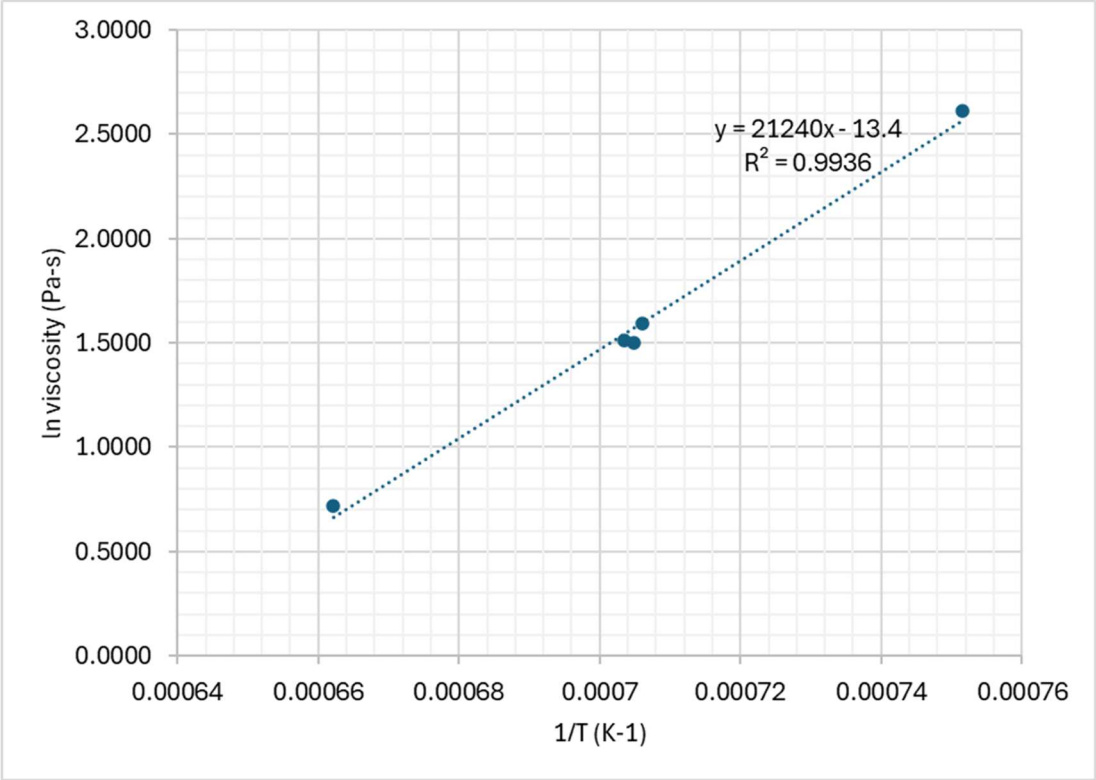


Figure G.3. Viscosity-Temperature Data and Arrhenius Equation Fit for LAWHNK-03.

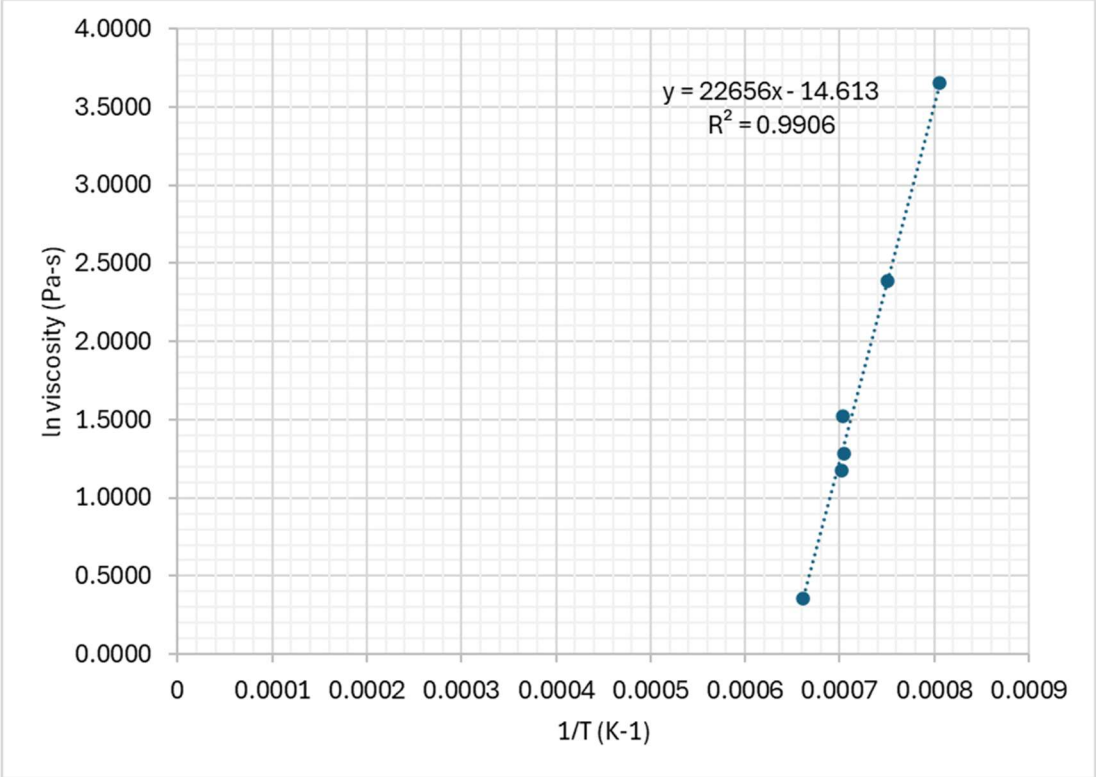


Figure G.4. Viscosity-Temperature Data and Arrhenius Equation Fit for LAWHNK-04.

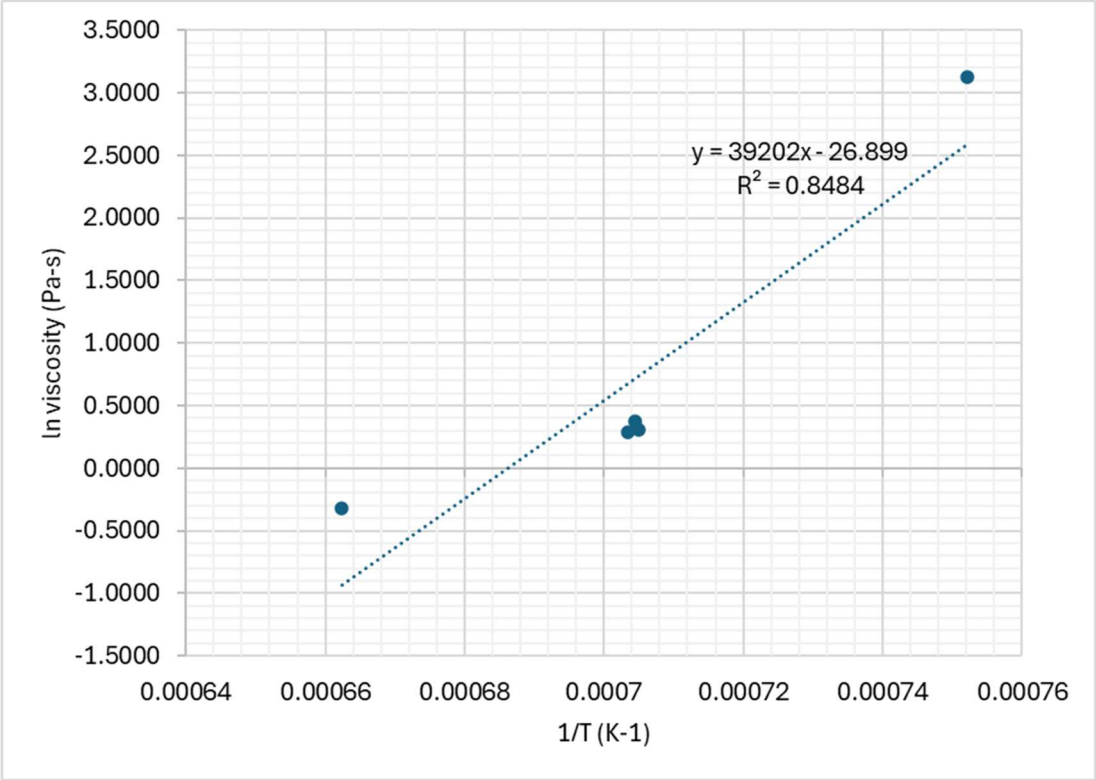


Figure G.5. Viscosity-Temperature Data and Arrhenius Equation Fit for LAWHNK-05.

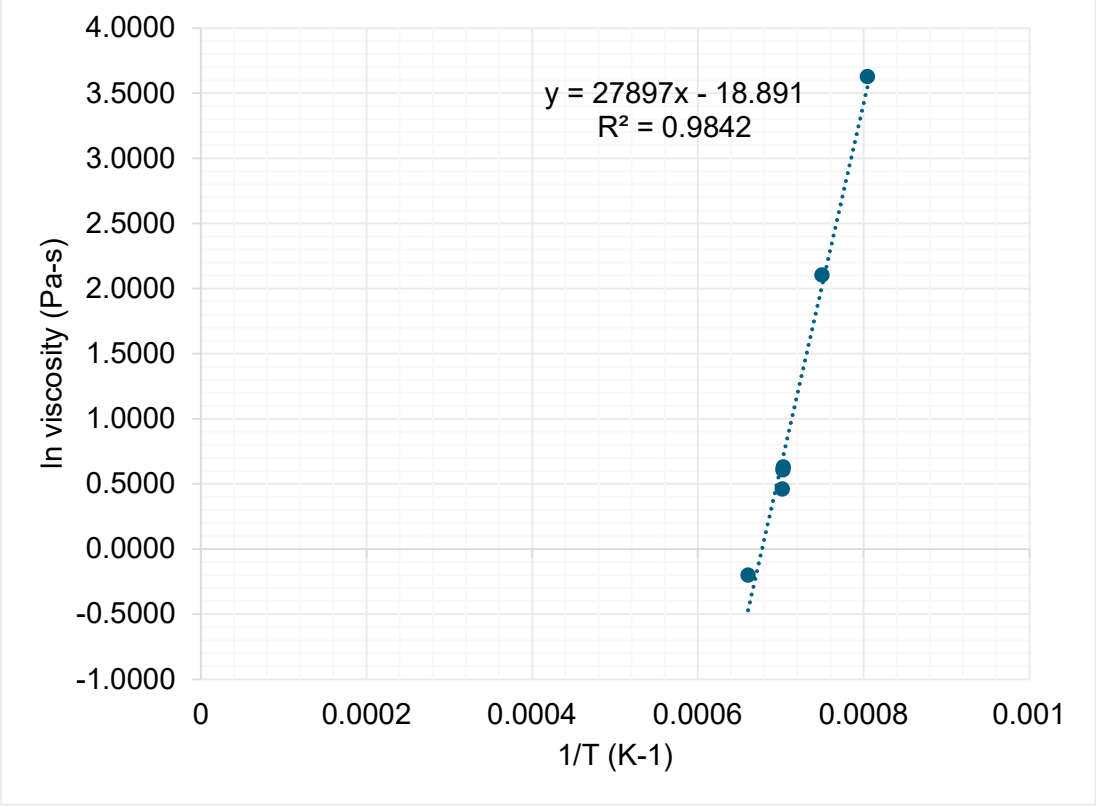


Figure G.6. Viscosity-Temperature Data and Arrhenius Equation Fit for LAWHNK-06.

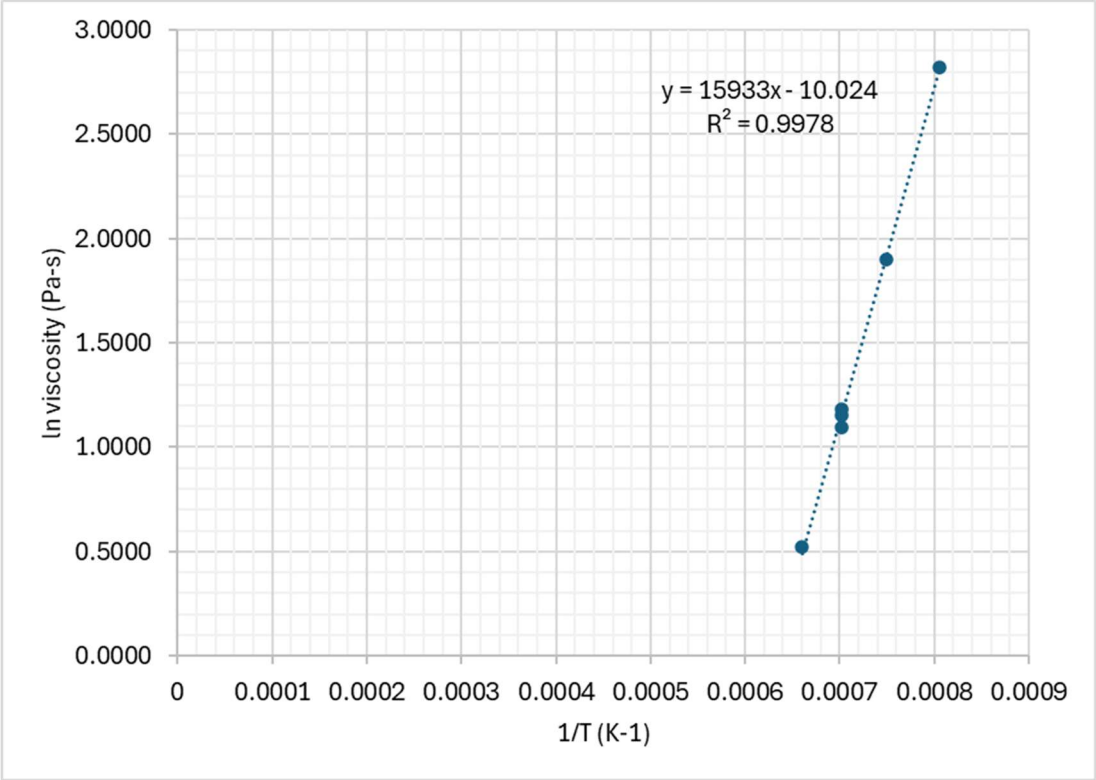


Figure G.7. Viscosity-Temperature Data and Arrhenius Equation Fit for LAWHNK-07.

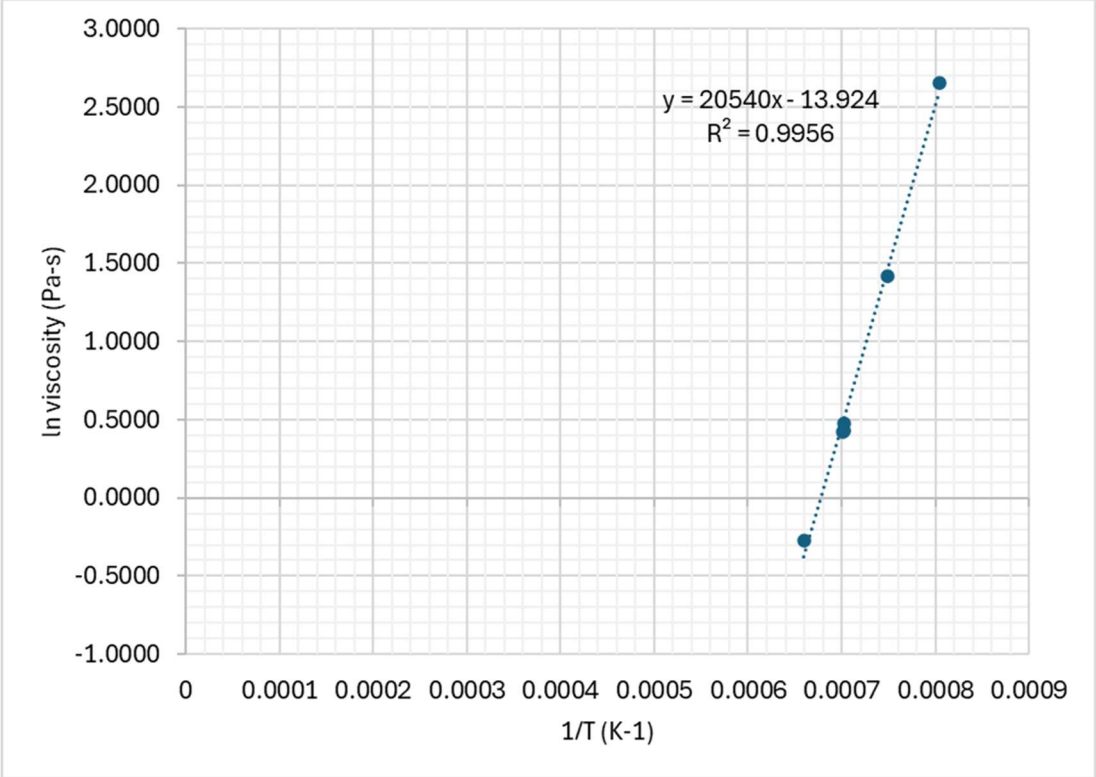


Figure G.8. Viscosity-Temperature Data and Arrhenius Equation Fit for LAWHNK-08.

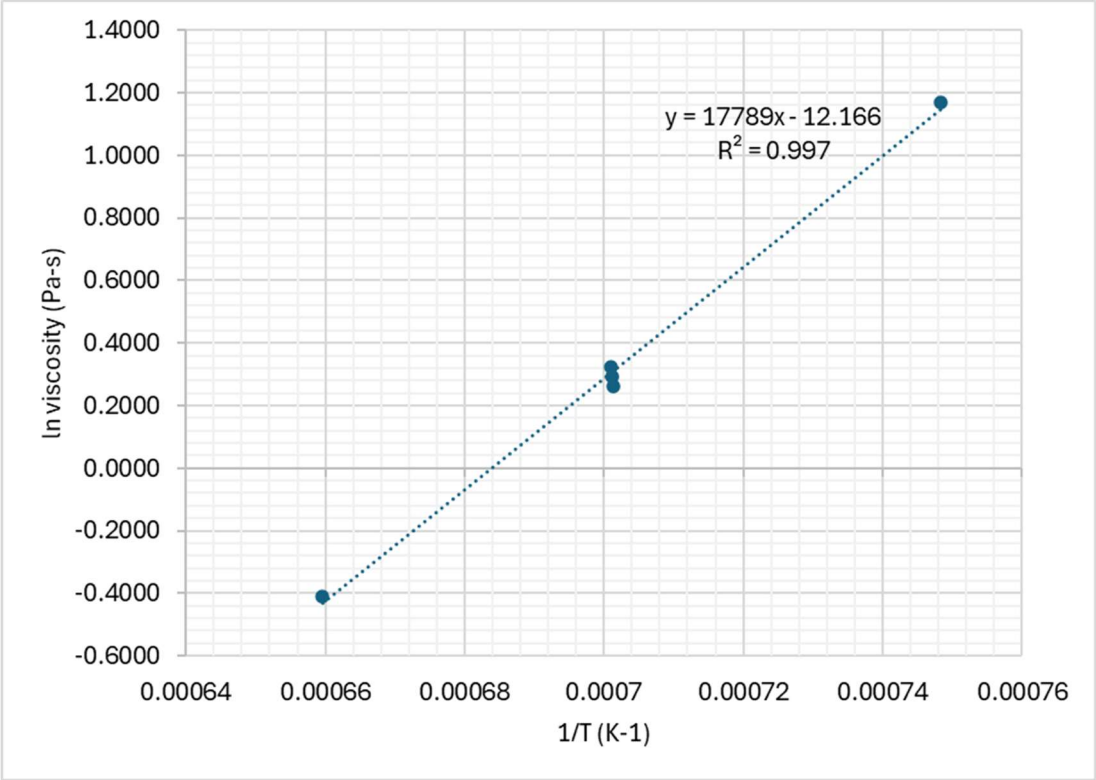


Figure G.9. Viscosity-Temperature Data and Arrhenius Equation Fit for LAWHNK-09.

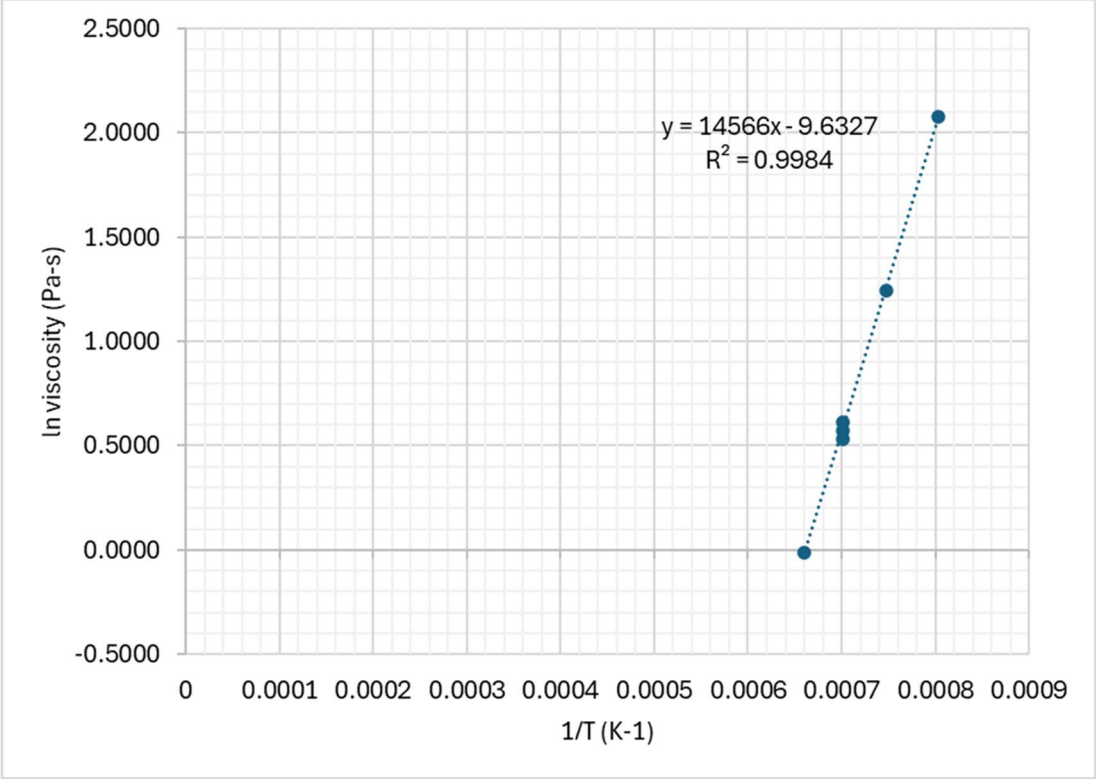


Figure G.10. Viscosity-Temperature Data and Arrhenius Equation Fit for LAWHNK-10.

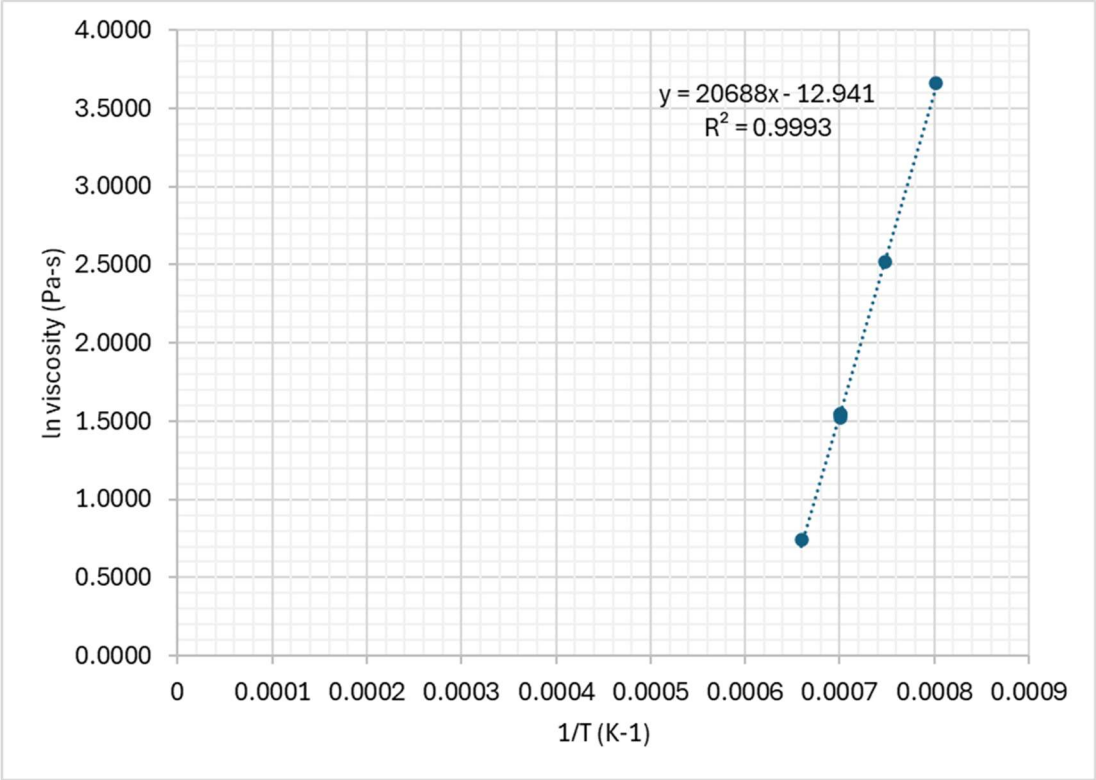


Figure G.11. Viscosity-Temperature Data and Arrhenius Equation Fit for LAWHNK-11.

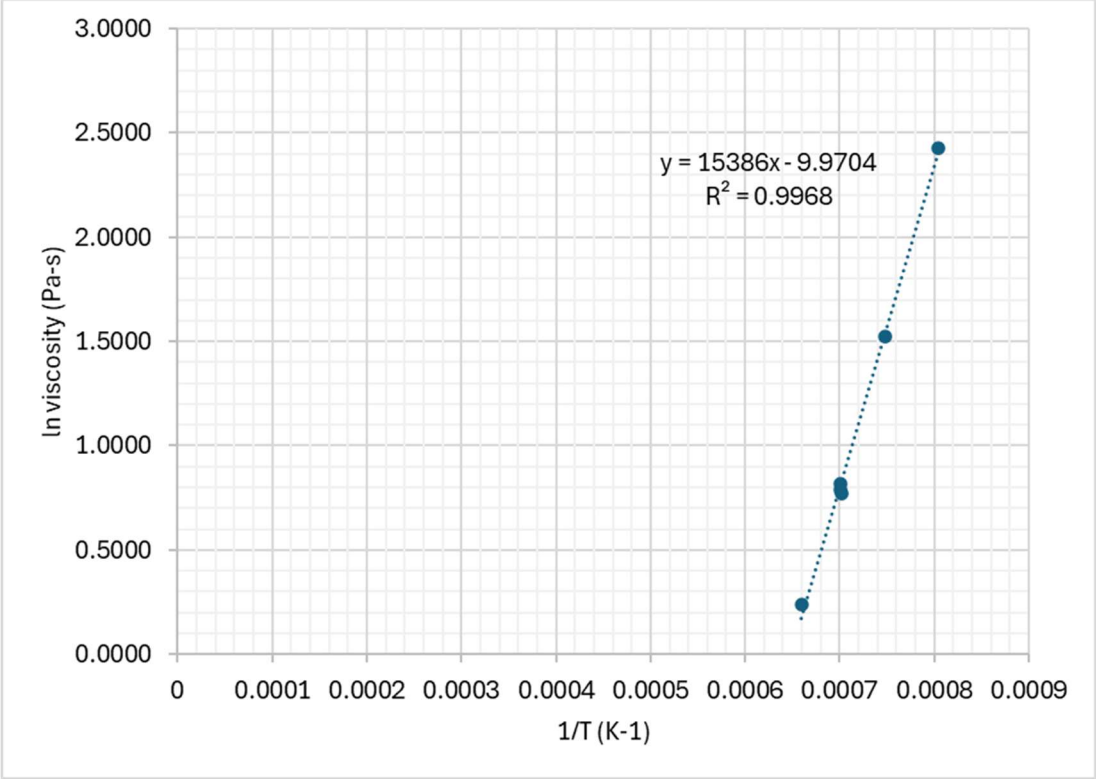


Figure G.12. Viscosity-Temperature Data and Arrhenius Equation Fit for LAWHNK-12.

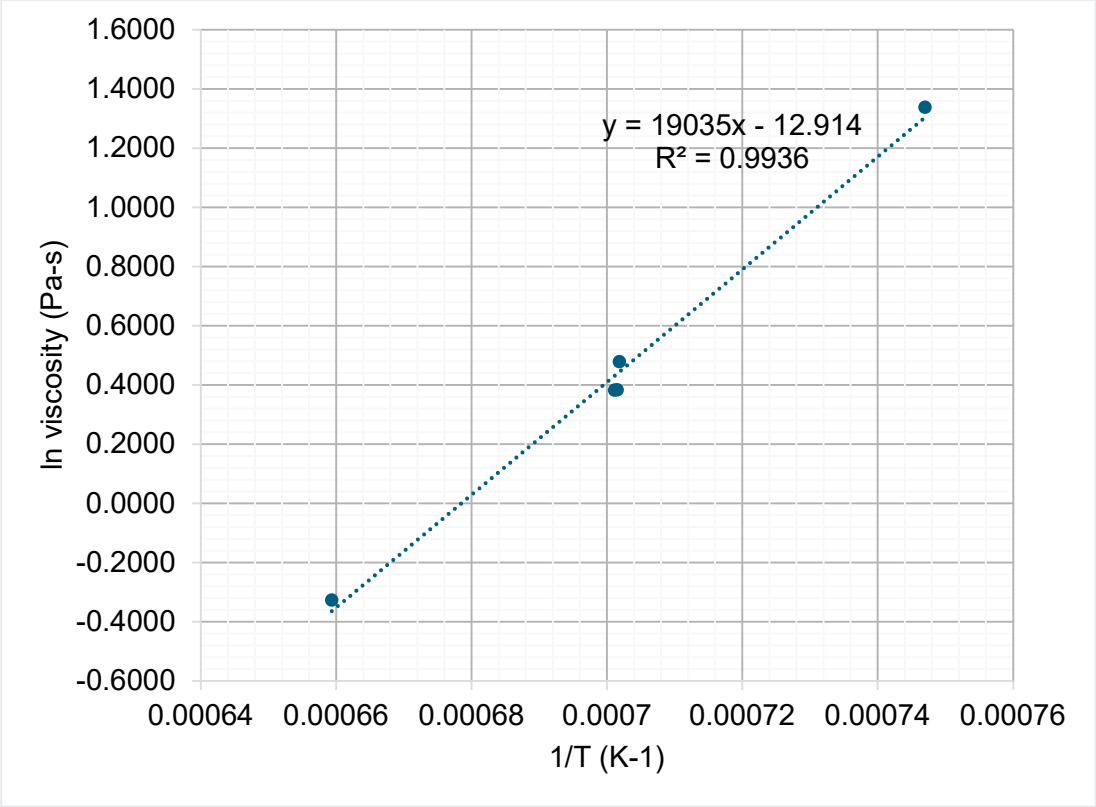


Figure G.13. Viscosity-Temperature Data and Arrhenius Equation Fit for LAWHNK-13.

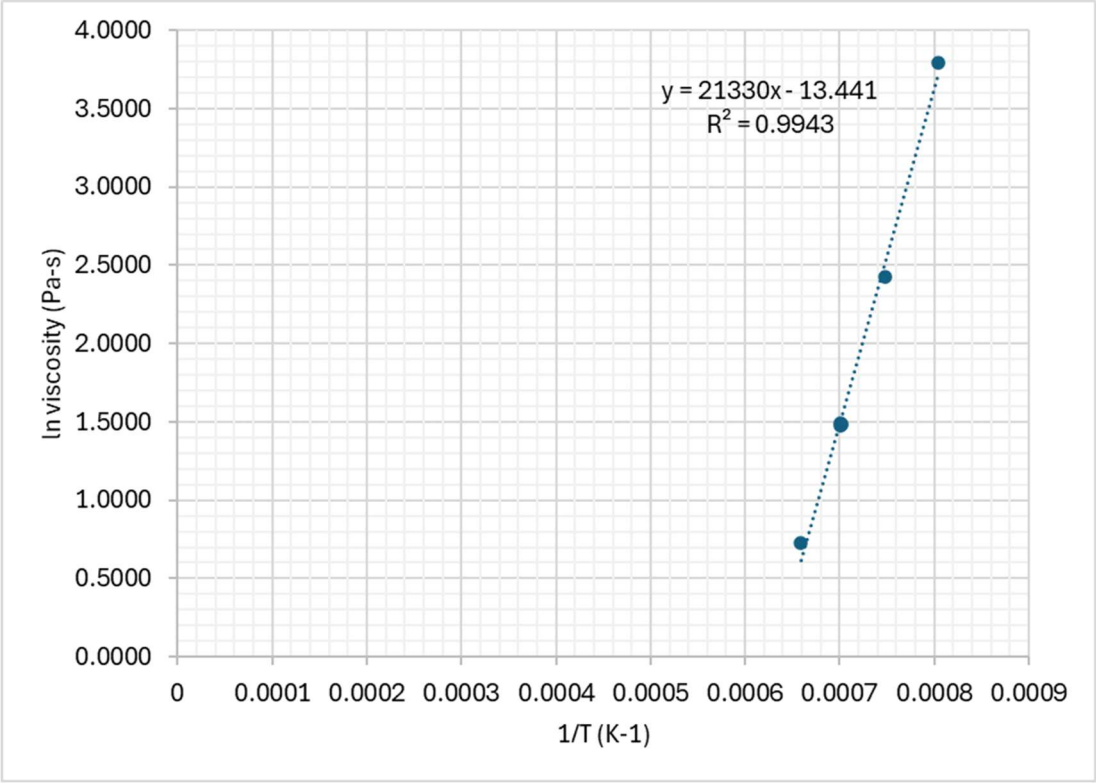


Figure G.14. Viscosity-Temperature Data and Arrhenius Equation Fit for LAWHNK-14.

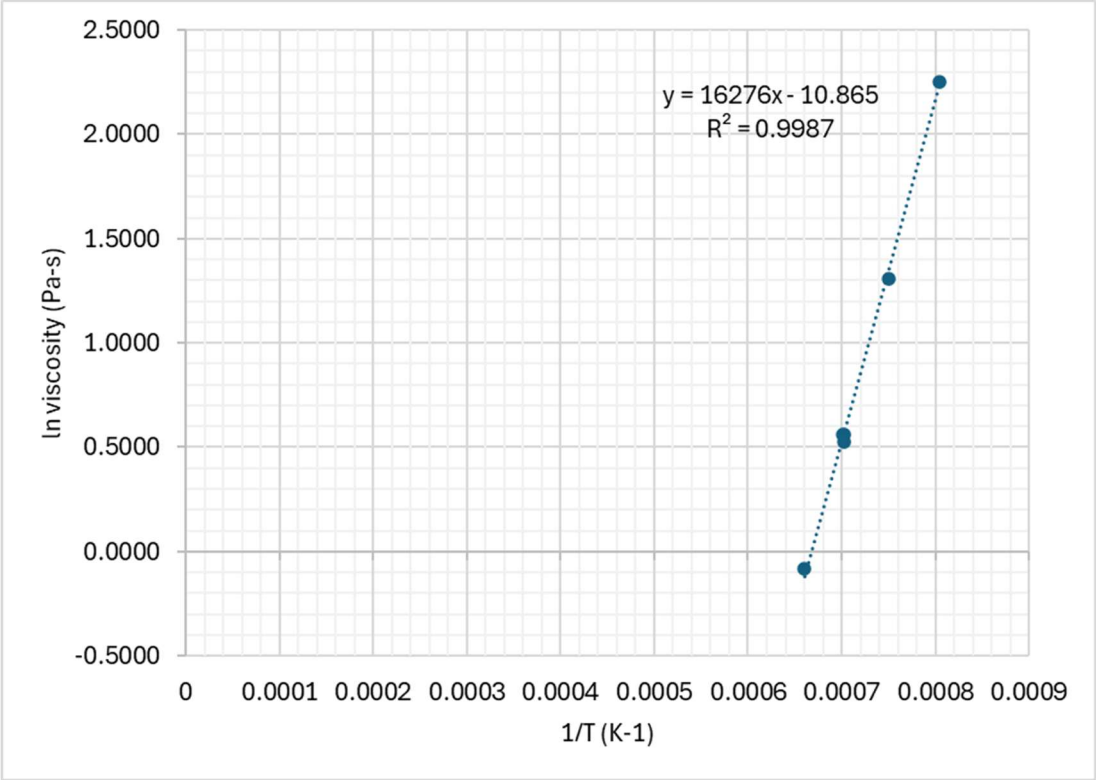


Figure G.15. Viscosity-Temperature Data and Arrhenius Equation Fit for LAWHNK-15.

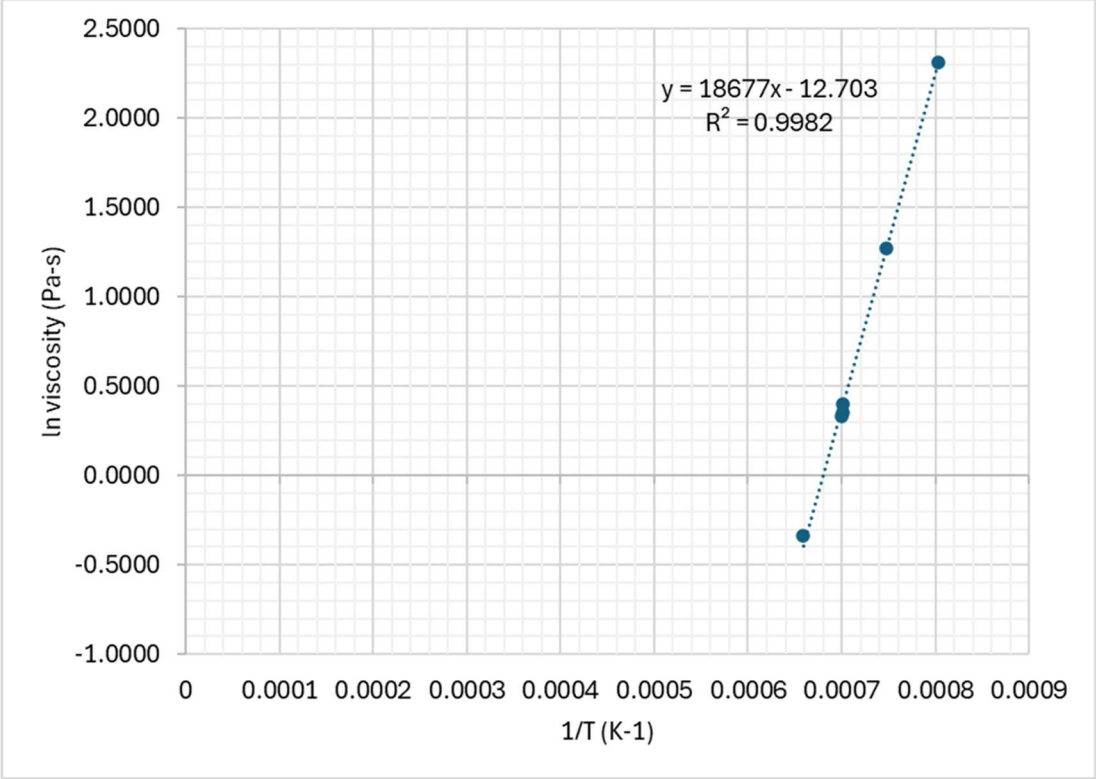


Figure G.16. Viscosity-Temperature Data and Arrhenius Equation Fit for LAWHNK-16.

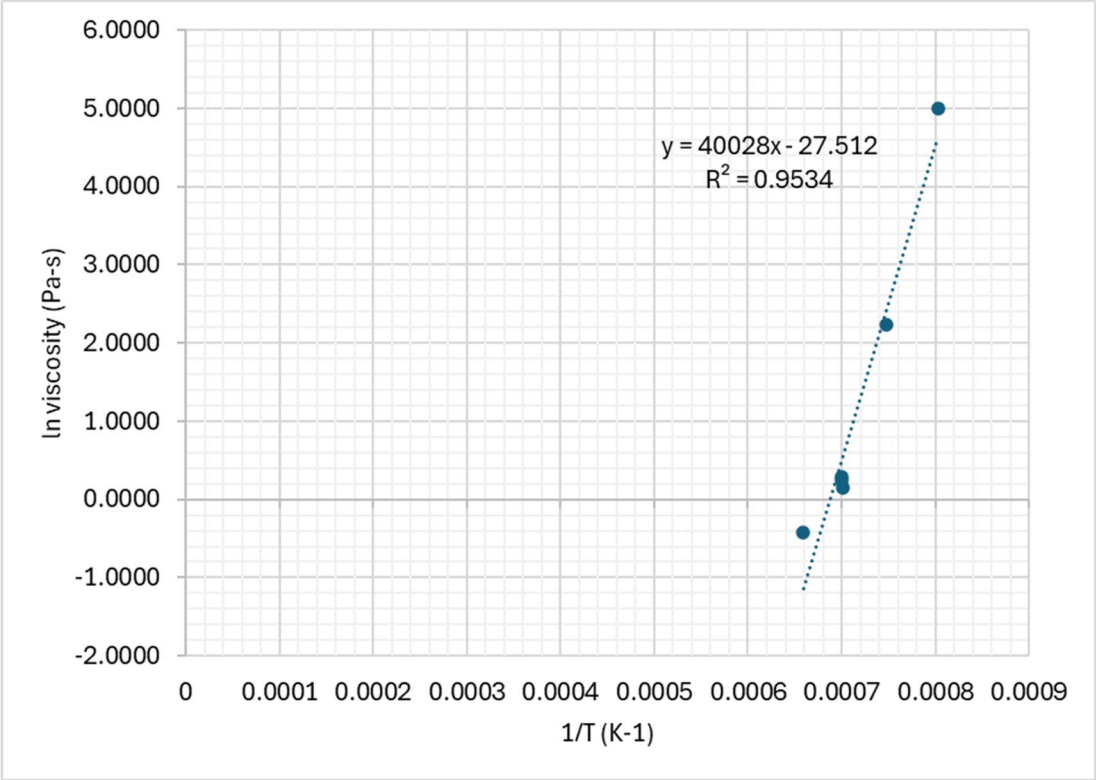


Figure G.17. Viscosity-Temperature Data and Arrhenius Equation Fit for LAWHNK-17.

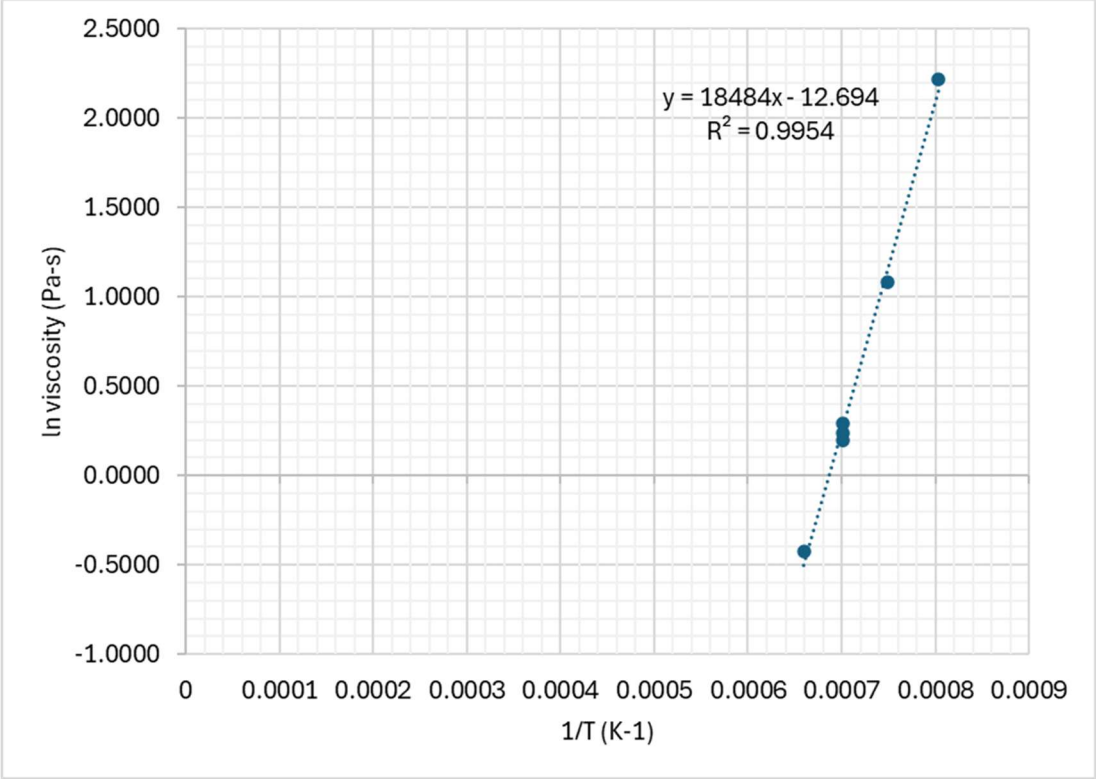


Figure G.18. Viscosity-Temperature Data and Arrhenius Equation Fit for LAWHNK-18.

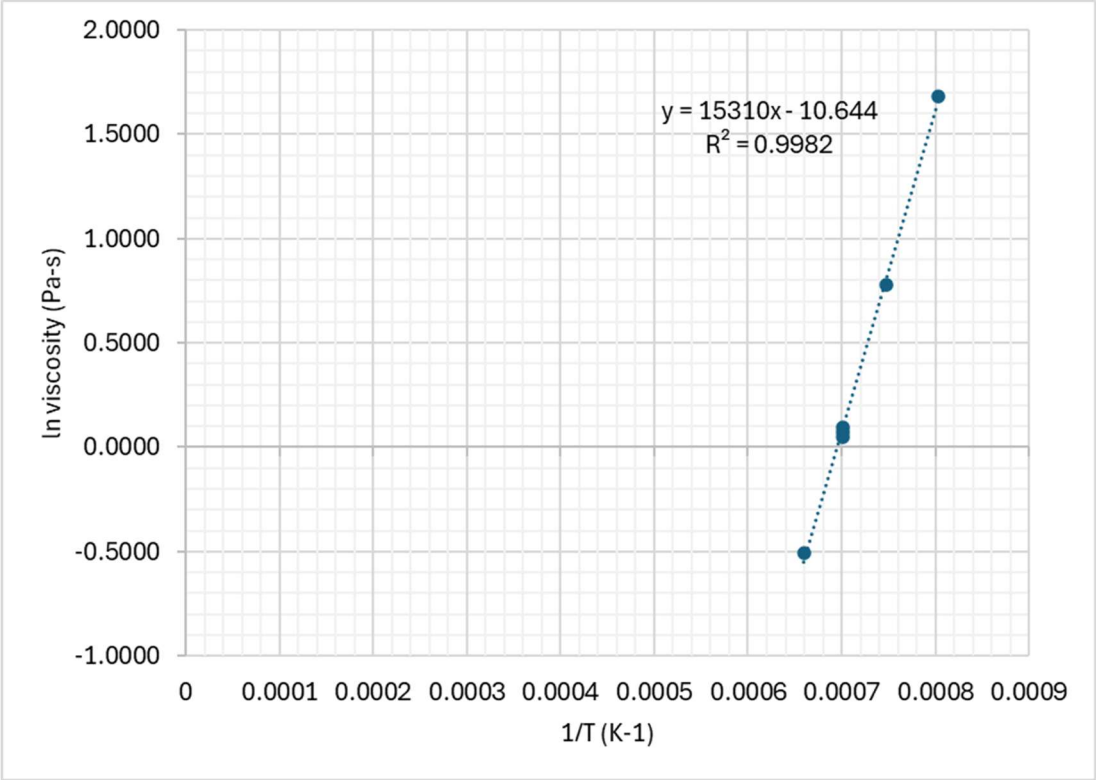


Figure G.19. Viscosity-Temperature Data and Arrhenius Equation Fit for LAWHNK-19.

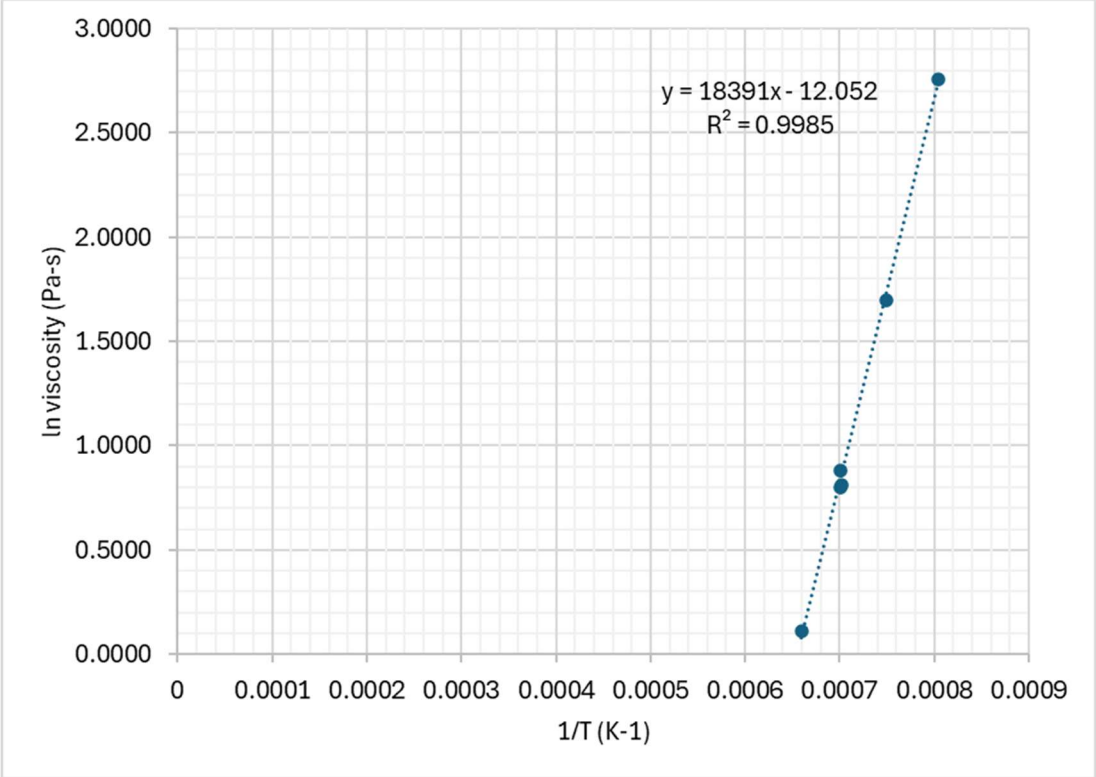


Figure G.20. Viscosity-Temperature Data and Arrhenius Equation Fit for LAWHNK-20.

Appendix H – Electrical Conductivity Measurements

This appendix contains the measured electrical conductivity data for each of the glasses in this matrix. The plots shown in this appendix are fitted to the Arrhenius equation:

$$\ln(\sigma) = A + \frac{B}{T_K}$$

where A and B are independent of temperature and temperature (T_K) is in K (T(°C) + 273.15).

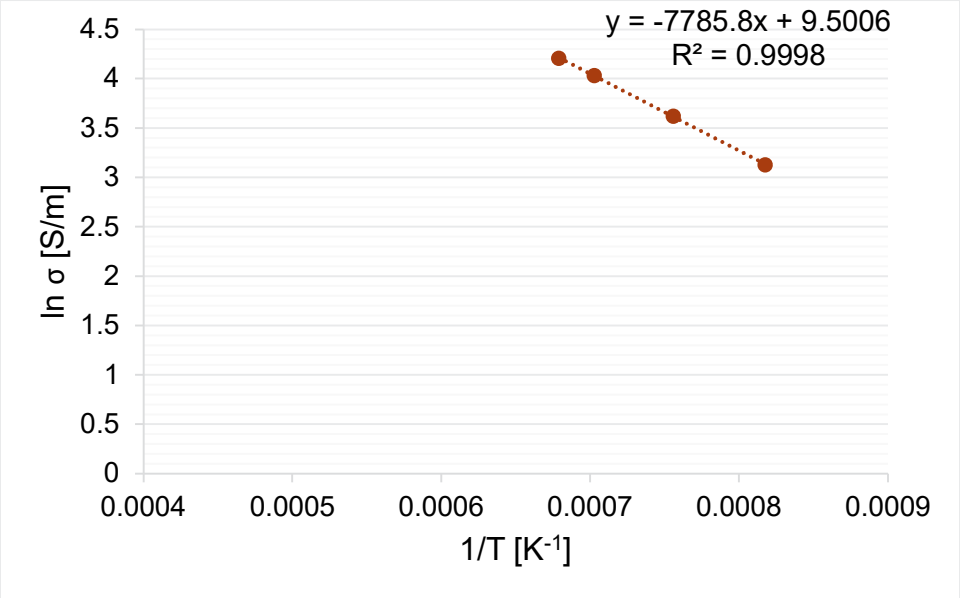


Figure H.1. Electrical Conductivity-Temperature Data and Arrhenius Equation Fit for LAWHNK-01.

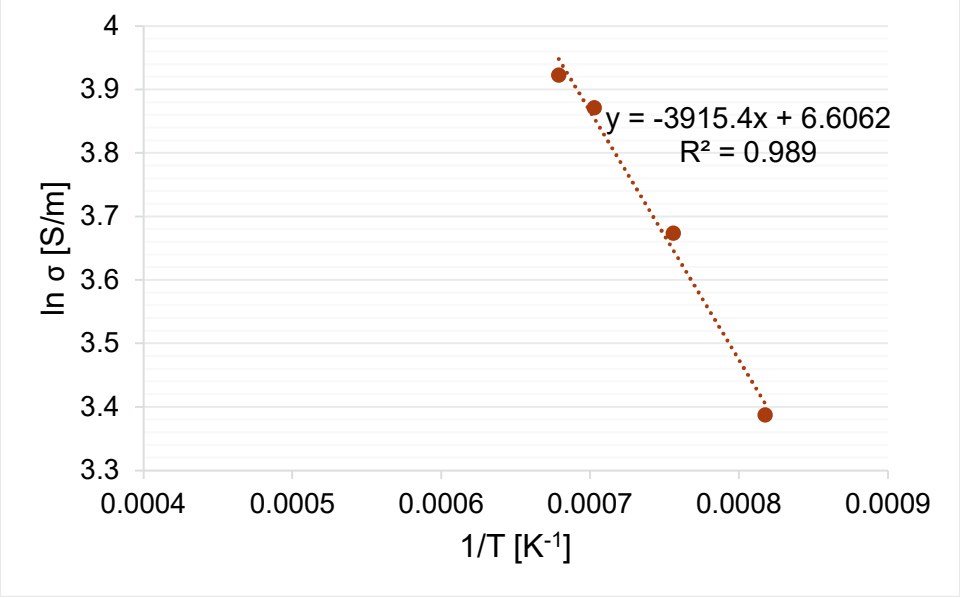


Figure H.2. Electrical Conductivity-Temperature Data and Arrhenius Equation Fit for LAWHNK-02.

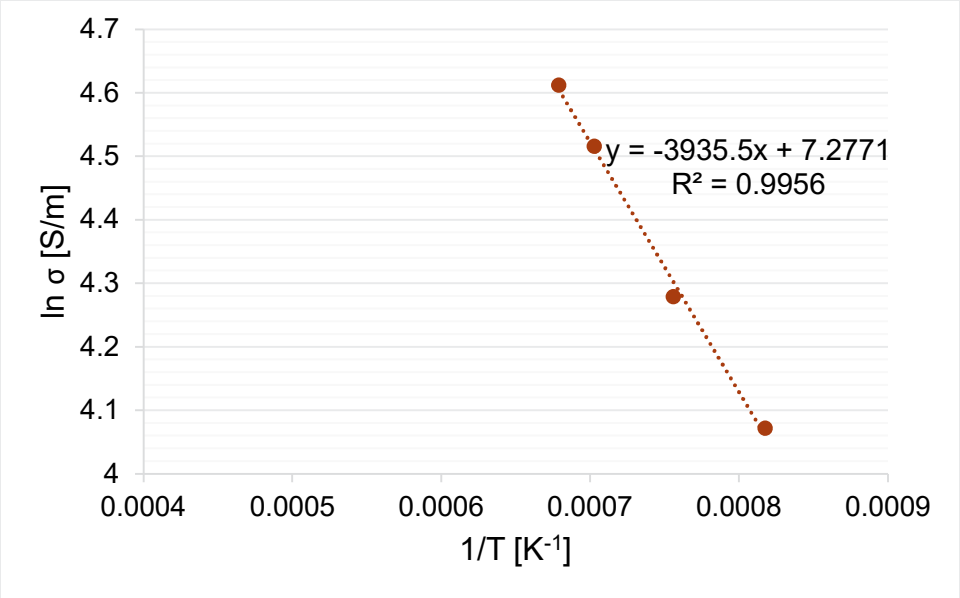


Figure H.3. Electrical Conductivity-Temperature Data and Arrhenius Equation Fit for LAWHNK-03.

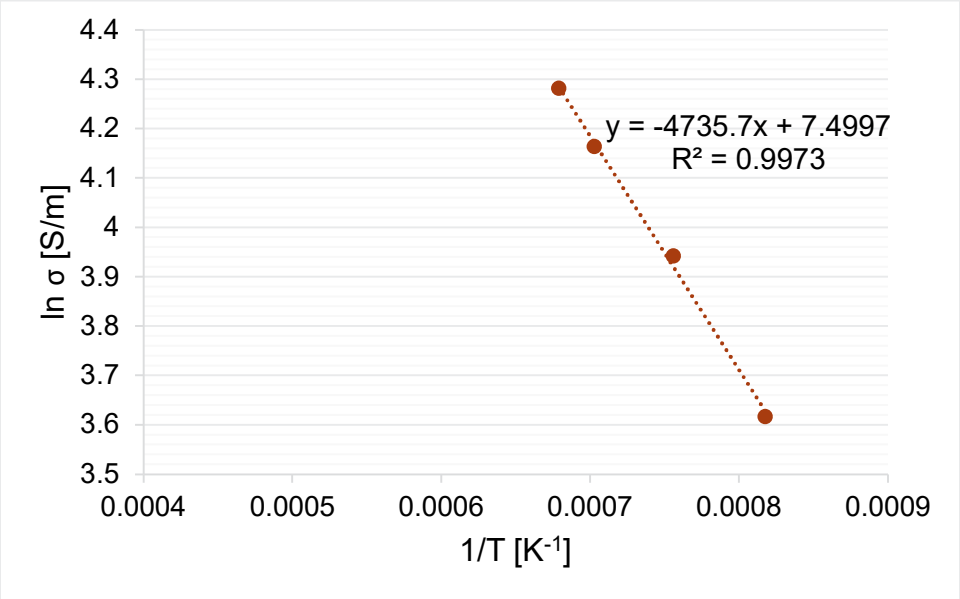


Figure H.4. Electrical Conductivity-Temperature Data and Arrhenius Equation Fit for LAWHNK-04.

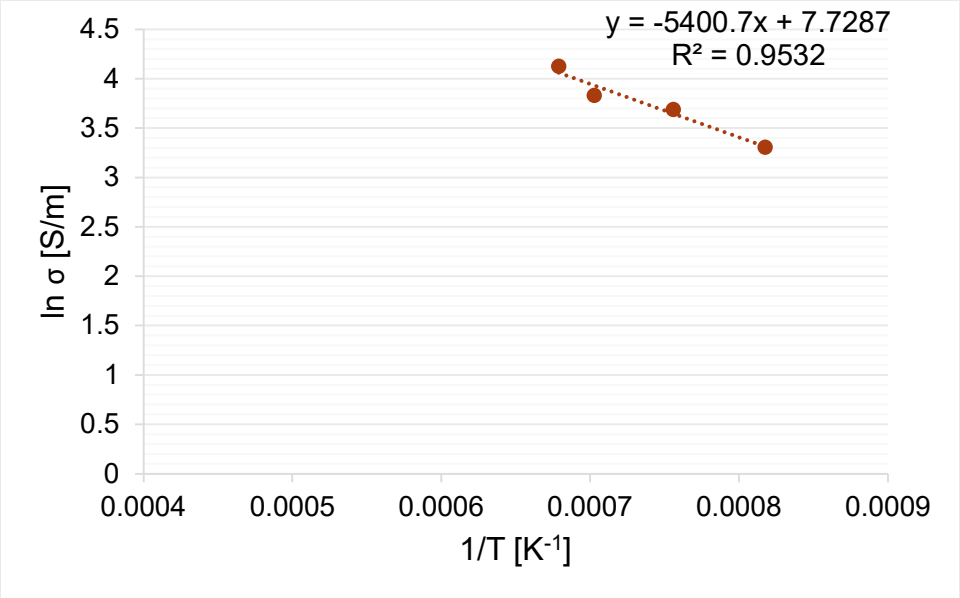


Figure H.5. Electrical Conductivity-Temperature Data and Arrhenius Equation Fit for LAWHNK-05.

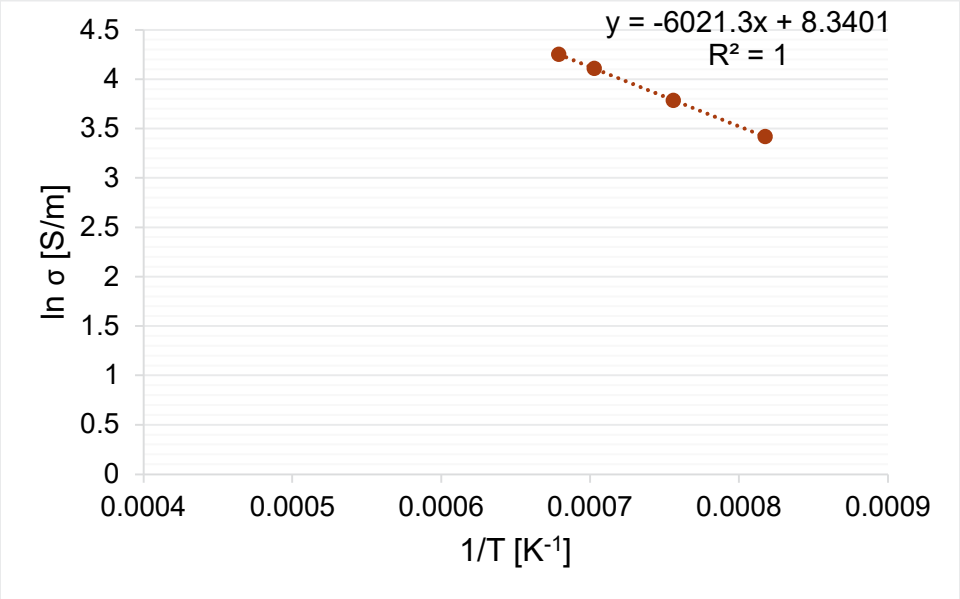


Figure H.6. Electrical Conductivity-Temperature Data and Arrhenius Equation Fit for LAWHNK-06.

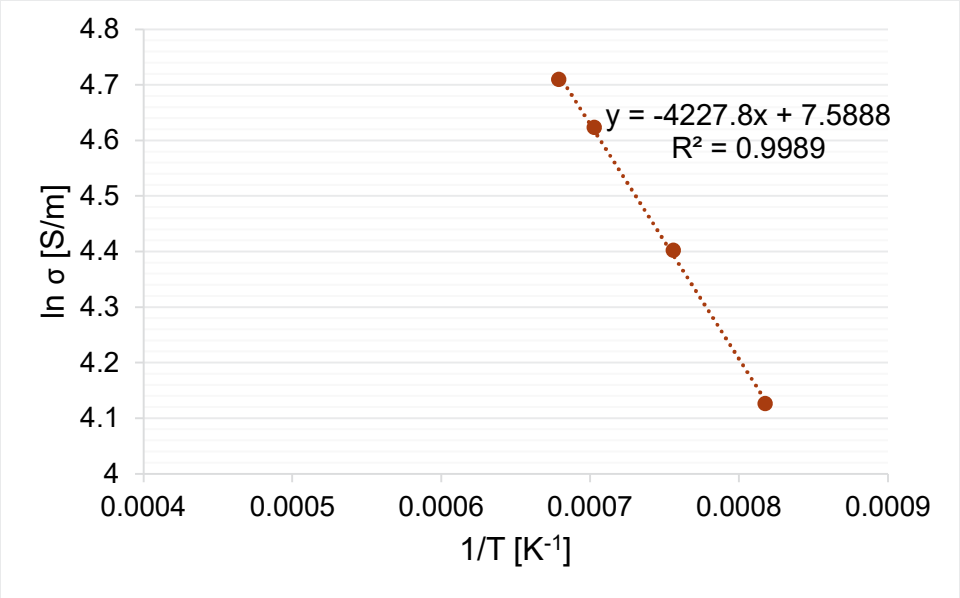


Figure H.7. Electrical Conductivity-Temperature Data and Arrhenius Equation Fit for LAWHNK-07.

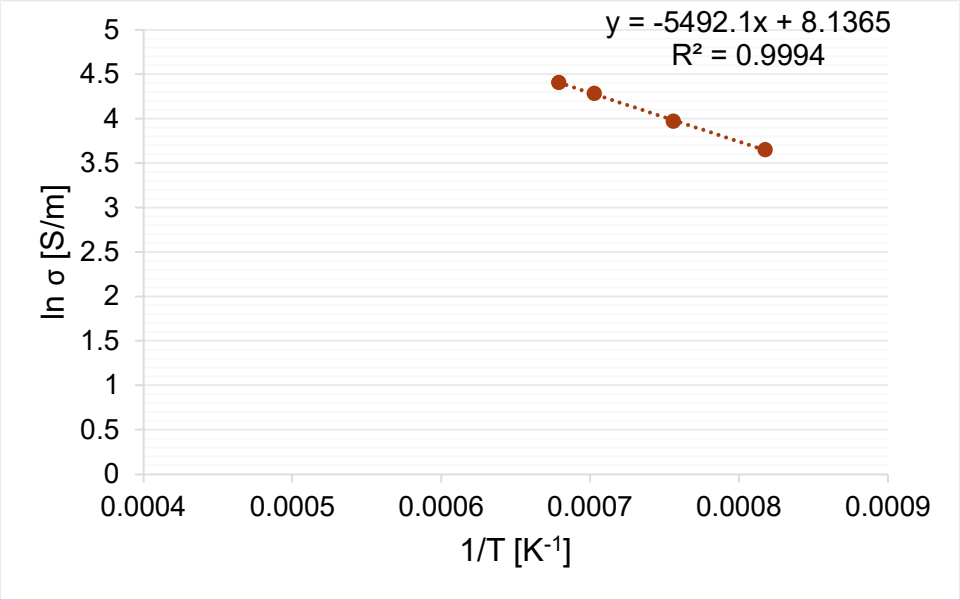


Figure H.8. Electrical Conductivity-Temperature Data and Arrhenius Equation Fit for LAWHNK-08.

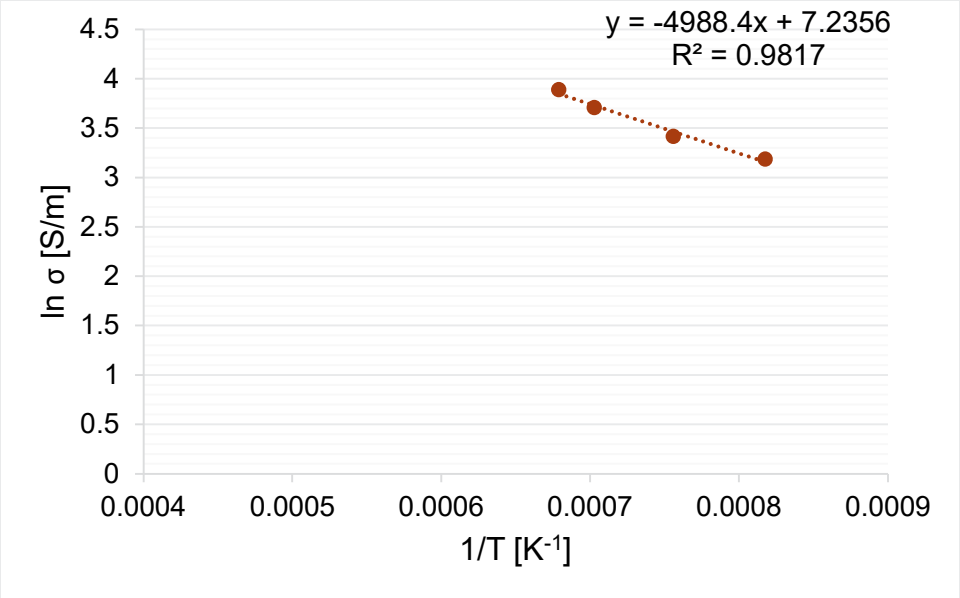


Figure H.9. Electrical Conductivity-Temperature Data and Arrhenius Equation Fit for LAWHNK-09.

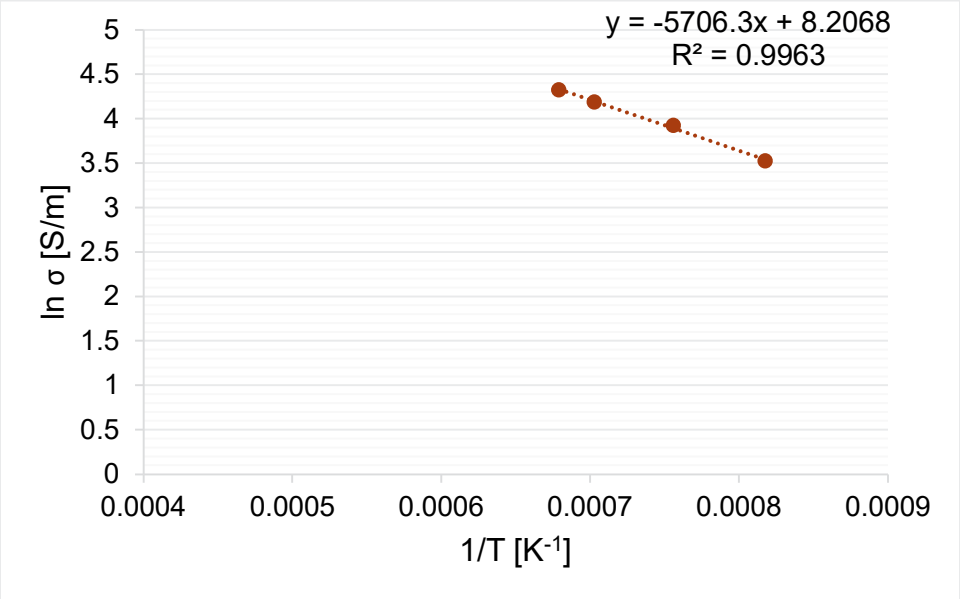


Figure H.10. Electrical Conductivity-Temperature Data and Arrhenius Equation Fit for LAWHNK-10.

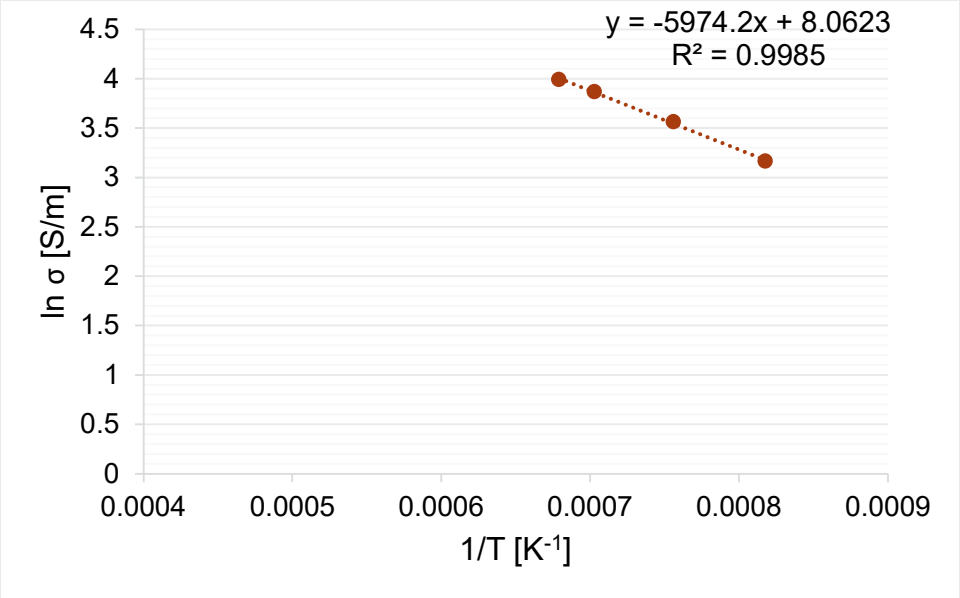


Figure H.11. Electrical Conductivity-Temperature Data and Arrhenius Equation Fit for LAWHNK-11.

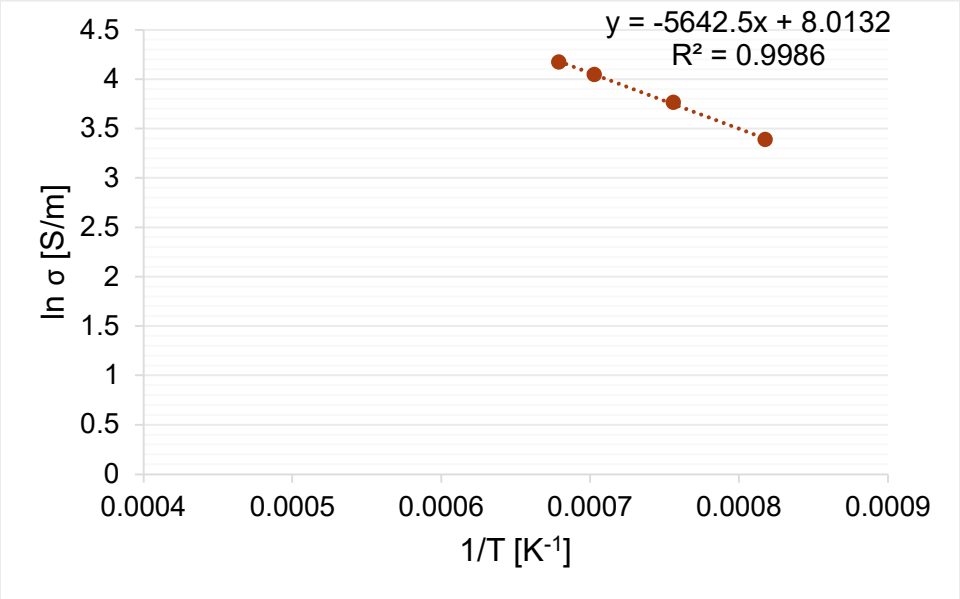


Figure H.12. Electrical Conductivity-Temperature Data and Arrhenius Equation Fit for LAWHNK-12.

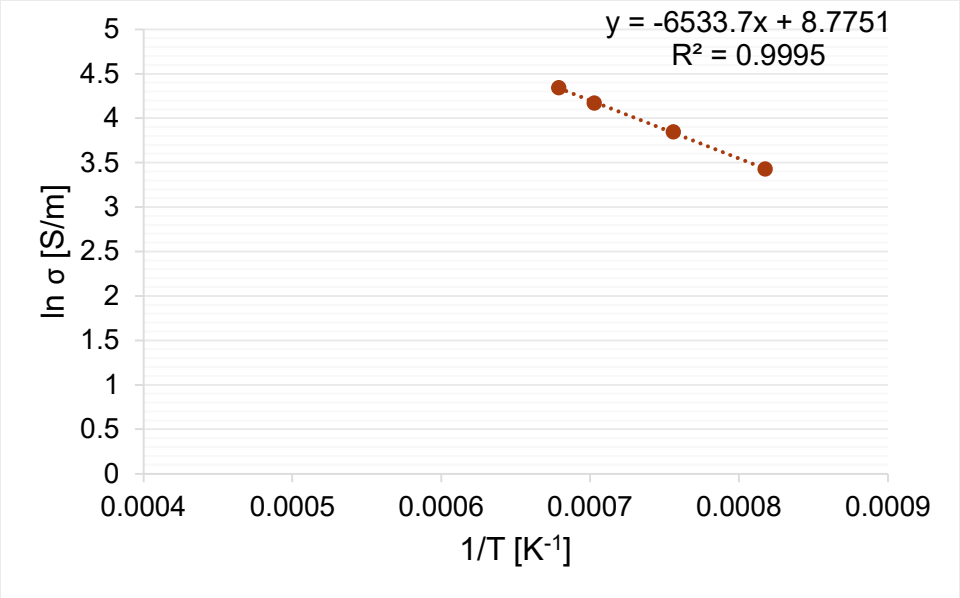


Figure H.13. Electrical Conductivity-Temperature Data and Arrhenius Equation Fit for LAWHNK-13.

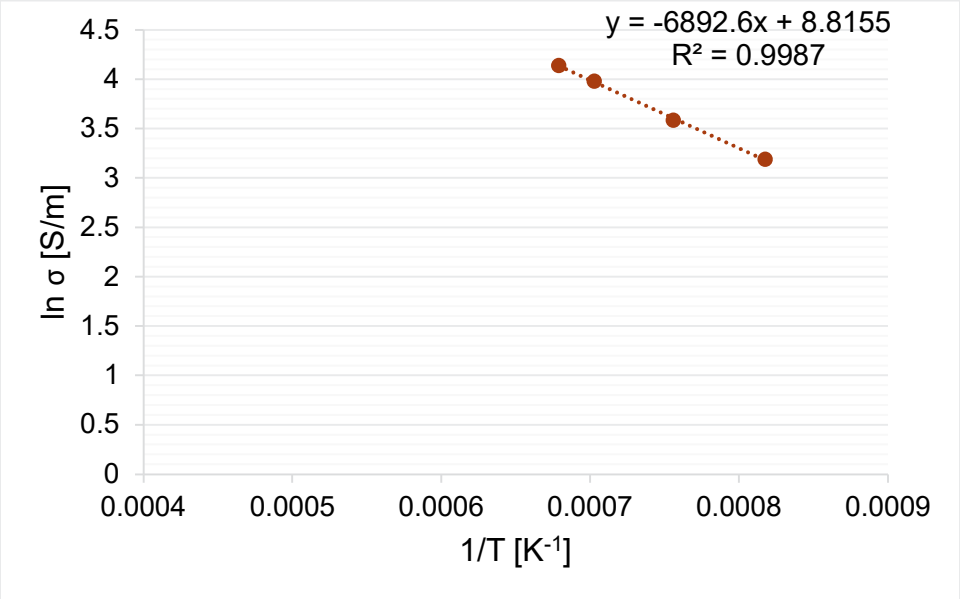


Figure H.14. Electrical Conductivity-Temperature Data and Arrhenius Equation Fit for LAWHNK-14.

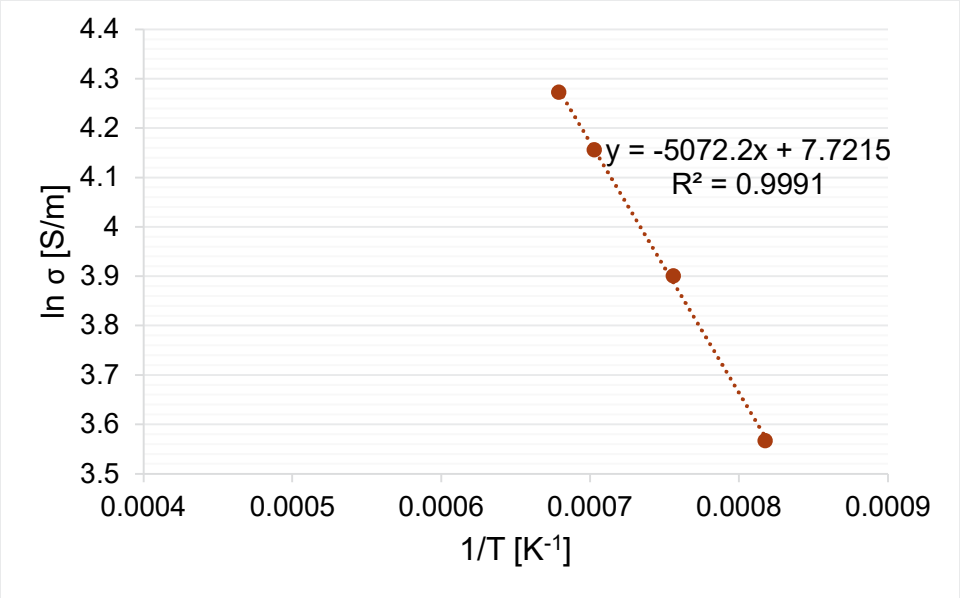


Figure H.15. Electrical Conductivity-Temperature Data and Arrhenius Equation Fit for LAWHNK-15.

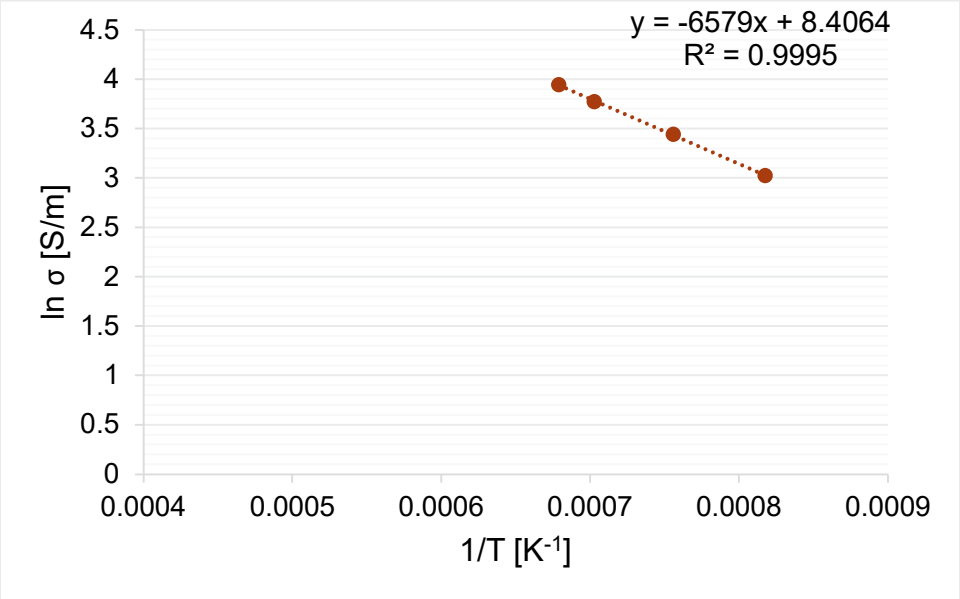


Figure H.16. Electrical Conductivity-Temperature Data and Arrhenius Equation Fit for LAWHNK-16.

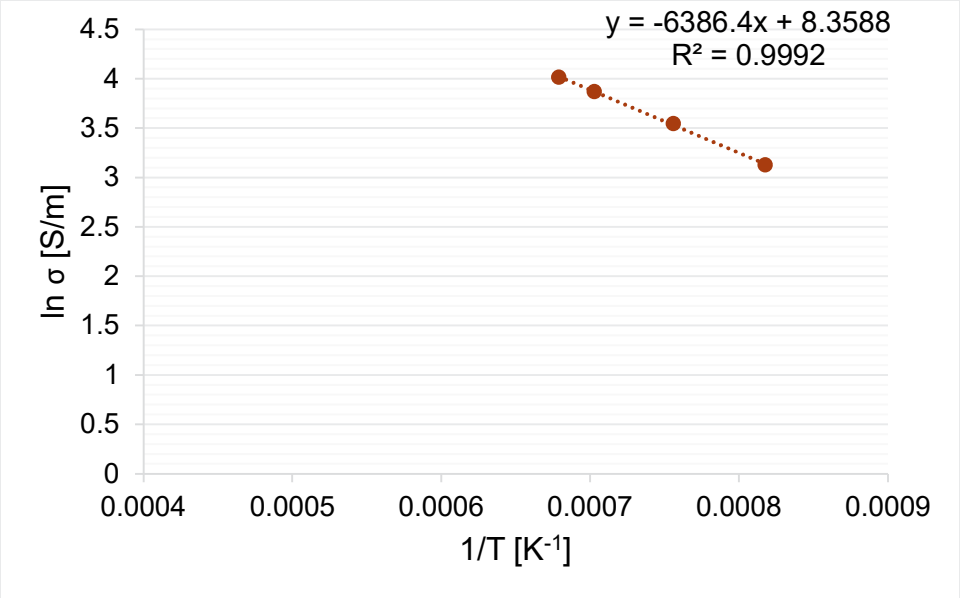


Figure H.17. Electrical Conductivity-Temperature Data and Arrhenius Equation Fit for LAWHNK-17.

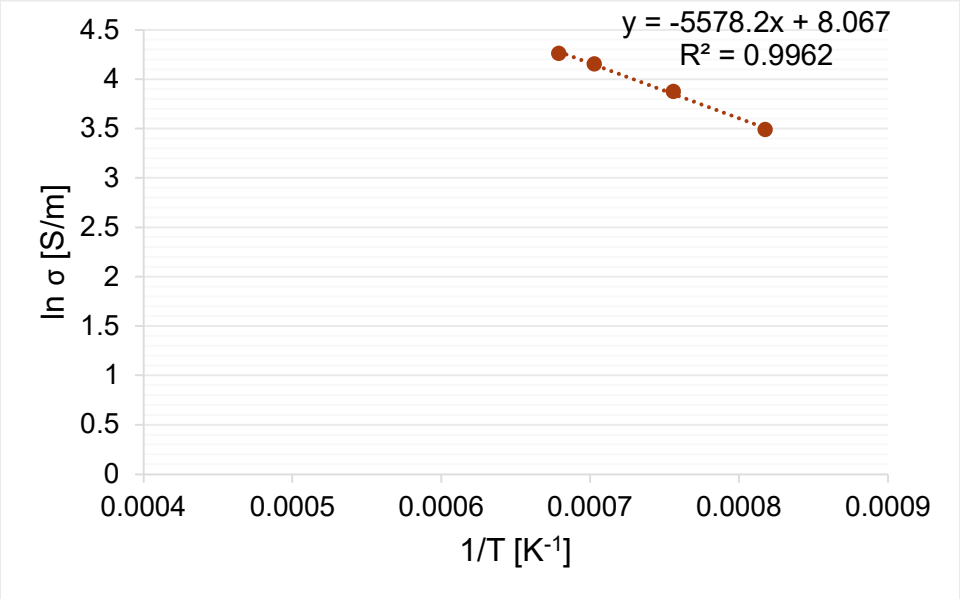


Figure H.18. Electrical Conductivity-Temperature Data and Arrhenius Equation Fit for LAWHNK-18.

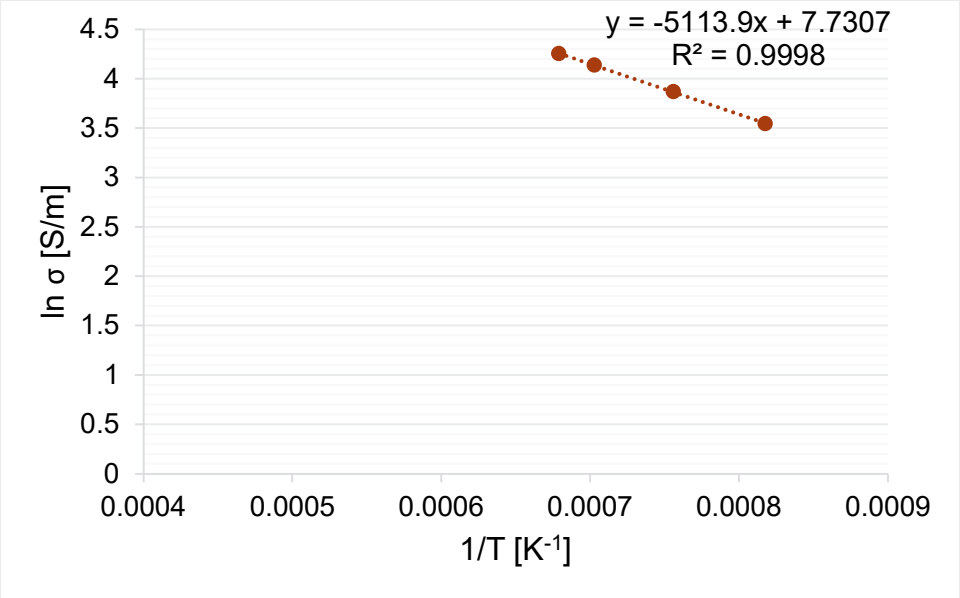


Figure H.19. Electrical Conductivity-Temperature Data and Arrhenius Equation Fit for LAWHNK-19.

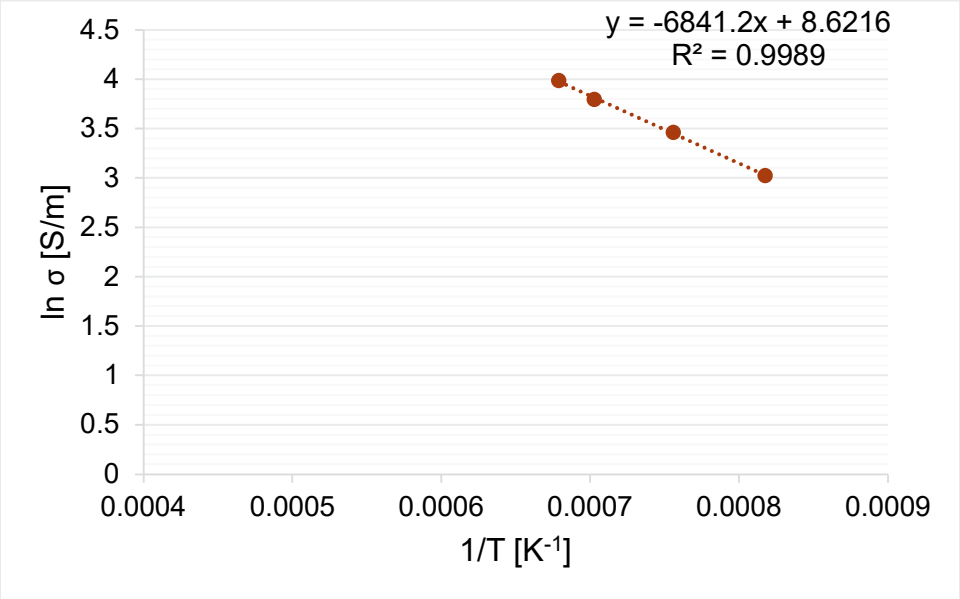


Figure H.20. Electrical Conductivity-Temperature Data and Arrhenius Equation Fit for LAWHNK-20.

Appendix I – PCT Full Results

The list of triplicate product consistency test (PCT) results for all quenched and container centerline cooled (CCC) glasses reported in the present study in g/L.

Table I.1. PCT normalized elemental mass losses (NL_i) in $g \cdot m^{-2}$ of B, Si, and Na for Q and CCC LAWHNK glasses.

	PCT normalized elemental mass losses, $g \cdot m^{-2}$			
Sample ID	Boron	Silicon	Sodium	Lithium
LAWHNK-01-Q-PCT-A	0.34	-1.28	0.66	0.42
LAWHNK-01-Q-PCT-B	0.35	-1.28	0.66	0.43
LAWHNK-01-Q-PCT-C	0.32	-1.30	0.63	0.41
LAWHNK-01-CCC-PCT-A	1.31	-1.42	1.06	0.80
LAWHNK-01-CCC-PCT-B	1.34	-1.42	1.10	0.87
LAWHNK-01-CCC-PCT-C	1.28	-1.46	1.04	0.79
LAWHNK-02-Q-PCT-A	0.74	-1.30	0.55	0.52
LAWHNK-02-Q-PCT-B	0.73	-1.30	0.55	0.51
LAWHNK-02-Q-PCT-C	0.73	-1.31	0.55	0.52
LAWHNK-02-CCC-PCT-A	3.87	-0.45	3.34	3.49
LAWHNK-02-CCC-PCT-B	3.87	-0.46	3.35	3.49
LAWHNK-02-CCC-PCT-C	3.87	-0.44	3.34	3.49
LAWHNK-03-Q-PCT-A	2.06	-1.06	1.52	1.07
LAWHNK-03-Q-PCT-B	2.07	-1.06	1.52	1.08
LAWHNK-03-Q-PCT-C	2.06	-1.05	1.53	1.10
LAWHNK-03-CCC-PCT-A	3.88	-0.09	3.09	2.47
LAWHNK-03-CCC-PCT-B	3.90	-0.08	3.11	2.47
LAWHNK-03-CCC-PCT-C	3.90	-0.08	3.11	2.47
LAWHNK-04-Q-PCT-A	0.23	-1.38	0.24	-0.69
LAWHNK-04-Q-PCT-B	0.22	-1.39	0.25	-0.69
LAWHNK-04-Q-PCT-C	0.25	-1.34	0.28	-0.64
LAWHNK-04-CCC-PCT-A	3.82	0.01	3.05	2.72
LAWHNK-04-CCC-PCT-B	3.82	-0.02	3.05	2.71
LAWHNK-04-CCC-PCT-C	3.82	-0.02	3.07	2.72
LAWHNK-05-Q-PCT-A	0.86	-0.91	0.75	0.49
LAWHNK-05-Q-PCT-B	0.86	-0.91	0.75	0.49
LAWHNK-05-Q-PCT-C	0.85	-0.90	0.75	0.49
LAWHNK-05-CCC-PCT-A	1.06	-0.75	0.87	0.77
LAWHNK-05-CCC-PCT-B	1.06	-0.75	0.88	0.77
LAWHNK-05-CCC-PCT-C	1.05	-0.76	0.87	0.77
LAWHNK-06-Q-PCT-A	-0.64	-1.00	0.19	-1.38
LAWHNK-06-Q-PCT-B	-0.63	-1.00	0.19	-1.38
LAWHNK-06-Q-PCT-C	-0.64	-1.00	0.19	-1.38
LAWHNK-06-CCC-PCT-A	3.79	1.23	3.34	3.24
LAWHNK-06-CCC-PCT-B	3.78	1.13	3.32	3.23
LAWHNK-06-CCC-PCT-C	3.78	1.16	3.33	3.24
LAWHNK-07-Q-PCT-A	0.38	-0.92	0.40	-1.22
LAWHNK-07-Q-PCT-B	0.39	-0.93	0.39	-1.24

	PCT normalized elemental mass losses, $g \cdot m^{-2}$			
Sample ID	Boron	Silicon	Sodium	Lithium
LAWHNK-07-Q-PCT-C	0.39	-0.91	0.40	-1.24
LAWHNK-07-CCC-PCT-A	3.90	0.73	3.28	2.74
LAWHNK-07-CCC-PCT-B	3.91	0.72	3.29	2.73
LAWHNK-07-CCC-PCT-C	3.90	0.72	3.28	2.73
LAWHNK-08-Q-PCT-A	0.62	-0.88	0.68	-0.17
LAWHNK-08-Q-PCT-B	0.62	-0.89	0.67	-0.17
LAWHNK-08-Q-PCT-C	0.59	-0.90	0.65	-0.21
LAWHNK-08-CCC-PCT-A	3.81	-0.15	3.02	2.70
LAWHNK-08-CCC-PCT-B	3.81	-0.24	3.02	2.70
LAWHNK-08-CCC-PCT-C	3.81	-0.17	3.01	2.70
LAWHNK-09-Q-PCT-A	0.96	-1.21	1.20	0.67
LAWHNK-09-Q-PCT-B	0.95	-1.21	1.20	0.61
LAWHNK-09-Q-PCT-C	0.95	-1.21	1.20	0.59
LAWHNK-09-CCC-PCT-A	2.52	-1.19	1.70	0.33
LAWHNK-09-CCC-PCT-B	2.53	-1.14	1.75	0.40
LAWHNK-09-CCC-PCT-C	2.52	-1.14	1.75	0.39
LAWHNK-10-Q-PCT-A	1.01	-1.28	0.80	0.90
LAWHNK-10-Q-PCT-B	1.01	-1.28	0.80	0.91
LAWHNK-10-Q-PCT-C	1.01	-1.28	0.80	0.91
LAWHNK-10-CCC-PCT-A	1.48	-1.02	1.12	1.35
LAWHNK-10-CCC-PCT-B	1.48	-1.01	1.13	1.35
LAWHNK-10-CCC-PCT-C	1.47	-1.01	1.12	1.34
LAWHNK-11-Q-PCT-A	2.60	0.57	2.28	1.19
LAWHNK-11-Q-PCT-B	2.60	0.57	2.27	1.16
LAWHNK-11-Q-PCT-C	2.61	0.59	2.28	1.21
LAWHNK-11-CCC-PCT-A	2.72	0.68	2.33	1.25
LAWHNK-11-CCC-PCT-B	2.74	0.70	2.33	1.25
LAWHNK-11-CCC-PCT-C	2.73	0.69	2.32	1.28
LAWHNK-12-Q-PCT-A	0.22	-1.35	0.12	-0.05
LAWHNK-12-Q-PCT-B	0.22	-1.34	0.13	-0.04
LAWHNK-12-Q-PCT-C	0.21	-1.35	0.11	-0.05
LAWHNK-12-CCC-PCT-A	1.54	-0.31	1.15	1.31
LAWHNK-12-CCC-PCT-B	1.53	-0.34	1.15	1.31
LAWHNK-12-CCC-PCT-C	1.52	-0.36	1.14	1.30
LAWHNK-13-Q-PCT-A	1.54	-0.17	1.45	1.37
LAWHNK-13-Q-PCT-B	1.53	-0.18	1.43	1.35
LAWHNK-13-Q-PCT-C	1.52	-0.19	1.43	1.35
LAWHNK-13-CCC-PCT-A	1.01	-0.45	1.37	0.70
LAWHNK-13-CCC-PCT-B	1.01	-0.46	1.37	0.70
LAWHNK-13-CCC-PCT-C	1.00	-0.46	1.37	0.70
LAWHNK-14-Q-PCT-A	-0.54	-1.14	-0.33	-1.22
LAWHNK-14-Q-PCT-B	-0.56	-1.19	-0.33	-1.21
LAWHNK-14-Q-PCT-C	-0.53	-1.18	-0.29	-1.16
LAWHNK-14-CCC-PCT-A	-0.54	-1.21	-0.40	-0.87
LAWHNK-14-CCC-PCT-B	-0.52	-1.19	-0.39	-0.86
LAWHNK-14-CCC-PCT-C	-0.53	-1.18	-0.39	-0.85

	PCT normalized elemental mass losses, $g \cdot m^{-2}$			
Sample ID	Boron	Silicon	Sodium	Lithium
LAWHNK-15-Q-PCT-A	1.86	0.16	1.65	1.59
LAWHNK-15-Q-PCT-B	1.87	0.17	1.66	1.60
LAWHNK-15-Q-PCT-C	1.86	0.17	1.65	1.59
LAWHNK-15-CCC-PCT-A	1.90	0.12	1.62	1.56
LAWHNK-15-CCC-PCT-B	1.90	0.11	1.61	1.55
LAWHNK-15-CCC-PCT-C	1.90	0.10	1.60	1.55
LAWHNK-16-Q-PCT-A	0.57	-1.03	0.47	0.31
LAWHNK-16-Q-PCT-B	0.56	-1.03	0.47	0.30
LAWHNK-16-Q-PCT-C	0.57	-1.02	0.47	0.31
LAWHNK-16-CCC-PCT-A	2.01	-0.62	1.57	1.38
LAWHNK-16-CCC-PCT-B	2.01	-0.63	1.57	1.39
LAWHNK-16-CCC-PCT-C	2.01	-0.64	1.57	1.39
LAWHNK-17-Q-PCT-A	0.05	-1.00	0.44	0.20
LAWHNK-17-Q-PCT-B	0.03	-1.01	0.42	0.20
LAWHNK-17-Q-PCT-C	0.03	-1.00	0.43	0.20
LAWHNK-17-CCC-PCT-A	2.87	0.50	2.42	2.45
LAWHNK-17-CCC-PCT-B	2.89	0.54	2.45	2.46
LAWHNK-17-CCC-PCT-C	2.89	0.53	2.45	2.47
LAWHNK-18-Q-PCT-A	0.24	-1.19	0.37	-0.15
LAWHNK-18-Q-PCT-B	0.23	-1.19	0.36	-0.16
LAWHNK-18-Q-PCT-C	0.22	-1.20	0.36	-0.16
LAWHNK-18-CCC-PCT-A	0.34	-1.11	0.37	0.01
LAWHNK-18-CCC-PCT-B	0.33	-1.14	0.37	0.01
LAWHNK-18-CCC-PCT-C	0.33	-1.13	0.38	0.02
LAWHNK-19-Q-PCT-A	0.97	-0.72	0.95	0.35
LAWHNK-19-Q-PCT-B	0.97	-0.72	0.96	0.36
LAWHNK-19-Q-PCT-C	0.97	-0.72	0.95	0.35
LAWHNK-19-CCC-PCT-A	0.92	-0.77	0.88	0.50
LAWHNK-19-CCC-PCT-B	0.91	-0.78	0.86	0.49
LAWHNK-19-CCC-PCT-C	0.92	-0.77	0.88	0.50
LAWHNK-20-Q-PCT-A	-0.20	-1.66	-0.02	0.00
LAWHNK-20-Q-PCT-B	-0.21	-1.67	-0.03	0.00
LAWHNK-20-Q-PCT-C	-0.22	-1.68	-0.04	0.00
LAWHNK-20-CCC-PCT-A	1.16	-0.85	1.00	0.00
LAWHNK-20-CCC-PCT-B	1.16	-0.85	1.01	0.00
LAWHNK-20-CCC-PCT-C	1.16	-0.84	1.01	0.00

Appendix J – VHT Images on Quenched Glasses

The photographs in this appendix show each quenched (Q) glass before and after vapor hydration test as described in Section 2.10. Duration of the test is specified in the picture caption.



Figure J.1. Left: LAWHNK-01 Q coupon pre VHT. Center: LAWHNK-01 Q coupon after 24 days VHT. Right: LAWHNK-01 Q coupon after 7 days VHT.

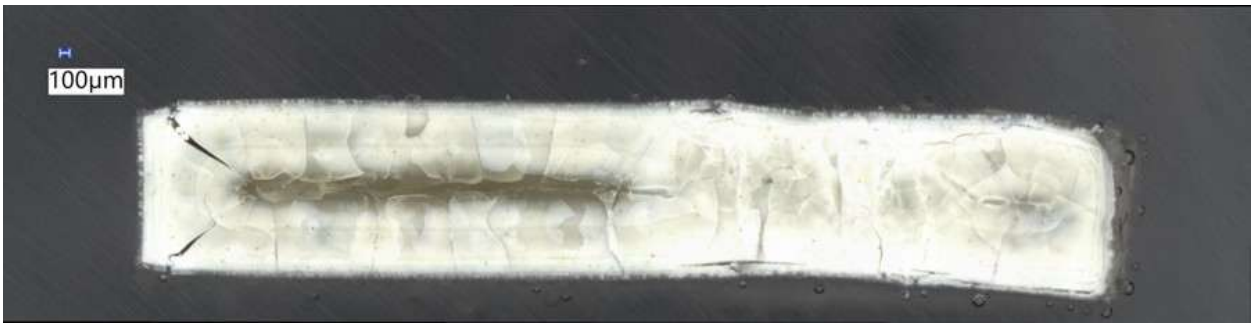


Figure J.2. Cross section of LAWHNK-01 Q coupon after 24 days VHT.



Figure J.3. Cross section of LAWHNK-01 Q coupon after 7 days VHT.



Figure J.4. Left: LAWHNK-02 Q coupon pre VHT. Center: LAWHNK-02 Q coupon after 24 days VHT. Right: LAWHNK-02 Q coupon after 7 days VHT.



Figure J.5. Cross section of LAWHNK-02 Q coupon after 24 days VHT.



Figure J.6. Cross section of LAWHNK-02 Q coupon after 7 days VHT.

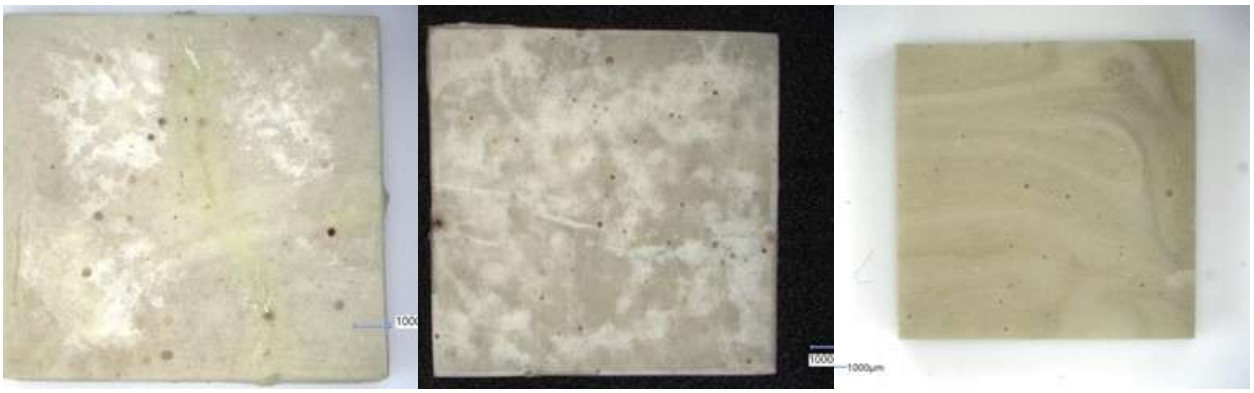


Figure J.7. Left: LAWHNK-03 Q coupon pre VHT. Center: LAWHNK-03 Q coupon after 24 days VHT. Right: LAWHNK-03 Q coupon after 7 days VHT.

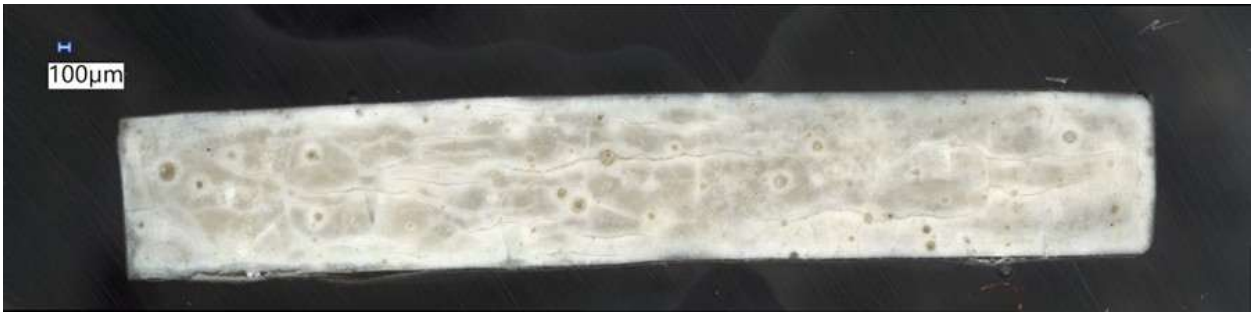


Figure J.8. Cross section of LAWHNK-03 Q coupon after 24 days VHT.



Figure J.9. Cross section of LAWHNK-03 Q coupon after 7 days VHT.



Figure J.10. Left: LAWHNK-04 Q coupon pre VHT. Right: LAWHNK-04 Q coupon after 24 days VHT.

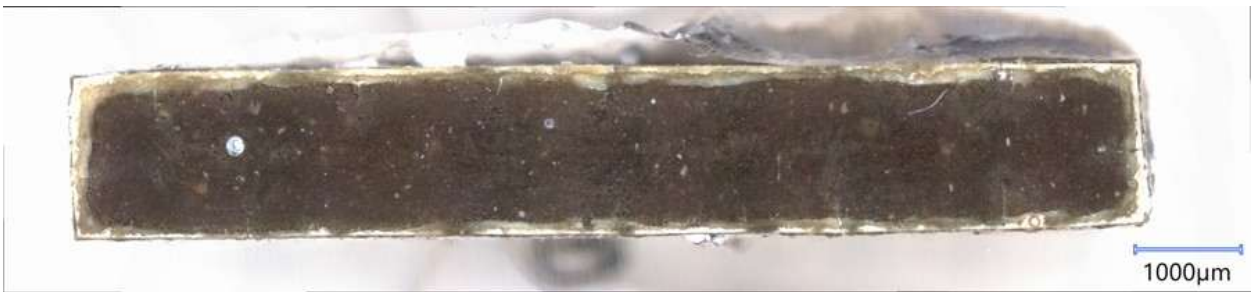


Figure J.11. Cross section of LAWHNK-04 Q coupon after 24 days VHT.



Figure J.12. Left: LAWHNK-05 Q coupon pre VHT. Center: LAWHNK-05 Q coupon after 24 days VHT. Right: LAWHNK-05 Q coupon after 7 days VHT.



Figure J.13. Cross section of LAWHNK-05 Q coupon after 24 days VHT.



Figure J.14. Cross section of LAWHNK-05 Q coupon after 7 days VHT.



Figure J.15. Left: LAWHNK-06 Q coupon pre VHT. Center: LAWHNK-06 Q coupon after 24 days VHT. Right: LAWHNK-06 Q coupon after 7 days VHT.



Figure J.16. Cross section of LAWHNK-06 Q coupon after 24 days VHT.



Figure J.17. Cross section of LAWHNK-06 Q coupon after 7 days VHT.



Figure J.18. Left: LAWHNK-07 Q coupon pre VHT. Center: LAWHNK-07 Q coupon after 24 days VHT. Right: LAWHNK-07 Q coupon after 7 days VHT.



Figure J.19. Cross section of LAWHNK-07 Q coupon after 24 days VHT.

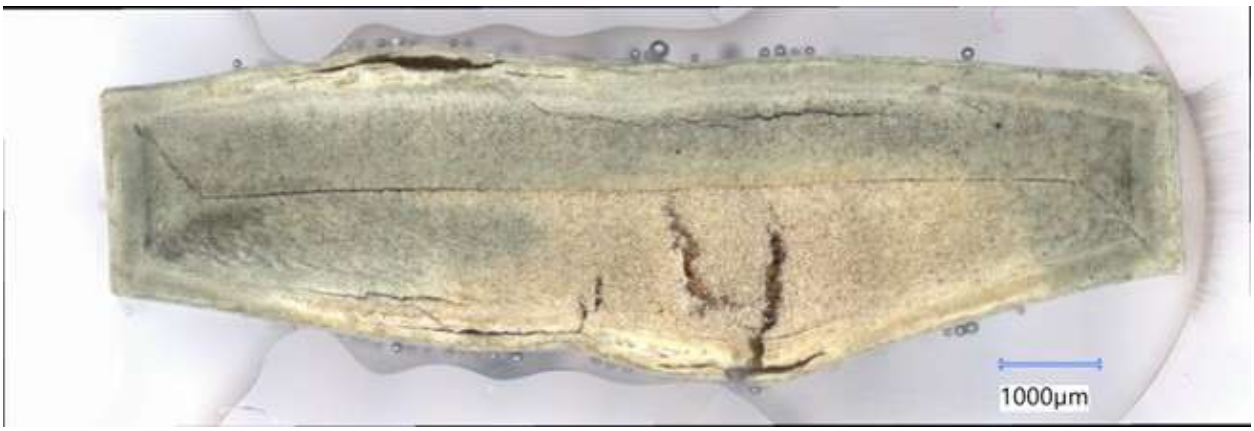


Figure J.20. Cross section of LAWHNK-07 Q coupon after 7 days VHT.



Figure J.21. Left: LAWHNK-08-Q coupon pre VHT. Center: LAWHNK-08 Q coupon after 24 days VHT. Right: LAWHNK-08 Q coupon after 7 days VHT.

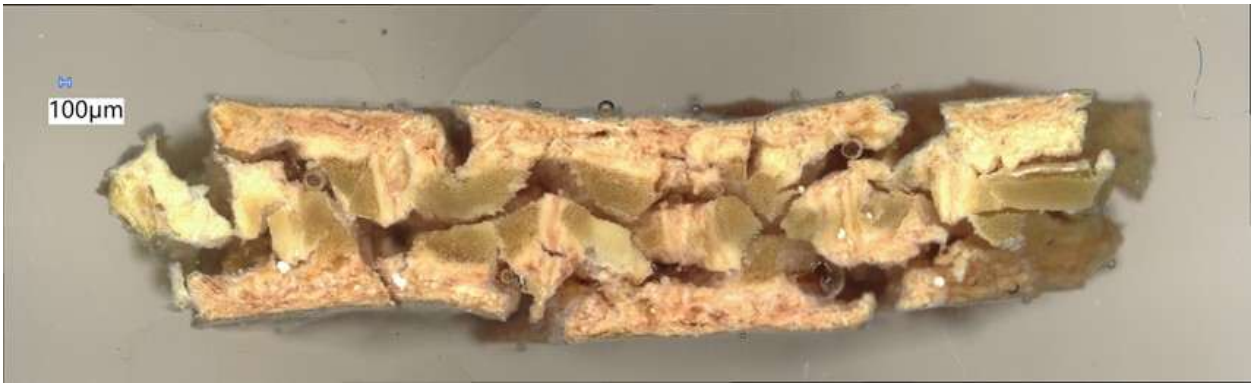


Figure J.22. Cross section of LAWHNK-08 Q coupon after 24 days VHT.



Figure J.23. Cross section of LAWHNK-08 Q coupon after 7 days VHT.



Figure J.24. Left: LAWHNK-09 Q coupon pre VHT. Center: LAWHNK-09 Q coupon after 24 days VHT. Right: LAWHNK-09 Q coupon after 7 days VHT.

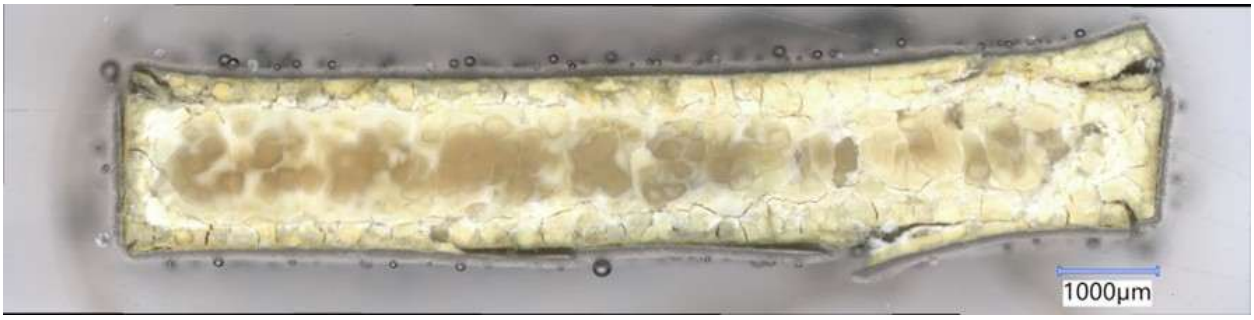


Figure J.25. Cross section of LAWHNK-09 Q coupon after 24 days VHT.

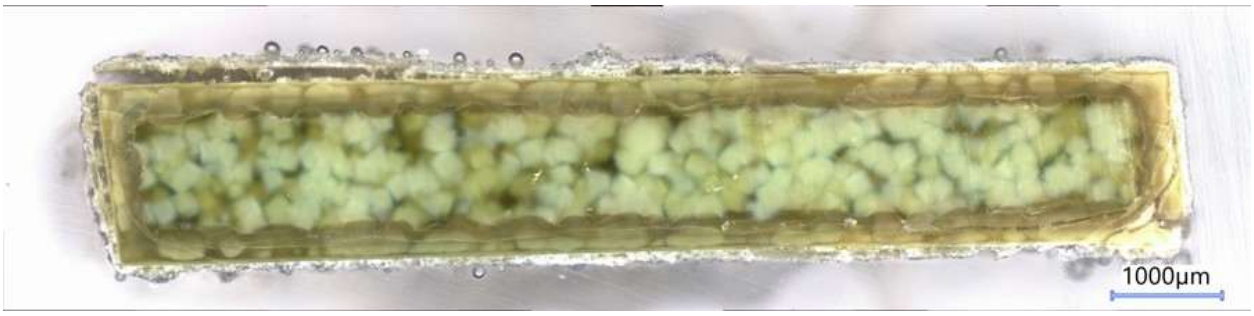


Figure J.26. Cross section of LAWHNK-09 Q coupon after 7 days VHT.



Figure J.27. Left: LAWHNK-10 Q coupon pre VHT. Center: LAWHNK-10 Q coupon after 24 days VHT. Right: LAWHNK-10 Q coupon after 7 days VHT.



Figure J.28. Cross section of LAWHNK-10 Q coupon after 24 days VHT.



Figure J.29. Cross section of LAWHNK-10 Q coupon after 7 days VHT.



Figure J.30. Left: LAWHNK-11 Q coupon pre VHT. Center: LAWHNK-11 Q coupon after 24 days VHT. Right: LAWHNK-11 Q coupon after 7 days VHT.



Figure J.31. Cross section of LAWHNK-11 Q coupon after 24 days VHT.



Figure J.32. Left: LAWHNK-12 Q coupon pre VHT. Center: LAWHNK-12 Q coupon after 24 days VHT. Right: LAWHNK-12 Q coupon after 7 days VHT.



Figure J.33. Cross section of LAWHNK-12 Q coupon after 24 days VHT.

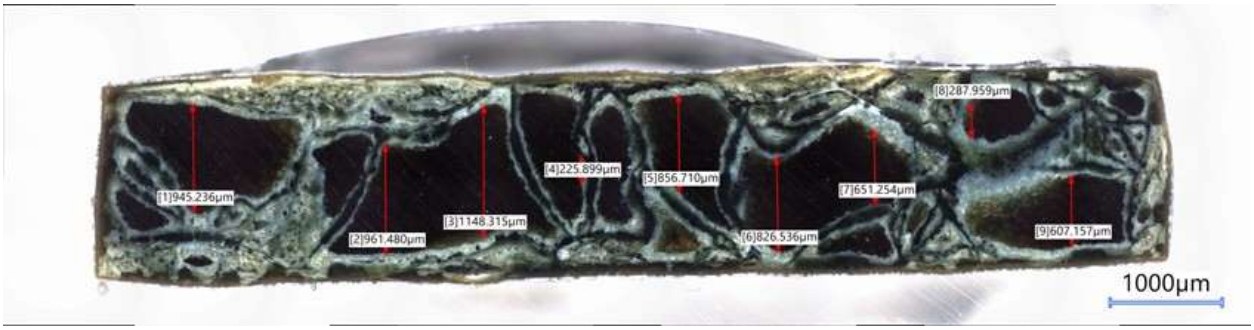


Figure J.34. Cross section of LAWHNK-12 Q coupon after 7 days VHT.



Figure J.35. Left: LAWHNK-13 Q coupon pre VHT. Center: LAWHNK-13 Q coupon after 24 days VHT. Right: LAWHNK-13 Q coupon after 7 days VHT.



Figure J.36. Cross section of LAWHNK-13 Q coupon after 24 days VHT.



Figure J.37. Cross section of LAWHNK-13 Q coupon after 7 days VHT.



Figure J.38. Left: LAWHNK-14 Q coupon pre VHT. Center: LAWHNK-14 Q coupon after 24 days VHT. Right: LAWHNK-14 Q coupon after 7 days VHT.



Figure J.39. Cross section of LAWHNK-14 Q coupon after 24 days VHT.



Figure J.40. Cross section of LAWHNK-14 Q coupon after 7 days VHT.



Figure J.41. Left: LAWHNK-15 Q coupon pre VHT. Center: LAWHNK-15 Q coupon after 24 days VHT. Right: LAWHNK-15 Q coupon after 7 days VHT.

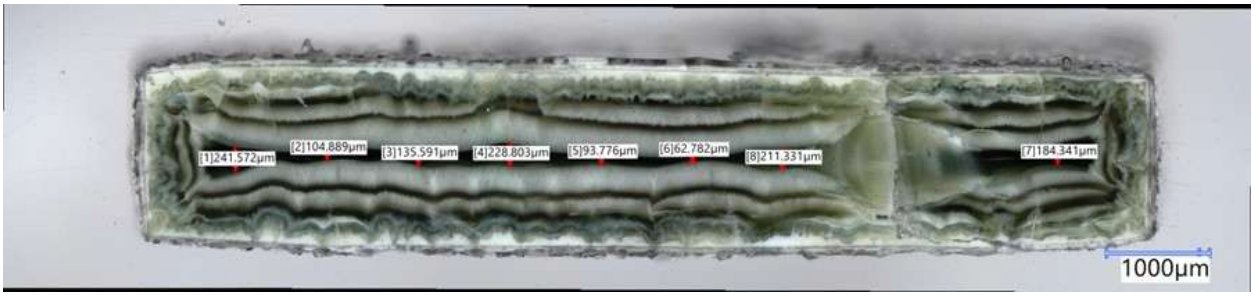


Figure J.42. Cross section of LAWHNK-15 Q coupon after 24 days VHT.

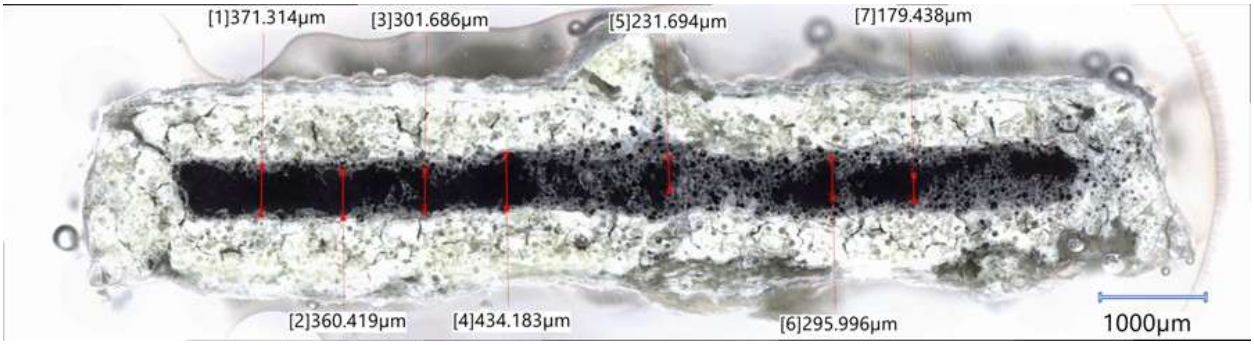


Figure J.43. Cross section of LAWHNK-15 Q coupon after 7 days VHT.

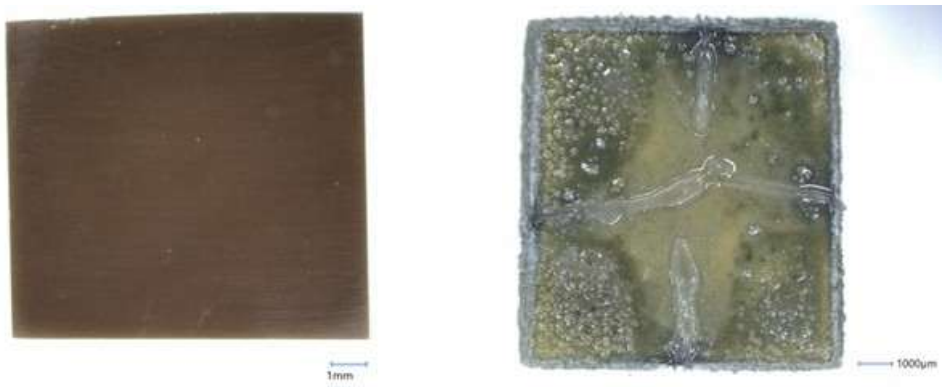


Figure J.44. Left: LAWHNK-17 Q coupon pre VHT. Right: LAWHNK-17 Q coupon after 24 days VHT.



Figure J.45. Cross section of LAWHNK-17 Q coupon after 24 days VHT.



Figure J.46. Left: LAWHNK-18 Q coupon pre VHT. Right: LAWHNK-18 Q coupon after 24 days VHT.

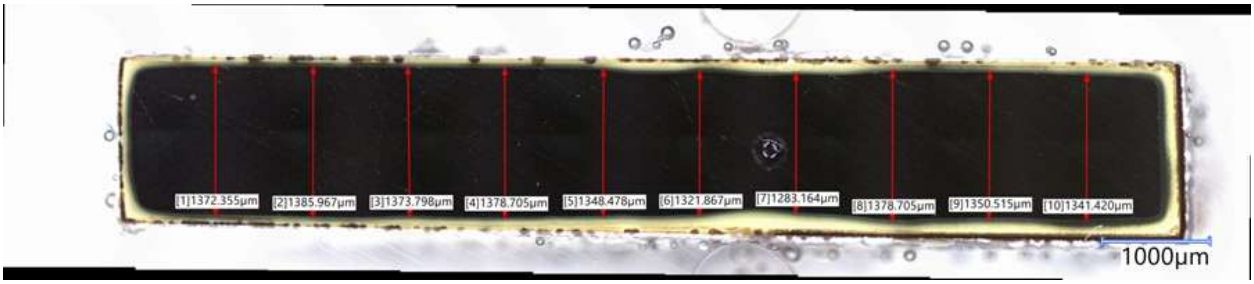


Figure J.47. Cross section of LAWHNK-18 Q coupon after 24 days VHT.



Figure J.48. Left: LAWHNK-19 Q coupon pre VHT. Right: LAWHNK-19 Q coupon after 24 days VHT.

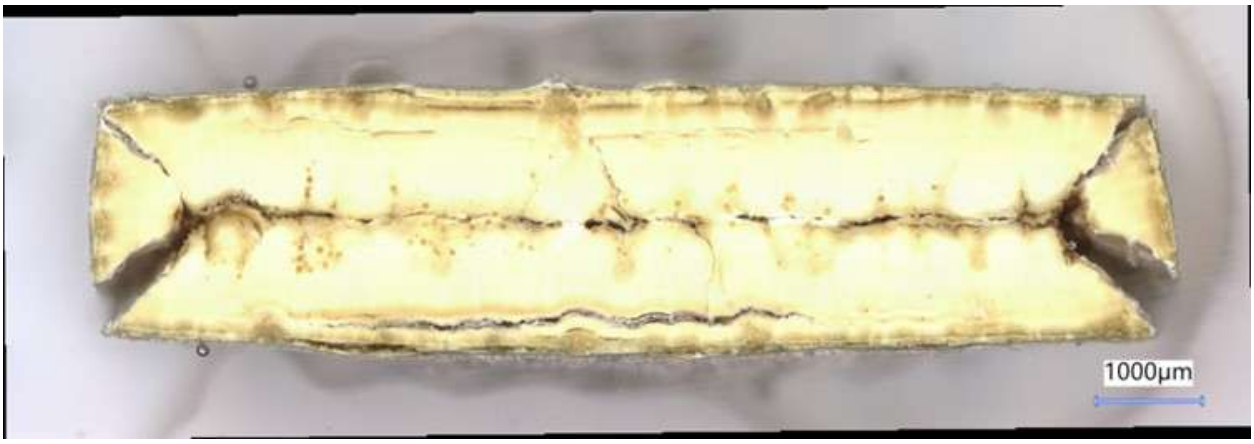


Figure J.49. Cross section of LAWHNK-19 Q coupon after 24 days VHT.

Appendix K – VHT Images on CCC Glasses

The photographs in this appendix show each CCC glass before and after vapor hydration test (VHT) as described in Section 2.10. Duration of the test is specified in the picture caption.



Figure K.1. Left: LAWHNK-01-CCC coupon pre VHT. Center: LAWHNK-01-CCC coupon after 24 days VHT. Right: LAWHNK-01-CCC coupon after 7 days VHT.



Figure K.2. Cross section of LAWHNK-01-CCC coupon after 24 days VHT.



Figure K.3. Cross section of LAWHNK-01-CCC coupon after 7 days VHT.

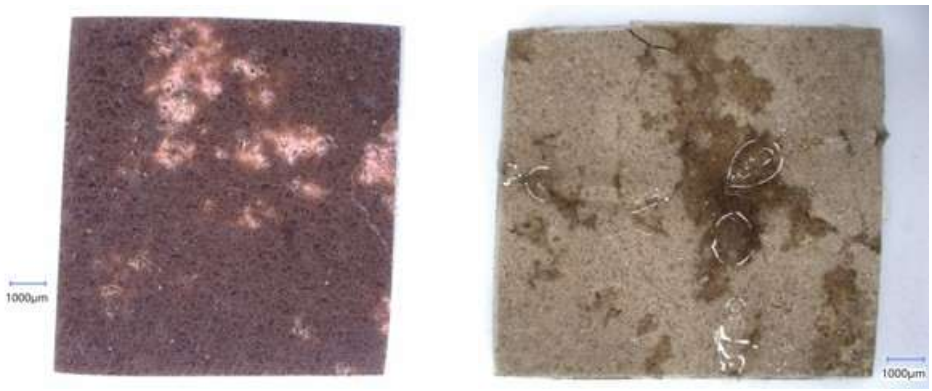


Figure K.4. Left: LAWHNK-02-CCC coupon pre VHT. Right: LAWHNK-02-CCC coupon after 24 days VHT. The 7-day VHT was not performed due to substantial alteration of the glass observed after 24.



Figure K.5. Cross section of LAWHNK-02-CCC coupon after 24 days VHT.

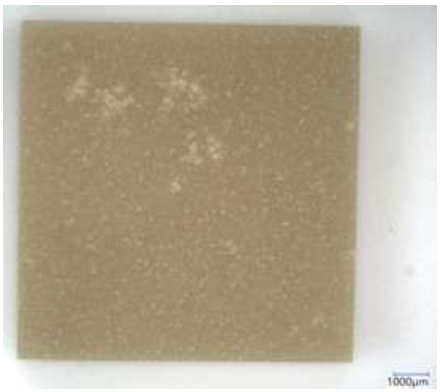


Figure K.6. Left: LAWHNK-03-CCC coupon pre VHT. VHT pictures were not taken because the coupon was completely corroded and crumbled before it could be pictured.

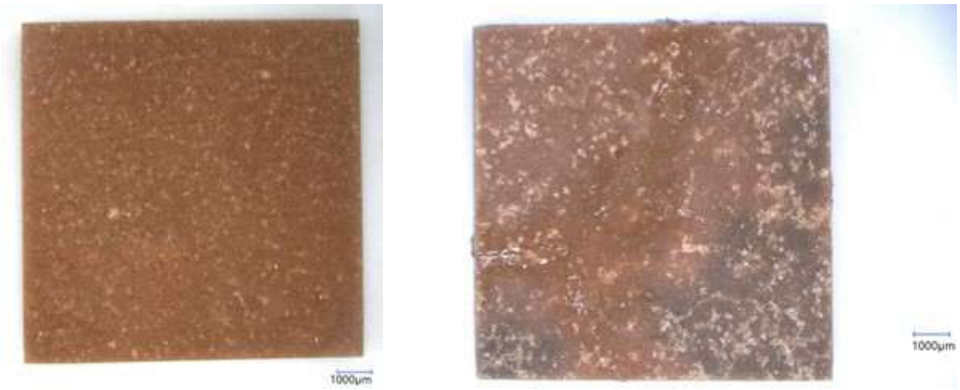


Figure K.7. Left: LAWHNK-04-CCC coupon pre VHT. Right: LAWHNK-04-CCC coupon after 24 days VHT. The 7-day VHT was not performed due to substantial alteration of the glass observed after 24.



Figure K.8. Cross section of LAWHNK-04-CCC coupon after 24 days VHT.



Figure K.9. Left: LAWHNK-05-CCC coupon pre VHT. Center: LAWHNK-05-CCC coupon after 24 days VHT. Right: LAWHNK-05-CCC coupon after 7 days VHT.



Figure K.10. Cross section of LAWHNK-05-CCC coupon after 24 days VHT.



Figure K.11. Cross section of LAWHNK-05-CCC coupon after 7 days VHT.



Figure K.12. Left: LAWHNK-06-CCC coupon pre VHT. Right: LAWHNK-06-CCC coupon after 24 days VHT. The 7-day VHT was not performed due to substantial alteration of the glass observed after 24.

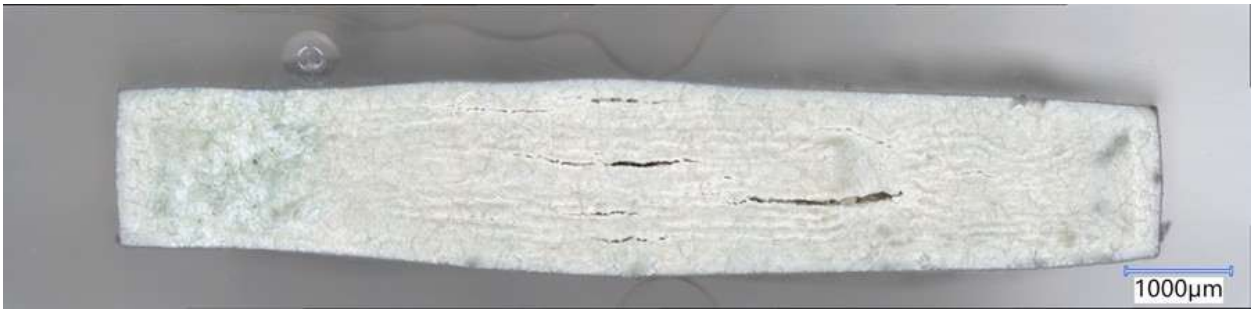


Figure K.13. Cross section of LAWHNK-06-CCC coupon after 24 days VHT.

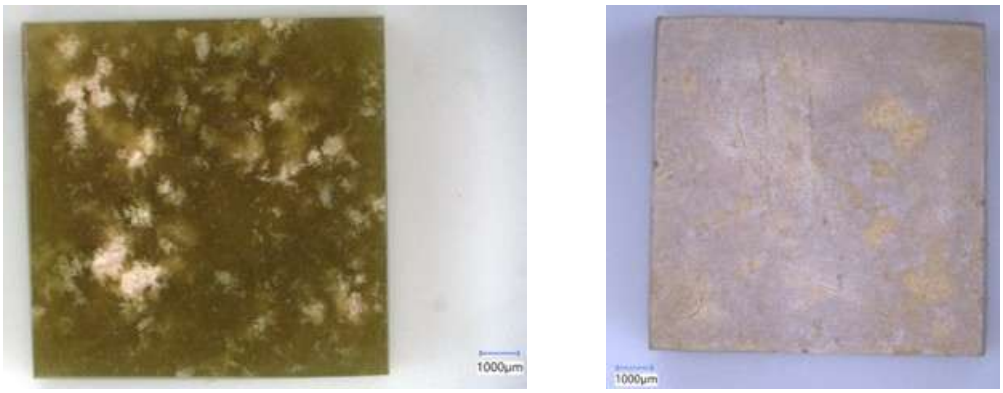


Figure K.14. Left: LAWHNK-08-CCC coupon pre VHT. Right: LAWHNK-08-CCC coupon after 24 days VHT. The 7-day VHT was not performed due to substantial alteration of the glass observed after 24.



Figure K.15. Cross section of LAWHNK-08-CCC coupon after 24 days VHT.



Figure K.16. Left: LAWHNK-10-CCC coupon pre VHT. Center: LAWHNK-10-CCC coupon after 24 days VHT. Right: LAWHNK-10-CCC coupon after 7 days VHT.

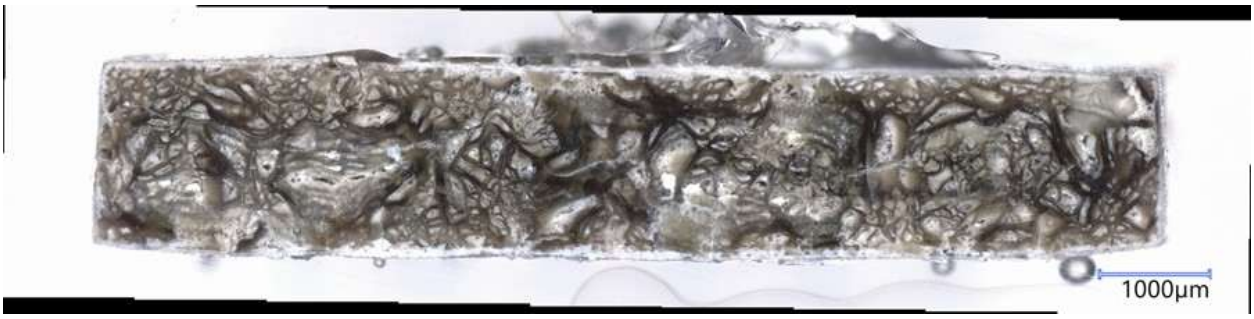


Figure K.17. Cross section of LAWHNK-10-CCC coupon after 24 days VHT.



Figure K.18. Cross section of LAWHNK-10-CCC coupon after 7 days VHT.



Figure K.19. Left: LAWHNK-11-CCC coupon pre VHT. Center: LAWHNK-11-CCC coupon after 24 days VHT. Right: LAWHNK-11-CCC coupon after 7 days VHT.

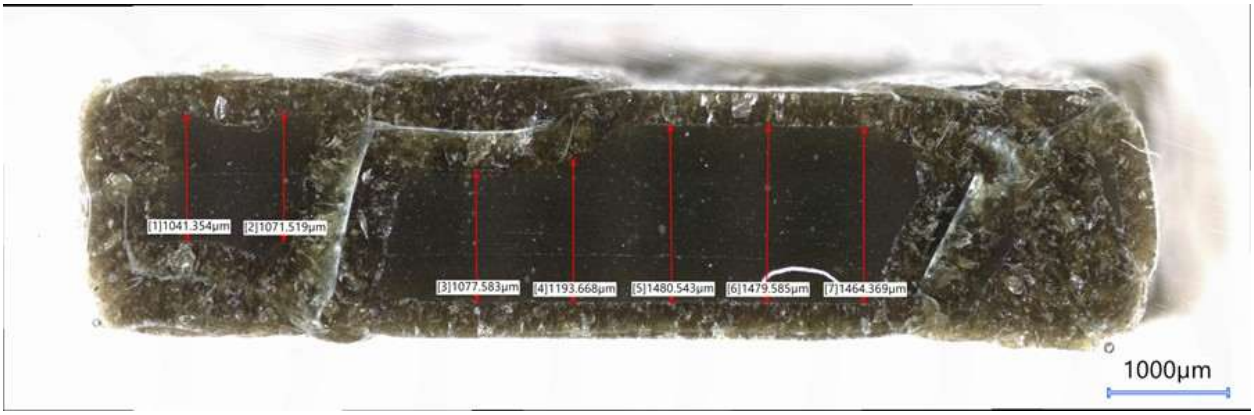


Figure K.20. Cross section of LAWHNK-11-CCC coupon after 24 days VHT.

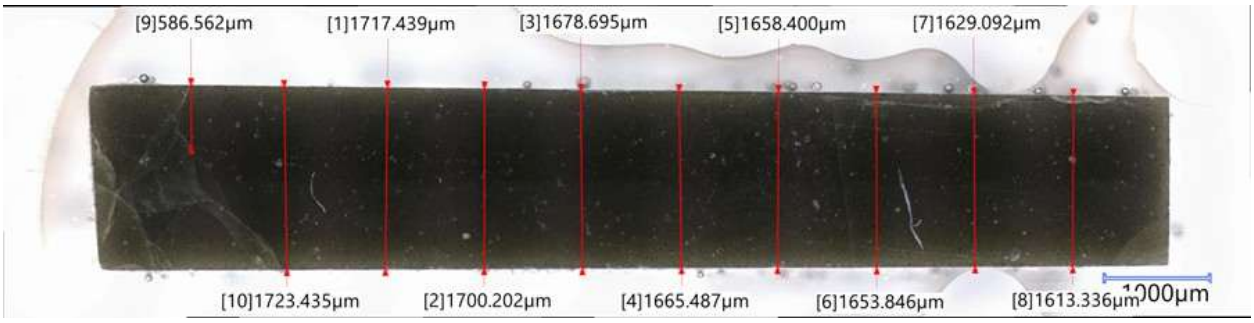


Figure K.21. Cross section of LAWHNK-11-CCC coupon after 7 days VHT.



Figure K.22. Left: LAWHNK-12-CCC coupon pre VHT. Center: LAWHNK-12-CCC coupon after 24 days VHT. Right: LAWHNK-12-CCC coupon after 7 days VHT.

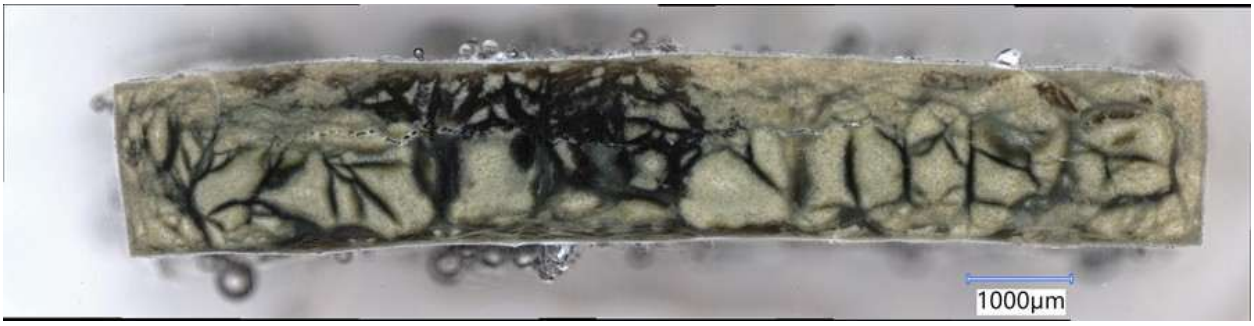


Figure K.23. Cross section of LAWHNK-12-CCC coupon after 24 days VHT.

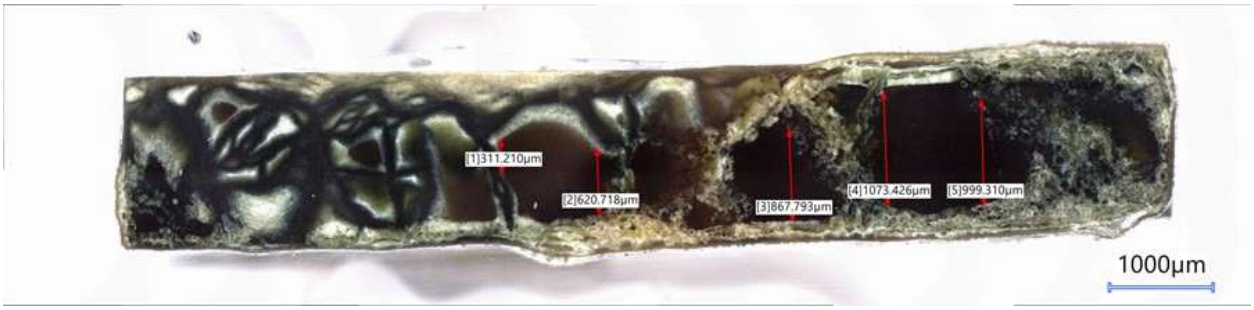


Figure K.24. Cross section of LAWHNK-12-CCC coupon after 7 days VHT.

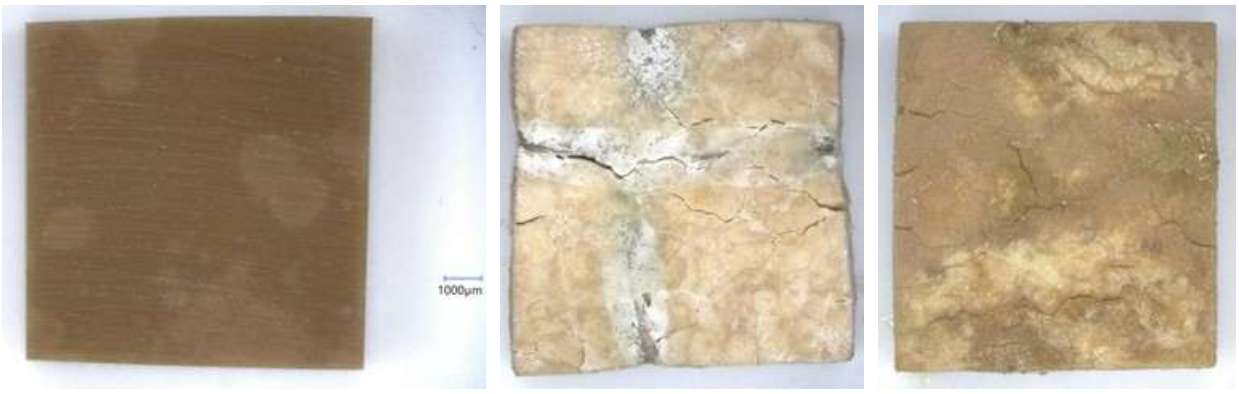


Figure K.25. Left: LAWHNK-13-CCC coupon pre VHT. Center: LAWHNK-13-CCC coupon after 24 days VHT. Right: LAWHNK-13-CCC coupon after 7 days VHT.



Figure K.26. Cross section of LAWHNK-13-CCC coupon after 24 days VHT.



Figure K.27. Cross section of LAWHNK-13-CCC coupon after 7 days VHT.



Figure K.28. Left: LAWHNK-14-CCC coupon pre VHT. Center: LAWHNK-14-CCC coupon after 24 days VHT. Right: LAWHNK-14-CCC coupon after 7 days VHT.



Figure K.29. Cross section of LAWHNK-14-CCC coupon after 24 days VHT.



Figure K.30. Cross section of LAWHNK-14-CCC coupon after 7 days VHT.

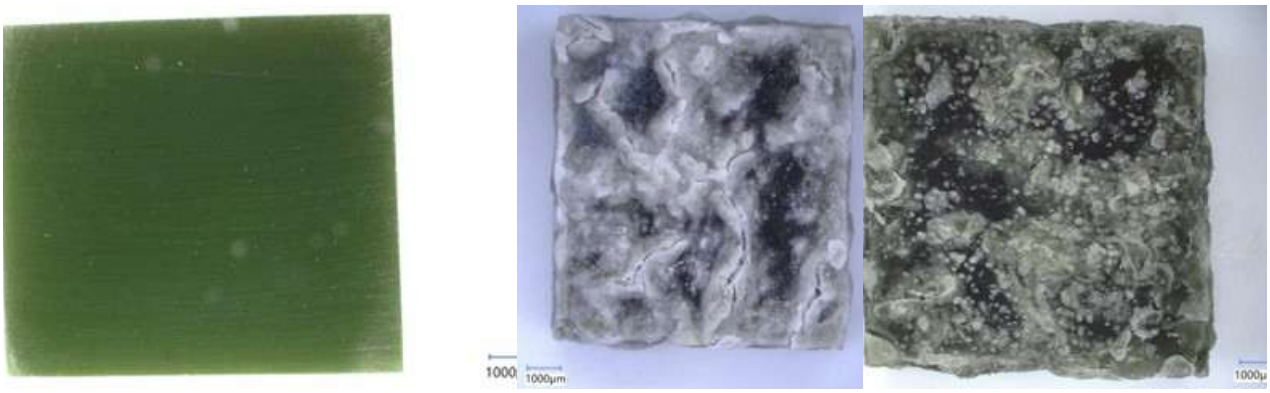


Figure K.31. Left: LAWHNK-15-CCC coupon pre VHT. Center: LAWHNK-15-CCC coupon after 24 days VHT. Right: LAWHNK-15-CCC coupon after 7 days VHT.

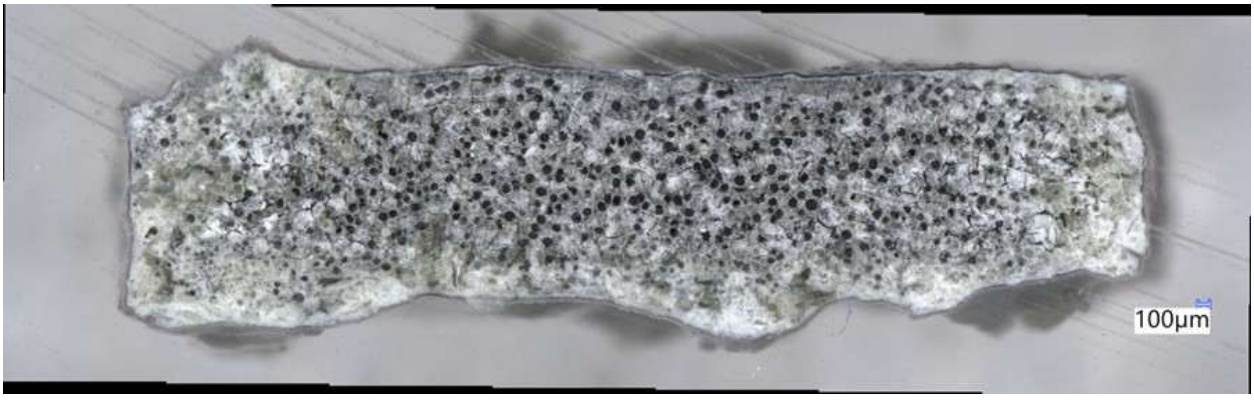


Figure K.32. Cross section of LAWHNK-15-CCC coupon after 24 days VHT.

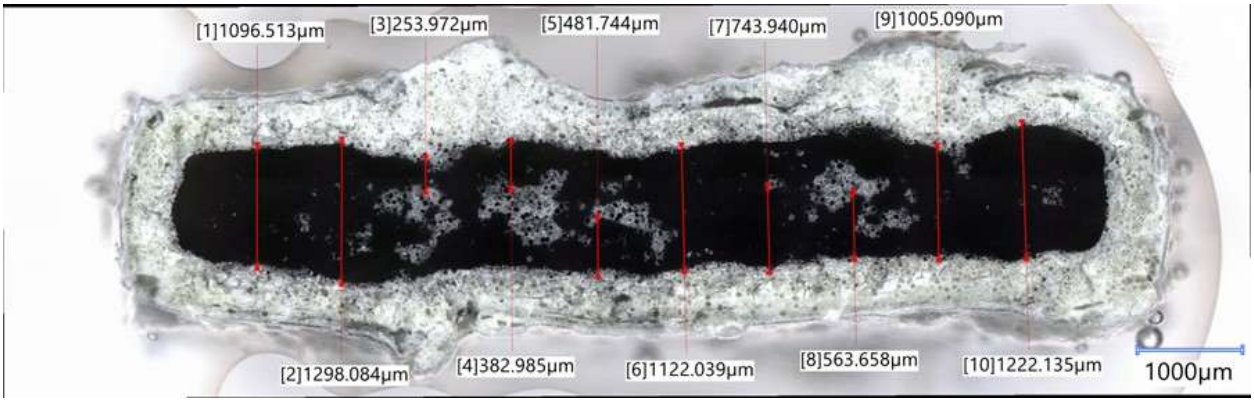


Figure K.33. Cross section of LAWHNK-15-CCC coupon after 7 days VHT.

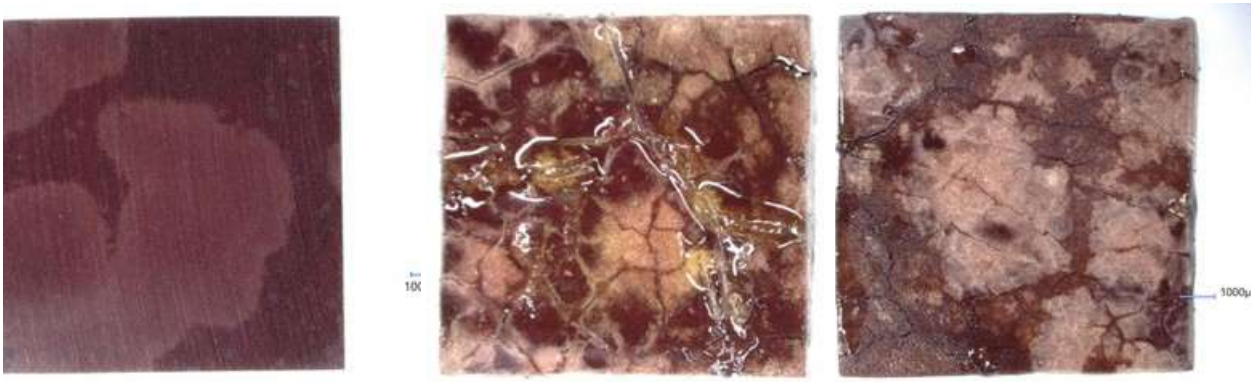


Figure K.34. Left: LAWHNK-16-CCC coupon pre VHT. Center: LAWHNK-16-CCC coupon after 24 days VHT. Right: LAWHNK-16-CCC coupon after 7 days VHT.



Figure K.35. Cross section of LAWHNK-16-CCC coupon after 24 days VHT.



Figure K.36. Cross section of LAWHNK-16-CCC coupon after 7 days VHT.



Figure K.37. Left: LAWHNK-17-CCC coupon pre VHT. Center: LAWHNK-17-CCC coupon after 24 days VHT. Right: LAWHNK-17-CCC coupon after 7 days VHT.

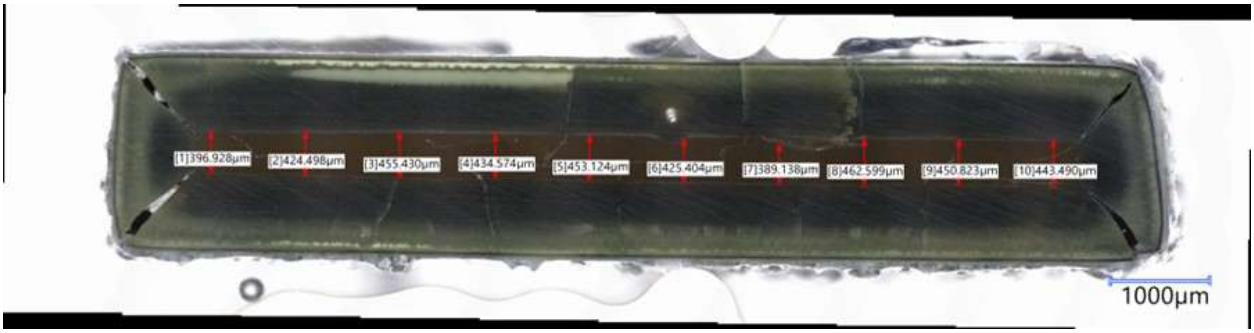


Figure K.38. Cross section of LAWHNK-17-CCC coupon after 24 days VHT.

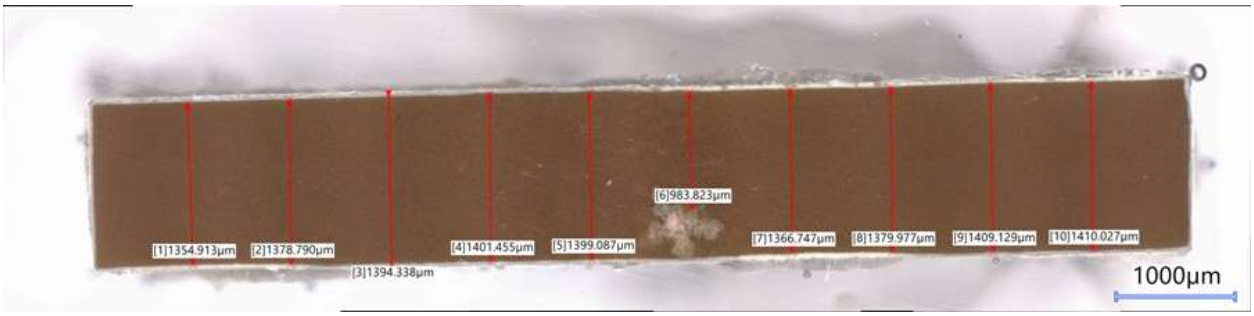


Figure K.39. Cross section of LAWHNK-17-CCC coupon after 7 days VHT.

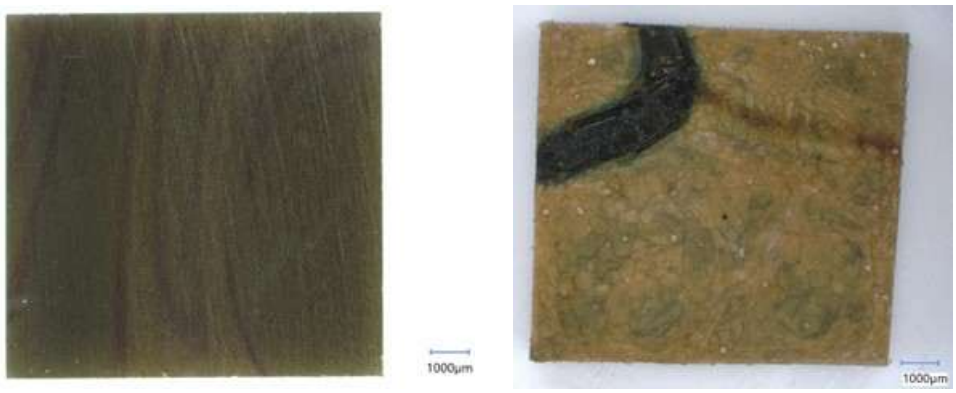


Figure K.40. Left: LAWHNK-18-CCC coupon pre VHT. Right: LAWHNK-18-CCC coupon after 7 days VHT.

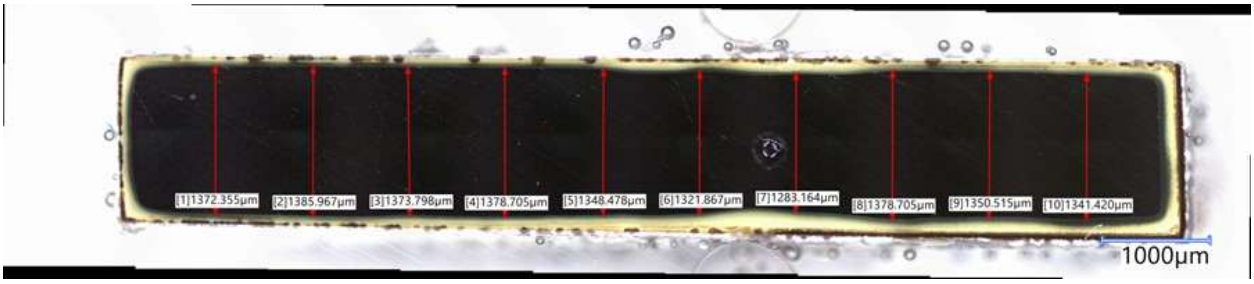


Figure K.41. Cross section of LAWHNK-18-CCC coupon after 7 days VHT.



Figure K.42. Left: LAWHNK-19-CCC coupon pre VHT. Center: LAWHNK-19-CCC coupon after 24 days VHT. Right: LAWHNK-19-CCC coupon after 7 days VHT.



Figure K.43. Cross section of LAWHNK-19-CCC coupon after 24 days VHT.

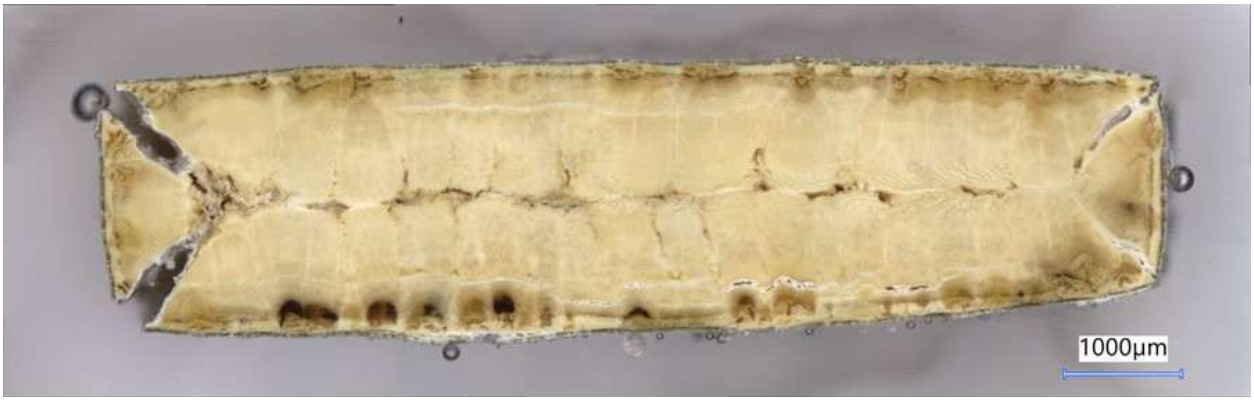


Figure K.44. Cross section of LAWHNK-19-CCC coupon after 7 days VHT.

Pacific Northwest National Laboratory

902 Battelle Boulevard
P.O. Box 999
Richland, WA 99354

1-888-375-PNNL (7665)

www.pnnl.gov